THERMAL PERFORMANCE OF MECHANICAL PIPE INSULATION SYSTEMS AT BELOW-AMBIENT TEMPERATURE

By

SHANSHAN CAI

Bachelor of Science
Huazhong University of Science and Technology
Wuhan, China
2007

Master of Science
Oklahoma State University
Stillwater, OK
2009

Submitted to the Faculty of the
Graduate College of the
Oklahoma State University
in partial fulfillment of
the requirements for
the Degree of
DOCTOR OF PHILOSOPHY
December, 2013

THERMAL PERFORMANCE OF MECHANICAL PIPE INSULATION SYSTEMS AT BELOW-AMBIENT TEMPERATURE

Dissertation Approved:

Dr. Lorenzo Cremaschi

Dissertation Adviser

Dr. Afshin Ghajar

Dr. Jeffery Spitler

Dr. James Smay

.

ACKNOWLEDGEMENTS

I wish to express my sincere appreciation and grateful to my advisor, Dr. Lorenzo Cremaschi, for his continuous support, patience and guidance. I would also like to extend my appreciation to my other committee members, Dr. Afshin Ghajar, for his help in the literature review and the first stage of this project, Dr. Jeffery Spitler, for teaching me VBA, and it becomes an important tool in my model, and Dr. James Smay, for all the suggestions given during my defense.

I should give my thanks to the person involved in this project: Kasey Worthington, who helped me design and construct the test apparatus; Jimmy Kim, who helped me in the construction work during the second stage; Auvi Biswas and Jeremy Smith, who helped me in the Labview program; Weiwei Zhu, who will continue the tests; I would also like to thank the other team members: Andrea Bigi, Ardi Yatim, Pratik Deokar, Xiaoxiao Wu for the help in the maintenance of the Psychrometric chamber. Without your help, I cannot go this far.

Special thanks to my parents for bringing me to the world, supporting me for my each decision and giving me their endless love.

Name: SHANSHAN CAI

Date of Degree: DECEMBER, 2013

Title of Study: THERMAL PERFORMANCE OF MECHANICAL PIPE INSULATION SYSTEMS AT BELOW-AMBIENT TEMPERATURE

Major Field: MECHANICAL ENGINEERING

Abstract: Mechanical pipe insulation systems are commonly applied to cold piping surfaces in most industrial and commercial buildings in order to limit the heat losses and prevent water vapor condensation on the pipe exterior surfaces. Due to the fact that the surface temperature of these pipelines is normally below the ambient dew point temperature, water vapor diffuses inside the pipe insulation systems often condenses when it reaches the pipe exterior surfaces. The water droplets accumulated in the pipe insulation system increase its overall thermal conductivity by thermal bridging the cells or the fibers of the insulation material. The moisture ingress into pipe insulation threatens the thermal performance and the overall efficiency of the building mechanical system.

The main objective of this research was to investigate the effects of water vapor ingress on the thermal conductivity of pipe insulation systems. A critical review of the state of the art literature in this field was included to clarify the similarities and differences on the apparent thermal conductivity of pipe insulation systems and flat slabs. A new experimental methodology was developed to isolate and quantify the effect of water vapor ingress to the pipe insulation systems. Seven fibrous and ten closed-cell pipe insulation systems were tested on the novel experimental apparatus under dry and wet, condensing conditions. Under dry condition, the apparent thermal conductivity was observed linearly varied with insulation mean temperature, and the presence of joint sealant may increase the apparent thermal conductivity by 15%. During moisture test, results showed that the moisture diffusion mechanism were different in fibrous and closed-cell pipe insulation systems. Compared to closed-cell, fibrous pipe insulation system behaved more sensitive to the moisture content and the thermal conductivity increased dramatically due to the formation of more thermal bridging and preferential paths. An analytical model was developed based on the diffusion mechanism to predict the moisture accumulation and the associated penalization of the apparent thermal conductivity in different pipe insulation systems operating below ambient room temperature. The model was validated with the experimental results and the data reported in the literature on the thermal conductivity ratio with different moisture content. The differences were within 10% for closed-cell pipe insulation, and within 15% for fibrous pipe insulation systems.

TABLE OF CONTENTS

LIST OF TABLES

LIST OF FIGURES

NOMENCLATURE

Latin symbols

a	=	fraction of series configuration	-
b	=	fraction of moistened pores	-
B_T	=	bias uncertainty	-
c_{rad}	=	radiation constant	Btu/hr-ft-R^4 (W/m-K^4)
C_1	=	coefficient C_1	-
C_2	=	coefficient C_2	-
D	=	diameter	in (mm)
D_v	=	water vapor diffusion coefficient	ft^2/s (m^2/s)
E	=	energy activation for permeation	Btu/lbmol (kJ/mol)
f_1	=	condensing coefficient	-
f_2	=	water vapor permeability correction factor	-
f_3	=	water retention coefficient	-
G	=	geometric factor	-
g	=	acceleration due to gravity	ft^2/hr (m^2/s)
h	=	latent heat of evaporation	Btu/hr-ft^2-F (W/m^2-K)
k	=	thermal conductivity	Btu-in/hr-ft^2-F (W/m-K)
L	=	length	in (mm)
$\dot{m}$	=	mass flow rate	lbm/min (kg/s)
m	=	mass	lbm (kg)
n	=	porosity	-
P	=	pressure	psi (Pa)
PIR	=	Polyisocyanurate	
PUR	=	Polyurethane	
Q	=	heat transfer rate	Btu/hr (W)
R	=	radius	in (mm)
R'	=	thermal resistance	hr-ft^2-F/Btu (m^2-C/W)
Rp	=	vapor resistance	(s-m^2-Pa/kg)
R_v	=	gas constant	Btu/lbm-R (J/kg-K)
T	=	temperature	℉ (℃)
V	=	volume fraction	-
Vol	=	volume	ft^3 (m^3)

Greek symbols

δ	=	thickness	in (mm)

ε	=	emissivity	-
β	=	coefficient of expansion	K^{-1}
σ	=	blackbody radiation constant	Btu/hr-ft^{2}R^4 (W/m^{2}K^4)
$\mathcal{P}$	=	water vapor permeability	ng/s-m-Pa

Dimensionless numbers

Nu = Nusselt number, $Nu = 1 + 1.44\left[1 - \frac{1708}{Ra_D}\right]^+ + \left[\frac{Ra_D^{\frac{1}{3}}}{18} - 1\right]^+$,[ ]$^+$indicates that if the quantity in the bracket is negative, it should be equal to zero

Pr = Prandtl number

Ra = Rayleigh number, $Ra = \frac{g\beta\Delta TD}{\nu^2}Pr$

CHAPTER I

1. INTRODUCTION

1.1 Background

When pipes are used for chilled water, glycol brines, refrigerants, and other chilled fluids, energy must be expended to compensate for heat gains through the wall of the pipes. Higher fluid temperature at the point of use decreases the efficiency of the end-use heat exchangers and increases the parasitic energy consumption, fans power for example. Mechanical pipe insulation systems are often used to save energy and avoid condensation and mold related problems in HVAC chiller pipeline systems for industrial and commercial buildings. These insulation systems play an important role for the health of the occupied space. When a chilled pipe is uninsulated or inadequately insulated, condensation might occur and water will drip onto other building surfaces possibly causing mold growth. Examples of wet pipe insulation and wet insulation with mold growth are shown in the Figure 1.1 and 1.2.

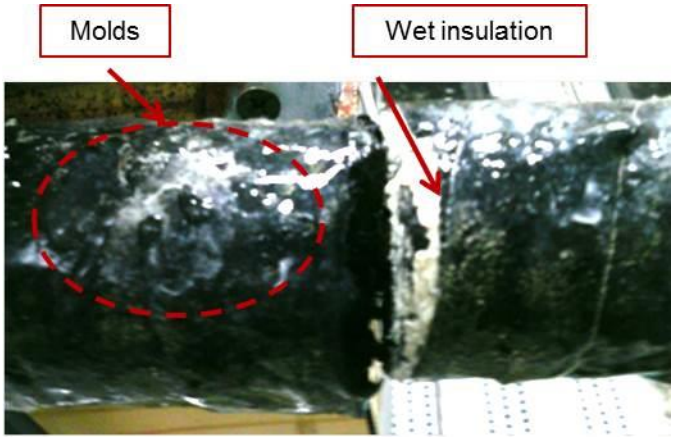

Figure 1.1: Example of wet insulation with mold growth on the surface (this photo was taken at Oklahoma State University Laboratory)

1.2 Critical issue with cold pipes

The critical issue with cold pipes is that the temperature difference between the pipe and its surrounding ambient air drives water vapor inside the insulation system, and condensation commonly occurs when the water vapor comes in contact the chilled pipe surface. This phenomenon inevitably lead to degradation of thermal performance and service life of the insulation; it affects the economics of performance, promote corrosion of piping and lead to system failure and downtime, which have large economic implications when shut-down and replacement is considered. Damage can also occur from leaking pipes and tubing, mold growth and contamination. To prevent these issues, engineers design pipe insulation systems with the aim of preventing such condensation, but pipe insulation product evaluations have not focused on these performance aspects. For below ambient applications, vapor barriers and jacketing are often adopted on the exterior of pipe insulation but a number of cases showed that water vapor can still permeated inside the insulation system through small gaps or pinholes formed in the jacketing.

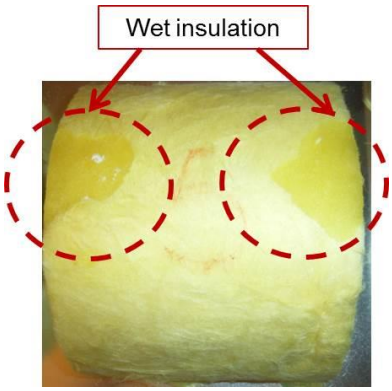

Figure 1.2: Example of wet pipe insulation (this photo was taken at OSU Laboratory)

An optimized solution that accounts for cost and system energy efficiency must consider the rate of moisture absorption at various operating conditions and the variation on pipe insulation thermal conductivity with moisture content. An accurate characterization of the thermal conductivity and moisture transport in pipe insulation systems would enable building distribution mechanical system designers to incorporate the most energy-efficient pipe insulation system for each application and to better estimate the actual heat gains during the life cycle of the insulation system. But what thermal conductivity should we use for pipe insulation system operating at below ambient temperature? This is not a trivial question, and it leads to the definition of apparent thermal conductivity. The apparent thermal conductivity is the inverse of the overall

thermal resistance between the pipe surface and the ambient air. It can be thought as an average thermal conductivity of the mechanical insulation system that consists of the pipe insulation material with cylindrical configuration, its split joints (see Figure 1.3), its sealant, and its vapor barrier or jacketing when present. Ultimately it is the parameter that the building distribution system designer is searching for to estimate the heat gains in the pipelines over the service period of the pipe insulation.

Figure 1.3: Example of split joins with either one or two seams used to facilitate the installation of pipe insulation over previously installed pipe (this photo was taken at Oklahoma State University Laboratory)

In current standards, there are no suitable testing procedures for measuring the apparent thermal conductivity of pipe insulation systems operating below ambient temperatures with moisture ingress. Although ASTM (American Society for Testing and Materials) C335 (2005) gives the standard on the measurement of heat transfer properties of pipe insulation, it is only based on the heated pipe with heat flow outward. In the literature it was pointed out that the direction of heat flow might be important and the apparent thermal conductivity data obtained from hot pipe tests might not be appropriate for cold pipe applications (see Figure 1.4). This is often the case in buildings air conditioning, in which the occupied zone is set to 68 to 77°F (20 to 25°C), relative humidity of 40 to 50% and the chilled water pipe surface temperatures are about 38 to 42°F (3 to 6°C). In addition, most of the data published were derived from the tests for insulation in flat slabs configuration. Mechanical HVAC engineers often directly use these values for pipe insulation systems and make an evaluation on the system thermal performance in wet conditions based on

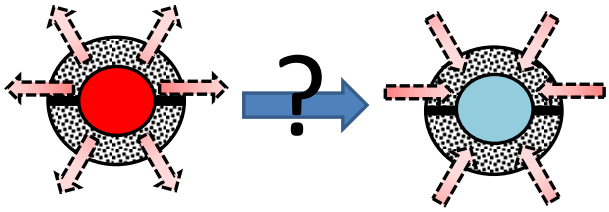

Figure 1.4: Can the apparent thermal conductivity measured from hot tests be applied to pipe operating at below ambient conditions?

similar material in flat slab configuration. Does this approach produce an accurate estimation of the apparent thermal conductivity for pipe insulation system at below ambient temperature (see Figure 1.5)? There is some debate because pipe insulation systems may behave differently from flat slabs due to the radial configuration, the presence of split joints, and of joint sealant adopted in the field. There is agreement that having a correct methodology for measuring the thermal conductivity of pipe insulation systems at sub-ambient temperatures will provide more meaningful data to practicing engineers.

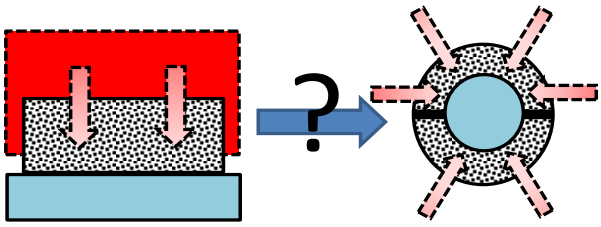

Figure 1.5: Can the thermal conductivity measured from flat slab tests be applied to pipe operating at below ambient conditions?

1.3 Objectives

The main objective of this research was to investigate the effects of water vapor ingress on the thermal conductivity of modern pipe insulation systems. This goal was achieved by conducting a critical review of the state-of-the art literature in this field, by developing a new experimental methodology that isolates and quantifies such effects for several representative pipe insulation systems, and by developing an analytical model that predicts the moisture accumulation and the associated penalization of the apparent thermal conductivity of pipe insulation systems operating below ambient room temperatures.

Step 1 was to conduct a critical literate review to clarify the similarities and differences on the apparent thermal conductivity data of pipe insulation systems and flat slabs. In the engineering field, the manufacturers typically publish the thermal behavior of the insulation materials, such as R-value and thermal conductivity, based on the test results from flat slabs. It is very common to extrapolate the thermal conductivity data provided in flat slabs for the estimation on the apparent thermal conductivity of pipe insulation systems. This review started with a discussion on the

methodologies that has been reported in the current field for the measurement on the pipe insulation thermal conductivity. The advantages and shortcomings of each technique were pointed out to help engineer or researcher choose the methodology that most appropriate for the test requirement. This literature review also provide a large data set on the thermal behavior of six insulation systems by summarizing the current values reported both in flat slab and cylindrical shape, under dry and wet conditions with moisture ingress.

The second step of my research work was the development of an experimental methodology to measure the apparent pipe insulation thermal conductivity in dry and wet operating conditions below ambient temperature and with water vapor ingress. This test apparatus improved the accuracy of the experimental data with respect to modern methodologies used for pipe insulation thermal conductivity measurements. The construction procedures are document in detail so that the same test apparatus can be rebuilt in other labs. This test apparatus will be tested on more than ten typical pipe insulation systems, which are commonly used in the low temperature engineering field, such as industrial freezer in the cryogenic application, chilled water pipes in HVAC&R, etc. The results derived from the measurement aimed to i) prove the feasibility and accuracy of the current test facility; ii) show the differences on the thermal behavior between pipe insulation and flat slabs, and how the behavior degrades when the insulation system was applied around the cold surface and gradually become wet; iii) update the handbooks so that engineers can use the specific values of the apparent thermal conductivity that directly measured from the pipe insulation systems. The specific objectives in the experiment section are summarized as follows:

a) Design an experimental test apparatus to measure the thermal conductivity of pipe insulation operating below ambient temperature and under both water vapor non-condensing and condensing conditions;
b) Construct a prototype apparatus and calibrate its instrumentation;

c) Demonstrate that the apparatus operates successfully through the evaluation of at least two typical insulation products at several pipe insulation mean temperatures;
d) Document the design of the apparatus in a way that others will be able to reproduce it
e) Measure various typical pipe insulation systems in both dry and wet conditions, and identify seminaries and difference (if any) between their thermal performance characteristics;
f) Investigate the impact of moisture ingress on the thermal conductivity of different types of pipe insulation systems.

The third step of my research was to develop a general model that can be applied in the industry field to help engineers predict the variation on the thermal behavior of different pipe insulation systems with moisture content and with time. The model aimed to be general so that it can be applied on various pipe insulation systems, fibrous or closed-cell, with joint sealant or with vapor jacketing. From this model, the mechanical engineers and designers are able to correlate the application with the ambient conditions to generate a deficiency profile of the insulation materials and make estimation on the lifetime of the pipe insulation systems. This will very helpful in selecting an optimal design between the system efficiency and economy cost. The specific aspects that aimed to reach in the modeling part are summarized as follows:

a) Verify, expand, and possibly improve the accuracy of the thermodynamic models in the open domain literature that predict the thermal conductivity of pipe insulation systems under dry conditions;
b) Develop an analytical model for the prediction of the apparent thermal conductivity of pipe insulation systems under wet, condensing conditions with moisture ingress;
c) Validate the model with both experimental data of the current thesis and the reported values from the open domain literature;

d) Document the limitations in the current model, and summarize potential improvements in follow up and future work.

1.4 Organization of this dissertation

This dissertation is organized in seven chapters:

1) Introduction: this section provides a research background on this topic and states project objectives that need to be achieved by the end of this research work;
2) Literature review: in this section, I reviewed the most up-to-date work available in the public domain on the measurement of pipe insulation thermal conductivity under both dry and wet conditions. The advantages and shortcomings of each technique were discussed at length with the challenges and future research needs in this area discussed at the end;
3) Test apparatus design and instrumentation: this section describes the test approach and test apparatus that developed for the measurement of pipe insulation system thermal conductivity. The construction procedures and facility improvements are documented in detail.
4) Measurements and data reduction: this section discussed the test conditions and summarized the test procedures applied during the experiment. A 2-D modeling approach was explained in the data analysis, followed with the equipment accuracy investigation and the measurement uncertainty analysis;
5) Experimental results: this section included all the findings that observed during each test and summarized the test results for more than ten pipe insulation systems under both dry and wet, condensing conditions. The test results were critically compared with possible explanations provided in detail.
6) Simulation model: in this section, an analytical model was developed for closed-cell and fibrous pipe insulation system, both under dry, non-condensing and wet conditions with

moisture ingress. The model has been validated with experimental data and reported data from the open domain literature. Limitations are also discussed in this section for further improvement;

7) Conclusions and recommendations: this section provides a conclusion of all the work I have done in this research. Recommendations for future work will be provided at the end.

CHAPTER II

2. LITERATURE REVIEW

Because there are limited experimental data of thermal conductivity of pipe insulation systems at below ambient temperature, mechanical HVAC engineers often extrapolate the thermal conductivity and moisture ingress rates of pipe insulation systems in wet operating conditions from experimental data originally obtained on the same type of insulation material but in flat slab configurations. Two studies (Cremaschi *et al*., 2012a; Wilkes *et al*., 2002) have reported a measurable difference on the effective thermal conductivity when considering flat slab and pipe insulation systems. In addition this approximation might not be suitable for all pipe insulation systems as it will be explained more in details later in the present report. Considering that the dissimilar values of thermal conductivity and moisture ingress rates are partially due to the method of testing, the test methodologies for measuring thermal conductivity of pipe insulation systems were critically reviewed with the intention to clarify the concept of apparent thermal conductivity associated with pipe insulation systems. To date there are not any standard methods of testing pipe insulation systems for below ambient applications. Research was conducted to extend test methodologies that were originally developed for flat slab configurations to pipe insulation systems. We will also present standard methods of testing used specifically for pipe insulation systems for above ambient applications, that is, heated pipes with outward heat flow. For cold pipes commonly used in building HVAC systems, an inward heat flow occurs through non-homogenous and anisotropic materials, and selecting the thermal conductivity for this application based on measurements with outward heat flow is another point of debate among

engineers, practitioners, and building owners. The first objective of this review section is to critically discuss all these aspects by an extensive literature review. The thermal conductivities of pipe insulation systems measured at various laboratories were compared with the data in the literature for flat slab configurations, and the second objective of the present review section is to highlight the differences and similarities between these two sets of data. In addition, the direction of heat flow is key when considering wet conditions, that is, when the pipe surface temperature is below the dew point temperature of the surrounding atmosphere. This is often the case in the building's air conditioning, in which the occupied zone is set to 20 to 25˚C (68 to 77˚F), when the relative humidity of 40 to 50%, and the chilled water pipe surface temperatures are about 3.3 to 5.6˚C (38 to 42˚F). In these conditions, water vapor enters the insulation systems and condenses on the pipe surfaces. The impact of moisture ingress on the actual pipe insulation thermal resistance is still an unresolved question. For wet insulation, four main methods for preparing the wet samples during laboratory measurements are identified in this review work and the third objective of this review is to evaluate the impact of each method on the measured apparent thermal conductivity of the pipe insulation system. The advantages and shortcomings of each moisturizing strategy are discussed at length, and the thermal conductivities of a few available pipe insulation systems in wet conditions are compared. The literature review presented in the next sections should assist system designers in selecting appropriate pipe insulation systems based on the thermal performance and operating conditions because, as it will be highlighted later in the present review section, some materials may perform very well under dry conditions, but condensate can easily accumulate leading to a fast degradation of the thermal performance.

2.1 Experimental methodologies for measurement of pipe insulation thermal conductivity under dry conditions

In the current open domain literature of experimental data involving thermal conductivity of cylindrical pipe insulation at below ambient conditions are scarce and mostly restricted to a few

insulation systems. Because there is debate on whether the thermal conductivity of pipe insulation systems can be derived from measurements on flat slabs, it is helpful to highlight some of the similarities and differences in the thermal conductivity measurements of these two forms. A comparison between measured thermal conductivity data from the various test methodologies on pipe insulation systems and flat slab systems may also illuminate this debate.

2.1.1 Brief background on the methodologies for thermal conductivity measurements of flat slabs

For flat slab insulation systems, steady-state and transient test methodologies are commonly used. The Guarded Hot Plate (GHP) is one of the most widely used steady-state methodologies for thermal conductivity measurement on flat slab materials (ASTM_C177, 2010; ISO_8302, 1991). In the GHP methods, the edge effect is minimized by the end guards. The Heat Flow Meter methods (HFM), which are mainly represented by ISO 8301 (1991), as well as ASTM C518 (2010) and BS-EN 12667 (2001), are also commonly used due to their simple concept and low requirements for the application of test specimens. The basic principles of both GHP and HFM methods are applicable to pipe insulation systems. Compared to the GHP method, which is normally applied below 200˚C (392˚F), there is no upper temperature limitation for the Thin Heater Apparatus (THA), which is typically used for refractory bricks and insulation panels. With considerably less mass than the combined central heater and guard heaters used in the GHP methods, the THA is able to shorten the time to reach steady-state and may also minimize drift errors (ASTM_C1114, 2006). However, currently this method is only available for testing flat slab configurations. Another method commonly used under steady-state is the Hot Box method (ASTM_C1363, 2011). Considering the severe requirements of the two temperature controlled boundary conditions on both sides of the test specimen, the same apparatus is not suitable to be used with material of cylindrical shapes because controlling the inner side might not be feasible in practice.

The Transient Hot Wire (THW) and the Transient Hot Strip (THS) methods are common techniques applied in transient conditions, and they are able to provide fast measurements of the thermal conductivity for small size test samples (Gustafsson *et al*., 1978; Ohmura, 2007). The Transient Plane Source technique (TPS), also referred to as "hot disk" or as "hot square", is developed for evaluation of anisotropic thermal property values by replacing the heating element with a very thin, double metal spiral heater (Gustafsson *et al*., 1994; Rides *et al*., 2009; Sabuga & Hammerschmidt, 1995). The thermal conductivity probe is a practical method used in the field, and it provides measurements of the thermal conductivity of regions of the insulation in which it is installed. It is generally viewed as a trade-off between accuracy and cost (Tye, 1969).

Compared to transient test methods, the thermal conductivity values from steady-state methods are simpler to be derived from the measured data if the uniform heat flux throughout the test specimen is a reasonable assumption. But providing a uniform heat flux in the entire test section is the main challenge for most steady-state methods. Pratt, referred by Tye (1969), mentioned that the steady-state methods are limited to only homogeneous materials with a thermal conductance of at least 6000 W/m2-K (1060 Btu/hr-ft2-˚F). In order to prevent end edge effects, the test samples normally need to be very large, and it takes a considerable amount of time for the test specimen to reach complete thermal equilibrium. Due to the large surface area, the surface contact resistances should not be neglected especially when the material thermal resistances are of the same order. For example, Salmon and Tye (2010) pointed out that the material thermal conductivity, measured by transient methodologies, are about 3% higher than the values derived from the GHP due to the effects of surface thermal contact resistance between the test specimens and the guarded plates. Transient methods are also not affected by the conditions of the surrounding environments, which may cause the test specimens to become chemically unstable or contaminated with long testing periods required by steady-state methods (Tye, 1969).

For the thermal conductivity measurement of insulating building materials, it seems that the steady-state heat flow techniques yield more accurate measurements than the transient techniques (Log, 1993). Using a calibrated insulation sample (McFadden, 1986), the accuracy of steady-state heat flow techniques can be significantly improved, and anisotropic materials, such as fiber materials with low bulk densities, can be successfully tested. Wulf *et al*. (2007) measured the thermal conductivities of both isotropic and anisotropic materials based on the GHP technique, the Guarded Heated Pipe technique, which will be discussed in the next section, and the THW technique. These three techniques showed excellent agreement for isotropic materials, but some discrepancies were observed in anisotropic materials. It was observed that the position of the heated wire in the THW technique affected the measured thermal conductivity of anisotropic materials. When dealing with low thermal conductivity materials, Woodbury and Thomas (1985) pointed out that probe wires could become highly conductive and created an alternative path for the heat losses. This would affect the accuracy of the measurements, and Suleiman (2006) provided recommendations to avoid this. On the other hand, GHPs show large differences when compare to other techniques at a temperature above 100˚C (212˚F) (Albers, 2002; Salmon & Tye, 2010). This is because the radiation heat transfer cannot be neglected at high temperatures. Tritt (2004) observed that in using a standard steady-state method for temperatures above 150˚C (302˚F), radiation loss became a serious problem, and a correction method to account for radiation was proposed based on Wiedemann-Franz law (Johns & March, 1985). To minimize the radiative heat transfer component, the surfaces need to be very emissive, especially for the low density materials (Miller & Kuczmarski, 2009).

Since the GHP and HFM methods measure an overall thermal conductivity on a relatively large area, they do not allow one to probe the insulation for a measurement of the thermal conductivity at specific identifiable locations in the sample, which can be considered as a shortcoming of these techniques in some cases (McFadden, 1988). By inserting the probe into the insulation, it is

possible to check the uniformity of the heat flux within the insulation and to determine if the moisture is absorbed uniformly in the insulation for wet conditions.

2.1.2 Review of the thermal conductivity measurements of pipe insulation systems

For pipe insulation systems, the heat transfer is in radial direction, due to the cylindrical shape, and heat conduction, which happens in radial symmetric geometries, was studied in the early literature (Glazebrook, 1922). Because of the cylindrical geometry, the heat transfer area varies from interior surface to the exterior surface, and this leads to a range of thermal resistances. The definition of mean insulation temperature is not clear in most reported studies. In some studies, it is reported as the arithmetic average temperature between the interior and exterior surfaces; in other studies, it is defined as the temperature of a center layer of insulation obtained by volume-weighted averages on the insulation samples. During the application of the pipe insulation systems, joint sealant is usually required between the top and bottom shells. The presence of longitudinal joints and of joint sealant affects the measured thermal conductivity of pipe insulation systems if compared to corresponding thermal conductivity data, which is obtained from flat slab configurations. All the above differences help to explain the reasons why the apparent thermal conductivity of the pipe insulation systems differs from the measured thermal conductivity of the insulation material, which is typically measured for flat slab configuration. In recent years, limited published work in the literature reported the comparison of the thermal performance and measurement methodologies between the pipe insulation systems and flat slabs of the same materials. Wilkes *et al.* (2002) concluded that for polyurethane insulation, the flat slab configuration had 2 to 5% higher thermal conductivity than the pipe insulation configuration. Cremaschi *et al*. (2012a; 2012b) observed that the joint sealant applied on pipe insulation during the installation might cause a non-negligible effect on the apparent insulation thermal conductivity. Moore *et al.* (1985) pointed that measuring the thermal conductivity of pipe insulation systems would be easier than measuring flat slabs since very long test specimens could

be used. Tritt (2004) disagreed because radial flow methods were relatively more difficult to apply when compared to the linear measurements, especially when the materials were tested below room temperature. However, Tritt (2004) agreed that the radiative heat loss, which was severe in the traditional longitudinal heat flow method under high temperatures, could be minimized when the heating source was placed internally.

From the standards of testing methods and literature reviews, the methodologies for measuring the thermal conductivity of pipe insulation systems were critically reviewed, and they are summarized next. The Guarded Heated Pipe method, which was developed from an early radial flow test apparatus designed by Flynn in 1963 (Tye, 1969), can be considered as a modification from the GHP method where the test pipe insulation shells are installed around a heated pipe. The entire test apparatus is required to be placed in a temperature controlled chamber (Kimball, 1974; Whitaker & Yarbrough, 2002; Wilkes *et al.*, 2002), or a test enclosure (Zehendner, 1983) to provide constant temperature boundary conditions. The main assumption of heat flux in the radial direction is reasonable only if the edge effects, at both ends of pipes, are minimized. The standard ISO 8497 (1994) and several studies in the literature provided guidelines on how to account for the end edge effects (ASTM_C335-05, 2005; BS-EN253, 2009; ISO_8497, 1994). The Calibrated Hot Box method, which was first presented by Musgrave (1979), is designed for testing pipe insulation systems around cold pipes. For this method, it is critical to reduce the humidity inside the box before the test, either by vacuuming or by dehumidification. In addition, proper sealing with vapor barrier systems are required, but achieving complete vapor barrier during the test conditions is critical. The Radial Heat Flow Meter method (concentric cylinder comparative method) is a modification of the HFM method, and it is applicable for testing pipe insulation with both inward and outward heat flux. Because of ease of installation, researchers used small pads as heat flux meters, substituting them for sleeve flux meters (Ramsden, 1985; Rawlins, 2005). However, the application of the heat flux pads seems to affect the shape of the test specimen --

either by compressing the insulation in some locations or by creating gaps of air between the test insulation and cold surface in other locations. This variation of the contact resistance should be properly accounted for when measuring the thermal performance of the pipe insulation systems.

While the Guarded Heated Pipe method is only suitable for the thermal conductivity measurement with the outward heat flow, the Calibrated Hot Box method is used for cold pipe with inward radial heat flux. For achieving accuracy, it is critical to design appropriate thermal guards at the ends, and water vapor condensate might be an issue during the thermal conductivity measurements. Radial heat flow meters are suitable for both heated and cold pipes, but they suffer similar issues when applied to cold pipes. When using the Radial Heat Flux Meter technique, they should be either designed as insensitive to the water vapor in the air and potential moisture accumulation on the meter, or the ambient has to be controlled such that the dew point temperature is below the surface temperature of the cold pipes. Another challenge with the Radial Heat Flux Meter is the possibility of forming thermal bridges between the two concentric pipes in the test apparatus. Cremaschi *et al.* (2012a; 2012b) pointed out that in order to obtain better accuracy during the measurement, the materials made for supporting sleeves in between the two concentric pipes need to be selected with a thermal conductivity of the same magnitude as the one of test specimen.

There are also some techniques that employed transient methods to measure the thermal conductivity of pipe insulation systems. Transient methods are suitable for the measurement of pipe insulation thermal conductivity under non-destructive testing and in the field. The THW method is applied for the measurement of thermal conductivity in the range from 0.08 to 2.0 W/m-K (0.55 to 13.9 Btu-in/hr-ft^2-˚F) (Kulkarni & Vipulanandan, 2006). Adl-Zarrabi (2005) tested the pipe insulation thermal conductivity by using the TPS method. By comparing to the results measured from the Guarded Heated Pipe method, all the values derived in the TPS apparatus were slightly higher. When considering the joint sealant and vapor jacketing of pipe

insulation systems, it is clear that transient methods provide a measurement of the local thermal conductivity in the material, instead of the system thermal performance.

A summary of interlaboratory/laboratory comparison results between steady-state and transient measurements is given in Table 2.1. This table summarizes the recent work in thermal conductivity measurements for pipe insulation systems, and the work is grouped into two main categories: steady-state techniques and transient techniques. Due to the lack of the reported uncertainty in some of the published data for pipe insulation systems, the range of application and corresponding accuracy for some of the studies are selected based on data published on flat slabs. These cases are indicated by the symbol (*) in the first column of Table 2.1.

Table 2.1: Summary of interlaboratory/laboratory comparison between steady-state and transient measurements (in SI units)

	Temperature Range	**Uncertainty steady-state measurement**		**Uncertainty transient measurement**	
		GHP	**HFM**	**Hot wire**	**Hot disk**
Zehendner(1983)	-60 - 80 ˚C	Pipe, < ±3%	--	--	--
*McCaa and Smith (1991)	24˚C	1.3 - 5.5%		--	--
*Albers (2002)	0 - 100˚C	< 2.5%	--	--	--
	100 - 1000˚C	24%	--	--	--
Wilkes *et al.*(2002)	5 - 45˚C	Slab, ±0.8% Pipe, ±0.8%	--	--	--
*Ohmura (2007)	-120 - 25˚C	< ±10%		> ±10%	±10%
	200 - 800˚C	--	--	±10%	--
	100 - 1300˚C	±10%		--	--
*Wulf*et al.* (2007)	0 - 1200˚C	GHP, radial flow and hot wire/disk method with test results within ±10%			
*Rides *et al.* (2009)	20 - 180˚C	HFM, hot wire/disk method with test results within ±7%			
*Hay *et al.* (2009)	10 - 23˚C	<2%	--	--	--
*Salmon and Tye(2010)	10-23˚C	±1.5%	±2%, if test on individual specimens (density differences), the difference up to 5%	±3%, 3% higher than GHP	
*Bezjak and Zvizdic(2011)	10 - 30˚C	<0.5%	--	<3.6%	--
Cremaschi *et al*. (2012a; 2012b)	10 - 25˚C	--	Pipe, < ±6%	--	--

*: Literature review results on flat slabs

2.2 Review of thermal conductivity variation in pipe insulation systems

In this section, a comparison of the thermal conductivity of both flat slab and pipe insulation is presented with the aim of documenting the methodologies discussed in the previous section. The differences in material properties, such as density, thickness, porosity, internal structure, anisotropy, blowing agent, manufacturing time, handling, and installation methods, may affect the results of the experimental measurements. However, there are no studies that provided detailed information on the materials being tested for the thermal conductivity of both pipe insulation systems and flat slabs. In one research study the authors compared these two configurations and pointed out the differences come from the material density and geometry between the pipe insulation and flat slabs (Wilkes *et al.*, 2002). In order to provide a general idea of how the thermal performance of the insulation system varies with the methodologies applied for thermal conductivity measurement, as well as with different types of materials and material densities, the reported values in the open literature are summarized in the following sections. The material properties, such as configurations of the test samples, densities and thicknesses are documented in the Tables of Appendix A. The thermal conductivity of both pipe insulation systems and flat slabs are compared between the materials with similar densities. Based on these criteria, nine insulation materials applied in HVAC field are discussed, and the data have been grouped in Figure 2.1 to 5.

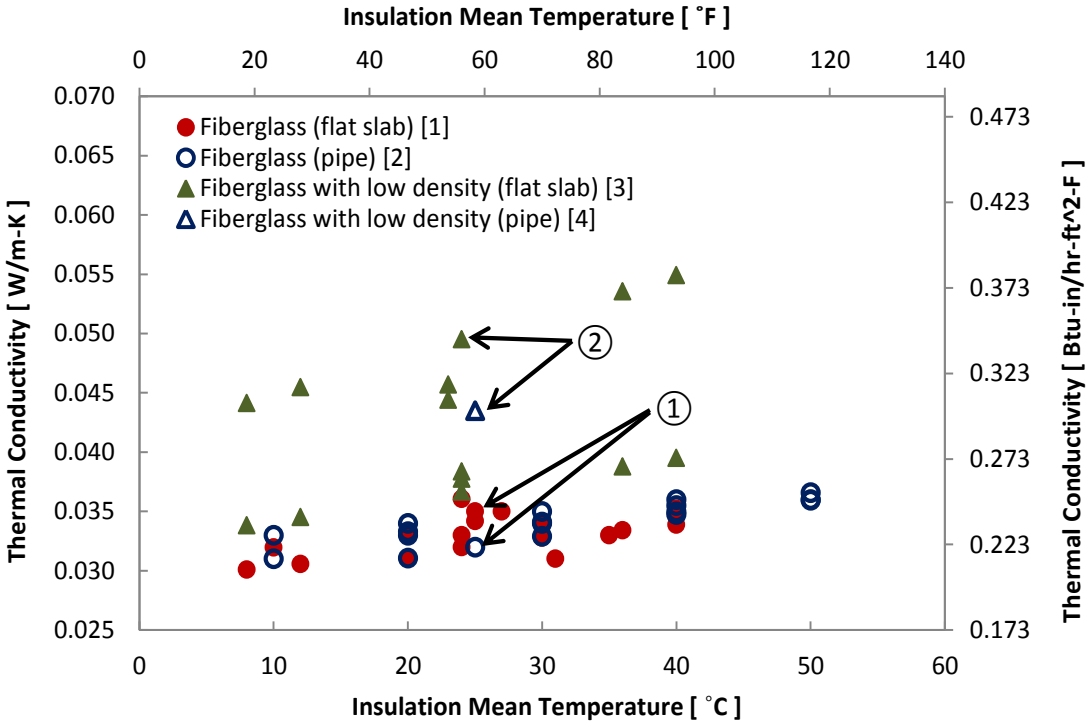

[1] Modi and Benner (1985), Moore *et al.*(1985), McFadden (1988), Wijeysundera and Hawlader(1988), Al-Hammad*et al.*(1994), Salmon (2001), Abdou and Budaiwi(2005)
[2] Chyu*et al.*(1997b), Wikes*et al.*(2002), Whitaker and Yarbrough (2002), Cremaschi*et al.*(2012a; 2012b)
[3] McCaa and Smith(1991), Abdou and Budaiwi(2005), Bezjak and Zvizdic(2011)
[4] Moore *et al.*(1985)

Figure 2.1: Thermal conductivity of fiberglass insulation

For fiberglass insulation, the thermal conductivities are linearly correlated with insulation mean temperatures (Abdou & Budaiwi, 2005; Cremaschi *et al.*, 2012b; Hay *et al*., 2009; Wilkes *et al.*, 2002). McCaa and Smith (1991) and Salmon (2001) also correlated the thermal conductivity with material density. From the data given in Figure 2.1 and the table in Appendix A, it appears that for fiberglass, the thermal conductivity of flat slabs and pipe insulation systems are fairly similar if one does not include the samples with low densities, which are shown as the solid and hollow triangle symbols. However, if one considers the samples with similar densities, by comparing the data reported by Wilkes *et al*. (2002) on the pipe insulation with a density of about 33kg/m^3

(2.1lbm/ft^3), and the data published by Al-Hammad *et al*. (1994) on the flat slab with a density between 32 to 37 kg/m^3 (2.0 to 2.3 lbm/ft^3), the measured thermal conductivity values on flat slab was about 10% higher than the pipe insulation, shown as group ① in Figure 2.1. The reported uncertainty is ±0.8% for the Guarded Heated Pipe method (Wilkes *et al*., 2002) and ±2% to ±4% for the GHP (Al-Hammad *et al*., 1994). When considering material samples with low densities, ranging from 12 to 27 kg/m^3 (0.75 to 1.7 lbm/ft^3) as shown in Appendix A, the thermal conductivity seems to increase as Langlais *et al*.(1982) pointed out. In this range, by selecting two samples with similar densities, 15 kg/m^3 (McCaa & Smith, 1991; Moore *et al*., 1985) and shown as group ② in the figure, the flat slab seems to be more conductive than the pipe insulation. The mean error for the measurement of thermal conductivity on the flat slab was reported with an imprecision around 3% (McCaa & Smith, 1991), and the uncertainty on the pipe insulation tester was not clarified in the literature.

For polyurethane, the density effect on the thermal conductivity seems not so significant as on fiberglass (Zehendner, 1983). The data summarized in Figure 2.2 suggests that the polyurethane insulation has different thermal conductivity when measured from flat slabs and pipe insulation systems; however, a measurable difference was only reported for one group of data by Ohmura (2007). Although this group of data was validated by both steady state and transient methods, within ±10% deviation, the material is affected by "aging" process since the blowing agent slowly diffuses out, and it is gradually replaced by air that fills in the cells. Kellner and Dirckx (1999) found that the thermal conductivity was increased by 7% to 30% depending on different aging methods. Blowing agent is another aspect that also needs to be considered during a critical comparison. Bhattacharjee *et al.* (1991) investigated both blowing agent and aging effects by comparing 20 specimens and concluded that different gas composition would vary the sensitivity on the thermal conductivity to the insulation mean temperatures. Biedermann *et al*. (2001) compared in detail the effect on thermal conductivity of 12 gas compositions, and the differences

in the 6 closed-cell specimens were found within 10%. Therefore, during the comparison of polyurethane insulation, both the fabricating time of these test samples and gas composition in the cells need to be critically considered. All the ranges on the measurements of polyurethane thermal conductivity are reported in the table in Appendix A.

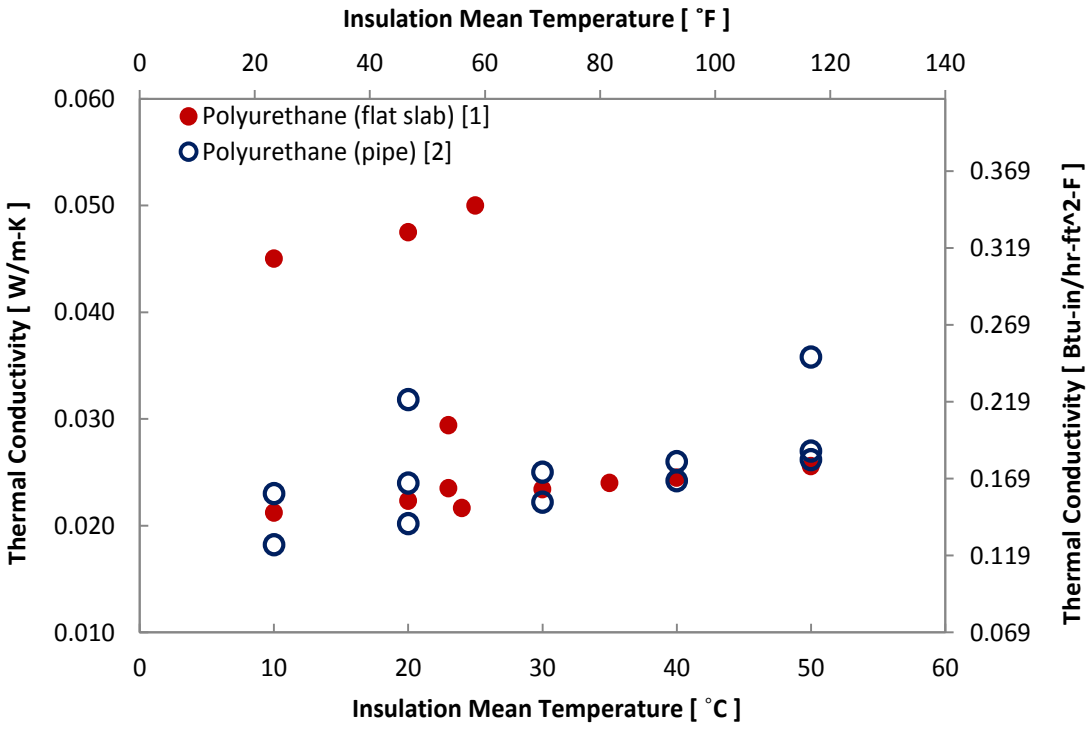

[1] Zehendner(1983), McFadden (1988), Al-Hammad*et al.*(1994), Abdou and Budaiwi(2005), Ohmura (2007), Bezjak and Zvizdic(2011)
[2] Adl-Zarrabi(2005), Chyu*et al.*(1997a)

Figure 2.2: Thermal conductivity of polyurethane Insulation

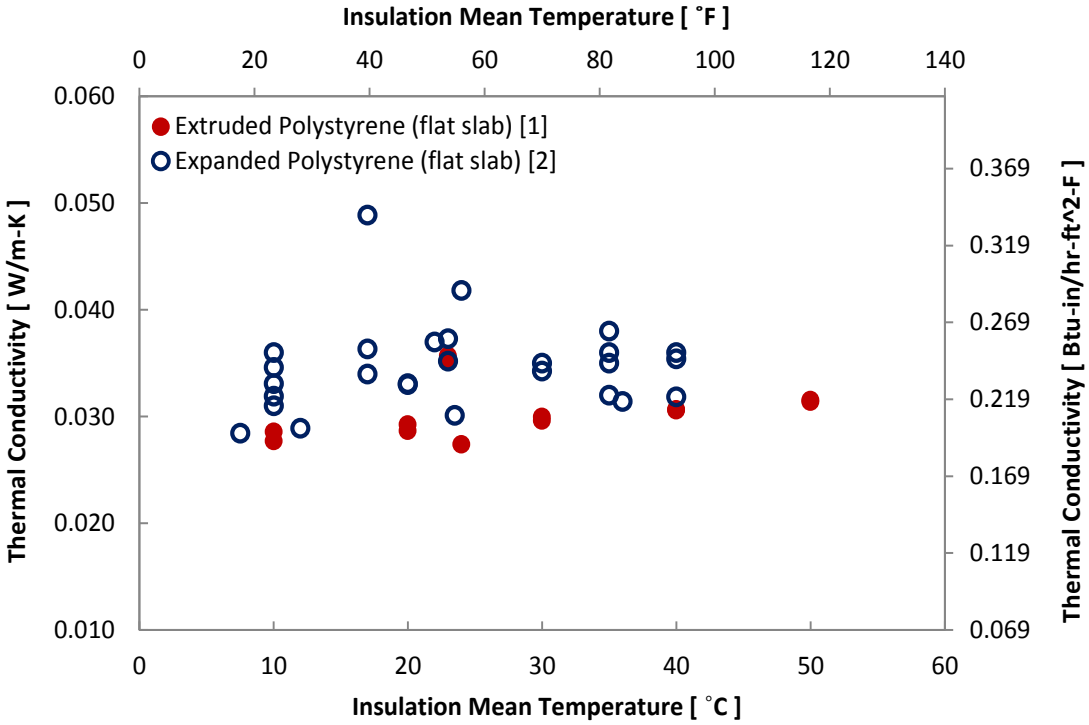

[1] McFadden (1988), Abdou and Budaiwi(2005), Bezjak and Zvizdic(2011)
[2] Pratt (referred by Tye(1969)), McFadden (1988), Al-Hammad*et al.*(1994), Salmon (2001),Abdou and Budaiwi(2005), Mar *et al.*(2008), Bezjak and Zvizdic(2011), Lakatos and Kalmar (2012), Jerman and Cerny(2012)

Figure 2.3: Thermal conductivity of extruded polystyrene (XPS) and expanded polystyrene (EPS)

Extruded and expanded polystyrene are two forms of foamed polystyrene insulation. Both extruded and expanded polystyrene are closed-cell foam insulation and for expanded polystyrene there are some small empty pockets in between the expanded beads (McFadden, 1988). Free convection in foams was shown to be negligible for the cell sizes to be less than 1.5mm (0.06 in), which includes most polystyrene foams, and the main heat transfer in foams is due to coupled conduction and radiation (Yajnik and Roux, 1990). Air fills in these pockets, and the overall thermal conductivity is higher than the one of extruded polystyrene. This is probably caused by a higher infrared heat transfer due to a lower extinction coefficient within the material. These findings are summarized in Figure 2.3. For extruded polystyrene, based on the current data

collected from the open literature, with densities varying from 35.8 to 49.3 kg/m^3 (2.2 to 3.1 lbm/ft^3), there was not an obvious pattern between the system apparent thermal conductivity and material density. This material is also subjected to an "aging" process (Stovall, 2009). Expanded polystyrene, on the other hand, is more sensitive to the material density, because the overall thermal conductivity of the material is affected by the radiative heat transfer within the material. Less dense materials are composed of more air pockets, which promote convective heat transfer and result in higher thermal conductivity. The numerical values are in the tables in Appendix A.

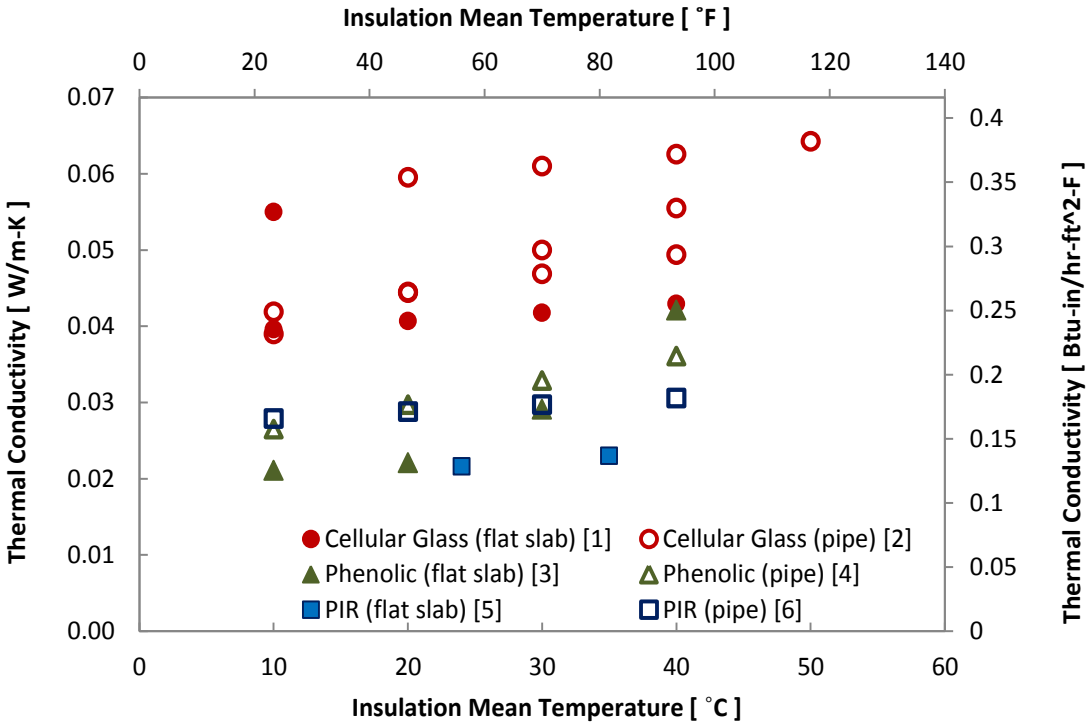

[1] Kaplar(1974), Pittsburgh Corning Co.
[2] Whitaker and Yarbrough (2002), Cremaschi*et al.*(2012a; 2012b)
[3] Tseng and Kuo(2002)
[4] Cremaschi*et al.*(2012a; 2012b)
[5] McFadden (1988), Al-Hammad*et al.*(1994)
[6] Cremaschi*et al.*(2012a; 2012b)

Figure 2.4: Thermal conductivity of cellular glass, phenolic and PIR insulation

Cellular glass, phenolic and polyisocyanurate (PIR), which has a similar thermal conductivity as polyurethane, are typically closed-cell insulation, and all these three materials require joint

sealant during the installation on pipes. As summarized in Figure 2.4 (and the tables in Appendix D), the densities of these closed-cell insulation materials are typically in a narrow range, and the thermal conductivity seems not to be sensitive on the material density. For cellular glass and phenolic pipe insulation systems, the thermal conductivity is about 20% higher than the thermal conductivity measured from flat slabs. Cremaschi *et al*. (2012b) explained that the difference might be due to the longitudinal joints and the sealant which was applied on these joints. For both phenolic and PIR insulation, the deterioration of self-performance in the test samples need to be considered since they are subjected to the aging process (Christian *et al*., 1998; Stovall, 2009). Thus the result reported in Figure 2.4 in which pipe insulation systems have 20 to 30% higher thermal conductivity than flat slabs must be carefully gauged due to different manufacturing time between the test samples. Similar to polyurethane insulation, different blowing agents are applied for PIR insulation, and the effect also needs to be accounted for during the comparison on the effective thermal conductivity (Zarr & Nguyen, 1994). For most closed-cell insulation, one critical issue that needs to be considered is some blowing agents, such as pentane, propane, which are defined as natural gas liquid, can be easily turned into liquid with the application of moderate pressure or freezing and dramatically reduce the thermal conductivity of the insulation.

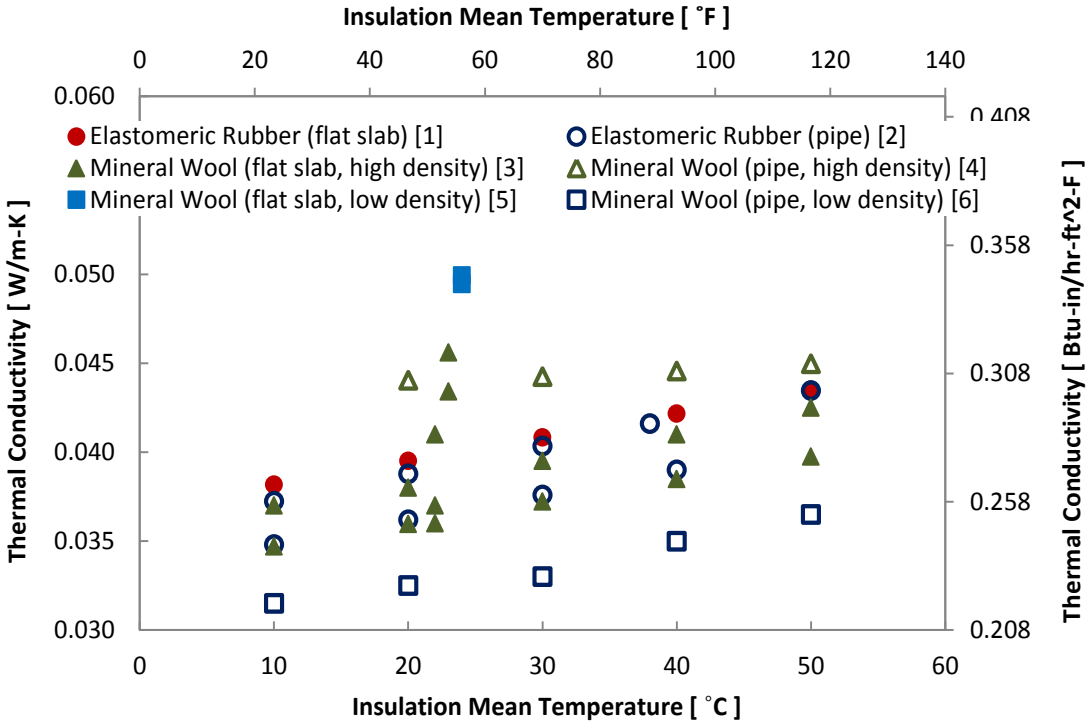

[1] Wikes *et al.*(2002), Cremaschi *et al.*(2012a; 2012b)
[2] Wikes*et al.*(2002)
[3] Abdou and Budaiwi(2005), Bezjak and Zvizdic(2011), Jerman and Cerny(2012)
[4] Whitaker and Yarbrough (2002)
[5] McCaa and Smith (1991)
[6] Zehendner(1983)

Figure 2.5: Thermal conductivity of elastomeric rubber and mineral wool

Elastomeric rubber insulation has either open-cell or closed-cell structure when present as foam insulation. Compared to the closed-cell, the open cell structure is affected by the portion of air pockets within the material. During the installation of elastomeric rubber pipe insulation, either a very thin layer of sealant is applied on the longitudinal joint, or a self-seal lap (SSL) tape is manufactured for the joint. Wilkes *et al.*'s (2002) results on the thermal conductivity of the elastomeric pipe insulation system are about 6 to 7% higher than Cremaschi *et al.*'s (2012b) measurements on a similar specimen with a higher density. The uncertainty for each test methodology is summarized in Appendix A. According to Wilkes *et al.*'s (2002) findings, pipe

insulation systems showed 1.5% to 2.5% lower thermal conductivity when compared to flat slabs with similar densities and thicknesses, as shown in Figure 2.5, and they considered it as a good match because the materials were not identical. Mineral wool is another type of fibrous insulation, and its thermal conductivity is quite sensitive to the material density. From the values summarized in the table in Appendix E, it seems that with similar densities, the cylindrical shaped mineral wool insulation has a thermal conductivity 20% higher than the flat slab configuration (Abdou & Budaiwi, 2005; Whitaker & Yarbrough, 2002). It is noted that one group of pipe insulation (the hollow rectangles in the figure) showed lower thermal conductivity than the flat slab which has a similar density. This is because during this group of tests, the test specimen is mineral fibers bound with synthetic resin (Zehendner, 1983).

2.3 Methodologies for measurement of pipe insulation thermal conductivity under wet condition and with moisture ingress

To date there are no set criteria for the testing methods of pipe insulation under wet conditions. In wet conditions, liquid water and water vapor will accumulate in the insulation by filling the air gaps between the cells, or replacing the gas in the cells if the cell wall is permeable. Water will be distributed in the insulation due to the gravitational effect and capillary force, and the partial pressure difference will be the driving force for the water vapor diffusion. From the present literature review it is found that the method of testing depends on the technique used for preparing the moist insulation sample. Four methodologies for the measurement of insulation thermal conductivity with moisture ingress are defined for the first time as shown in Table 2.2.

Table 2.2: Common methodologies for insulation thermal conductivity measurements with moisture ingress

Experiments	Moisturization	Materials	Moisture content	Method	Uncertainty on thermal conductivity
Batty *et al.* (1981)	Immersion/Squeeze	Fiberglass	1.8 - 6.2%	Probe	--
Hay[1]	Injection	Extruded polystyrene		GHP	--
Modi and Benner (1985)	Conditioned ambient with cold surface	Fiberglass	18%	GHP	--
		Cellulose	19%		
McFadden (1988)	Laboratory pre-conditioning and materials from field	Fiberglass	8%	GHP Probe	--
		Polyurethane and polyisocyanurate	7%		
		Extruded expanded polystyrene	21%		
		Molded expanded polystyrene	10%		
Kumaran(1987)	Injection	Fiberglass	12 - 19%	HFM	--
Chyu*et al.*(1997a)	Immersion	Polyurethane	70%	HFM	9%
Kehrer*et al*. (2002)	Chamber	Fiberglass	11.6% (by mass)	GHP	--
Cremaschi*et al.* (2012a; 2012b)	Conditioned ambient with cold surface	Fiberglass	12%	Radial HFM	$< \pm 6\%$, considered axial distribution
		Phenolic	5%		

[1]: referred by McFadden(1986)

The first group, flooded methods, consists of completely immersing the test specimens in water to provide a certain amount of moisture and uniform distribution. There exists the assumption that by immersing the insulation sample in the water would be able to provide the upper limit for the insulation thermal conductivity. However, a simple immersion without temperature difference between the two surfaces of the pipe insulation test sample would lead to the water permeation less than the situation with driving force from the water vapor pressure differences across the insulation. If immersing the pipe insulation test sample in a water reservoir with the inner surface maintained at a low temperature and controlling the water temperature in the reservoir, the thermal conductivity can be measured under isothermal conditions. The water absorption is determined directly from the water volume variation in the reservoir (Chyu *et al.*, 1997a, 1997b; Kaplar, 1974). Several more or less cumbersome techniques are proposed to control the desired amount of water content in the test specimen (Batty *et al.*, 1981; Kumaran, 2006; Langlais & Klarsfeld, 1984). Full immersion, partial immersion, and immersion under pressure may lead to different internal moisture distribution (Chalumeau & Felix-Henry, 2006; Kaplar, 1974). In addition, it is pointed out that the temperature of the water reservoir might affect the moisture ingress and the apparent thermal conductivity of the test sample. This is due to surface tension effects (Chyu *et al.*, 1997a) and heat transfer processes which are caused by the natural convection phenomenon. The convection heat transfer is particularly relevant for fiberglass and mineral wool insulation. The flooded method is more appropriate on testing insulation systems applied around pipelines below ground or in deep sea application. However, in the HVAC field, the insulation systems are applied around pipelines which are normally placed in either indoor or outdoor environment. Flooded methods create different boundary conditions on the test samples from the actual field applications, and thus it is difficult to extrapolate the data from these methods of wet testing.

Spraying or injecting water into pipe insulation systems and flat slabs belong to the second group of methodologies for measuring the thermal conductivity in wet conditions (Langlais *et al.*, 1982; Wijeysundera *et al.*, 1996). The moisture distribution inside the insulation might be in transient conditions since water at the hot surface will be vaporized and transported to the cold surface (Kumaran, 1987). During the transient conditions, the insulation thermal conductivity is a function of the location of the high moist regions (McFadden, 1986), and the thermal conductivity of pipe insulation systems depend on whether the high moist regions are closer to the hot side or to the cold side. This group of methodologies requires a great amount of time to reach steady state when the moisture content, both in the form of liquid and gas, is completely redistributed to the cold surface. Once it reaches steady state, the thermal conductivity of insulation systems is independent of the initial moisture distribution of the test samples. Results show that when the water content is less than 1% by volume, the heat flux through the material is 3 to 4 times higher than the dry insulation during transient conditions, but the material will perform as dry insulation under steady state when the moisture is completely transported to the cold surface (Kumaran, 1987). Considering the sensitivity of the positions of the high moist regions to the thermal conductivity of pipe insulation systems, spray/injection methods would fail in simulating the water distribution in the pipe insulation systems applied in the HVAC field.

The third category is defined as laboratory pre-conditioning methods, and it consists of placing the insulation test specimens in the air with very high humidity before the thermal conductivity measurements. Several researchers point out that the moisture content accumulated inside the insulation is lower than the moisture content in the actual operating conditions (Batty *et al.*, 1984; Kehrer *et al.*, 2002; Kumaran, 1987; Langlais *et al.*, 1982; McFadden, 1988). This is due to a weak vapor driving potential during the pre-conditioning process of the insulation test specimens. The other disadvantage of these methods is that water distribution in the insulation systems is

different from the real field, and any water redistribution will affect the thermal conductivity measurements.

The fourth group includes methods that adopt a temperature, humidity and air speed controlled ambient and simultaneously impose a cold surface/cold pipe on one side of the insulation test specimen (Cremaschi *et al.*, 2012a; Cremaschi *et al.*, 2012b; Modi & Benner, 1985; Mumaw, 2002; Peuhkuri *et al.*, 2008). Cremaschi *et al.*(2012a) tested several pipe insulation systems in a psychrometric chamber. Their approach required a large amount of equipment, and it had a very high capital cost. The psychrometric chamber is able to better replicate the actual operating conditions of the pipe insulation systems as those of real service in the chiller applications. Moisture is driven into the insulation due to a gradient in the water vapor partial pressure across the insulation specimen, and the water vapor ultimately condenses when it reaches the cold pipe surface. A great amount of time is required to achieve measurable moisture contents, but accelerated type of tests can be conducted by increasing the temperature and humidity gradients to help drive water vapor ingress into the insulation specimen (Cremaschi *et al.*, 2012a; Mumaw, 2002).

If the test samples are prepared according to the two techniques mentioned above (Spray/injection methods and pre-conditioning methods), steady-state methods are not suitable for the thermal conductivity measurements with moisture ingress. Kehrer *et al*. (2002) measured the thermal conductivity of fiberglass insulation by placing the sample, which had moisture content of about 11.6% by mass, in a GHP test apparatus. The insulation thermal conductivity was approximately 5 to 6% higher when compared to that of the dry sample. The reason is due to the latent heat convection effects with moisture that evaporates at the hot plate and condenses at the cold surface. They concluded that "the real thermal conductivity of the insulation material in equilibrium with 80% RH is not higher than in the dry state". Langlais *et al.*(1983) tested a fiberboard with moisture sprayed on the cold and hot surfaces. The thermal conductivity was

measured using the GHP method; it increased rapidly in the first two hours and gradually dropped in the next five hours. The similar phenomenon was observed by other researchers (Benner & Modi, 1986; Wijeysundera *et al.*, 1993, 1996). Langlais *et al.*(1983) explained that the redistribution of the moisture inside the insulation led to a water vapor enthalpy flow, which was interpreted as heat conduction by the thermal conductivity test apparatuses. Thus, the steady-state methods yield to overestimation of the material thermal conductivity under wet conditions. Sandberg (1995) highly recommended that with redistribution phenomenon, the measurement should not be taken with a large temperature difference or in a long time, which are the steps required for both the GHP and HFM methods. These observations suggest that steady-state methods are not suitable for the thermal conductivity measurements of moisture insulation with low heat fluxes. Only if the test sample is continuously in contact with a cold surface or a cold pipe, then steady-state methods can be successfully applied (Cremaschi *et al.*, 2012a). In this method, the water distribution in the pipe insulation is fairly similar to the real chilled water application. Water redistribution is minimized because a continuous driving force for the moisture is established during the tests by the water vapor pressure difference between the cold surface and the ambient.

For improving the accuracy of the measurement in presence of moisture ingress, the end sections of the test specimens must be given special considerations in order to avoid longitudinal moisture ingress that can skew the measurements (Simonson *et al.*, 1996). Batty *et al.* (1984) concluded that traditional GHP methods were impractical for the thermal conductivity measurements of moist insulation due to moisture redistribution, and they proposed using a line-source thermal conductivity probe. With this transient method, the short measuring time and small temperature gradient overcome the limitation of vapor redistribution that exists in most steady-state methods. Woodbury and Thomas (1985) concluded that when measuring with a thermal conductivity probe, the moisture content was quite sensitive to the thermal conductivity at low concentration,

and the thermal conductivity increased dramatically when the insulation becomes slightly wet. Yu *et al*. (2009) derived a similar conclusion on the thermal conductivity probe when using the device to determine the effects of moisture content on the uncertainty during sand thermal conductivity measurements. If the moisture content is higher than 25% (by volume), the thermal conductivity is measured accurately by the probe because the evaporation rate and capillary forces are low. However, if the moisture content is low, such as in pipe insulation systems, the regions adjacent to the heating tip of the probe may be easily dried out, and this local dry out phenomenon can bring a large error in the measurement of the actual thermal conductivity of the wet insulation. Some other challenges include the heat loss from the high conductive probe wire (Woodbury & Thomas, 1985), the limitation of the sample size based on the probing length (Suleiman, 2006), and the estimation of the bulk thermal conductivity measured at a finite number of specific locations.

In order to correlate the thermal conductivity with moisture content in the insulation systems, scale method is the most common way to measure the water content in the systems (Mumaw, 2002; Vrana & Bjork, 2008). Other techniques for quantifying the moisture content in the test insulation specimen exist but are costly and require extensive calibration, such as, computing the water volume from the immersion in a tank (Chyu *et al.*, 1997a), using gamma-ray attenuation phenomenon (Freitas *et al.*, 1991), and measuring the electric capacitance of the test samples (Rywotycki, 2003).

2.4 Review of the thermal conductivity variation with moisture content in pipe insulation systems

Variations of the thermal conductivity with water content are shown in Figure 2.6 for four types of insulation systems. A summary of the data is provided in Tables 3 and 4.

Fiberglass becomes fairly conductive at the room temperature if a certain amount of water accumulates in the insulation. This is because when the strands are gradually covered by water, the conduction heat transfer is intensified through larger surface areas along the fiber strands and the intersection regions among the strands (McFadden, 1988). If considering the density and temperature effects, most of the results published for either flat slabs or pipe insulation showed similar trends (solid circles in Figure 2.6). When the moisture content reaches about 12% by volume, the thermal conductivity of fiberglass insulation increases up to 2~3 times of the corresponding thermal conductivity in dry conditions (in which moisture content is less than 0.1% by volume). As more water accumulates into the fibrous material, an excess amount of water drains out from the insulation (Cremaschi *et al.*, 2012a). Comparing the published data on denser fibrous materials to the ones with lower densities, the thermal conductivity of the insulation at lower densities performs less sensitive to the amount water. This can be explained by the presence of a smaller number of fiber strands and intersections among the fibers. Because smaller internal surface areas are coated with water, the heat conduction results are less sensitive to the moisture content in fibrous insulation. The density also affects the convection heat transfer during condensing conditions, but this is a secondary mechanism when compared to conduction in fibrous insulation.

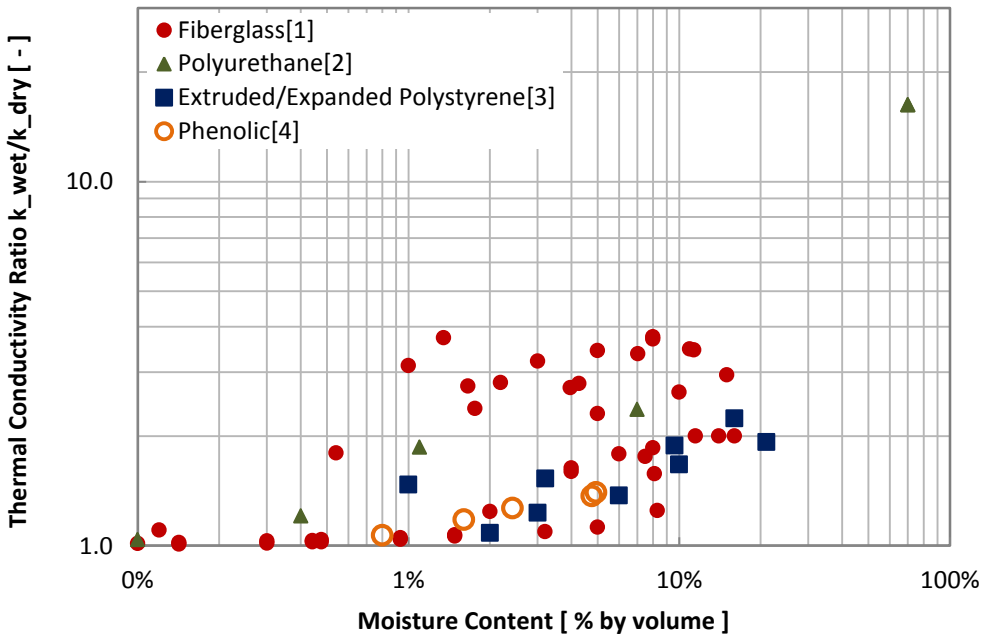

[1] Kaplar(1974), Batty *et al.*(1981), Langlais *et al.* (1982), Langlais*et al.* (1983) Langlaisand Klarsfeld(1984), Modi and Benner (1985), McFadden (1988) Kehrer*et al.*(2002), Cremaschi*et al.*(2012a; 2012b)

[2] Chyu*et al*. (1997a), McFadden (1988)

[3] Kaplar(1974), Hay (referred by McFadden (1986)), McFadden (1988)

[4] Cremaschi*et al.*(2012a; 2012b)

Figure 2.6: Thermal conductivity of four common insulation materials with moisture effect

For the three types of closed-cell insulation reported in Table 2.4, the thermal conductivity of the test specimens increased with moisture ingress because i) water accumulates on the cell walls, which increases the wall thickness and offers a better heat flow path; and ii) water fills in the small air gap and therefore enhances the heat conduction. It should be noted that at one point of the polyurethane pipe insulation (solid triangle in Figure 2.6), the moisture content reached 70%, and its thermal conductivity was measured almost 16 times higher than the dry condition. However, this point was measured by flooded method, and researchers prepared the moist test specimen by immersing it in the water tank (Chyu *et al.*, 1997a) It was the only data that reported a very large increase of the thermal conductivity for wet polyurethane insulation. Extruded polystyrene shows an increase on the system thermal conductivity in moist conditions by about

2.2 times with respect to the values in dry conditions (McFadden, 1988). This increase is reported for a moisture content of 16% by volume. For expanded polystyrene, the water content is around 21% by volume, and the thermal conductivity increases up to 1.9 times of the value in dry condition. Phenolic is tested as pipe insulation, and it shows that the thermal conductivity increases by 1.6 times when the moisture content is about 4.9% by volume (Cremaschi *et al.*, 2012a; Cremaschi *et al.*, 2012b).

Table 2.3 and 2.4 provide a quick one glance summary of the experimental methods and test results for insulation systems with moisture ingress. Most of the published data are for flat slabs, and the thermal conductivity of pipe insulation systems with moisture ingress are reported in only 2 studies in the open domain literature. Expanding the database for pipe insulation systems at below ambient temperatures in wet conditions with moisture ingress is a natural extension of the current efforts in this field and should be considered for future research. Developing thermal conductivity correlations with moisture content as the ones published for flat slab configurations might also be helpful. Since pipe insulation systems have more complex geometries than flat slabs and consist of multiple C-shell sections and various materials (i.e. Presence of joint sealant and vapor retarder at the butt joints for example), a generalized correlation that works for all the systems, even for only the ones with the same insulation material, might not be possible. These questions should be addressed by future research in this field.

Table 2.3: Comparison among experimental methods and test results for fiberglass insulation with moisture ingress (in SI units)

Fiberglass									
Literature	Mean temperature	Thermal conductivity			Moisture content	Type	Method	Thickness	Description
		wet	dry	ratio					
	˚C	W/m-K		-	% by volume			mm	
Kaplar (1974)					29.7%	board	-	101.6	-
Langlais *et al.* (1982)	24	0.032	0.032	1.00	0.0%	board	Spray, GHP, HFM (spray on cold surface)	25.4	dry density 70kg/m^3
		0.1	0.032	3.13	1.0%				
		0.11	0.032	3.44	5.0%				
		0.12	0.032	3.75	8.0%				
	24	0.032	0.032	1.00	0.0%	board	Spray, GHP, HFM (spray on cold surface)	25	dry density 70kg/m^3
		0.035	0.032	1.09	3.2%				
		0.036	0.032	1.13	5.0%				
		0.04	0.032	1.25	8.3%				
Jesperson [1]	10	0.036	0.036	1.00	0.0%	board	-	-	dry density 65.6kg/m^3
		0.083	0.036	2.31	5.0%				
		0.095	0.036	2.64	10.0%				
		0.0106	0.036	2.94	15.0%				
Modi and Benner (1986)	20	0.052	0.033	1.58	8.1%	board	Conditioned ambient with cold surface, GHP	51	dry density 45.8kg/m^3
	27	0.07	0.035	2.00	16.0%				
Wijeysundera and Hawlader (1988)	28	0.123	0.033	3.73	1.4%	board	Spray, GHP	25.4	dry density 131kg/m^3
	29.5	0.0557	0.031	1.80	0.5%		Spray, probe		
	28.7	0.0739	0.031	2.38	1.8%				
	30	0.087	0.031	2.81	2.2%				
	29	0.0843	0.031	2.72	4.0%				
McFadden (1988)	24	0.0365	0.036	1.01	0.1%	board	Laboratory pre-conditioning or from field, GHP and probe	>3.2	[2]$k=k_0+0.03\%M$ $(0<\%M<2)$
		0.0447	0.036	1.24	2.0%				
		0.1157	0.036	3.21	3.0%				[2]$k=0.73+0.024\%M$ $(3<\%M<8)$
		0.1330	0.036	3.69	8.0%				
Kehrer *et al.*(2002)	10	0.041			11.6% by mass	board	Laboratory pre-conditioning, GHP	-	-
	35	0.046			11.6% by mass				

(continuted): Comparison among experimental methods and test results for fiberglass insulation with moisture ingress (in SI units)

Fiberglass									
Literature	Mean temperature	Thermal conductivity			Moisture content	Type	Method	Thickness	Description
		wet	dry	ratio					
	˚C	W/m-K		-	% by volume			mm	
Abdou and Budaiwa(2013)	14	0.0340	0.0333	1.02	0.1%	board	Spray, HFM	50	dry density 27kg/m^3
		0.0343	0.0333	1.03	0.3%				
		0.0346	0.0333	1.04	0.5%				
	34	0.0375	0.0371	1.01	0.1%				
		0.0377	0.0371	1.02	0.3%				
		0.0380	0.0371	1.02	0.5%				
	14	0.0323	0.0313	1.03	0.4%				dry density 84kg/m^3
		0.0329	0.0313	1.05	0.9%				
		0.0335	0.0313	1.07	1.5%				
	34	0.0344	0.0336	1.02	0.4%				
		0.0350	0.0336	1.04	0.9%				
		0.0357	0.0336	1.06	1.5%				
Cremaschi *et al.*(2012a)	40	0.0340	0.036	1.10	0.1%	pipe	Conditioned cold pipe, HFM (cold pipe)	50.8	dry density 70kg/m^3
		0.0343	0.036	2.75	1.7%				
		0.0346	0.036	2.79	4.3%				
		0.0375	0.036	3.37	7.0%				
		0.0377	0.036	3.45	11.3%				
		0.0380	0.036	3.47	10.9%				

Table 2.4: Comparison among experimental methods and test results for other common insulations with moisture ingress (in SI units)

Literature	Mean temperature	Thermal conductivity wet	Thermal conductivity dry	Thermal conductivity ratio	Moisture content	Type	Method	Thickness	Description
	˚C	W/m-K		-	% by volume			mm	
Polyurethane									
Kaplar (1974)	-	-			1.63% (14 days)	board	-	50.8	dry density 35.9kg/m^3
Chyu *et al.* (1997a)	23.89	0.3462	0.019	16.26	70.0%	pipe	Flooded, Radial HFM	38.1	dry density 46.5kg/m^3
	60.00	0.3462	0.0242	16.26	70.0%				dry density 140kg/m^3
McFadden (1988)	24	0.0229			0.1%	board	Laboratory pre-conditioning or from field, GHP and probe	>3.2	[2] $k=k_0+0.085\%M$ (0<%M<0.5)
		0.0265			0.4%				
		0.0410			1.1%				[2] $k=0.27+0.013\%M$ (1<%M<7)
		0.0490			0.1%				
Extruded Polystyrene									
Kaplar (1974)	4.4	0.036			1.00%	board	-	50.8	dry density 53.8kg/m^3
Hay[1]		0.0229		-	3.2%	board	Spray/Injection	-	[3] $k=0.17+0.03W$
		0.0265	0.0245	1.53	9.6%	board			
		0.0410	0.0245	1.88	16.0%	board			
McFadden (1988)	24	0.0427	0.029	1.47	1.0%	board	Laboratory pre-conditioning or from field, GHP and probe	>3.2	[2] $k=0.29*\exp(0.014\%*\%M)$
		0.0484	0.029	1.67	10.0%				
Expanded Polystyrene									
McFadden (1988)	24	0.0314	0.029	1.08	2.0%	board	Laboratory pre-conditioning or from field, GHP and probe	>3.2	[2] $k=k_0+0.0089\%M$
		0.0229	0.029	1.47	21.0%				
Jerman and Cerny (2012)	-	0.0265	0.029	1.67	1.0%	board	Immersion, IM	20	[4] $k=-0.4757*\%M^2+0.2198*M+0.0394$
		0.0410	0.029	1.08	10.0%				

[1]: referred by McFadden(1986); [2]: IP units: k and k_0 (Btu-in/hr-ft^2-˚F), %M: the percent by volume of moisture in the sample;
[3]: IP units: k (Btu-in/hr-ft^2-˚F), W: weight ratio; [4]: SI units: k (W/m-K), %M: the percent by volume of moisture in the sample

Table 2.4 (*continued*): Comparison among experimental methods and test results for other common insulations with moisture ingress (in SI units)

Phenolic									
Literature	Mean temperature	Thermal conductivity			Moisture content	Type	Method	Thickness	Description
		wet	dry	ratio					
	˚C	W/m-K		-	% by volume			mm	
Cremaschi *et al.* (2012a)	35	0.0369	0.0345	1.07	0.8%	pipe	Conditioned cold pipe, HFM (cold pipe)	50.8	dry density 50-60 kg/m^3
		0.0407	0.0345	1.18	1.6%				
		0.0438	0.0345	1.27	2.4%				
		0.0473	0.0345	1.37	4.8%				
		0.0484	0.0345	1.40	4.9%				

[1] referred by McFadden(1986);
[2] IP units: k and k_0 (Btu-in/hr-ft^2-˚F), %M: the percent by volume of moisture in the sample
[3]: IP units: k (Btu-in/hr-ft^2-˚F), W: weight ratio
[4]: SI units: k (W/m-K), %M: the percent by volume of moisture in the sample

2.5 Challenges with the current methodologies for measuring the pipe insulation apparent thermal conductivity with moisture ingress and future research needs

Some challenges are identified for moist tests: 1) How to prepare the test specimen with controlled and uniform moisture? 2) What are the appropriate techniques that can replicate similar boundary conditions across the test specimen as the ones observed during pipe insulation systems field service? Flooded, spray/injection and laboratory conditioning methods are the most common methodologies adopted for inducing moisture ingress. However, all of these methods have some trade-off, and ultimately the laboratory conditions deviate from the actual field conditions. Conditioned ambient with cold surface/pipe method provides a more reliable measurement on the apparent thermal conductivity of pipe insulation systems. The temperature and humidity regulated psychrometric chamber, together with a low temperature maintained at the pipe insulation interior surface, would provide appropriate pressure gradients to help vapor condensate on the cold surface and lead to water accumulation in the insulation materials. This will help simulate the moisture distribution in the real application fields. However, the entire test apparatus, including the psychrometric chamber and the thermal conductivity sensors, may take a large space and a considerable amount of time for construction, control and calibration. The equipment maintenance is also a high cost and large capital investment. It is believed that a compact, easy to install, and inexpensive sensor is still needed in future research.

Any inhomogeneity that exists in the material interior structure would create preferential paths for moisture transportation and would form wet regions around those preferential paths. The formation of the wet regions affects the moisture test due to the following two reasons. First, the preferential paths lead more water to pass through. In this case, when the weight of the water that accumulates around the surface of the wet spot overcomes the material surface tension, the water condensate drips out of the insulation material, and some of the water condensate is lost to the ambient. Once this phenomenon occurs, the experiment has to be terminated since the partial loss

of water condensate makes it difficult to correlate the true accumulated moisture content in the insulation test sample with time. A second reason is that when the test material becomes partially wet, the thermocouple sensors, which are evenly placed on the insulation surface, read a larger temperature difference due to a higher thermal conductivity around the wet regions. For example, for fiberglass pipe insulation, after 10 days of test in the moist ambient, the temperature difference on the insulation surface increased from 1.7˚C (3˚F) to 6.1˚C (11˚F) (Cremaschi *et al.*, 2012a). The non-uniformity of the temperature distribution may affect the direction of the heat flow, and the assumption of one-dimensional flow becomes arguable. For pipe insulation systems, large temperature variations along the cylindrical surfaces imply that axial heat transfer has to be considered. This is the same consideration typically made for flat slabs in which large variations of the insulation surface temperatures produce longitudinal heat transfer in the slab, and the assumption of unidirectional heat conduction is no longer valid.

For most pipe insulation systems, it is required to use joint sealant or adhesive during the installation procedure. Joint sealant, which is served as a thermal conductive chemical, may increase the apparent thermal conductivity of the insulation material. The joint sealant may also absorb moisture and can create preferential paths for water accumulation (Cremaschi *et al.*, 2012a). Both effects deteriorate the apparent insulation thermal performance. This can be an explanation as to why most of the manufacturers' data, which are tested on flat slabs, under-predict the thermal performance and water absorption of pipe insulation systems. Mumaw (2002) measured the moisture content in the pipe insulation by using the Calibrated Hot Box method, and he pointed out that the measured moisture content was much higher than the value predicted from the simplified model because the model neglect the effects of the joints and lap seals in the vapor retarders. By dissecting the specimens, he observed that water absorption, lack of curing, and shrinkage of insulation materials away from the joints occurred near the sealed joints. Two technical challenges should be addressed in future studies on joint sealant effects: i) Joint sealant

is usually first applied as a thin layer on the cross section of one or both half shells, and the two half shells of the pipe insulation are compressed towards each other to make a good contact between the insulation materials. In this case, it is unfeasible to accurately measure the thickness of joint sealant. One way to determine it is to first measure the perimeter of the pipe insulation before applying the test specimen around the cold pipe. Once the insulation is installed on the cold pipe, the perimeter of the test specimen with joint sealant will be measured again. The joint thickness is computed from the difference between the diameters before and after the installation procedure. As second challenge is that ii) there are no accurate data for the thermal conductivity of the joint sealants in the open literature.

On this topic, other areas that can potentially be investigated in future research include the effects of the split joints, insulation bulk densities, wall thicknesses, insulation jacketings, contact resistances between pipe and insulation, interior structures and types of fillers and aggregates (Kulkarni & Vipulanandan, 2006) on the apparent thermal conductivity of pipe insulation systems. For some closed-cell insulation, aging is a common phenomenon that degrades the thermal performance of the pipe insulation systems, and very limited work is reported in the literature on this process (Biedermann *et al.*, 2001; Christian *et al.*, 1998; Kellner & Dirckx, 1999; Stovall, 2009). Insulation thickness affects the volume available for the storage of the gas, and thus it directly impacts the deterioration of the insulation thermal performance during aging (Eriksson & Sunden, 1998). The impacts of the exterior water vapor jacketing systems, as well as of the split joints and seams, are not clear, and the results are sporadic and sometimes contradictory. The above additional features of the pipe insulation systems and the anisotropic features of the pipe insulation material on the radial and angular directions, seem to affect the behavior of the pipe insulation systems during dry and wet operating conditions.

In wet condensing conditions with moisture ingress, the moisture migration inside pipe insulation systems can result in a temperature re-distribution on the radial and angular directions. What are

the predominant forces that drive the moisture from one region to another in different types of pipe insulation systems, and what are the geometric inner structures that promote or prevent microscopic water vapor mass transfers inside the pipe insulation are still open questions. Some works that pioneered in this research topic were studied on a "wick" concept, and they focused on the methods to limit water moisture accumulation in pipe insulation systems (Guldbrandsen *et al.*, 2011; Korsgaard, 1993). These studies reported that the microscopic capillary actions inside fibrous pipe insulation systems were responsible for the removal of moisture from the inside of the material outward. It is believed that there are opportunities to improve their models for better prediction of the apparent pipe insulation thermal conductivity in wet conditions and to expand further their original models to other types of pipe insulation systems beside fibrous type insulation. A model that describes and predicts water accumulation in pipe insulation systems will advance the state-of-the-art knowledge of these mechanical insulation systems in cold pipe applications. It will also cause an enormous potential in the industry for developing sensors that can detect failure of the insulation systems and local moisture traps in the pipelines, and this technique can be used for operational and management of the building cooling system.

2.6 Conclusions

This section discussed the experimental methodologies for measuring the apparent thermal conductivity of pipe insulation systems with the aim of providing some clarification on the existing thermal conductivity data for pipe insulation systems. Steady-state and transient methods were discussed, and the measurements from these two methods were critically compared. It is observed that steady-state methods for pipe insulation systems are commonly adopted for measuring an average thermal conductivity, which is defined as apparent thermal conductivity of the pipe insulation systems. Steady-state methods are simpler, more direct, and easier to make than transients methods in dry operating conditions. However, steady-state methods often need a considerable amount of time to reach thermal equilibrium, large test sample size to eliminate edge

effects, and a limited temperature range to prevent radiation. In addition, when considering steady-state methods for pipe insulation systems, the flow direction seems to affect the apparent thermal conductivity. Transient methodologies provide fast measurements, simple installations, and they can be easily applied to pipe insulation systems. However, these methodologies are indirect measurements of the thermal conductivity and adopt more or less cumbersome models to reduce the data from the original measurements. Transient methodologies also provide local values of thermal conductivity in various regions of the test specimen, and the apparent thermal conductivity is strongly depended on the number and locations of the probing sensors. The accuracy and repeatability of transient methods for pipe insulation systems are not as well defined as steady-state methodologies.

During the measurement of the thermal conductivity of pipe insulation with moisture content, four moisturizing strategies used to prepare the wet samples were identified as flooded method, spray/injection method, laboratory pre-conditioning method, and conditioned ambience with cold surface/pipe method. The advantages and shortcomings of each moisturizing strategy were discussed at length. It is pointed out in the this review that steady-state methods in wet conditions with moisture ingress seem to be inadequate because the enthalpy flow occurs due to redistribution of the water condensate in the insulation systems. Using accelerated types of techniques, such as high humidity ambient with a cold surface on one side of the test specimen, seem to provide similar moisture ingress as the ones in the fields but in a shorter time. However, this technique requires a large investment for the equipment and control of the ambient conditions. Transient methods applied to wet pipe insulation systems may be sensitive to the moisture content in the regions adjacent to the probe installed in specific locations of the insulation samples.

The thermal conductivities of several pipe insulation systems were compared under dry conditions, and some data were discussed for wet conditions with different water content. To date, challenges still exist in the measurement of apparent thermal conductivity of insulation with

moisture ingress. The main aspects that must be properly considered are non-uniformity of the pipe surface temperatures, the lack of information on the thermal performance of joint sealants, and the moisture redistribution in radial configurations of the pipe insulation systems. These aspects can be investigated further in future research in order to develop reliable predictive models that estimate the pipe insulation apparent thermal performance in chillers for building air conditionings applications.

CHAPTER III

3. EXPERIMENTAL APPARATUS DESIGN AND INSTRUMENTATION

This chapter provides an overview of the test apparatus and test facility. The experimental methodology and design criteria will be further discussed in the following sections. The experimental apparatus consisted of three parts: the pipe insulation tester (PIT), a refrigeration system, and a psychrometric chamber. The PIT was installed inside the psychrometric chamber at OSU laboratory, which provided accurate control of the ambient temperature and humidity. This project is separated to two stages. In the second stage, the pipe insulation testers (PITs) and the refrigeration system were modified based on original protocol, and both test apparatus in these two stages are included in this chapter.

3.1 Pipe insulation tester (PIT)

In the first stage of this research, two pipe insulation testers (PITs), shown in Figure 3.1a, were constructed and were installed in series with respect to the refrigerant flow. Each PIT was 11.6 ft (3.5 m) long and had two end sections acting as thermal guards. Each PIT was consist of a ½ in. (12.7 mm) inner copper tube, sand filling, and an aluminum pipe of 3 in. (76.2 mm) NPS (Nominal Pipe Size). This test apparatus was improved in the second stage (2012) by adding two more PITs on top of the wood cage, as shown in Figure 3.1a and b, and the four PITs were changed from series in the refrigeration loop to a parallel configuration. Figure 3.2 shows a schematic of one PIT with relevant dimensions. The test specimen is 4 ft (1.2 m) long but the actual measuring section is only the center 3ft (0.9m) of the pipe insulation system. The copper

pipe is centered and aligned inside the aluminum pipe.

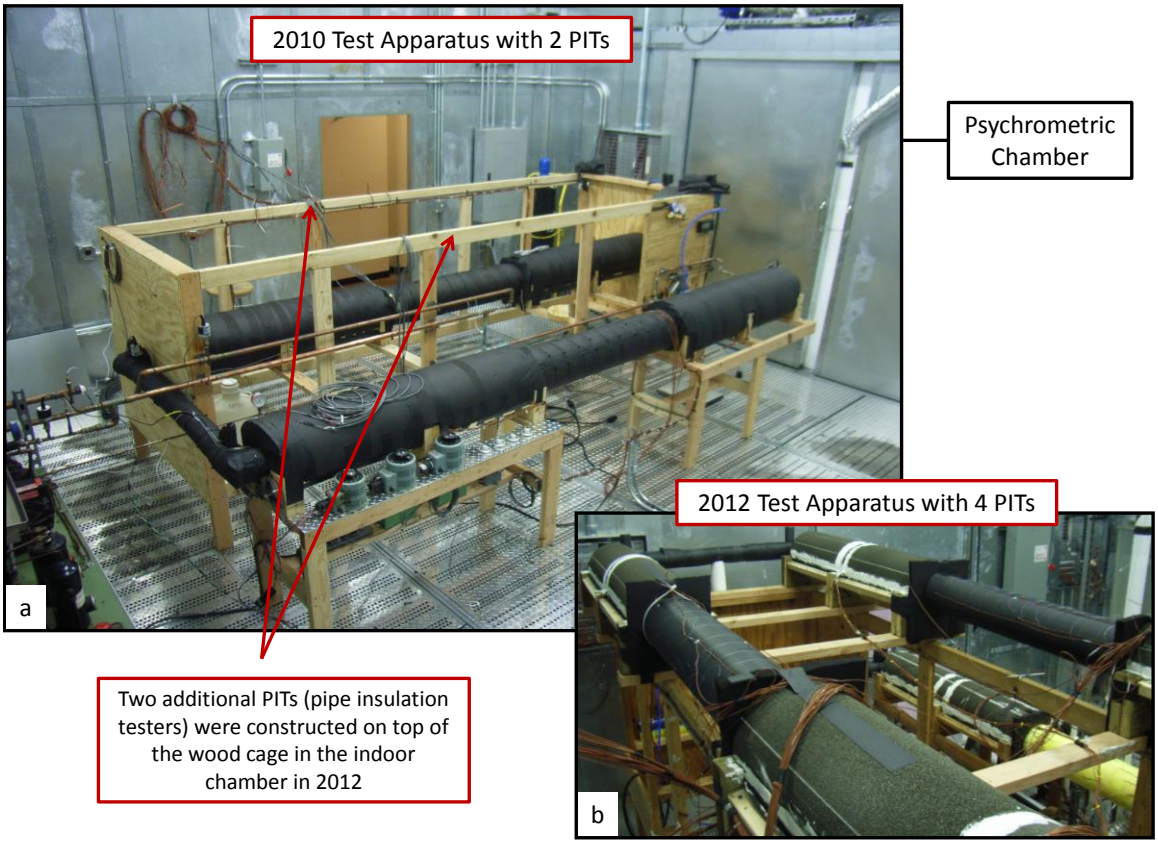

Figure 3.1 Photo of the two Pipe Insulation Test apparatus (PIT); first PIT is used to measure the thermal conductivity of the test insulation specimen while the second PIT is used to measure its moisture content

The aluminum surface temperature was adjusted between 38 to 40.5 ℉ (3.3 to 4.7 ℃) to be close to typical surface temperatures in chilled water applications. With reference to Figure 3.2, low temperature refrigerant circulated in the inner copper tube. The chilled copper tube at the central core of the aluminum pipe created a thermal gradient across the sand, which was the filling material for the annulus region between the copper pipe and the aluminum pipe. The temperature gradient controlled the inward heat flux, and the refrigerant side needs to provide a uniform temperature distribution along both axial and angular directions of the aluminum pipe. Thus axial

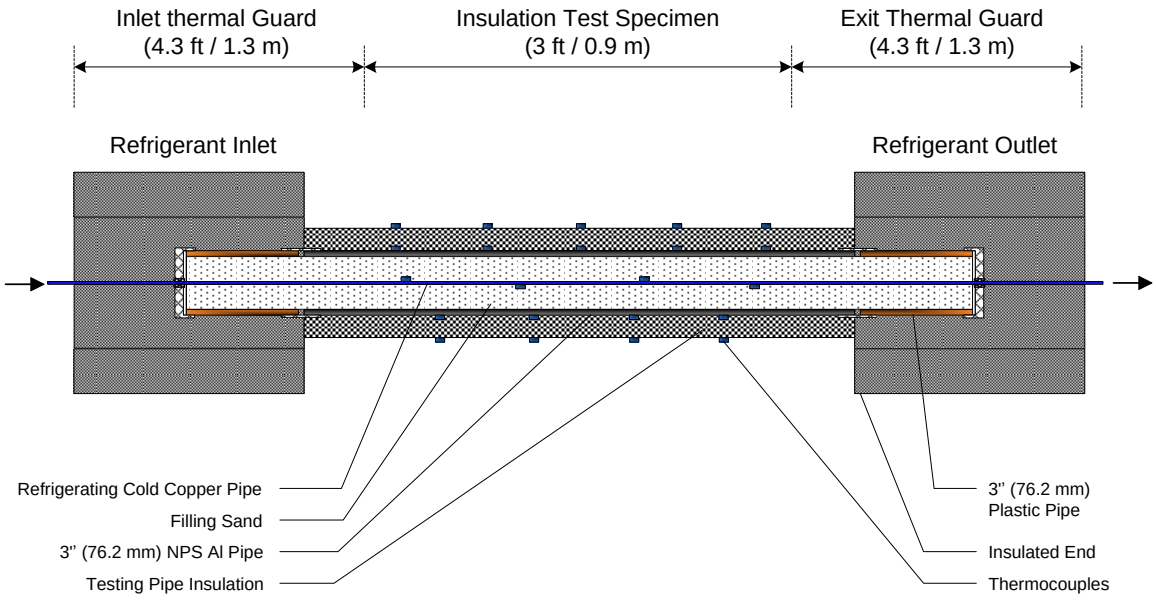

Figure 3.2: Schematic of the Pipe Insulation Test apparatus (PIT) (technical CAD drawings are reported in Appendix B)

heat losses were minimized. The refrigeration system was different during the two stages of this research project. In the first stage, a two-phase refrigerant, R134a, was selected in the refrigeration system. By controlling the refrigerant as a two-phase vapor and liquid mixture in the PIT section, the cold pipe surface temperature was close to the saturation temperature, and it remained constant along the entire length of the copper pipe with small changes in the refrigerant vapor thermodynamic quality and local pressure. In the second stage, dynalene HC50, which is a single-phase refrigerant, was selected in the system. The temperature uniformity was controlled by maintaining the coolant at a high flow rate in the cold pipe through the test section. The refrigeration systems will be discussed in detail in the following section. Pre-dried play sand was selected because of easiness of filling, compact structure, and appropriate thermal conductivity for the radial heat flux measurements. The suitable thermal conductivity of sand provided large temperature gradients between the inner copper tube and aluminum pipe surface during the experiments. Sand was inexpensive and available in several local warehouses. It filled the

annulus region in between the copper tube and the aluminum pipe without requiring special tools or any pre-fabrication processes. Sand formed a fairly homogenous and compact filling in the entire space inside the aluminum pipe, and it was replaced two times without damaging the thermocouples attached on the inner copper tube. When water vapor diffused into the aluminum pipe, sand provided some resistance to the local water accumulation because it limited water traps due to its compactness. However, sand did not repel water vapor and the sealing of the end sections of the aluminum pipe was performed with vapor resistance mastic. Other fillings, such as waxes or plastics, could be used and might be more vapor repellent than sand. In the present work it was found that waxes, plastic or any other insulation materials could not fill the aluminum pipe without the risk of damaging the surface thermocouples anchored to the copper pipe. It was also found that other fillings did not have adequate thermal conductivity for accurately measuring the radial heat flux typical of pipe insulation systems. In addition to prevent possible moisture ingress into the sand, it was sealed in vapor barrier plastic bags, and plastic plugs were used to seal each side of the aluminum pipe. Figure 3.3 illustrates the end sides of the aluminum pipe, the plastic bags and plastic plugs used as vapor barrier for the sand, and various phases of the assembly process of the aluminum pipe core section. It should be emphasized that during the sand filling task, the sand needs to be poured in the aluminum pipe with a very slow rate and with frequent tapping on the aluminum pipe wall to promote sand layering in a compact structure inside the pipe. Any large air gap in the sand should be avoided because it introduces a systematic error in the radial heat flux measurements. Four cross-shaped plastic supports, shown in Figure 3.4, were inserted inside the aluminum pipe to align the copper pipe at the center line of the aluminum pipe. These supports are necessary to prevent that cold copper pipe, which is almost full with liquid refrigerant during the experiments, bends under the weight stress and compresses the sand at the bottom. Any misalignment of the copper pipe with the aluminum pipe and any non-uniformity of the sand in the annulus region could cause a systematic error in the radial heat flux measurements. Figure 3.6 shows a sample of the failure we detected in both PITs with moisture

penetrating into the system. This failure was caused by an incomplete seal of the sand (without the use of plastic bags) and showed a bending happened to the copper tube without the plastic supports. Preliminary tests were conducted to check that the entire device was assembled satisfactorily. In these tests the temperature distribution along the aluminum pipe surface was measured, and it was uniform along both axial and angular direction as it is discussed later in more detail.

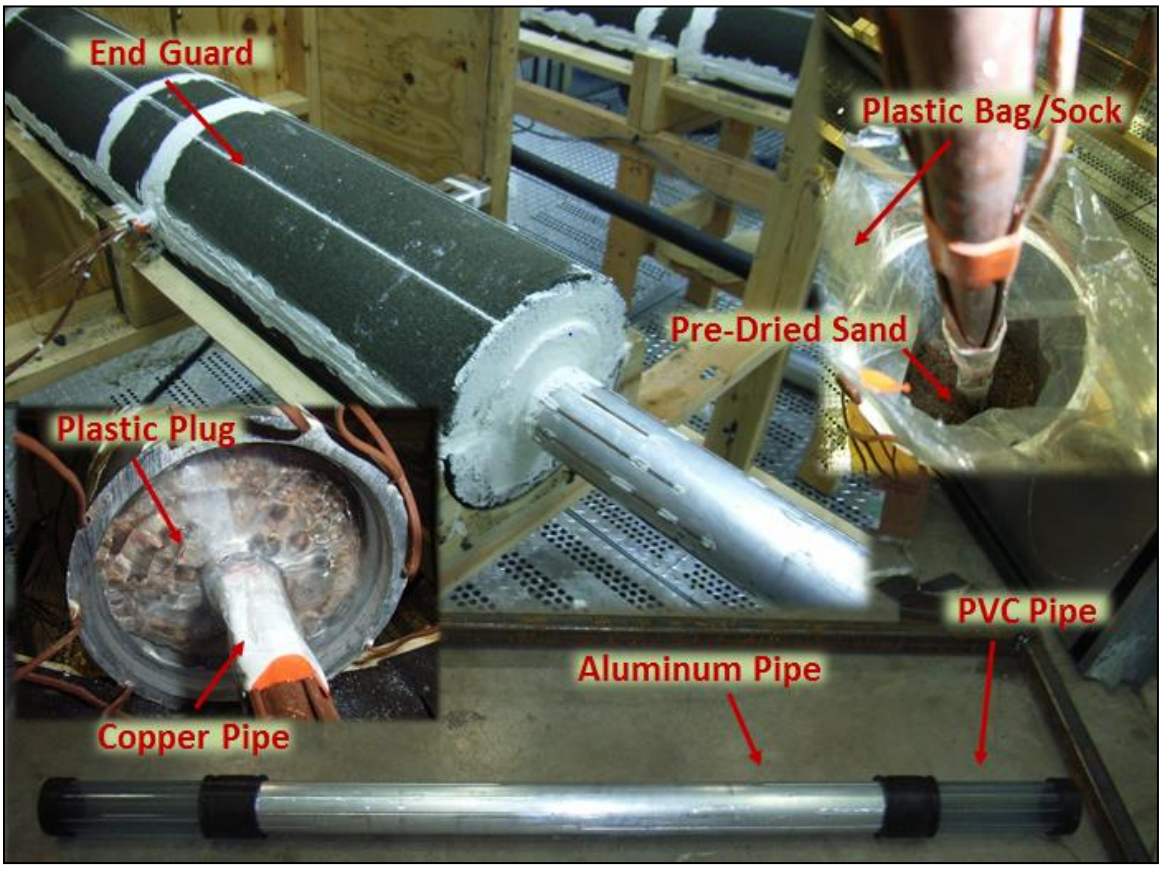

Figure 3.3: Photos of the construction stages of Pipe Insulation Test apparatus (PIT)

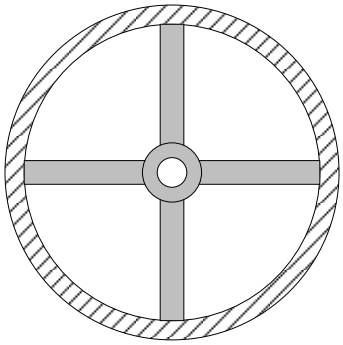

Figure 3.4: Pipe support for the copper pipe inside the PIT

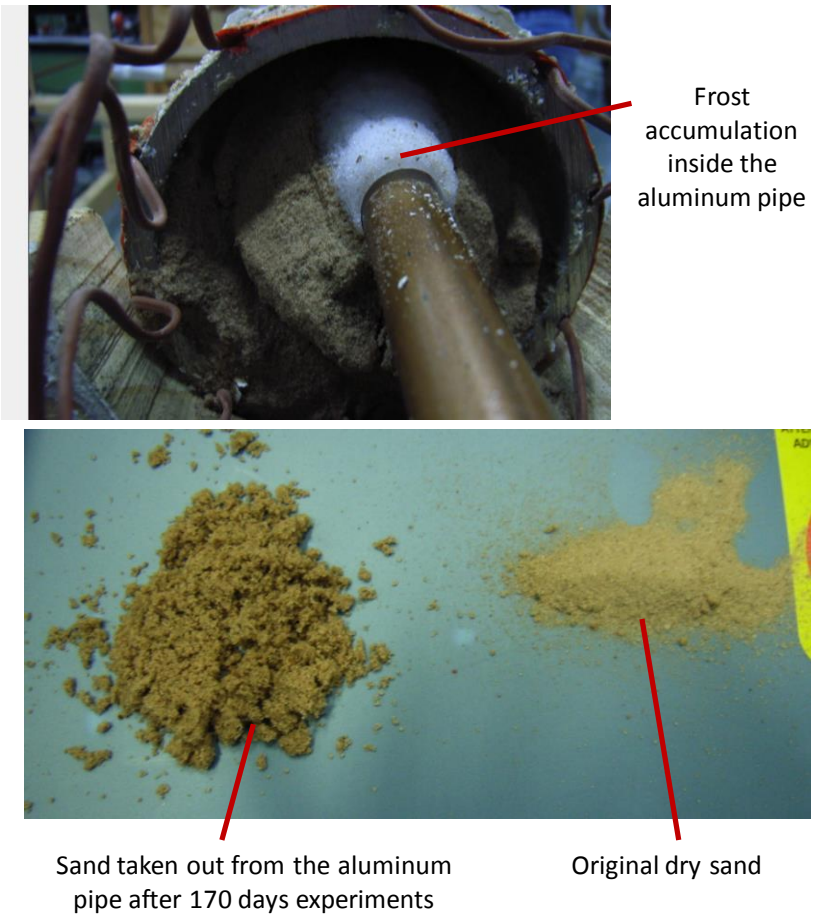

Figure 3.5: Photos of one incident of frost accumulated in the wet sand inside PITs

When the axial temperature gradient along the pipe surface was small, then the axial heat losses were also small. In such a scenario, the heat flux in the PIT occurred mainly along the radial

direction and from the aluminum pipe toward the inner copper pipe. The radial heat flux was computed from the surface temperature readings by the thermocouples and from the sand thermal conductivity. Thermal conductivity of the test insulation specimen was calculated by applying a 1-D heat balance equation to the PIT. For the two PITs constructed in the first stage, the temperature measurements were taken with 20 in-situ and in-house calibrated thermocouples distributed evenly on the aluminum pipe surface. The pipe insulation specimen was instrumented with another 20 in-situ and in-house calibrated thermocouples distributed on its exterior surface. Six (6) in-situ and in-house calibrated thermocouples were mounted on the inner copper pipe surface. Fewer in-situ and in-house calibrated thermocouples were applied on the other two PITs constructed in the second stage: 12 around the aluminum pipe, 12 on the insulation exterior surface, and 6 for the inner copper pipe. Although the total amount of the temperature sensors at each surface decreased when compared to the first stage, these thermocouples were calibrated with a better accuracy, which will be discussed in the next chapter. The thermocouple wires on the aluminum pipe created small air gaps between the inner surface of the pipe insulation and the outer surface of the aluminum pipe. To avoid this air gap, 20 longitudinal grooves (12 grooves in the second stage), with dimensions of 1/8 by 1/8 in. (3.2 by 3.2 mm), were machined on the aluminum pipe surface. The grooves accommodated the thermocouple wires on the aluminum pipe, as shown in Figure 3.6.

Considering the fact that these thermocouple grooves may become potential paths for the water vapor transmission, the surfaces of the aluminum pipes for all PITs were sealed with aluminum adhesive tape during the second stage, as shown in Figure 3.7. The gaps between the test pipe and the end guards were sealed with silicone gel. In order to decrease the radiation effect that caused by the low emissivity of the aluminum surface, the aluminum pipe was further pained as flat black, and the photos for the blackened pipes are shown in Figure 3.9.

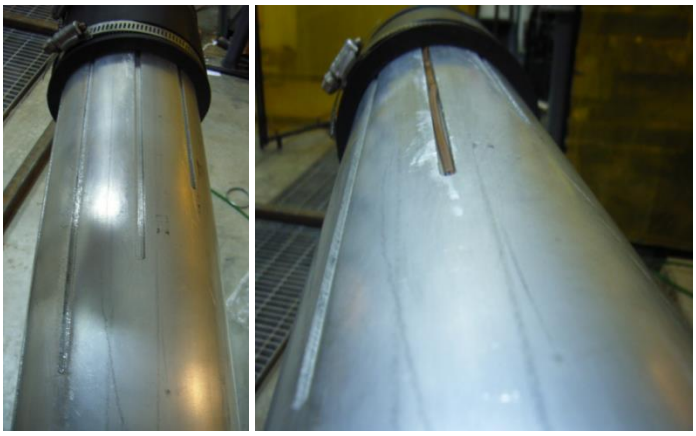

Figure 3.6: Photos of the grooves for inserting the thermocouple wires on to the aluminum pipe exterior surface (CAD drawings are in Appendix B)

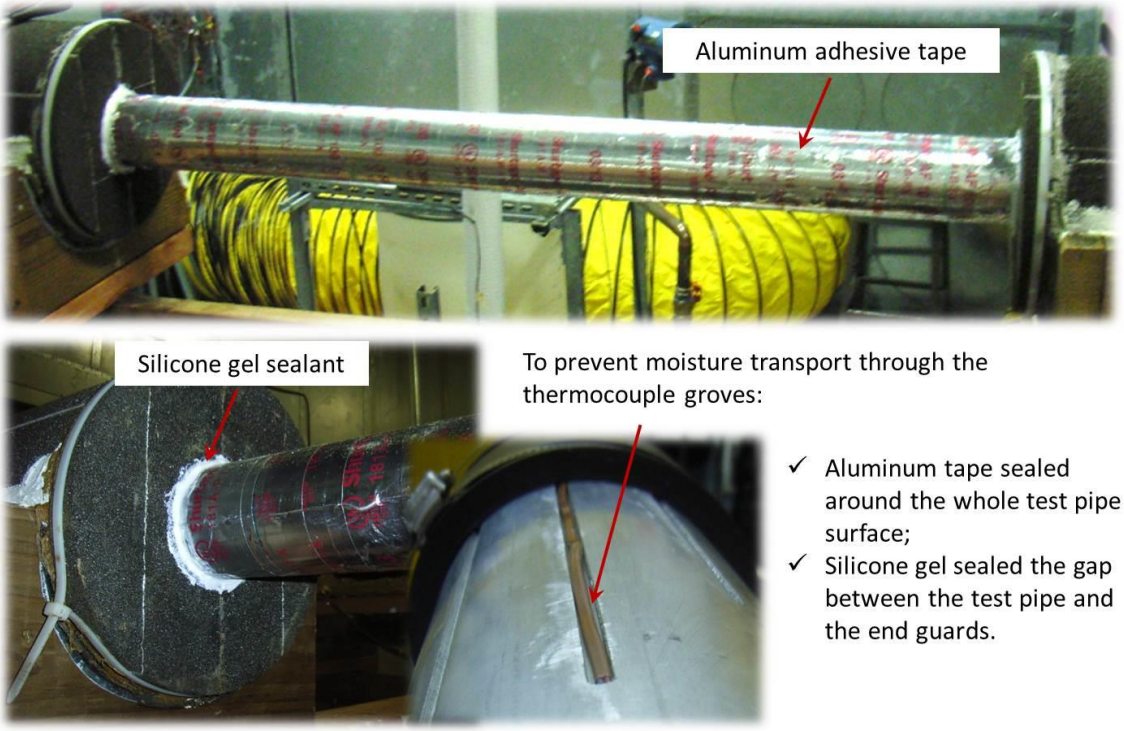

Figure 3.7: Photos of the grooves sealed with aluminum adhesive tape and edge seal with silicone gel

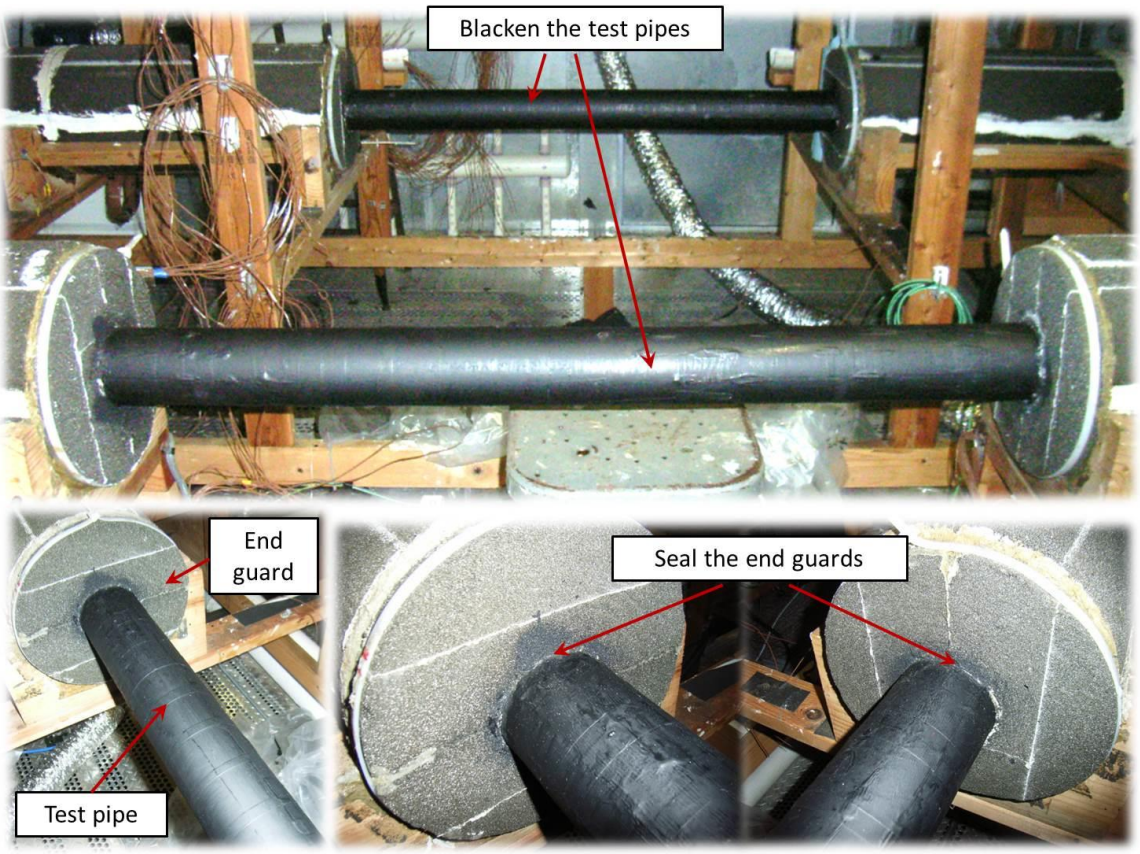

Figure 3.8: Photos of the blackened pipe and edge seals

The six thermocouples attached to the copper tube were glued on to the outer surface using Omega thermal conductive epoxy (model type OMEGABOND 100 and 101), which had thermal conductivity of about 7.2 Btu-in/hr-ft^2-F (1.0 W/m-K). The thermal epoxy had low nominal electrical conductivity, and it was estimated that the electrical insulation volume resistance was between 10^{12} to 10^{15} ohm-inch. Test apparatus was also electrically grounded to minimize electric noise from the thermocouples. The thermocouples were spaced evenly along the angular and axial directions, that is, following a spiral path along the outer surface of the copper pipe. Similarly, the thermocouples on the aluminum pipe were glued using the same thermal epoxy and installed evenly along a spiral path on the outer surface of the aluminum pipe. The thermocouples on the

pipe insulation outer surface were positioned along a spiral path with the tips of the thermocouples immersed in silicone beads. The tips of these thermocouples were covered by a low thermal conductivity silicone gel beads to create a thermal barrier from the surrounding air. Using silicon beads was preferred than using small square patches of neoprene insulation because the readings from the thermocouples with silicon beads were closer estimations of the local pipe insulation exterior surface temperatures.

The pipe insulation specimens were exactly cut to fit the 3 ft (0.9m) long center section of the PITs. The pipe insulation dimensions were measured according to the standard ASTM C585 (ASTM, 2009) before installation. Joint sealant was applied to the longitudinal joints, depending on the characteristics of the test insulations and on the manufacturer recommendations.

The end thermal guards were designed as two 48-in long (1.2 m) sections, with an outer diameter of 10½-in (266.7 mm), as illustrated in Figure 3.2. The nominal wall thickness of the pipe insulation at the thermal end guards was 3½-in. (88.9 mm). By adding a large thermal resistance at two ends of the test section of the apparatus, it was estimated that the axial heat transfer was reduced to within 0.5% of the radial heat flux. Cellular glass was used as insulator for the end thermal guards because it has low water vapor permeability. This property minimizes moisture ingress into the end thermal guard sections, phenomena that interferes with the thermal conductivity and moisture content measurements of the PIT. Two plastic pipes of nominal 3-in NPS (7.6 mm) size and 12-in (0.3 m) long were positioned at each end of the aluminum pipe. Rubber couplings were used to join the two plastic pipes to the central aluminum pipe, and about ½-in (12.7 mm) air gap was maintained in between the plastic pipes and aluminum pipe in order to minimize thermal bridge in the aluminum pipe. Polyethylene foam rubber, which has a thermal conductivity of 0.25 Btu-in/hr-ft^2-F (0.036 W/m-K) and a low vapor permeability, was inserted inside the plastic pipes, and rubber caps were installed at the ends. Rubber caps were excellent vapor retarders but unfortunately they were also good thermal conductors when compared to the

other components of the PIT. Two cellular glass cylindrical inserts were mounted in between the rubber caps and the refrigerating cold copper pipe in order to eliminate any direct contact between rubber caps and the copper pipe surface. The external surface of the plastic pipes was insulated by using cellular glass insulation with 3½-in (88.9mm) of nominal wall thickness.

In the first stage, two PITs were connected in series with respect to the refrigerant flow, and both PITs were required for the measurement of the apparent thermal conductivity in one pipe insulation system. Theses two PITs were identical and were built at the same time. The temperature sensors on the first PIT aimed to measure the thermal conductivity of the pipe insulation specimen, while the second PIT served a dual purpose. First, it allowed monitoring the sand thermal conductivity during the dry tests. If we assume that the PIT is perfectly sealed and that vapor cannot penetrate into the aluminum pipe, then the second PIT might not be required for the dry tests. An objective of the second PIT was to validate this hypothesis with the prototypes constructed in this project. A second objective of the second PIT was to measure the moisture content in the pipe insulation system at intermediate time intervals during the wet tests. The measurements of moisture content from the second PIT provided an indication of the moisture accumulation rate and transitional phase (Mcfadden, 1988) in the pipe insulation system during the wet test period. Although the second PIT increased the total cost for the test apparatus it was necessary to demonstrate the feasibility of the test apparatus of this project. The second PIT is also recommended if water vapor absorption rate must be experimentally estimated during the period of exposure of the pipe insulation system to the humid ambient with moisture ingress. A flexible strip electric heater was installed along the surface of the aluminum pipe of the second PIT during the dry tests. A large amount of insulation was wrapped around the heater to limit radial heat gain from the surrounding ambient. The power to the heater was controlled to obtain similar aluminum surface temperature in the second PIT as the one measured in the first PIT during the dry tests. Since the two PITs were of identical geometry, constructed at the same time,

and maintained at the same temperature and humidity boundary conditions, we postulated that any variation in the sand conductivity measured with the second PIT was reflected with an equivalent variation of the sand conductivity inside the first PIT. In other words, while the absolute values of the sand thermal conductivity for the two PITs were slightly different, the increase of the sand thermal conductivity due to moisture ingress into the aluminum pipe of the first PIT was assumed to be proportional to the increase of sand thermal conductivity measured in the second PIT, if present. This approach allowed us monitoring the thermal conductivity of the sand and detecting any change of the sand thermal conductivity due to potential failure of the sealing and moisture ingress inside the aluminum pipe.

In the second stage, with an improved procedure on the calibration test, which represents the tests for the measurement on the sand thermal conductivity, the PITs can work independently during the dry test, and these four PITs were connected in parallel with respect to the refrigerant flow. However, under moisture test, two PITs were stilled required at the same time for the measurement on the apparent thermal conductivity and moisture content. In the following descriptions, I named the PIT used for the thermal conductivity measurement as the first PIT, and the one used to determine the moisture content in the pipe insulation systems as the second PIT.

3.2 Refrigeration systems

Two different refrigeration systems were used to maintain the cold copper tube in a temperature range from -20 to +25°F (-29 to -4°C) in the two stages of the experiment.

3.2.1 Refrigeration system in the first stage

In the first stage, two PITs were connected in series with respect to the refrigerant flow, that is, the outlet of the first PIT was connected to the inlet of the second PIT as shown in Figure 3.9. Both PITs were connected to a two-phase refrigeration system as an evaporator and the refrigerant absorbed heat from the sand via two-phase flow boiling in the inner copper tube.

Under the heat flux conditions of the laboratory tests for this project, the temperature of the coolant must be controlled in a fairly large range. Refrigerant R134a was the primary choice for pipe insulation systems with moderate thermal conductivity. Refrigerant R404A was the second choice for pipe insulation systems that have a very-low thermal conductivity. For the latter case, a very low temperature of the refrigerant was required in order to create a measurable radial heat flux across the pipe insulation specimen. A two-phase flow boiling approach was chosen because it provides a good distribution of surface temperature along the axial direction of the pipe. It was also stable with time, which is a desirable feature for the time-extensive experiments in wet ambient conditions. Refrigerants entered and exited the PIT at constant temperature and in the two-phase vapor and liquid mixture thermodynamic state. The vapor refrigerant thermodynamic quality increased slightly from inlet to outlet of the PIT but it remained in the two-phase saturated region.

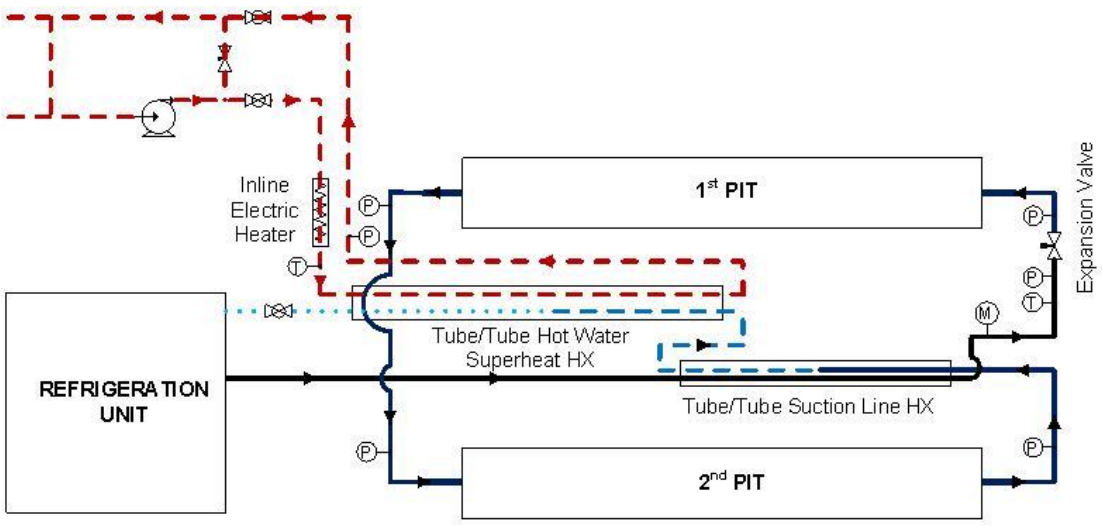

Figure 3.9: Schematic of the test facility consisting of two PITs in line with the refrigeration system (Stage 1)

Considering the cooling capacity required for the two PITs, a tube-in-tube suction line heat exchanger (HX), referred in Figure 3.9 as Tube/Tube Suction Line HX, was installed after the

second PIT to increase the overall cooling capacity of the refrigeration unit. The suction line heat exchanger was required to increase the cooling capacity of our refrigeration unit and to shift the vapor refrigerant thermodynamic quality at the inlet of the first PIT toward the saturated liquid curve. The suction line HX was made in house by welding a 48-in (1.2 m) long, ½-in. (12.7 mm) OD copper pipe around the system 3/8-in (9.5 mm) copper tube with tee and reducer fittings to keep the two fluid streams independent. The in-house manufacturing process of the tube-in-tube suction line HX is shown in Figure 3.10. Before returning to the compressor, proper degree of superheat at the compressor suction was achieved by an auxiliary water-to-refrigerant tube-in-tube heat exchanger. The superheat HX was made using a 72-in (1.8m) long, 1-in (25.4 mm) nominal copper pipe with a tube insert of ½-in (12.7 mm) copper pipe. Warm water was circulated in an auxiliary loop, which had a pump, a flow valve, and an in-line heater. The power to the in-line heater was adjusted to guarantee proper refrigerant temperature at the compressor suction. It should be noted that electric heaters applied directly on the surface of the cold copper pipelines were intentionally avoided in the test apparatus because they created large axial temperature gradients in the refrigeration copper pipelines used inside the PITs. These large axial temperature gradients might be the results of heat conduction across the walls of the pipes and they greatly affect the uniformity of the surface temperature along the axial direction of PIT. In a preliminary prototype of the PIT, it was observed that electric tape heaters, which used along the copper pipe to provide refrigerant superheated vapor to the compressor, altered the temperature profile of the copper pipes inside the PITs upstream the suction line HX as well as introduced a systematic error during the measurements of pipe insulation thermal conductivity. Thus, we purposely avoided to use any electric heater directly in contact with the copper pipes of the test facility of Figure 3.9 .

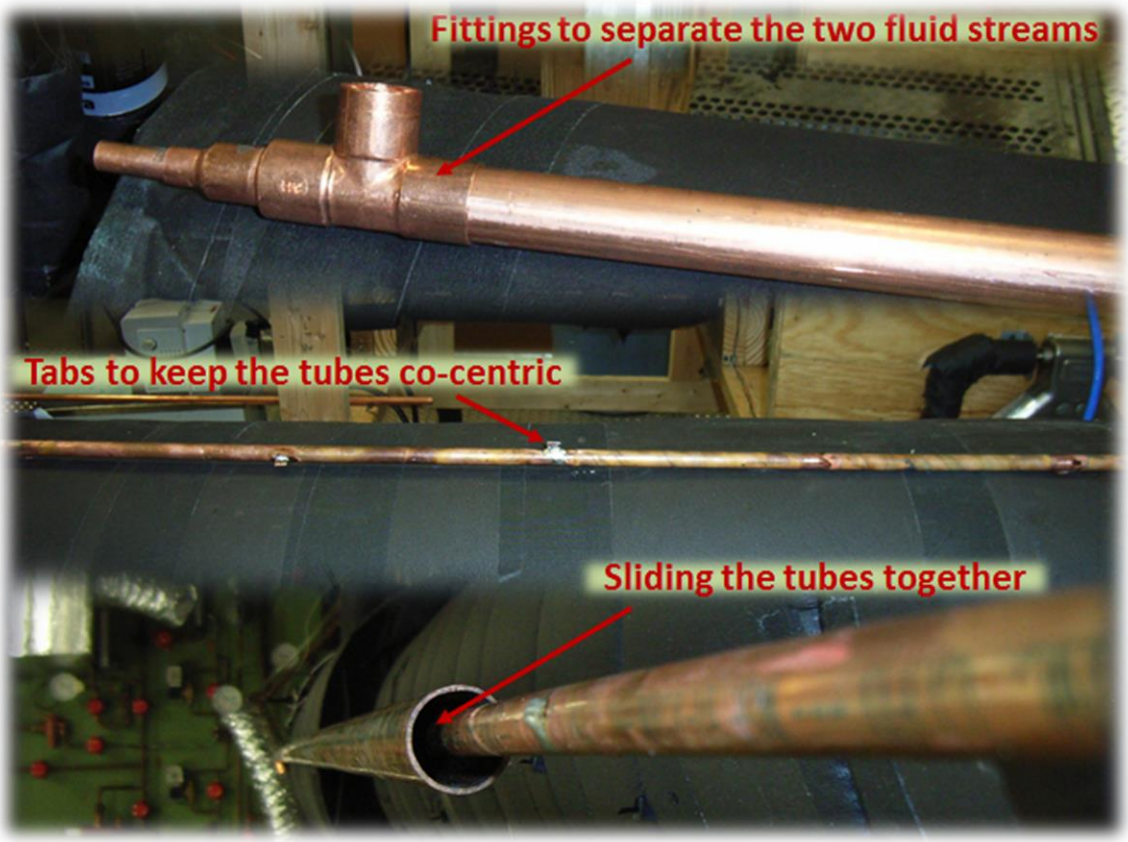

Figure 3.10: Photos of the construction stages of the tube and tube heat exchangers

3.2.2 Refrigeration system in the second stage

A completely different refrigeration system was designed in the second stage of the project. Due to the fact that in the previous design, the air-cooled refrigeration unit was constructed in the indoor chamber next to the PIT test sections, the cooling capacity provided to the condenser was very limit and highly dependent on the indoor ambient conditions. For example, in the normal case, the moisture test need to be maintained as a hot and humid environment, and the room was set at 107˚F (41.7˚C), 83% relative humidity. Under this severe condition, there was not enough cooling provided to the condenser by passing warm air through the fin-and-tube heat exchanger, and this results in a difficulty to maintain the refrigerant as two-phase in the test sections. The room ambient was very unstable due to the heat generated from the compressor and the warm air

blowing through the air-cooled condenser. Considering these disadvantages, in the second stage, the refrigeration unit was separated from the test environment, and was designed outside the indoor chamber. Instead of using a two-phase refrigerant, which has a high requirement on the control of the system pressure and the ambient condition, a single-phase refrigerant, Dynalene HC50, was selected as a substitute. A portable water cooled chiller was connected in the system to maintain the processing liquid at a low temperature. The inlet temperature of Dynalene HC50 to the chamber can be controlled within ±0.1˚F (±0.06˚C) of the set point temperature. The system requires a high flow rate to minimize the temperature increase in the single-phase refrigerant through each PIT test section. It should be noted that in the second stage, two more PITs were added next to the original PITs built in the first stage. Considering the requirements on the high flow rate and similar inlet temperatures, these four PITs were designed in a parallel configuration, as shown in Figure 3.11.

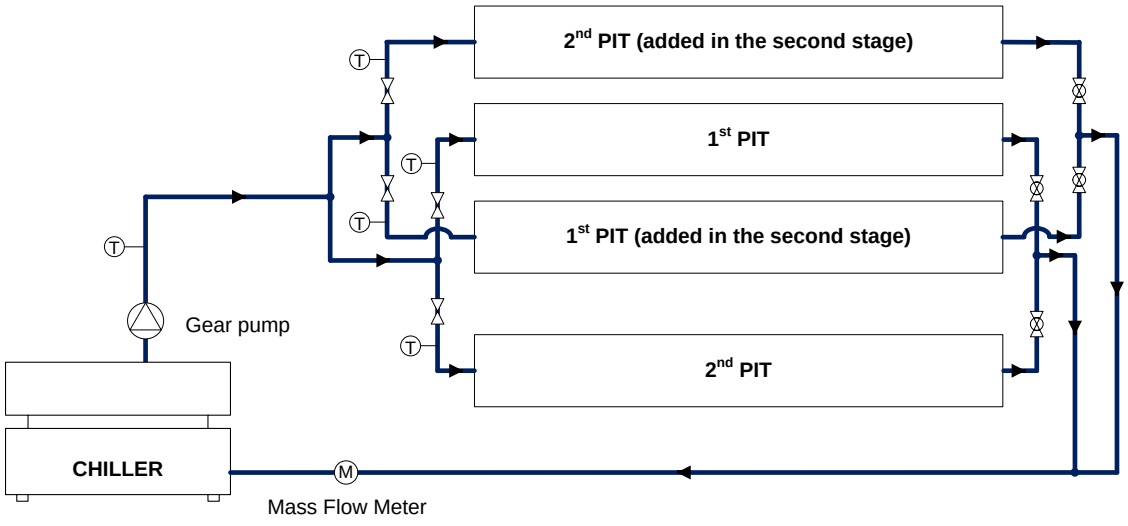

Figure 3.11: Schematic of the test facility consisting of four PITs in line with the refrigeration system (Stage 2)

Piping needs to be appropriately designed to balance the pressure drops among the four branches. During the second stage, all the four PITs can be used for thermal conductivity measurement

under dry condition, and four pipe insulation systems could be tested simultaneously. The variation on the sand thermal conductivity would still be monitored by the periodical calibration tests applied on all the four PITs. The test results derived from each PIT would be corrected based on a specific correlations developed on the sand thermal conductivity with time between the two calibration tests. The procedures for the calibration tests will be explained in detail in the section 4.2.2.

3.3 Psychrometric Chamber

Measuring of the actual thermal conductivity of pipe insulation systems under controlled ambient temperature and humidity could be performed in psychrometric chambers. In this project, a psychrometric chamber was designed so that a slow motion of the air was maintained during the tests, with air ascending in the room from a perforated floor. This displacement ventilation system, shown in Figure 3.12, was consist of a conditioning loop, an under floor air plenum supply, and a set of adjustable ceiling filters. Air was circulated through the conditioning loop first, shown on the right side in Figure 3.12, by using a variable speed fan. The air flow rate was adjusted with the fan motor speed and a set of electro-mechanical dampers. With reference to Figure 3.12, during the first process, the air stream goes inside the conditioning loop is cooled down and dehumidified through the water-to-air cooling coils. The coils' surface temperature and capacity were controlled by a system with a variable speed pump, electronic mixing valves and bypass valves. These parameters were adjusted so that the air is cooled and dehumidified at about 43°F (6°C) of air dew point temperature. This was the minimum air dew point temperature that the cooling coils of the chamber were able to provide. To achieve proper dry non-condensing conditions, the ambient air dew point temperature must be below the aluminum pipe surface temperature of 40°F (4.5°C) in the first stage and below 38°F (3.3°C) in the second stage.

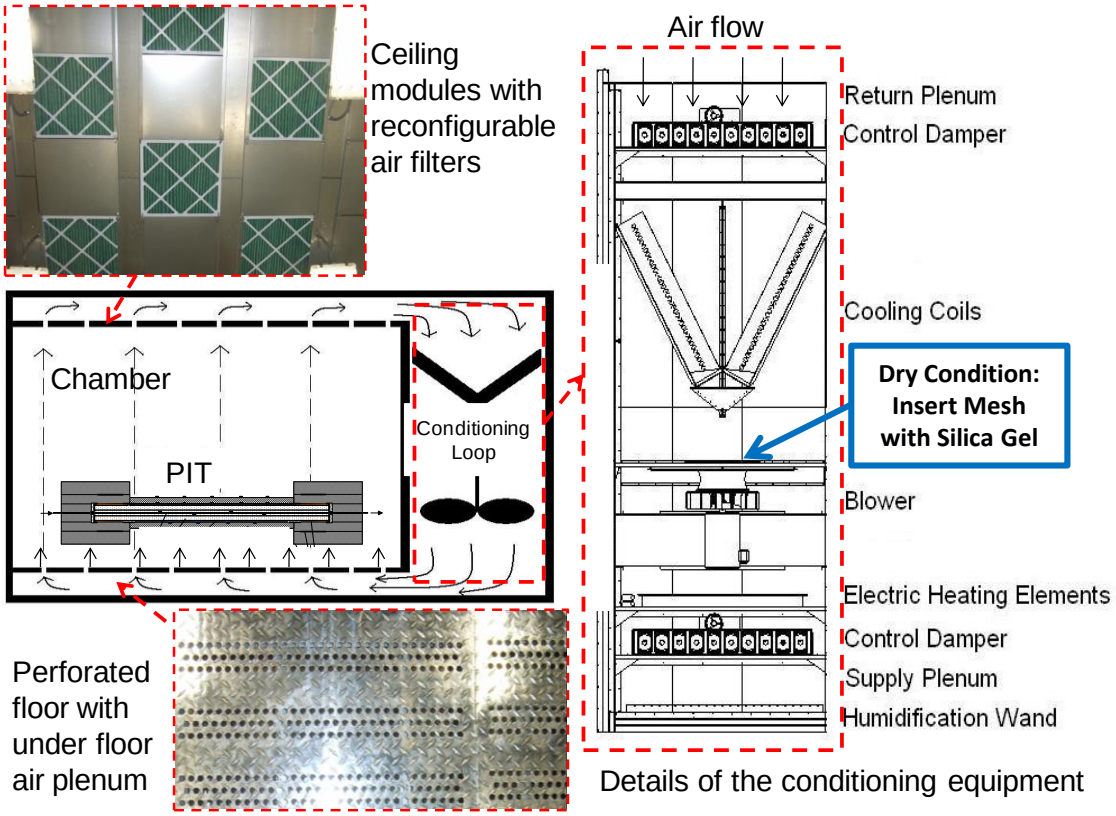

Figure 3.12: View of psychrometric chamber with details of the ceiling with reconfigurable air filters, of the perforated floor with under floor air plenum, and of the chamber conditioning equipment to create dry and wet conditions of the ambient air surrounding the PIT

In order to reach such conditions, two different methodologies were applied during the two stages of the project. In the first stage, a mesh with solid desiccant silica gel material was inserted after the cooling coils and installed against the air stream inside the conditioning loop, shown in Figure 3.12. The solid silica gel material was replaced periodically to insure that the room humidity was maintained low enough throughout the dry tests. However, there were several cumbersome procedures need to follow when replacing the silica gel in the conditioning area, and the drying efficiency of the silica gel decreases fast after each time of baking. Therefore, in the second stage, the drying technique was improved by utilizing two cooling coils in the indoor chamber, as shown in Figure 3.13.

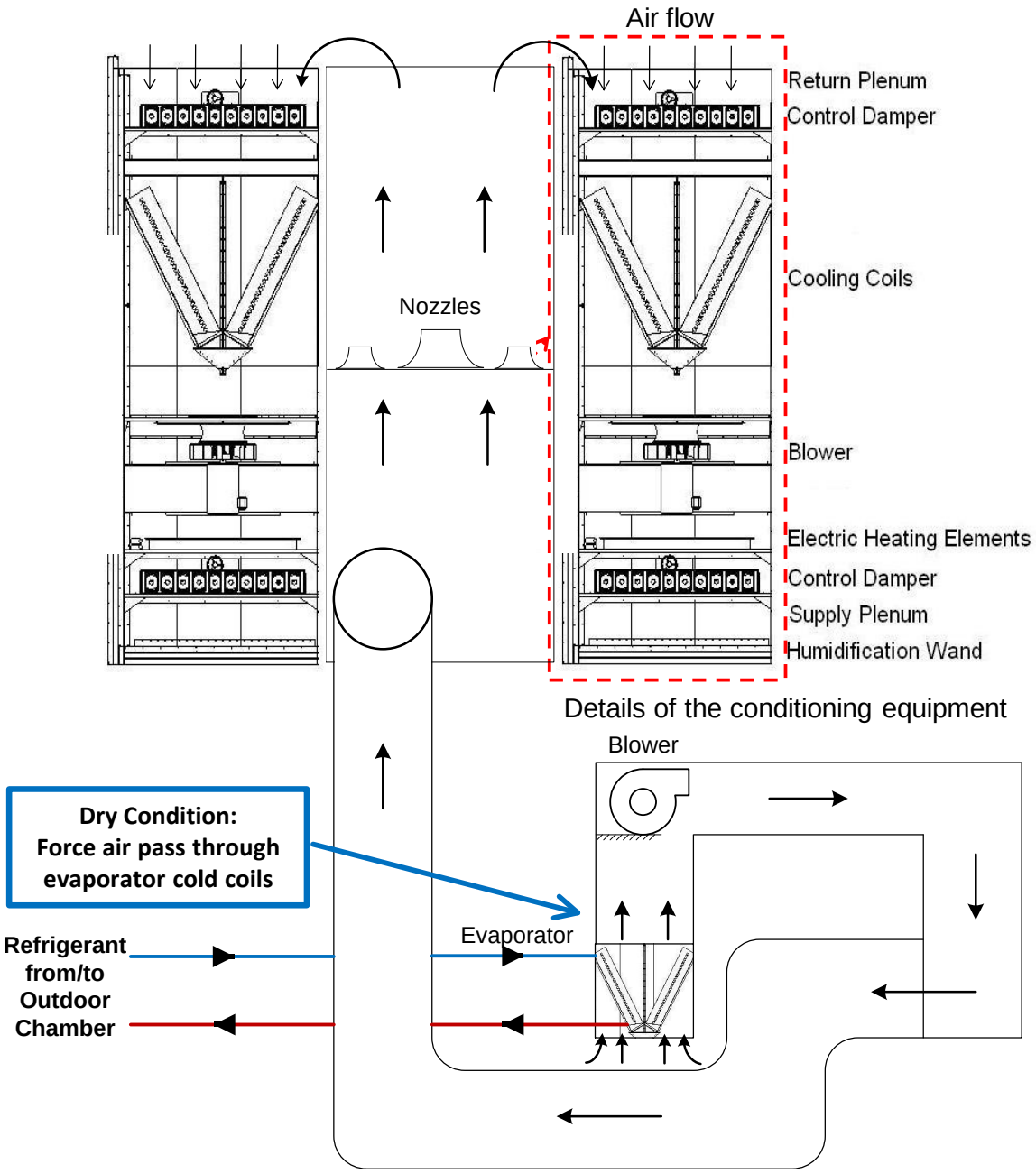

Figure 3.13: View of psychrometric chamber and of the chamber conditioning equipment to create dry conditions of the ambient air surrounding the PIT (second stage)

These two coils were parts of a heat pump unit, but they could be served as an evaporator by reversing the heat pump cycle. By maintaining the coil surface temperature lower than the required test temperature on the aluminum pipe, the water vapor in the air would be condensed on

the cold surface when the air passed through the cold coils, and the air was dehumidified with the dew point temperature lower than the aluminum pipe surface temperature. Then the dry air was sent back to the conditioning area, mixed with the air returned from the ceiling and back to the conditioning loop. Experiments showed that the second drying technique performs much better than the silica gel method, and the relative humidity could be maintained below 10% when the ambient temperature was around 90˚F (32˚C). However, there are several disadvantages in this method. First, frost accumulation degraded the coil performance, and the refrigeration unit needs to be off for defrost cycle every two to three days. During the defrost cycle, the ambient temperature and humidity would be disturbed and the PIT systems may lose the steady-state condition. Second, the heat pump unit can only work in a limited temperature range. When the indoor room temperature is too high, there will be too much heating load in the evaporator side, and this will lead to a very high discharge temperature on the compressor. Considering the pros and cons in both methods, the appropriate drying technique should be selected based on the specific requirements on the ambient conditions during the dry tests.

After being cooled and dehumidified by following the procedures that explained in previous sections, the air stream was guided to a series of electric resistance heating coils, which would raise the air temperature up to the required ambient temperature for the dry tests. The electric heaters of the psychrometric chamber allowed for precise temperature control and rapid response time during the test period. PID control was designed to adjust the heaters' power until the average room dry bulb temperature next to the PITs was within ±0.1°F (±0.05°C) of the desired set point temperature.

For the wet tests, the ambient condition was required to maintain the humidity at a high level, and the air stream was humidified using an electric stream humidifier. Moisture was added from the bottom section of the conditioning loop by steam wands, shown as 'Humidification Wand" in Figure 3.12. It is important to emphasize that the introduction of moisture to the ambient air was

far away from the PITs, and this would guarantee enough time for proper mixing in the under-floor plenum before the moist air stream reaches the PITs. This strategy is critical since uniform ambient conditions must be achieved around the PITs. In the first stage, two small room humidifiers were used to provide water vapor and maintain adequate moisture level in the ambient air during the draining periods of the main humidifier of the chamber. The small room humidifiers were synchronized so that water vapor was continuously supplied to the room during the 40 to 50 minute period required for the main humidifier to perform its daily self cleaning and draining cycles. In the second stage, the draining cycle was expanded to 7 to 10 days because of the usage of soft water, and soft water would lead to a lower rate of forming scaling in the humidifier water system.

Two dry bulb and two wet bulb probes were used to measure the dry-bulb and wet-bulb temperatures of ambient air surrounding the PITs. The probes measured an average value of the ambient air at various locations along the two sides of the PITs. The sampling tree of the dry-/wet-bulb probe is made of plastic white PVC and is shown in Figure 3.14 on the left side next to the PIT. Four additional humidity sensors and six thermocouples were installed around the PIT to measure the local air humidity and local dry-bulb temperature, respectively. A panel of elastomeric rubber insulation was positioned directly underneath the pipe insulation test specimen as shown on the bottom of Figure 3.14. This configuration avoided direct impingement of the air on the bottom exterior surface of the insulation specimen, which stood at least 33 in. (0.8 m) high from the perforated floor. Each PIT was supported from the two end side thermal guard sections by a wood frame. The specifications of the wood cage were attached in Appendix A. The measurements of the air dry-bulb temperature and humidity in the various locations surrounding the PITs indicated uniform ambient conditions. The local ambient dry-bulb temperatures were within ±0.3°F (0.15°C) of the average room dry-bulb temperature and the local relative humidity measurements were within ±4% RH of the average relative humidity in the room.

Figure 3.14: View of Pipe Insulation Test apparatus (PIT) with location of ambient dry-bulb temperature sensors and relative humidity sensors

CHAPTER IV

4. MEASUREMENTS AND DATA REDUCTION

This chapter discussed the test procedures for the apparent thermal conductivity measurement under both dry and wet, condensing conditions. A 1-D heat conduction model was used in the data reduction, and the system uncertainty analysis was provided in detail at the end of this chapter.

4.1 Experimental Test Conditions

According to the design criteria and controlled strategy described in previous chapter, the developed test apparatus is expected to guarantee uniform conditions for the ambient air in both dry (non-condensing) and wet (condensing) tests. Different types of pipe insulation systems with nominal wall thickness from 1 to 2-in (25.4 to 50.8 mm) were investigated in dry tests. Dry conditions were achieved by removing all possible water vapor from the room, which took several hours. The ambient relative humidity was limited to be below 15% to 30% RH depending on the ambient dry bulb temperature. In dry tests the air dew point temperature was always lower than the aluminum pipe surface temperature; thus avoiding the risk of condensation on the aluminum pipe surface. The thermal conductivity of the pipe insulation specimen was measured for insulation mean temperatures ranging from 55 to 73°F (13 to 23°C), that is, a cold surface side of 38 to 41°F

(3.3 to 4.4°C), and a hot surface side from 72 to 105°F (22 to 40.5°C). The hot surface temperature was controlled by varying the ambient temperature of the surrounding air from 77 to 110°F (25 to 43.4°C). For both PITs constructed in the first stage, more than 50 temperature sensors were used to monitor the interior and exterior local surface temperatures of the pipe insulation specimens. An example of the axial and angular temperature measurements is shown in Figure 4.1. Pipe insulation surface temperatures were measured by 20 thermocouples positioned around the exterior surface of insulation specimen and following a similar spiral configuration. By blocking the air stream right below the test apparatus with a panel of elastomeric rubber insulation, the temperature distribution of the pipe insulation exterior surface was within ±0.95 ℉ (±0.5°C). 20 additional thermocouples were positioned on the exterior surface and they were installed inside longitudinal grooves of about 1/8-in (3.2 mm) depth. The grooves were cut out in the aluminum pipe so that the thermocouple wires did not interfere with the installation of the pipe insulation around the aluminum pipe. The local surface temperatures of the aluminum pipe were within ±0.5 ℉ (±0.3°C) when considering both axial and angular directions, as shown in the central plot of Figure 4.1. Finally, 6 thermocouples were attached to the copper tube, and the temperature variation in both axial and angular directions was within ±1.1 ℉ (±0.6°C), as shown in the bottom plot of the figure. The average copper surface temperature was 2 to 3.5 ℉ (1 to 2 ℃) higher than the refrigerant saturation temperature inside the copper pipe. For the two additional PITs constructed during the second stage, fewer, but better calibrated thermocouples were used for surface temperature measurements. The numbers of the sensors attached to the insulation exterior surface, aluminum pipe surface and copper surface are 12, 12 and 6. An example of the axial and angular temperature distribution on the latter PITs is shown in Figure 4.2. The axial temperature differences along the copper and aluminum pipe surfaces were almost the same as the values derived on the PITs built in the first stage, but the temperature difference measured

from the exterior surface was greatly decreased from 2.7°F (1.5°C) to 0.8°F (0.4°C) with the newly installed temperature sensors.

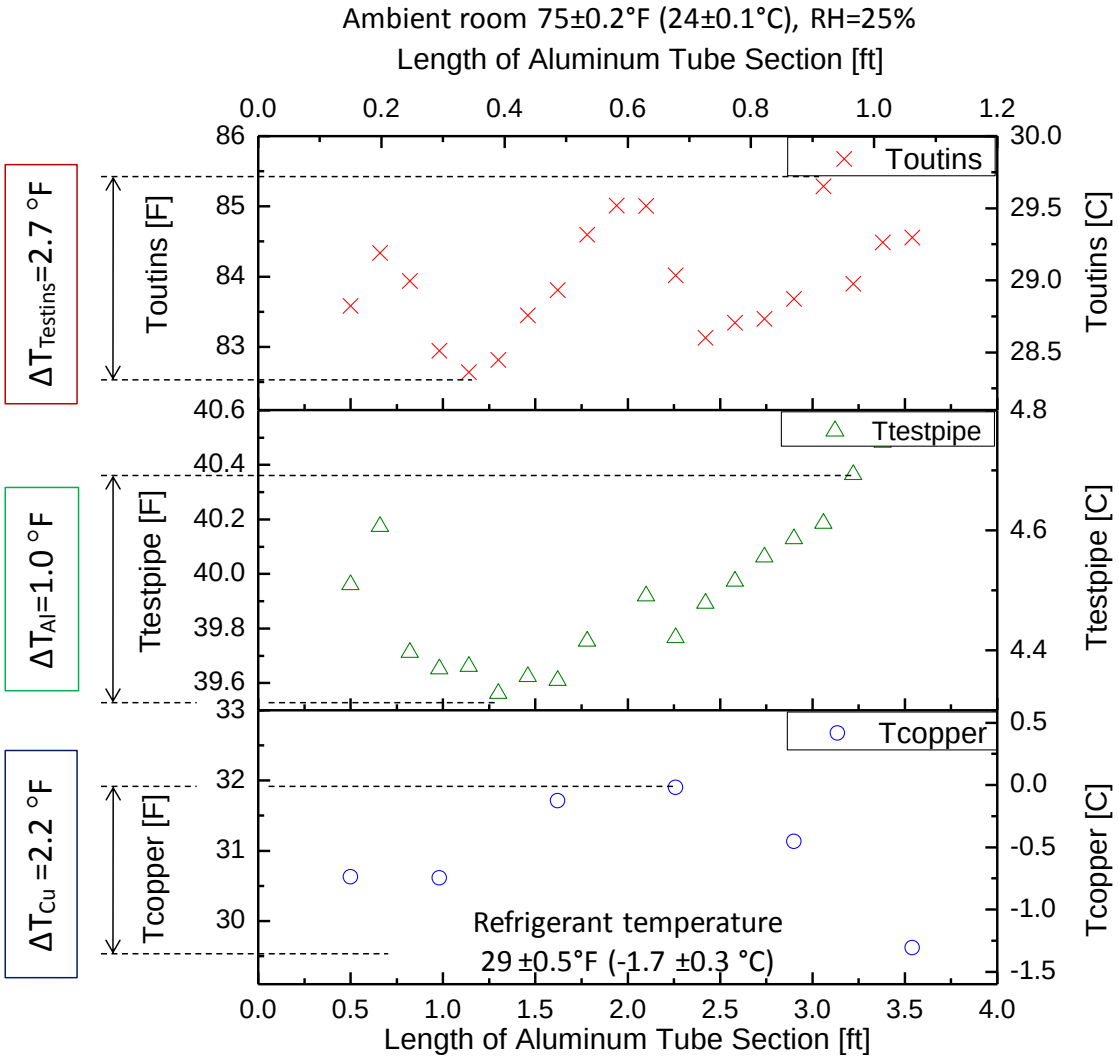

Figure 4.1: Example of surface temperature measurements during a dry test on fiberglass – the first stage (note that thermocouples are positioned along the axial and angular directions that follow a spiral path along the pipe surface)

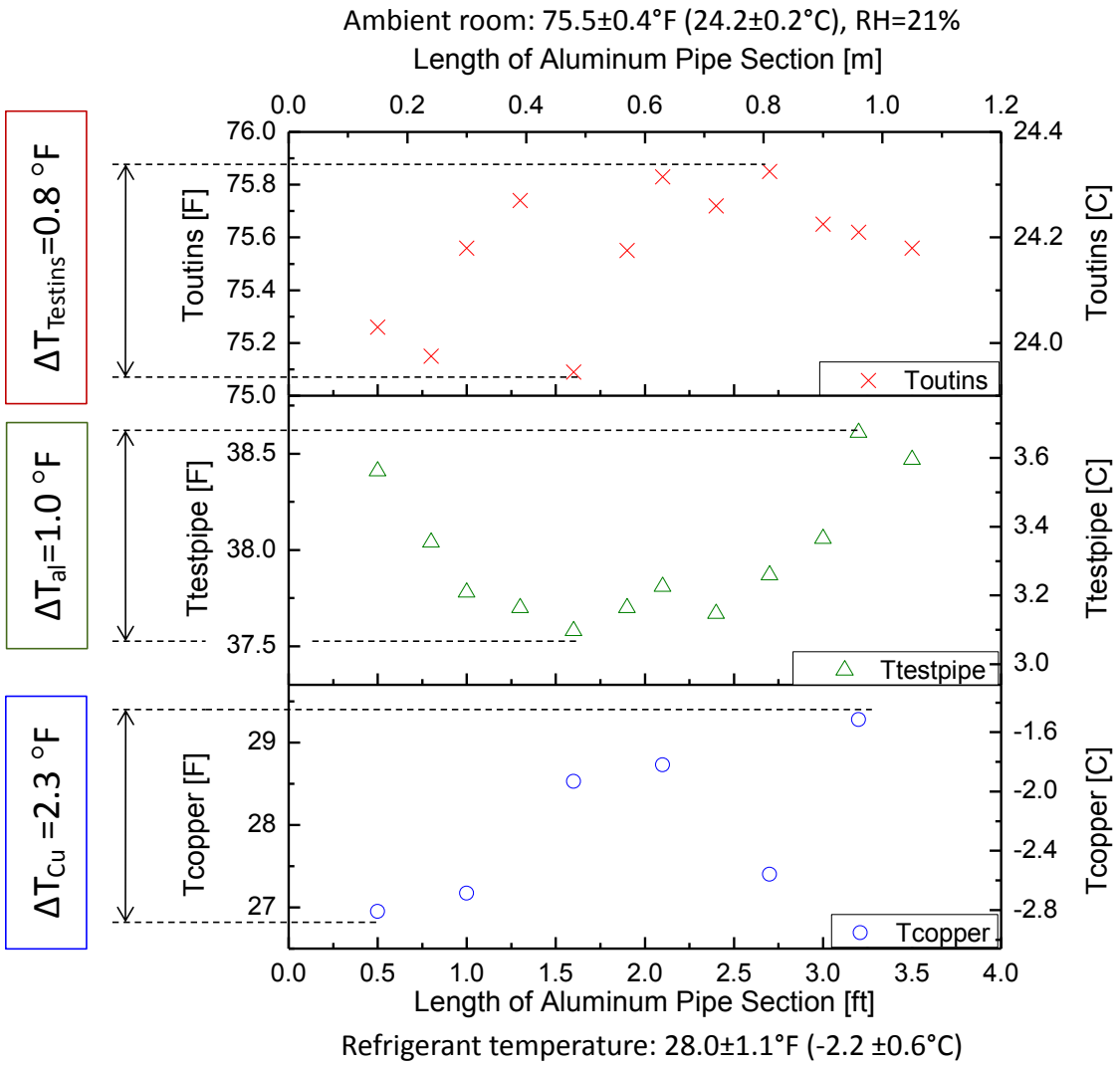

Figure 4.2: Example of surface temperature measurements during a dry test on fiberglass – the second stage (note that thermocouples are positioned along the axial and angular directions that follow a spiral path along the pipe surface)

During the wet tests the ambient was controlled at a high temperature and high humidity to accelerate the moisture absorption in the pipe insulation systems. The ambient temperature was normally controlled between 90 to 107 ℉ (32 to 42 ℃), with the average relative humidity adjusted between 81 to 87%. Under such conditions, the air dew point temperature was significantly higher than the aluminum pipe surface temperatures and ranged from 84 to 100.4 ℉

(29 to 38 ℃). Figure 4.3 shows the surface temperature measurements on the first day of fiberglass pipe insulation wet test. While the aluminum pipe surface temperature was controlled to about 40°F ± 0.6°F (4.5°C ± 0.3°C) for both the dry-test and for the wet test, the ambient temperature were 75°F in Figure 4.1 (fiberglass in dry non-condensing conditions) and 100°F in Figure 4.3 (first day of fiberglass in wet condensing conditions). The temperature distributions along the surfaces were quite similar for both cases and the discrepancy of all temperature sensors reading the pipe insulation exterior surface increased by 0.3 ℉ (0.17 ℃), that is, from $\Delta T_{testins}$ of 2.7°F in dry non-condensing condition (see Figure 4.1) to $\Delta T_{testins}$ of 3.0°F for the first day of the wet-test (see Figure 4.3). The temperature distribution on the surfaces after 10 days of exposure to humid ambient conditions for fiberglass pipe insulation is shown in Figure 4.4. The temperature profiles on the copper tube, aluminum pipe and insulation specimen exterior surfaces were not as uniform as the ones measured for dry tests. This was due to local wet regions created by water condensate that accumulated around the thermocouples on the exterior surface of the pipe insulation specimen. These wet regions were visually observed and documented during the wet tests using digital photos. Due to the insulation structure and the gravity effects, preferential wet regions developed on the insulation specimen and water droplets accumulated at the bottom shells. The increase of the temperature difference along the vertical direction is evident in Figure 4.4, in which $\Delta T_{testins}$ gradually increased from 3 ℉ (1.67 ℃) at day 1 up to 11 ℉ (6.1 ℃) at day 10. It should be noted that a large temperature difference might be due to local values of the temperature readings in which the water condensate droplets were adjacent to the thermocouple beads. Thermal bridges might have been occurred due to local regions of wet insulation. The temperature readings were not uniform because of the insulation material was not homogeneously wet along the axial and angular directions. Since 20 thermocouples were used on each surface, the average surface temperatures calculated from all temperature readings were still a good representation of the exterior temperatures of the aluminum pipe and pipe insulation surfaces.

With all 3D effects introduced for wet insulation conditions, the assumption of a 1-D heat transfer model is an approximate approach that was simple but accurate enough to be useful in practice. The thermal conductivity value calculated in wet conditions was representative of the average conductance of heat across the pipe insulation specimen in wet conditions with moisture accumulated (non-uniformly) on the insulation material.

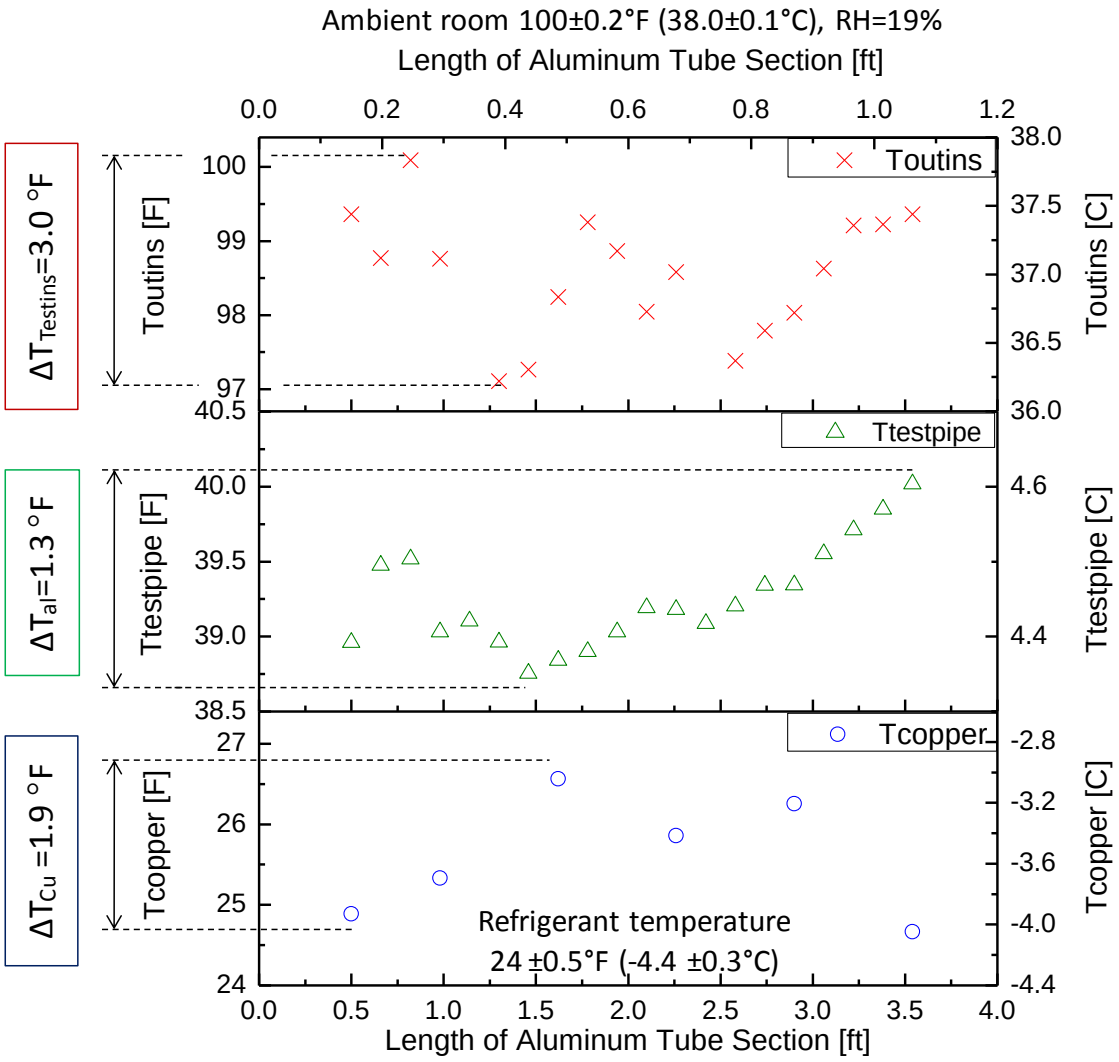

Figure 4.3: Example of surface temperature measurements on the first day of fiberglass moisture test (note that thermocouples are positioned along the axial and angular directions that follow a spiral path along the pipe surface)

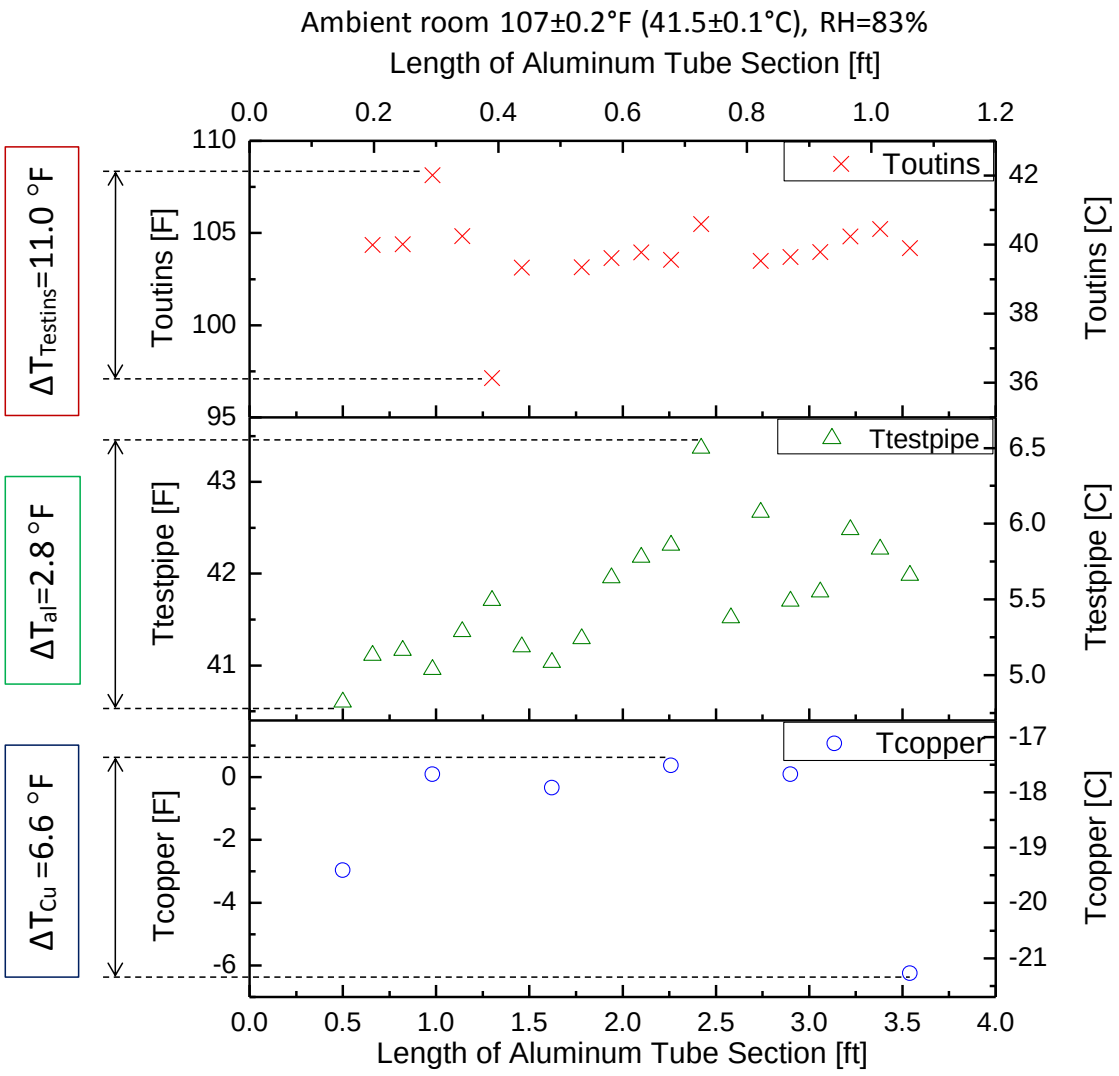

Figure 4.4: Example of surface temperature measurements on the 10th day of fiberglass moisture test (note that thermocouples are positioned along the axial and angular directions that follow a spiral path along the pipe surface)

4.2 Experimental procedures

4.2.1 Experimental procedures for calibration test

Calibration tests were required at the beginning of each dry test and at the end of each moisture test, as a periodically check on the effective thermal conductivity of the sand. Although the sand was completely sealed in the plastic bag, with two plugs tightly blocked at the ends of the test pipe, a calibration test was necessary to detect any potential moisture penetration into the aluminum pipe from the small cracks of the seals between plugs and metal pipe surfaces, if present. The calibration results served for correcting any potential variation of the sand thermal conductivity due to moisture accumulation.

During the calibration, two tape electric heaters were installed evenly on the surface of the aluminum pipe, and they were controlled by a variable transformer. A watt transducer was used to measure the power to the electric heater. A large volume of rubber foam insulation was applied around the heaters to limit the heat gains from the ambient. From preliminary tests, it was found that thermocouple readings were quite sensitive to the power of the tape heaters due to the electric interferences from the direct contact of the electric tape heater with the aluminum pipe surface. Therefore, a layer of wax paper was tightly wrapped below the tape heaters to provide an extra layer of electrical insulation. Another layer of thin film aluminum foil was tightly sandwiched between the tape heaters and the exterior rubber foam insulation in order to evenly distribute the heat from the electric heater to the aluminum pipe and avoid local hot spots that could potentially damage the thermocouple wires. The entire aluminum pipe and corresponding thermocouples were electrically grounded to reduce electric noise.

4.2.2 Experimental procedures for dry non-condensing testes

For the apparent thermal conductivity measurement under dry conditions, two different procedures were proposed at different stages of this project. These procedures will be explained in detail in the following paragraphs.

Procedure in the first stage

In the first stage, two PITs were required during one single test. The first PIT was served for the thermal conductivity measurement, while the second PIT was tested simultaneously to monitor the sand thermal conductivity. The steps to calculate the apparent thermal conductivity of one pipe insulation system are shown in the algorithm of Figure 4.5. The first PIT measured the radial heat flux across the sand, and the thermal conductivity of the pipe insulation system was obtained from the sand thermal conductivity and temperature measurements across the pipe insulation system. The sand thermal conductivity was determined during the initial calibration of the apparatus. The second PIT was operated under similar thermal boundary conditions as the ones of the first PIT. During the dry test period, the thermal conductivity of the sand in the second PIT was constantly monitored by measuring the electric power to the heaters and the temperature gradient across the sand. If the thermal conductivity of the sand showed an obvious deviation from the initial values then the test on the first PIT was paused. The measured anomaly on the second PIT was assumed to be an indicator that water vapor diffused inside the aluminum pipe. The assumption made was that if the second PIT experienced a failure then the first PIT might have experienced a failure during the same time. With the dry test paused, an intermediate calibration of the sand thermal conductivity in the first PIT was conducted to assess whether the sand thermal conductivity in the first PIT also experienced a measurable variation from its initial value. With updated values of the sand thermal conductivity in the first PIT, the dry test was then re-started again. At the end of the dry test, a final check of the sand thermal conductivity on the first PIT was conducted to assess the overall variation of the sand thermal conductivity during the period of the dry test, if present. This variation was usually small unless water vapor penetrated in

the aluminum pipe and frosted inside the sand. If we assume that there is not any water vapor diffusion into the aluminum pipe then the second PIT is not required for the dry tests. However, the purpose of the second PIT was to verify the above hypothesis and to take corrective actions if anomalies in the sand thermal conductivity were to be detected during the dry tests. Experimental correlations for the sand thermal conductivity on the first PIT were developed to correct the initial sand thermal conductivity to its instantaneous value depending on heat flux, sand average temperature, and time. The algorithm of Figure 4.5 allowed detecting any potential moisture intrusion into the aluminum pipe, stopping the dry test instantly and taking proper corrective actions. Anomaly represents a fluctuation in sand thermal conductivity more than 20%.

While the steps in procedure of Figure 4.5 might seem redundant, we experienced one instance at the beginning of the project in which moisture diffused into the sand inside the aluminum pipe during a dry test. This anomaly was detected by the second PIT and the test was paused to correct and account for the augmented sand thermal conductivity in the first PIT. After re-testing the 2-in (50.8 mm) cellular glass pipe insulation system (system V-CG2 as shown in Table 5.2 of chapter 5), the sand was replaced with new dry sand, and we added a plastic bag and plastic caps in the original design to seal the interior space of the aluminum pipe. We also employed a larger amount of sealant at the end caps with respect to the first prototype. With these improvements on the PITs, which was described in the previous chapter (section 3.1), moisture ingress into the aluminum pipe was never observed. The variation of the sand thermal conductivity during the entire period of testing was within 20% with respect to value obtained from the initial calibration. This variation was estimated to be due to small condensation of water vapor in the aluminum pipe from pre-existing ambient air inside the aluminum pipe.

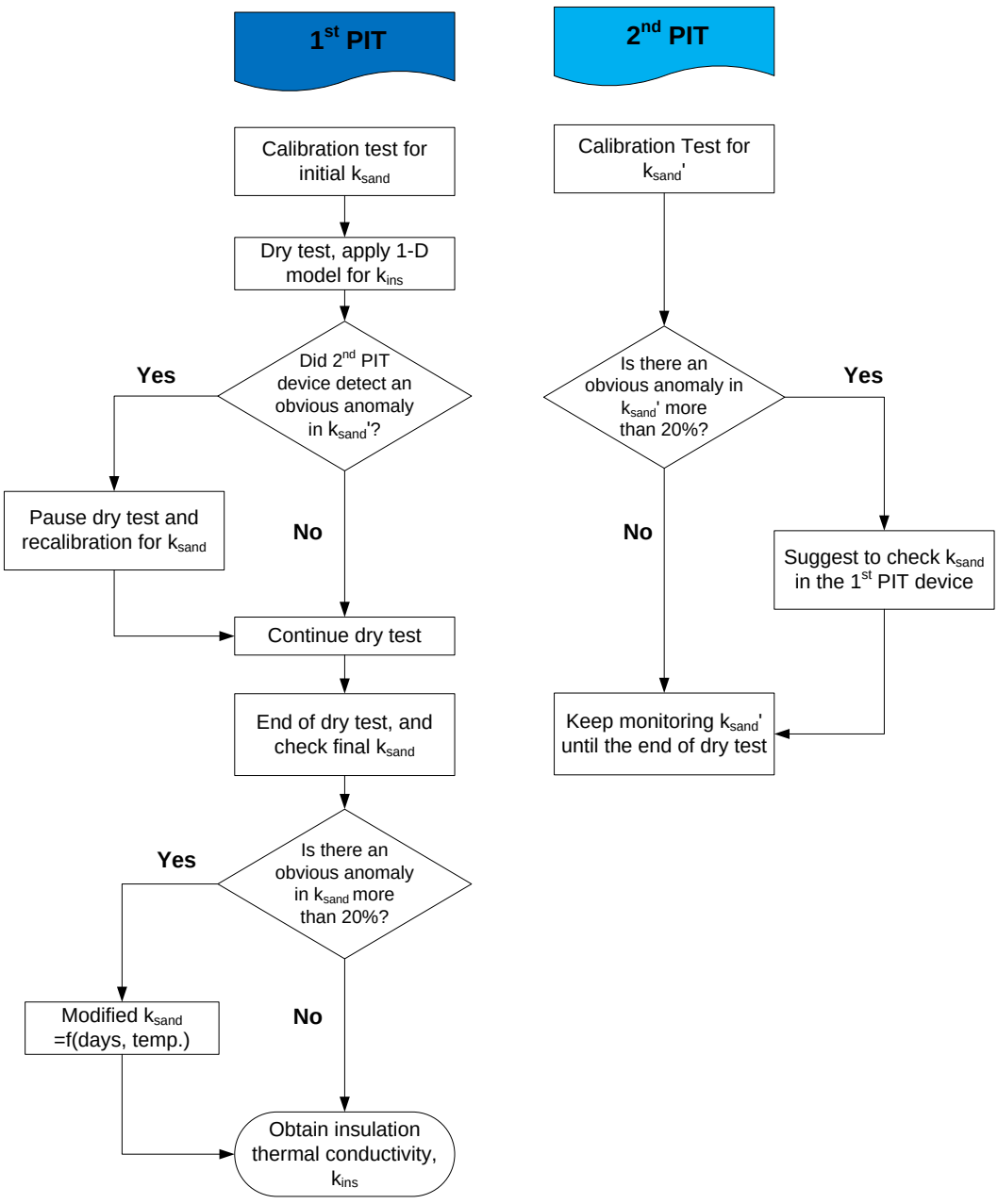

Figure 4.5: Algorithm used in the first stage for measuring the thermal conductivity of pipe insulation, k_{test}, using the first PIT as the main apparatus and the second PIT monitors k_{sand}' (k_{sand} represents the sand thermal conductivity measured in the first PIT, and k_{sand}' represents the sand thermal conductivity measured in the second PIT)

Procedure in the second stage

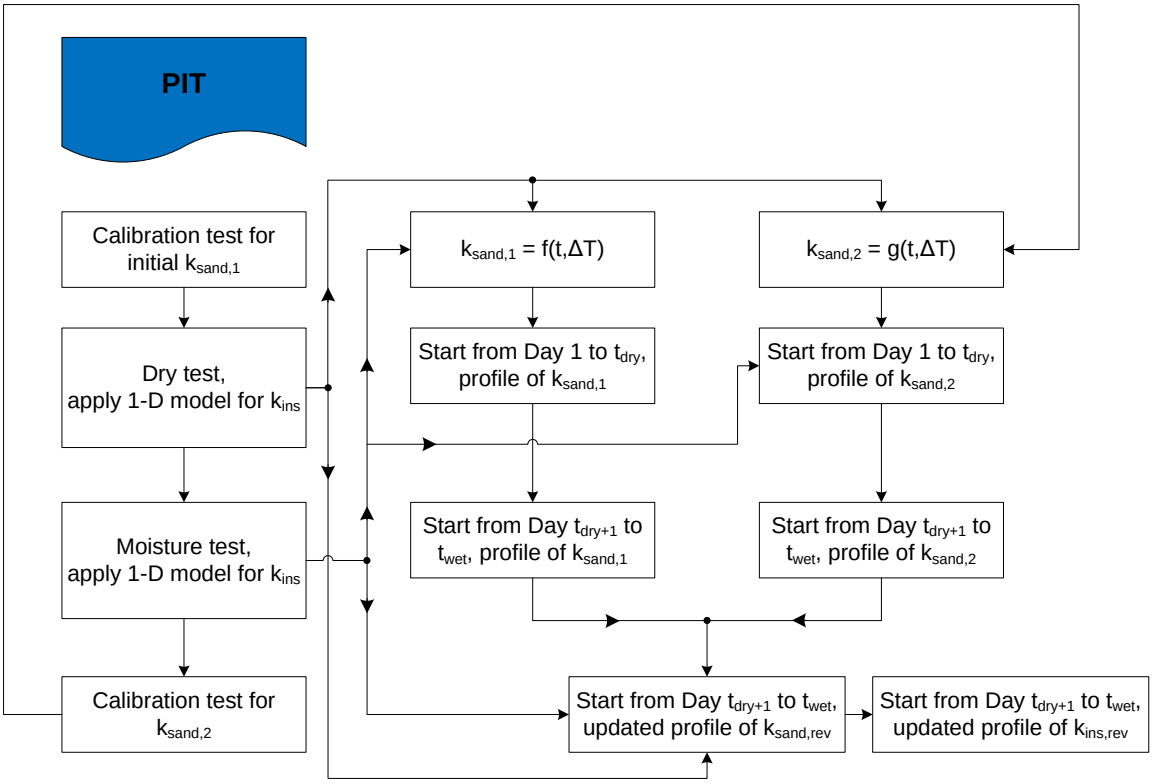

Figure 4.6: Algorithm used in the second stage for measuring the thermal conductivity of pipe insulation, k_{test}, using the revised $k_{sand,rev}$ ($k_{sand,rev}$ represents the sand thermal conductivity integrated between two functions of k_{sand} developed from two calibration tests: one at the beginning of the dry test, and one at the end of the moisture test)

Although the procedure mentioned above did help us detect one vital failure happened in both PITs, the steps in this procedure seem redundant. Pause the dry test for re-calibration, and then continue the dry test is not quite feasible due to the fact that once the pipe insulation system is removed from the PIT, the same test sample is not recommended to be used again because of the attachment to the joint sealant and possible damages from the sample removal. Some of the samples are fragile and can easily be damaged when breaking the longitudinal and butt joints. If continue the dry test with another new piece of the same test sample, it brings in extra errors to the pipe insulation system because of the differences existed between test samples and insulation system installation. Therefore, in the second stage of the project, the experimental procedure was

improved to avoid any interruption during one single test. The steps for the improved procedure are shown in the flow chart provided in Figure 4.8. By following this new procedure, it is not required a second PIT to monitor the variation on the sand thermal conductivity, and each PIT can be served for thermal conductivity measurement independently. This means with the improved method, four pipe insulation systems can be tested at one time under dry conditions. Before each dry test, a calibration test is required to determine the initial correlation of sand thermal conductivity with the sand average temperature and the exterior temperature difference between the ambient and the cold pipe surface, $k_{sand,1} = f(T,\Delta T)$ for example. After the calibration test, the dry test starts and will be followed by the moisture test. By the end of the moisture test, a second calibration test will start immediately for periodical check on the sand thermal conductivity, and the new correlation from the second calibration is $g(T,\Delta T)$, for example ($k_{sand,2} = g(T,\Delta T)$). By only considering $k_{sand,1}$ or $k_{sand,2}$ in the dry and moisture test, I can derive two sets of sand thermal conductivity regarding to the same temperature profile. Assume the sand thermal conductivity varies linearly with time, the revised values on $k_{sand,rev}$ can be interpolated from the two sets of data. For example, according to the temperature profile recorded on the x^{th} day from the beginning of the dry test ($t=t_x$), the sand thermal conductivity is computed as $k_{sand,1x}$ by applying the correlation $f(T,\Delta T)$, which is developed from the initial calibration. With the same temperature profile, but applying the other correlation, $g(T,\Delta T)$ from the second calibration test, the sand thermal conductivity is $k_{sand,2x}$. Therefore, on day x, the revised sand thermal conductivity ($k_{sand,revx}$) is corrected as:

$$k_{sand,revx} = k_{sand,1x} + \frac{t_x - 1}{(t_{dry} + t_{wet}) - 1}(k_{sand,2x} - k_{sand,1x}) \qquad (4.1)$$

Where t_x is the days for testing, t_{dry} is the total days for dry test, and t_{wet} is the total days for moisture test. It should be noted that the first day is considered as $t=1$.

The apparent thermal conductivity of the pipe insulation system measured in both dry and wet conditions will be corrected by the revised sand thermal conductivity, as shown in Equation (4.1). By following this procedure, the variation on the sand thermal conductivity will be considered automatically without spending a spare PIT to monitor any changes that may happen on the sand thermal properties.

4.2.3 Experimental procedures for wet (condensing) test with moisture ingress

Before each wet test, it was critical to determine an initial reference point for the thermal conductivity of the pipe insulation system. Similar cylindrical insulation systems might not have the same thermal conductivity, even if taken from the same material bun. Location in the bun, transportation, storage, and actual installation has an effect on the actual thermal conductivity of the pipe insulation system. To eliminate these effects, the pipe insulation system was installed on the PIT and its thermal conductivity was measured in dry conditions first. Before the moisture test, vapor repellent sealant was applied at two end sides of the pipe insulation test specimen, which were in contact with the insulation of the end thermal guards. At the same time, a second test specimen of the same insulation material batch was cut into six cylindrical sections. Each section was about 6-in (152.4mm) long. Then, the sections were mounted to the second PIT and served to measure the moisture content accumulated in the pipe insulation system during the wet test period. Figure 4.7 shows a schematic of the PITs and the locations in which vapor sealant was applied. Vapor sealan and a plastic film were applied in between each section to prevent axial moisture diffusion from one section to the adjacent one. Each of the 6-in (152.4mm) samples was removed at regular time intervals from the second PIT and replaced with another dry sample of the same insulation material and dimensions. Each sample is weighed, conditioned in an oven, and weighed again to obtain the amount of water mass accumulated in the insulation sample. It should be noted that for fiberglass insulation, the initial moisture content may affect the amount of moisture accumulated in the sample during the wet test. In other words, the initial

moisture content for the fiberglass specimen might have been affected by the ambient relative humidity of the storage space (office room at about 72°F (22.2°C) and 40 to 50% RH). A 6-in (152.4 mm) section of the fiberglass, which was stored in the same storage space, was conditioned at the beginning of the test. The initial moisture content was lower than the accuracy of the scale, that is, less than 0.002 lbm (1 g). Thus, the calculated initial moisture content of the fiberglass was less than 0.4% in volume of insulation, and we assumed that the initial moisture content of the fiberglass sample was negligible. For the closed-cell pipe insulation, some of them are subjected to an "aging" process, and the test specimens were required to be conditioned in the oven at maximum temperature of 158°F (70°C) for three days before the test. Therefore, the initial moisture content was practically zero after the baking process. The amount of water mass accumulated in the sample was obtained as the difference of moisture content between the wet sample and the dry sample. At the end of the wet test period, the last 6-in (152.4mm) sample on the second PIT is removed almost at the same time when the entire test specimen is removed from the first PIT. We postulate that similar moisture diffusion occurred in the two pipe insulation systems during the wet test. Since the insulation test specimens are identical and are exposed to similar thermal and humidity boundary conditions, the above assumption seems reasonable.

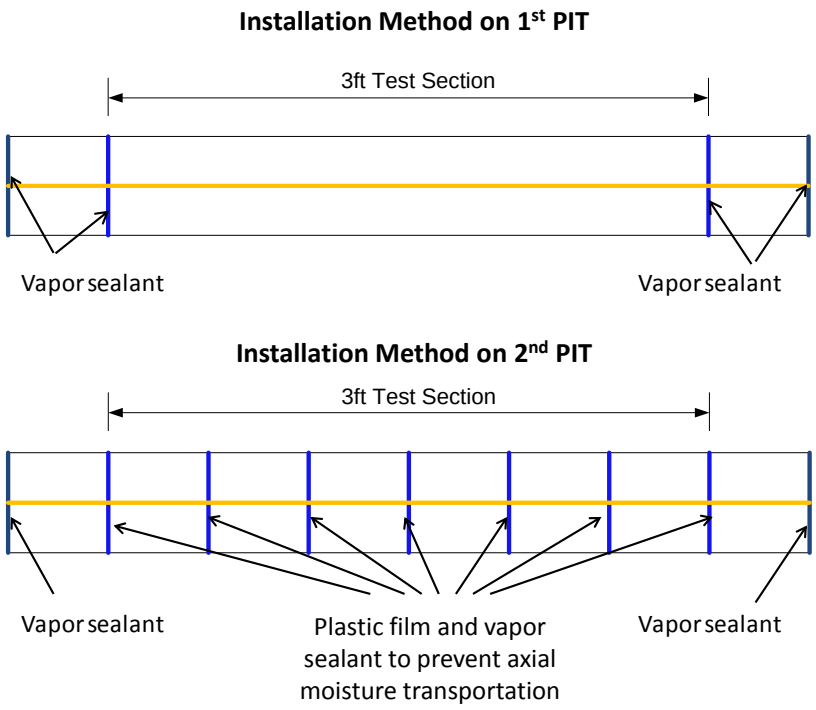

Figure 4.7: Schematic showing the preparation of the insulation test specimens for the wet test

The moisture content of the insulation test specimen is directly measured only at the beginning and at the end of the wet test period. The rate of moisture absorption in the pipe insulation test specimen was obtained by data regression of the moisture content measurements obtained from the samples removed at regular time intervals from the second PIT. A specific sample was shown in chapter 5 section 5.5.1. The water mass accumulated on the pipe insulation system was measured by using the difference in weight of the test specimen in wet conditions with respect to dry insulation. This weight difference represented the moisture mass accumulated in the insulation system during the period of exposure to the wet ambient conditions. For some types of pipe insulation, such as phenolic, cellular glass and PIR, joint sealant was required to apply between two C-shells along the longitudinal joints. Vapor sealant was applied to fill in the gaps in between each 6-in (152.4mm) sample. According to the preliminary in-house tests, both insulation adhesive and vapor sealant absorbed a small amount of moisture. A procedure to

remove the adhesive and vapor sealant by cutting a piece of pure insulation out of the test specimen (taken from the second PIT) is shown in Figure 4.8. The pure insulation sample, i.e. without any adhesive and vapor sealant, is placed in the oven at a baking temperature between 170 to 250 ℉ (77 to 121 ℃) for at least 8 hours. The baking time and baking temperature varied with moisture content and types of insulation. Usually for the highly permeable materials, such as fiberglass, the drying process for baking the entire pipe insulation test specimen was up to three days. Each insulation sample was conditioned in the oven for an enough long period such that its weight did not change in between two consecutive weight measurements. Each weight measurement took place in the ambient room temperature every 12 to 24 hours. If two consecutive weight measurements of the same sample were within 0.0044 lb_m (2 grams) after a baking period, then the insulation sample was considered to have achieved dry conditions. The final weight measurement after the baking process was assumed to be the weight of the dry insulation test specimen. The total amount of water mass accumulated in the insulation system during wet operating conditions was determined from the difference between the wet weight of the sample and the dry weight of the insulation sample.

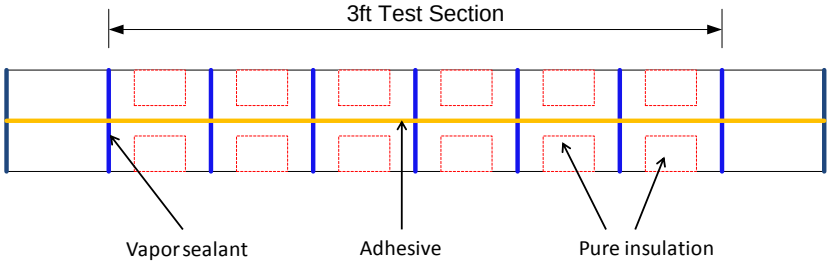

Figure 4.8: Schematic showing the insulation cuts for collecting insulation material without any vapor sealant and adhesive before baking

In order to better compare the system thermal conductivity measured in the moisture test to the value derived under dry condition, a mapping test was added before the moisture test to provide a correlation between the pipe insulation system thermal conductivity and the aluminum pipe

surface temperature. This mapping test was required to be completed with the ambient at the same dry bulb temperature as the one required for the following wet test. However, the ambient humidity should be much lower to maintain the pipe insulation system as dry sample. The correlation derived from the mapping test would help correct the reference value of the pipe insulation thermal conductivity under dry conditions based on different aluminum pipe surface temperatures. With more PITs involved in the moisture test, different types of pipe insulation systems were tested simultaneously under one condition, that is, the same ambient temperature, humidity and the same refrigerant inlet temperature. Considering different properties and installation methods, such as pipe insulation wall thickness, water vapor permeability, usage of vapor retarder and joint sealant, the pipe insulation systems would behave differently during the moisture test, and it might not be possible to maintain the aluminum surface temperatures in all PITs at the same required condition. The mapping test aimed to expand the range of the reference data by including an allowance on the test pipe surface temperature. For example, if the dry test is completed with the aluminum pipe surface temperature maintained at 38˚F (3.3˚C), the mapping test will expand the temperature range to 38 ± 2˚F (3.3 ± 1.1˚C). When the pipe insulation gradually become wet, the aluminum pipe surface may not be able to maintain at 38˚F (3.3˚C) and increased to 39˚F (3.9˚C) due to the enhanced heat transfer. Then the dry reference point would be computed based on the latter aluminum surface temperature to include the change on the boundary conditions.

4.3 Installation of pipe insulation systems

Pipe insulation systems need to be appropriately installed and sealed to eliminate any possibility for moisture penetration from the end edges and any incomplete seals between the insulation joints. For the insulation systems with two C-shells, the joint sealant must be applied as a thin film to cover the entire area, as shown in Figure 4.9a. The two ends of the insulation installed in the center 3-ft (0.9 m) section were required to be sealed with appropriate water vapor sealant, as

shown in Figure 4.9b. The same method was applied on the butt joints between the end guard and the end section next to the test insulation system. It should be emphasized that different pipe insulation systems require different water vapor sealant, and the detailed information on the vapor sealant applied in the specific pipe insulation system was document in detail in chapter 5, from Table 5.12 to 5.14. It was also recommended to seal the cross section of the end guard to completely avoid water vapor transmission (see Figure 4.9). If the pipe insulation system requires any vapor retarder or insulation jacketing, a circumferential seal was recommended on the exterior surface of the vapor retarder next to the end guards to prevent water transmission beneath the vapor retarder and along the exterior surface of the pipe insulation, as shown in the schematic in Figure 4.9. Vapor strip was required if there was joint between two pieces of the vapor retarder.

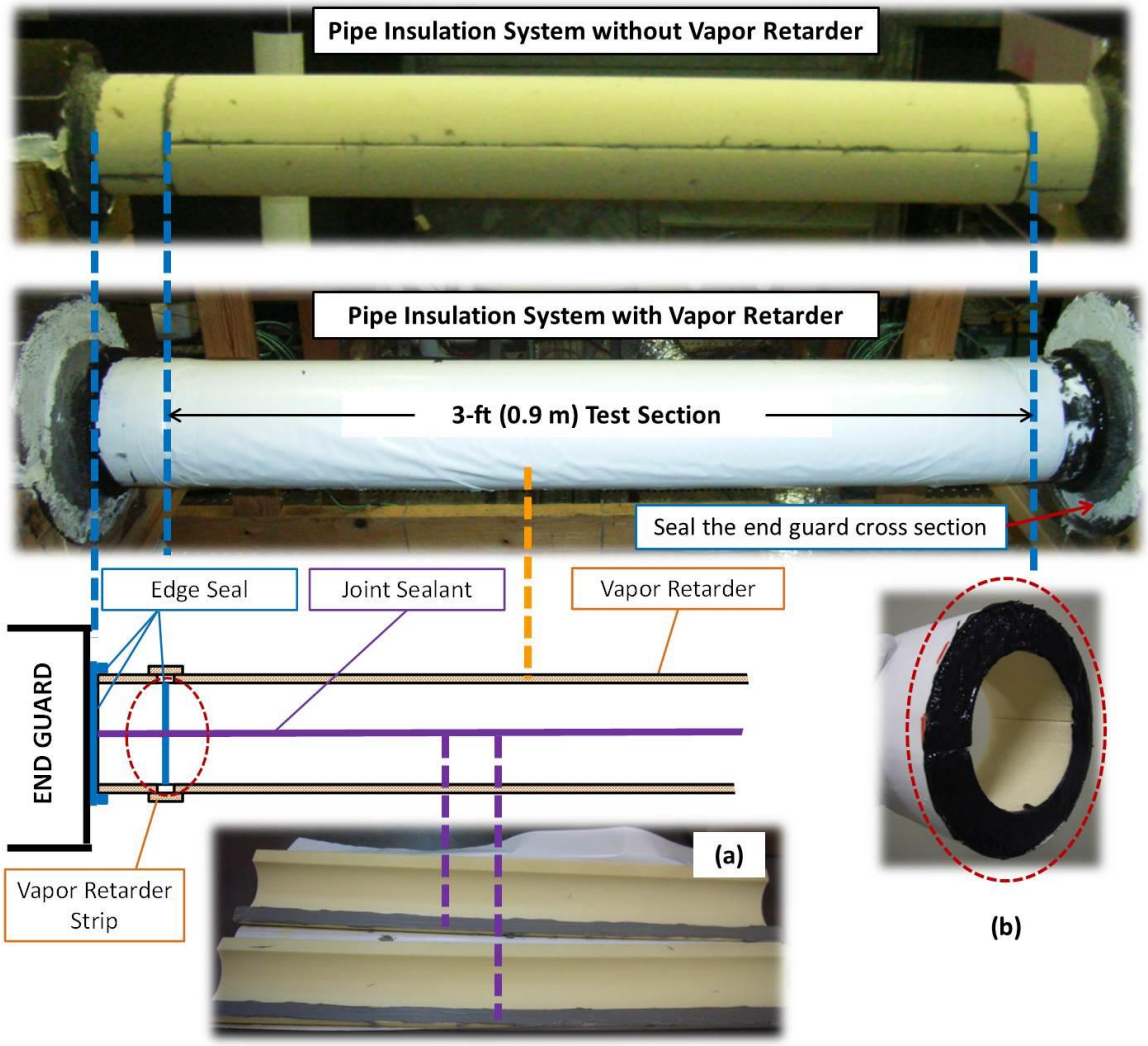

Figure 4.9: Installation and sealing of the pipe insulation systems

4.4 Data reduction

4.4.1 Calibration of the PIT

Calibration was conducted before each dry test to determine the actual thermal conductivity of the sand that filled in the 3-in (76.2 mm) NPS aluminum pipe. The cross section of the radial flux meter that used in the calibration test is shown in Figure 4.10.

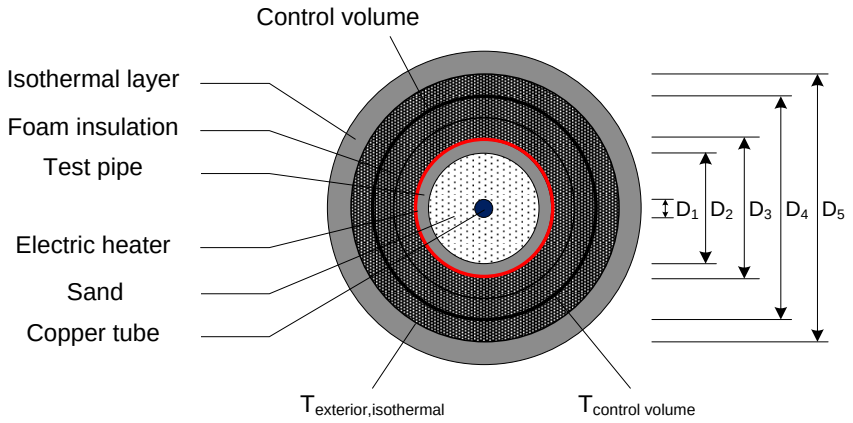

D_1: D_{copper} D_2: $D_{interior,Al,pipe}$ D_3: $D_{exterior,Al,pipe}$ D_4: $D_{control\ volume}$ D_5: $D_{interior,isothermal}$

Figure 4.10: Cross section of radial flux meter inside the PIT

When the electric heater was energized, the total heat transfer into the aluminum pipe, $Q_{Al,pipe}$, was estimated by considering both the electric power in the tape resistor heater, Q_{heater}, and a small amount of heat transfer leaking in from the surrounding ambient through the foam rubber insulation layer and from the end sections of the test apparatus due to axial heat conduction, $Q_{leak,in}$, as given in equation (4.2):

$$Q_{Al,pipe} = Q_{heater} + Q_{leak,in} \tag{4.2}$$

where $Q_{Al,pipe}$ is the total heat transfer rate into the aluminum pipe; Q_{heater} is the heating capacity measured by the watt transducer; $Q_{leak,in}$ is the heat transfer rate leaking in from the environment.

The control volume was selected as shown in Figure 4.10. $Q_{leak,in}$ is estimated by using the following expression for conduction heat transfer in a cylindrical insulation material, as shown in Equation (4.3).

$$Q_{leak,in} = \frac{2\pi k_{foam} L(T_{interior,isothermal} - T_{control\ volume})}{ln\frac{D_{interior,isothermal}}{D_{control\ volume}}} \tag{4.3}$$

Where k_{foam} is the estimated thermal conductivity of outside rubber foam insulation; $D_{interior,isothermal}$ is the interior diameter of the isothermal layer (see Figure 4.10); $D_{control\ volume}$ is the diameter of control volume (see Figure 4.10); L is the length of test section; $T_{interior,isothermal}$ is the interior surface temperature of the isothermal layer; $T_{control\ volume}$ is the surface temperature of the control volume (see Figure 4.10).

During the calibration of the PIT the ambient temperature was adjusted such that the temperature difference across the insulation on the outside of the electric heater was within 5.4°F (3°C). This caused $Q_{leak,in}$ to vary from 3.5 to 4.2 Btu/hr (1.0 to 1.2 W), which represent 7 to 10 percent of the total heat measured from the heater. $Q_{leak,in}$ was accounted for during the calibration procedures to eliminate a systematic error on the actual thermal conductivity of the sand filling the aluminum pipe. It should be emphasized that the actual thermal conductivity of the sand inside the aluminum pipe was slightly different than the thermal conductivity of pure dry sand because the measured values during the calibration procedure accounted for the end effects of the thermal guards, the contribution due to small axial heat flow, and the effects due to the non-uniformity and non-homogenous properties of the sand inside the aluminum pipe. The thermal conductivity of the sand also depended on the percent of quartz and residual moisture in the sand batch used for filling the pipe. Calibration of the aluminum pipe at the same thermal conditions, as the ones occurring during the actual experiments, allowed estimating a value of the sand thermal conductivity that can be used during the dry and wet tests to calculate the radial heat flux. The sand thermal resistance and the axial heat conduction effects of the PIT were approximated as an equivalent sand thermal conductivity that could be used in a 1-D heat conduction equation following Fourier's law. According to the energy balance applied on the aluminum pipe surface: there is:

$$Q_{Al,pipe} = Q_{sand} \tag{4.4}$$

Where Q_{sand} represents the heat transfer rate into sand filling the aluminum pipe.

The axial temperature gradient along the aluminum pipe was less than 0.43% of the radial temperature gradient across the sand. Based on this finding it is reasonable to assume that the axial heat losses on the aluminum pipe are small and a heat balance across the sand yields

$$Q_{sand} = \frac{2\pi k_{sand} L(T_{Al,pipe} - T_{cold,copper,pipe})}{ln\frac{D_{interior,Al,pipe}}{D_{cold,copper,pipe}}} \quad (4.5)$$

where k_{sand} is the effective thermal conductivity of sand; $D_{interior,Al,pipe}$ is the inside diameter of test pipe, Figure 4.10; $D_{cold,copper,pipe}$ is the diameter of copper tube, Figure 4.10; $T_{cold,copper,pipe}$ is the surface temperature of copper tube.

The average sand temperature is

$$T_{sand} = \frac{T_{copper} + T_{Al,pipe}}{2} \quad (4.6)$$

By measuring the power of the electric heater and the temperatures, the thermal conductivity of the sand inside the aluminum pipe was obtained using equations (4.1) to (4.5).

It should be noted that according to (4.3), $Q_{leak,in}$ is highly dependent on the ambient conditions. When the test condition is controlled at a higher temperature, the temperature difference between the exterior surface of the pipe insulation and the aluminum pipe increases, and $Q_{leak,in}$ weights more in Q_{sand}, when compared to the low temperature condition. In order to include the impact from the variation on the boundary conditions, the calibration test was required to be applied at two different ambient temperatures: 56˚F (13.3˚C) and 90˚F (32.2˚C). Two correlations between sand thermal conductivity and average sand temperatures were derived from the measurements under these two ambient conditions in the calibration test. With interpolation between these curves, the sand thermal conductivity was developed as a second power correlation to both the average sand temperature and the exterior temperature difference between the ambient and the

aluminum pipe, shown in Equation (4.7) This improved correlation included the impact of the variation on the boundary conditions and further enhance the system accuracy.

$$k_{sand} = b_1 T_{sand}^2 + b_2 T_{sand} + b_3 \Delta T_{exterior}^2 + b_4 \Delta T_{exterior} + b_5 \quad (4.7)$$

Where b_1 to b_5 are empirical coefficients, $\Delta T_{exterior}$ represents the temperature difference between the ambient and the aluminum pipe.

4.4.2 Pipe insulation system thermal conductivity measurements

Once the thermal conductivity of the sand filling the aluminum pipe, k_{sand}, was obtained from the calibration procedure, a 1-D heat balance equation along the radial direction was applied to the PIT, as shown in the schematic of Figure 4.11. As a result, the pipe insulation thermal conductivity, k_{ins}, was determined directly by the following expression (4.8):

$$k_{ins} = k_{sand} \times \frac{(T_{Al,pipe} - T_{cold,copper,pipe})}{(T_{exterior,ins,specimen} - T_{Al,pipe})} \times G_f \quad (4.8)$$

Where G_f is a geometry factor that depends on the ratios of pipe insulation exterior diameter, the aluminum pipe outer diameter, and refrigerating copper tube outer diameters, as shown in Figure 4.11. The diameters of the pipe insulation were measured according to the standard ASTM C585 (ASTM, 2009).

The average temperature of the test insulation specimen was calculated from the measurements of the surface temperature sensors as follows:

$$T_{avg,ins,specimen} = \frac{T_{Al,pipe} + T_{exterior,ins,specimen}}{2} \quad (4.9)$$

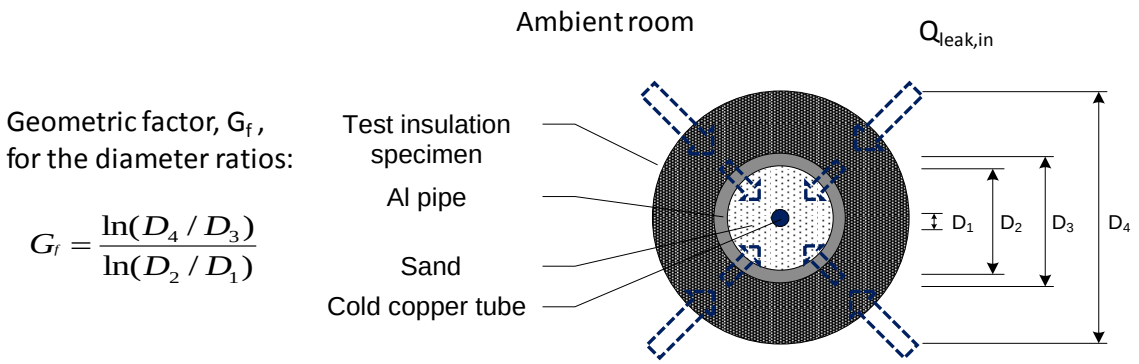

Figure 4.11: Schematic of the 1-D model of the Pipe Insulation Tester (PIT) and corresponding diameters

4.4.3 Moisture Content Measurements in the Pipe Insulation System

The moisture content in the pipe insulation systems during the wet tests was calculated as percentage of the water volume per unit volume of pipe insulation. Moisture mass was measured from the weight difference of the samples in wet and dry conditions. Then the water mass was divided by a reference density of water, which was assumed constant at 62.43 lbm/ft^3 (1000 kg/m^3) (at 39.2 ℉/ 4 ℃). The volume of pipe insulation system was measured from its actual geometry. The overall expression for moisture content is as follows:

$$V_{moisture}(\%) = \frac{(m_{wet,specimen} - m_{dry,specimen})}{\rho_{water}} \cdot \frac{1}{V_{specimen}} \times 100 \cdot \qquad (4.10)$$

Where $V_{moisture}$ is the volume of water present in the insulation system; $V_{specimen}$ is the volume of the insulation system; $m_{wet,specimen}$ is the weight of the wet insulation system; $m_{bake,specimen}$ is the weight of the dry insulation system after being conditioned in the oven; ρ_{water} is the water density at 39.2 ℉ (4 ℃).

4.5 Experimental Uncertainty

4.5.1 Uncertainty on the thermal conductivity of pipe insulation system

A complete uncertainty analysis was conducted and calculations were carried out by using a numerical model of the test apparatus that was developed in EES (Engineering Equation Solver, (Klein, 2006). The experimental data for the axial and radial temperature measurements were input to the numerical model of the PIT device. The uncertainty on the system apparent thermal conductivity was estimated according to the Taylor series expansion method as follows (Taylor, 1997):

$$U_Y = \sqrt{\sum_i (\frac{\partial Y}{\partial X_i})^2 U_{Xi}^2} \tag{4.11}$$

where U_Y represents the uncertainty of the variable Y and U_X represents the precision accuracy of the measured variable X. The uncertainty on the pipe insulation thermal conductivity was calculated following a similar approach and it resulted as in equation (4.12):

$$\begin{aligned} U_{k\,ins}^2 = {} & (\frac{\partial k_{ins}}{\partial k_{sand}})^2 U_{k\,sand}^2 + (\frac{\partial k_{ins}}{\partial k_{Al,pipe}})^2 U_{T\,Al\,pipe}^2 \\ & + (\frac{\partial k_{ins}}{\partial k_{cold,copper,pipe}})^2 U_{T\,cold,copper,pipe}^2 \\ & + (\frac{\partial k_{ins}}{\partial k_{exterior,ins,specimen}})^2 U_{T\,exterior,ins,specimen}^2 + (\frac{\partial k_{ins}}{\partial G_f})^2 U_{G\,f}^2 \end{aligned} \tag{4.12}$$

Where each term in parenthesis represents the coefficient of sensitivity for the variable of interest (X_i) and the U_{Xi} on the right hand side of equation (4.12) are the uncertainty associated with the variable X_i. The uncertainty on the thermal conductivity depended on the thermocouple accuracy and on the time averaged spatial uniformity of the temperatures along the axial and angular

directions of the PIT device. All temperature sensors were calibrated in-situ and the bias uncertainty was computed according to the approach provided by Johnson *et al*. (1998) and summarized below:

$$B_{Tdistribution} = (T_{max} - T_{min}) / N \quad (4.13)$$

$$B_T = \sqrt{B_{Tdistribution}^2 - B_{Tuniform}^2} \quad (4.14)$$

Where $B_{Tdistribution}$ is the bias uncertainty resulting from the actual non-uniform temperature distribution, $B_{Tuniform}$ is the bias uncertainty present even with a uniform temperature distribution and it was estimated from equation (4.13) with T_{max} and T_{min} set as the acceptable limits for ideal condition of uniform surface temperature, B_T is the total bias uncertainty, and N is the total number of measuring points in the grid.

Accuracy and precision of the sensors used during the measurements for both stages are given in Table 4.1 and 4.2. The uncertainties on the effective thermal conductivity of sand and the apparent thermal conductivity of test specimen were plotted with unit heat flux, as shown in Figure 4.12a and b. (Figure 4.12a represents the first stage and Figure 4.12b represents the second).

It is observed that in both cases the uncertainty on the effective thermal conductivity of the sand filling the aluminum pipe is the main factor affecting the uncertainty of the pipe insulation system thermal conductivity. The two uncertainties follow similar trends with the latter being amplified by the accuracy of the temperature measurements. Due to the better calibration on the temperature sensors in the second stage, as shown in Table 4.2, the uncertainty was significantly improved, especially in the low heat flux range. In the current test apparatus, when the radial heat flux was larger than 10.4 Btu/hr-ft (10 W/m) it was estimated that the uncertainty on the pipe

Table 4.1: Accuracy and maximum spatial variation of the temperature measurements of the PIT (Phase I)

Parameter	Manufacturer	Model	Accuracy	Max Spatial Variation	Uncertainty
Foam insulation thermal conductivity	Armacell	Armaflex	± 10%		± 10%
Watt transducer	Flex-Core	AGW-001E	± 0.05% F.S. (± 0.25W)		± 0.04% F.S. (± 0.25W)
Thermocouples (copper tube)	Omega	T-type	± 0.36 ℉ (± 0.2 ℃)	± 1.5 ℉ (± 0.8 ℃)	± 0.44 ℉ (± 0.25 ℃)
Thermocouples (aluminum pipe)	Omega	T-type	± 0.18 ℉ (± 0.1 ℃)	± 0.8 ℉ (± 0.4 ℃)	± 0.18 ℉ (± 0.1 ℃)
Thermocouples (insulation)	Omega	T-type	± 0.18 ℉ (± 0.1 ℃)	± 2.1 ℉ (± 1.2 ℃)	± 0.21 ℉ (± 0.12 ℃)
Diameter (copper pipe)	N/A	N/A	± 0.010 in (± 0.254 mm)	N/A	± 0.010 in (± 0.254 mm)
Diameter (aluminum pipe)	N/A	N/A	± 0.015 in (± 0.381 mm)	N/A	± 0.015 in (± 0.381 mm)
Diameter (pipe insulation)	N/A	N/A	± 0.0625 in (± 1.6 mm)	N/A	± 0.0625 in (± 1.6 mm)

Table 4.2: Accuracy and maximum spatial variation of the temperature measurements of the PIT (Phase II)

Parameter	Manufacturer	Model	Accuracy	Max Spatial Variation	Uncertainty
Foam insulation thermal conductivity	Armacell	Armaflex	± 10%		± 10%
Watt transducer	Flex-Core	AGW-001E	± 0.04% F.S. (± 0.2W)		± 0.04% F.S. (± 0.2W)
Thermocouples (copper tube)	Omega	T-type	± 0.14 ℉ (± 0.08 ℃)	± 1.8 ℉ (± 1.0 ℃)	± 0.33 ℉ (± 0.18 ℃)
Thermocouples (aluminum pipe)	Omega	T-type	± 0.11 ℉ (± 0.06 ℃)	± 1.1 ℉ (± 0.6 ℃)	± 0.14 ℉ (± 0.08 ℃)
Thermocouples (insulation and ambient)	Omega	T-type	± 0.14 ℉ (± 0.08 ℃)	± 1.3 ℉ (± 0.7 ℃)	± 0.18 ℉ (± 0.10 ℃)
Diameter (copper pipe)	N/A	N/A	± 0.010 in (± 0.254 mm)	N/A	± 0.010 in (± 0.254 mm)
Diameter (aluminum pipe)	N/A	N/A	± 0.015 in (± 0.381 mm)	N/A	± 0.015 in (± 0.381 mm)
Diameter (pipe insulation)	N/A	N/A	± 0.0625 in (± 1.6 mm)	N/A	± 0.0625 in (± 1.6 mm)

insulation system thermal conductivity was about ±5 % and the uncertainty of the sand thermal conductivity was within ±4%, as shown in Figure 4.12. With the temperature boundary conditions of the aluminum pipe surface temperature at 38°F (3.3°C) and room temperature between 56 to 90˚F (13.3 to 32.2˚C), the PITs improved in the second stage could accurately measure the pipe insulation system thermal conductivity with a heat flux as low as 8.2 Btu/hr-ft (7.9 W/m). Compared to the uncertainty profile derived from previous apparatus, which showed a dramatic increase on the uncertainty of sand thermal conductivity when the radial heat flux was below 8.6 Btu/hr-ft (8.3 W/m), the present system was able to maintain the uncertainty in a larger range, especially in the low heat flux region. This is a significant improvement because under dry condition, the heat transfer through pipe insulation systems remains at a low level, around or even below 10.4 Btu/hr (10 W/m) in most cases. With the improved test apparatus, more pipe insulation systems, such as those with larger wall thicknesses and lower thermal conductivity, can be tested with acceptable uncertainties. However, it should be noted that the uncertainty might increase dramatically when the heat flow drops below 8.2 Btu/hr-ft (7.9 W/m). This limitation was due to the fact that the measured heat transfer from the tape heaters during the calibration process becomes too small and in particular becomes lower than 1% of the maximum range of the watt transducer. In these conditions the uncertainty on the power measurements increased drastically. In the low range of the electric heater, the heat from the ambient into the sand became a higher fraction of the total heat gain, and the uncertainty on the heat gain from the ambient became a significant contributor to the overall uncertainty of the sand thermal conductivity.

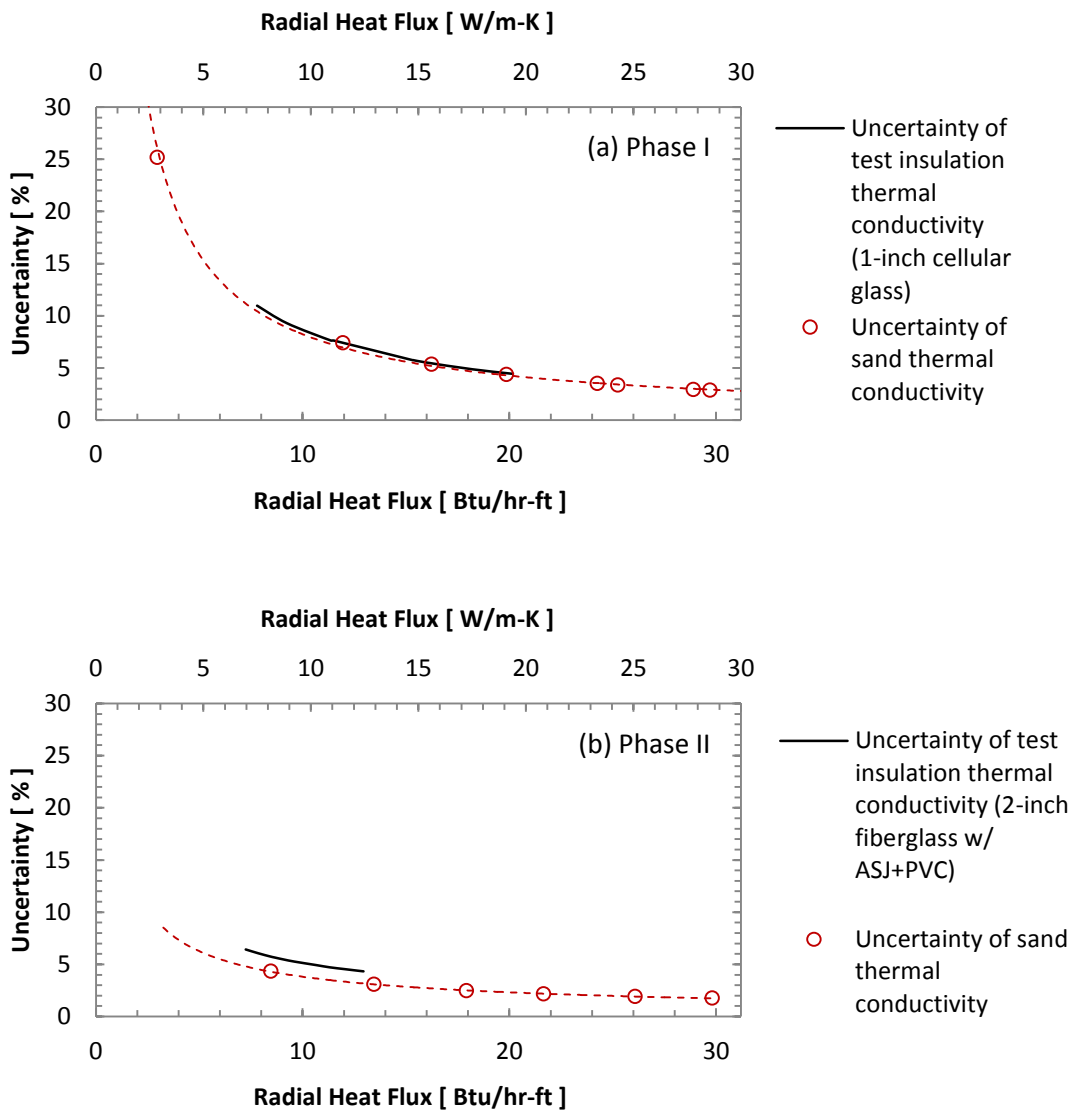

Figure 4.12: Uncertainties of the sand thermal conductivity and pipe insulation system thermal conductivity versus radial heat flux per unit length (data from the calibration phase of the PIT with electric heater around the aluminum pipe)

4.5.2 Uncertainty on the moisture content in the pipe insulation system

The moisture content was computed from the water mass divided by the volume of the pipe insulation system, which was estimated from the insulation actual geometry. The uncertainty on

the moisture content was determined by the accuracy of the scale, and the human error in the measurement of the insulation dimensions, as listed in Table 4.3.

Table 4.3: Accuracy of the moisture gains measurement during the tests in wet conditions

Moisture Gains Uncertainty Table				
Parameter	**Manufacturer**	**Model**	**Nominal Value**	**Accuracy**
Scale	AMW	AMW-13	0 ~ 13 lb (0 ~ 6 kg)	±0.1oz (3 g)
Length/Thickness/Diameter	N/A	N/A		±1/8 in (0.381 mm)

The relative uncertainty of the moisture content decreased with water content in the insulation, as shown in Figure 4.13. The relative uncertainty would be high when the water content was below 2% by volume while it would be within ±5% if the water content is above 4% by volume. The scale accuracy was the limiting factor in determining the uncertainty of the moisture content.

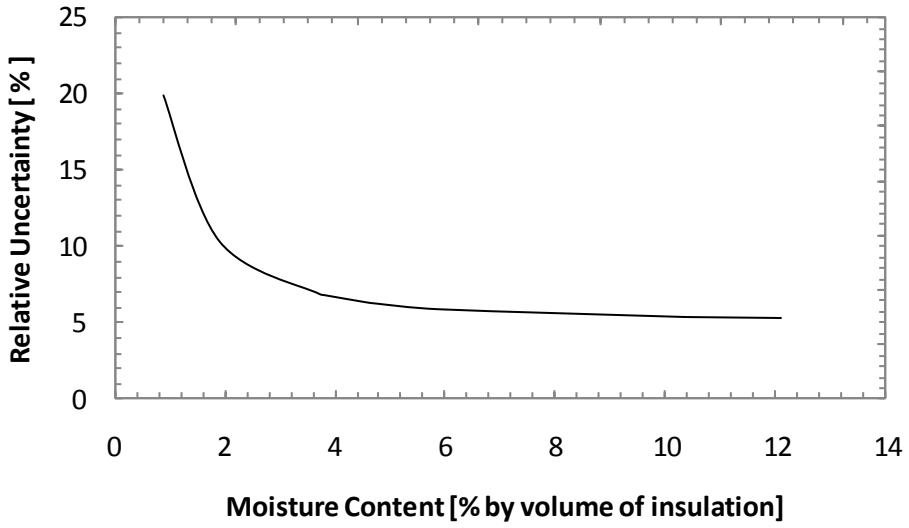

Figure 4.13: Relative uncertainty on the moisture content measured in the pipe insulation specimen

CHAPTER V

5. EXPERIMENTAL RESULTS

The capability of the test apparatus and test methodology described in previous chapters was demonstrated by the validation tests on four pipe insulation systems, and the test results will be present in this chapter. Fifteen pipe insulation systems, including both fibrous and closed-cell pipe insulation with different thicknesses, were tested for system thermal conductivity under dry conditions. The test results were documented and critically compared. Ten pipe insulation systems were selected for the moisture test under wet, condensing conditions. The variation on the system thermal conductivity and moisture content in the pipe insulation systems were discussed in detail at the end of this chapter.

5.1 Thermal conductivity validation test results for two types of pipe insulation systems

During the validation phase two types of pipe insulation systems, cellular glass and polyiscoyanurate (PIR) were tested on the experimental apparatus which was constructed in the first stage. All the pipe insulation systems were tested without insulation jacketing, and more information on the systems is listed in Table 5.1. The pipe insulation mean temperature was varied between 50 to 77 ℉ (10 to 25 ℃). The ambient temperature was varied from 68 to 117 ℉ (20 to 47 ℃), with the cold copper pipe surface temperature controlled from 12 up to 39 ℉ (-11 to 4 ℃) depending on radial thermal gradients required to maintain the aluminum pipe surface temperature at 40.5 ℉ ± 0.5 ℉ (4.7 ℃ ± 0.3 ℃). The chamber humidity was set as low as possible

to reduce any moisture effect, and the dew point temperature of the ambient air was below the aluminum pipe surface temperature.

Table 5.1: Pipe insulation systems in the validation test

Test Systems (Ref. No.)	Thickness in (mm)	Joint Sealant	Edge Seal
Cellular Glass (V-CG1)	1 (25.4)	Boss 368 Butyl Rubber Sealant	Boss 368 Butyl Rubber Sealant
Cellular Glass (V-CG2)	2 (50.8)		
Polyisoyanurate (V-PIR1)	1 (25.4)		
Polyisoyanurate (V-PIR2)	2 (50.8)		

5.1.1 Cellular glass pipe insulation systems V-CG1 and V-CG2

Cellular glass insulation is a lightweight, rigid insulating material that is used in industrial and commercial applications. Composed of completely sealed glass cells, which are defined as insulating spaces, this material is filled with CO_2 as the main gas without any significant aging effect.

Two thicknesses of cellular glass pipe insulation were selected during the validation phase: 1-in (25.4 mm) and 2-in (50.8 mm). Due to manufacturing constraints, the test samples were provided with a full length of 2-ft (0.61 m) (ASTM_C552, 2012). As shown in Figure 5.1, the top C-shells and bottom C-shells of the test insulation were staggered installed on the aluminum pipe. All the joints were sealed with Boss 368 butyl rubber sealant. The sealant thickness was about 1/8-in (3.175 mm) and it was applied following an "S" pattern on the edge of the pipe shells. Then the two C-shells were tightly pressed together around the PIT, and the sealant was flattened in a thin layer. It should be noted that this insulation system was the first type tested in the PIT. The application method of the joint sealant was different from the method used on the rest of the insulation systems. The joint sealant was usually applied as a thin layer through the entire longitudinal joints of the C-shells for the remaining insulation systems in both dry and wet tests.

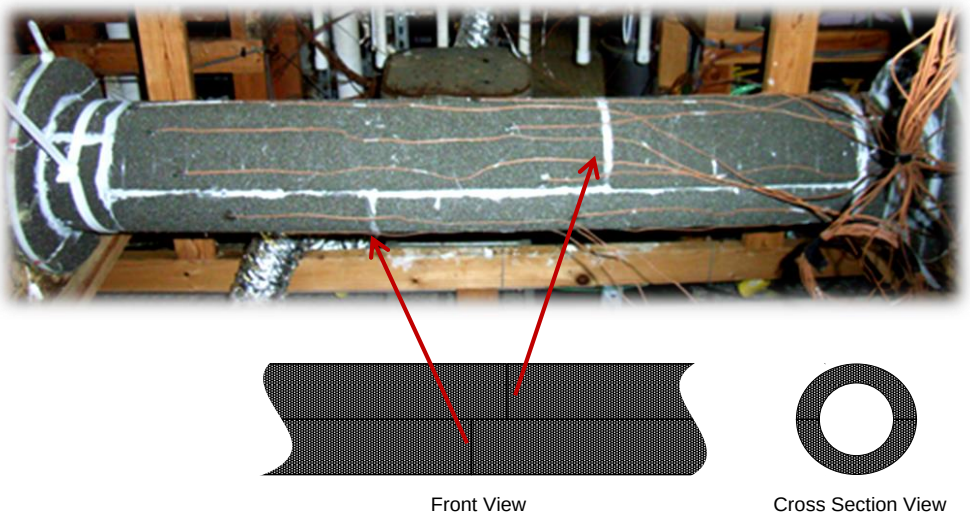

Figure 5.1: Schematic of the installation of the cellular glass test specimen on the PIT

The test results on these two cellular glass pipe insulation systems were listed in Table 5.2, with detailed measurement values tabulated in Appendix B. Based on the previous works from the literature (Wilkes *et al*., 2002; Macfadden, 1988), the correlation between the insulation thermal conductivity and insulation mean temperature was highly possible to follow a linear trend. Figure 5.2 compares the measured thermal conductivity versus insulation mean temperature at 1-in (25.4 mm) and 2-in (50.8 mm) nominal wall thickness of cellular glass pipe insulation systems. The error bar in the figure represents the maximum deviation of experimental data from a linear fit curve.

The data in Figure 5.2 were obtained by using droplets of silicone gel covering the tips of the thermocouples to attach the thermocouples on the exterior surface of the pipe insulation. Silicone gel beads had a low thermal conductivity of 0.7 to 6.9 Btu-in/hr-ft^2-F (0.1 to 1.0 W/m-K). They acted as adhesive and created a large thermal barrier at the interface between the tip of the thermocouples and the air film boundary layer surrounding these sensors. The data in Figure 5.2 might suggest that the cellular glass thermal conductivity was depended on the insulation wall thickness. However, one fact should be taken into account before drawing the above conclusions.

Table 5.2: Validation experiment results of cellular glass pipe insulation systems

Test Systems (Ref. No.)	Cellular Glass Thickness in. (mm)	Thermocouple Attachment	System Thermal Conductivity $^{*}k_{pipe,insulation} = a \cdot T + b$ Btu-in/hr- ft^2- ℉ (W/m-K)		Heat flux per unit length Btu/hr-ft (W/m)
			a	b	
Cellular Glass (V-CG1)	1 (25.4)	Silicone	0.0010 (0.00025)	0.2425 (0.0394)	14.6 (14.1)
Cellular Glass (V-CG2)	2 (50.8)	Silicone	0.0021 (0.00055)	0.1643 (0.0335)	9.8 (9.4)
Manufacturer Catalog	-	-	0.0006 (0.00014)	0.2498 (0.0386)	---

*: T is in ℉ (℃)

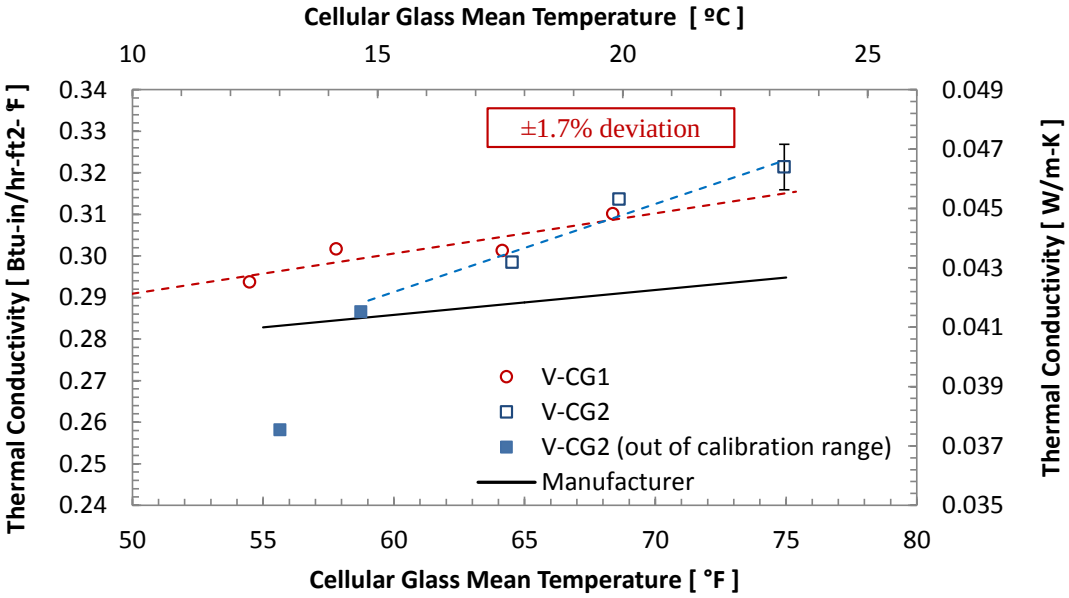

Figure 5.2: Thermal conductivity of cellular glass pipe insulation systems V-CG1 and V-CG2

For cellular glass pipe insulation system V-CG2 with 2-in (50.8 mm) nominal wall thickness, two points were measured with the radial heat flux lower than the calibration range of the test apparatus, which was about 8.6 Btu/hr-ft (8.3 W/m-K). Measured with this low heat flux, not only the uncertainty for the sand thermal conductivity increased, a systematic error was also present.

The systematic error could not be eliminated because it was caused by the physical limitations of the end sections to act as adiabatic thermal guards. Thus, the assumption of negligible axial heat conduction was not valid when the heat flux was below the calibration lower limit.

Compared to the manufacturer's data, which was obtained on 1-in (25.4 mm) flat slabs according to the standard ASTM C518 (ASTM, 2010), the thermal conductivity of cellular glass pipe insulation at different mean insulation temperatures is given in Table 5.3. The maximum discrepancy was 9.2% for cellular glass pipe insulation system V-CG2 and 7.7% for the system V-CG1.

Table 5.3: Comparison cellular glass data of the present work with manufacturer catalog

Mean Insulation Temperature ˚F (˚C)	**Thermal Conductivity Btu-in/hr- ft^2-F (W/m-K)**			**Percentage Difference %**	
	V-CG1	V-CG2	manufacturer catalog	V-CG1 v.s. manufacturer	V-CG2 v.s. manufacturer
75 (23.9)	0.318 (0.4589)	0.322 (0.4645)	0.295 (0.0426)	7.7	9.2
65 (18.3)	0.308 (0.0444)	0.301 (0.0434)	0.289 (0.0417)	6.5	4.2
60 (15.5)	0.303 (0.0434)	0.209 (0.0301)	0.286 (0.0413)	5.8	1.6
55 (12.8)	0.298 (0.0430)	0.280 (0.0404)	0.283 (0.0408)	5.2	-1.1

5.1.2 Polyisocyanurate (PIR) pipe insulation system V-PIR1 and V-PIR2

Two polyisocyanurate (PIR) pipe insulation systems with different nominal wall thicknesses, 1-in (25.4 mm) and 2-in (50.8 mm), were selected as a second type of material to demonstrate the capabilities of the developed test apparatus. Unfortunately PIR is subjected to aging phenomena and the system thermal conductivity will be a function of time. In order to eliminate the aging effects, two groups of test samples, radial C-shells and flat slabs, were taken from a same batch of the insulation material. The flat slab insulation specimens were tested at Oak Ridge National Laboratory while the cylindrical C-shell specimens were tested on the PIT at the OSU laboratory

at approximately the same time. The results of the experiments are shown in Figure 5.3, and the correlations for the pipe insulation system thermal conductivity are given in Table 5.4. Similar to the system V-CG2, the PIR pipe insulation system V-PIR2 with 2-in (50.8 mm) nominal wall thickness performed more sensitive to the temperature when compared to the system V-PIR1, which was at 1-in (25.4 mm) nominal wall thickness. One possible reason was that the radial heat flux in the system V-PIR2 was below the lower calibration limit of the test apparatus. The effective thermal conductivity of sand was not measured for heat flux below 11.5 Btu/hr-ft (11.1 W/m) at the time the validation tests on systems V-PIR1 and V-PIR2 were conducted. While extrapolation of the sand thermal conductivity for heat fluxes of about 9.7 Btu/hr-ft (9.3 W/m) might be still considered acceptable, heat fluxes in the range of 5.14 Btu/hr-ft (4.94 W/m) were clearly out of the calibration range of the apparatus. By the end of the validation test on the system V-PIR2, a failure was detected on the second PIT for moisture migration into the aluminum pipe, and both PITs were disassembled right after the test to replace the wet sand with new dry sand. The re-constructed PITs could reach a lower limit on the radial heat flux, around 8.6 Btu/hr-ft (8.3 W/m-K), as the one applied for the cellular glass pipe insulation system V-CG2. In order to improve the uncertainty of the test apparatus, it would be necessary to decrease the aluminum pipe surface temperature to below 40°F (4.5°C) and provide a larger radial temperature gradient. The PIR pipe insulation system V-PIR1 was measured at a higher radial heat flux, and results showed that differences existed on the measured thermal conductivity between the pipe insulation system and the flat slab specimens, which were tested by the Building Envelopes Research Group at OakRidge National Laboratory. The differences were up to 8.8%. These differences might be due to the edge effects of the longitudinal split joints and the presence of the joint sealants along the joints between the two C-shells. The anisotropy of the PIR cells is another potential factor that could explain this discrepancy. The PIR samples were cut out at different locations of the same batch, and this might result in some differences on the physical properties of the test samples.

Table 5.4: Experimental results for PIR pipe insulation systems

Test Systems (Ref No.)	Thermocouple Attachment	System Thermal Conductivity $^{*}k_{pipe,insulation} = a \cdot T + b$ Btu-in/hr- ft^2- ℉ (W/m-K)		Heat flux per unit length Btu/hr-ft (W/m)
		a	b	
V-PIR1	Silicone	0.0004 (0.00009)	0.1748 (0.0270)	9.70 (9.33)
**V-PIR2	Silicone	**0.0032 (0.00083)	-0.0284 (0.0107)	5.14 (4.94)

*: T is in ℉ or ℃

**: k_{sand} is out of the calibration range – these data have larger uncertainty

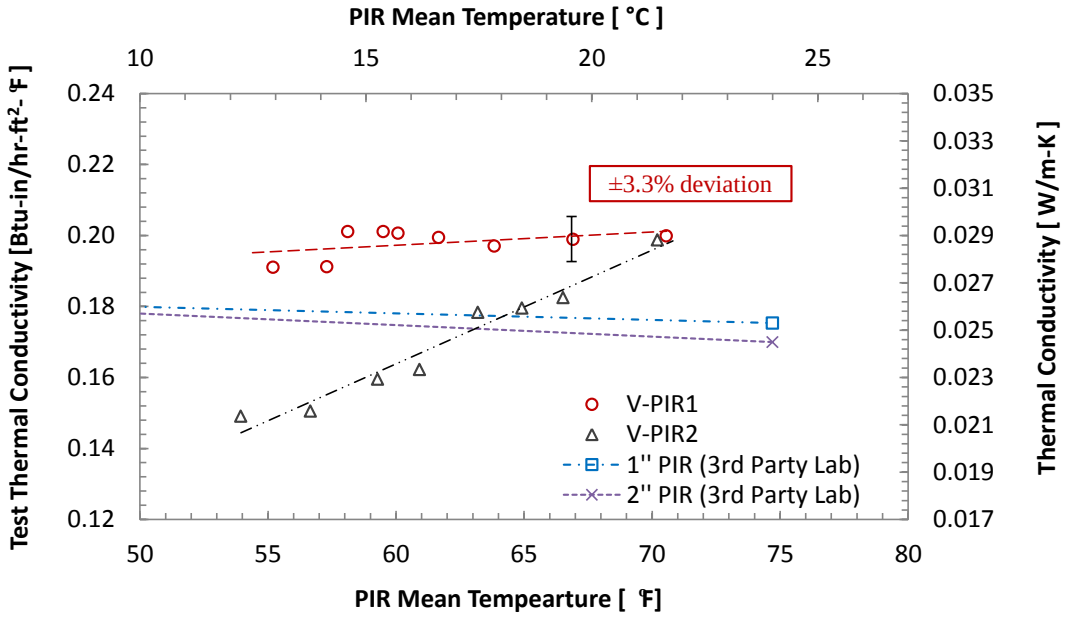

Figure 5.3: Thermal conductivity of PIR pipe insulation systems V-PIR1 and V-PIR2

5.2 Thermal conductivity tests results under dry non-condensing conditions (in the first stage)

The thermal conductivity of fiberglass, elastomeric rubber and phenolic pipe insulation systems was measured during the first stage of this project in dry non-condensing ambient conditions. Detailed information on the tested pipe insulation systems is listed in Table 5.5.

Table 5.5: Pipe insulation systems tested under dry conditions (in the first stage)

Test Systems (Ref. No.)	Thickness in (mm)	Joint Sealant	Edge Seal
Fiberglass (P1-FG)	2 (50.8)	N/A	Foster 90-66 and Foster 30-80
Elastomeric Rubber (P1-ER)	2 (50.8)	Aeroseal	Aeroseal
Phenolic (P1-P1)	1 (25.4)	Boss 368 Butyl Rubber Sealant	Boss 368 Butyl Rubber Sealant
Phenolic (P1-P2)	2 (50.8)		

The nominal wall thicknesses of these pipe insulation systems were between 1-in (25.4 mm) to 2-in (50.8 mm), and the insulation mean temperatures were varied from 57 to 74 ℉ (14 to 23 ℃). Any vapor barrier and external jacketing was removed from the pipe insulation systems. Correlations of the pipe insulation thermal conductivity were developed based on the insulation mean temperature and the wall thicknesses. It is found that the thermal conductivity of these four insulation systems increased linearly with the insulation mean temperature, as shown in Figure 5.4, and this result agrees with previous observations provided in the literature (Abdou & Budaiwi, 2013; Budaiwi *et al.*, 2002; Litovsky *et al.*, 2008; Saxena *et al.*, 1989). The coefficients of the linear correlations are given in Table 5.6, and the experimental data fit well in these linear interpolation curves with deviations less than ±1.2%. It should be noted that for fiberglass, elastomeric rubber, and phenolic pipe insulation systems, the experiments were based on the re-constructed PITs with updated calibrations on the test apparatus. Learning from the previous tests with PIR, more data points were collected in the low radial heat flux region. In the calibration of the re-constructed PITs, the heat transfer rate in a 3-ft (0.9 m) long section ranged from 23.8 Btu/hr (6.97 W) to 103.7 Btu/hr (30.4 W), that is, a heat flow per unit length from 7.9 Btu/hr-ft (7.6 W/m) to 34.6 Btu/hr-ft (33.3 W/m). However, in order to maintain the uncertainty below

±10%, the minimum radial heat flux across the pipe insulation system should be 8.6 Btu/hr-ft (8.3 W/m-K). The average heat flux for the four pipe insulation systems are listed in Table 5.6, and the values in systems P1-FG, P1-ER, and P1-P1 are within the range for which the calibration of the test apparatus was conducted. Phenolic pipe insulation was tested in two systems, P1-P1 and P1-P2 with different nominal wall thicknesses. The experimental findings in Figure 5.4 and the coefficients in Table 5.6 suggests that there might be a slight change in the slope of the pipe insulation system thermal conductivity when the nominal wall thickness increases from 1-in (25.4 mm) to 2-in (50.8 mm). This might due to the edge effects of the split joints, that is, the lateral sections of two C-shell joints. It should be noted that the change of slope might also be caused by the test apparatus limitations since the heat flux for phenolic pipe insulation system P1-P2 at 2-in (50.8 mm) nominal wall thickness was about 7.1 Btu/hr-ft (6.9 W/m), and it was slightly below the calibration limit of the test apparatus of 7.9 Btu/hr-ft (7.6 W/m). Thus the uncertainty on the data points for the 2-in (50.8 mm) phenolic was larger (more than ±10%).

Table 5.6: Thermal conductivities of pipe insulations under dry condition

Test Samples (Ref. No.)	**System Thermal Conductivity** $^{*}k_{pipe,insulation} = a \cdot T + b$ **Btu-in/hr- ft^2-F (W/m-K)**		**Heat flux per unit length Btu/hr-ft (W/m)**
	a	**b**	
Fiberglass (P1-FG)	0.0004 (0.00010)	0.2101 (0.0320)	7.91 (7.61)
Elastomeric Rubber (P1-ER)	0.0005 (0.00014)	0.2144 (0.0334)	8.38 (8.06)
Phenolic (P1-P1)	0.0007 (0.00018)	0.1821 (0.0297)	13.2 (12.7)
Phenolic (P1-P2)	0.0012 (0.00032)	0.1217 (0.0233)	7.13 (6.86)

*: T is in ℉ or ℃

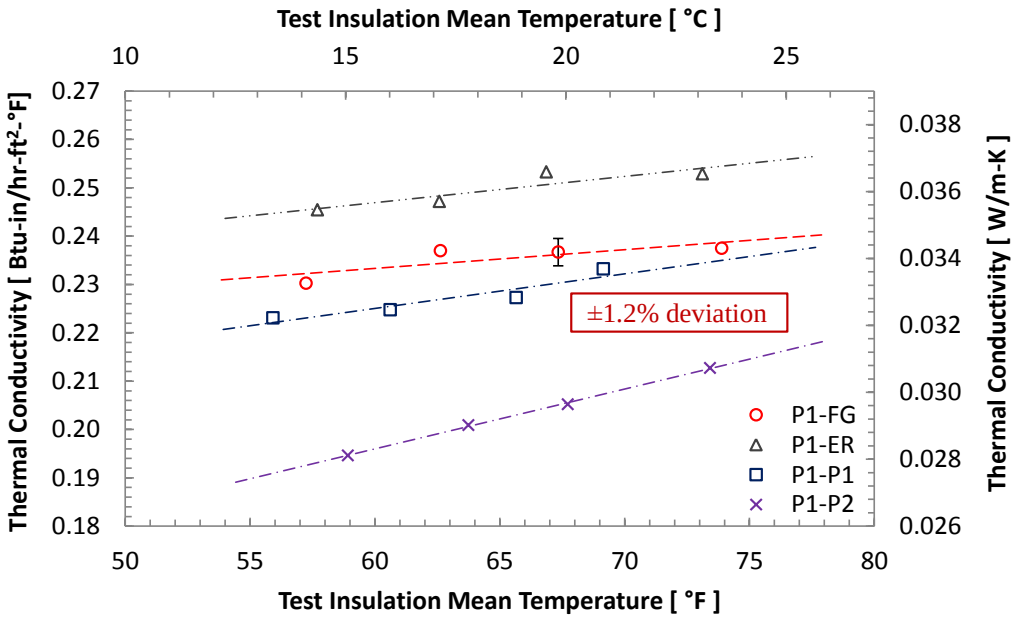

Figure 5.4: Thermal conductivities of fiberglass, elastomeric rubber (flexible elastomeric) and phenolic pipe insulation systems with 1 to 2-in (25.4 to 50.8 mm) nominal wall thickness

The effect of joint sealant on the measured thermal conductivity of mechanical pipe insulation systems was further investigated based on phenolic pipe insulation systems P1-P1 and P1-P2 with different nominal wall thicknesses. Applying joint sealant is a recommended installation procedure by the manufacturer, and we investigated edge effects that the compound might have on the actual thermal conductivity of the pipe insulation system. Figure 5.5 shows the data derived from the tests on the 1-in (25.4 mm) thick phenolic pipe insulation systems both with and without joint sealant along the longitudinal joints. The thermal conductivity of the pipe insulation system with joint sealant was higher than the one without joint sealant. The thermal bridge at the edges might cause an increase in the system apparent thermal conductivity. The joint sealant was first applied all the way through the cross sections of the longitudinal joints with a thickness around ¼-in (6.4mm) when the C-shells were open. Then the C-shells were tightly assembled around PITs, and the actual thickness of the joint sealant was not directly measurable. It seems

that the edge effects from the joint sealant applied on the longitudinal joints of the C-shells increased the actual thermal conductivity by as much as 15%.

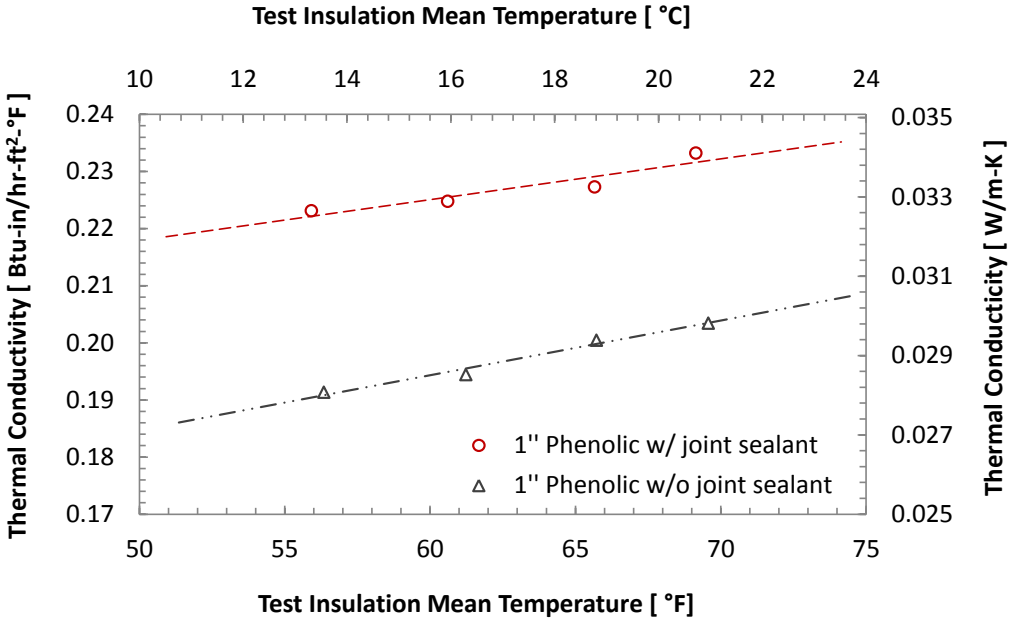

Figure 5.5: Effect of joint sealant on the thermal conductivity of phenolic pipe insulation system with 1-in (25.4 mm) nominal wall thickness

The joint sealant effect was further investigated by considering an overall thermal resistance that combines insulation material, air gap and joint sealant, as shown in the schematic of Figure 5.6. Any additional layer of joint sealant between the two half shells of the pipe insulation might create a thin layer of air gap between the aluminum pipe and interior pipe insulation interface. The thermal resistances of joint sealant along the longitudinal joints can be considered as in parallel to the insulation thermal resistances, and the conductive joint sealant may create thermal bridging in the insulation systems. With reference to Figure 5.6 an equivalent overall thermal resistance can be calculated as follows:

$$R'_{combined} = R'_{airgap} + \frac{1}{\frac{1}{R'_{joint\ sealant}} + \frac{1}{R'_{ins}}} \tag{5.1}$$

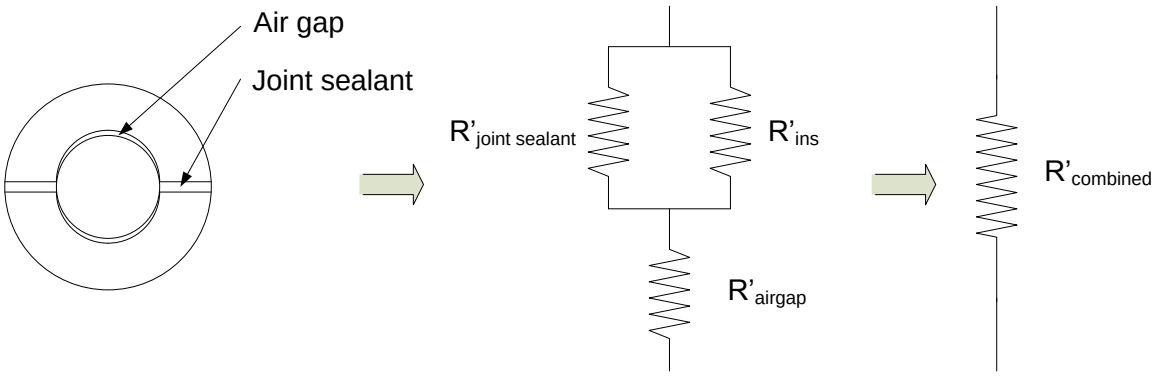

Figure 5.6: Sketch of combined thermal resistance when considering joint sealant in the pipe insulation

The value for the equivalent combined thermal resistance is dependent on the joint sealant thermal conductivity and thickness. Figure 5.7 shows the experimental and simulation results on the phenolic pipe insulation system P1-P1. The triangles in the figure represent the measured thermal conductivity of phenolic pipe insulation without joint sealant, while the circles provide the measured thermal conductivity of the same phenolic pipe insulation specimen with joint sealant. The experimental data without joint sealant were used to calculate R'_{ins} in the Equation (5.1). Then, a sensitivity study was conducted in an attempt to replicate the experimental data with joint sealant as shown in Figure 5.7. An example is reported below to illustrate the effects of joint sealant. Equation (5.1) was applied by assuming that the thickness of joint sealant varied from 1/16-in (1.59mm) to 1/10-in (2.54 mm), and the sealant thermal conductivity varied between 2.8 Btu-in/hr-ft^2-F (0.4 W/m-K) and 4.9 Btu-in/hr-ft^2-F (0.7 W/m-K). The sensitivity of the combined thermal conductivity to the joint sealant thickness and thermal conductivity is quite large. The combined thermal conductivity computed from equation (5.1) could be within 0.5% of

the experimental data when the joint sealant was assumed to have a thickness of 1/16-in (1.59 mm) and a thermal conductivity of 4.44 Btu-in/hr-ft^2-F (0.64 W/m-K). Based on this sensitivity analysis, the joint sealant edge effect was postulated to be the factor that increased the thermal conductivity of phenolic pipe insulation system.

Example of sensitivity of the combined thermal conductivity of the pipe insulation to joint sealant (the first points shown as round dot and triangle in Figure 5.7)

pipe insulation mean temperature = 55.9°F (13.3°C)

joint thermal conductivity = 4.44Btu-in/hr-ft^2-F (0.64 W/m-K)

joint sealant thickness =1/16 in. (1.59 mm)

R'_{ins}= 1.5 hr-F/Btu (2.9 C/W)

k'_{ins}=0.19 Btu-in/hr-ft^2-F (0.027 W/m-K)

$$R'_{joint\ sealant} = \frac{D_{exterior,ins} - D_{exterior,Al,pipe}}{4k_{joint\ sealant}\delta_{joint\ sealant}L} = 7.2 \text{ hr-F/Btu (13.7 C/W)}$$

Where $D_{exterior,ins}$ is the exterior diameter of the pipe insulation with joint sealant; $D_{exterior,Al,pipe}$ is the exterior diameter of test pipe; L is the length of test section; $k_{joint\ sealant}$ is the thermal conductivity of the joint sealant; $\delta_{joint\ sealant}$ is the thickness of the joint sealant.

$$R'_{airgap} = \frac{\ln[(D_{exterior,Al,pipe} + \delta_{airgap})/D_{exterior,Al,pipe})]}{2\pi k_{airgap}L} = 0.03 \text{ hr-F/Btu (0.06 C/W)}$$

Where k_{airgap} is the thermal conductivity of the air gap; δ_{airgap} is the thickness of the air gap.

And finally

$R'_{combined}$= 1.3 hr-F/Btu (2.5 C/W)

$$k'_{combined} = \frac{\ln(D_{exterior,ins}/D_{exterior,Al,pipe})}{2\pi R'_{combined} L} = 0.22 \text{ Btu-in/hr-ft}^2\text{-F } (0.032 \text{ W/m-K})$$

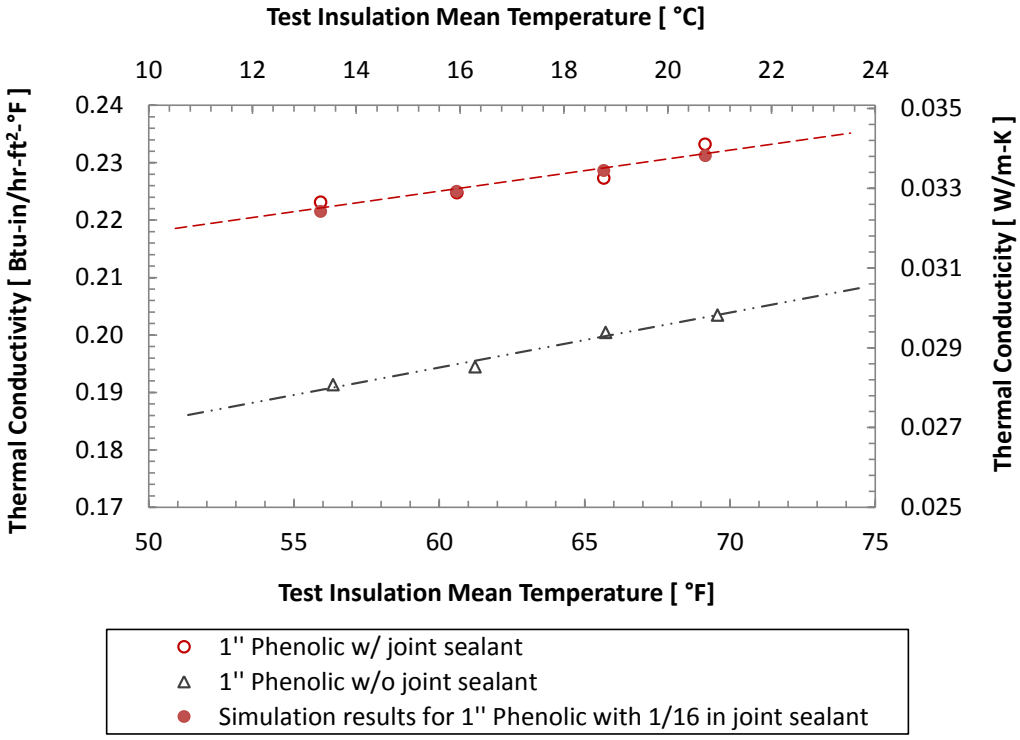

Figure 5.7: Simulation results by considering the joint sealant effect on the thermal conductivity of phenolic pipe insulation system with 1-in (25.4 mm) nominal wall thickness

5.3 Sensitivity analysis of the joint sealant on the thermal conductivity measurements in dry, non-condensing conditions

A sensitivity analysis was conducted to investigate the impact of the thickness and thermal conductivity of joint sealant based on the experimental results on cellular glass pipe insulation system V-CG1 with 1-in (25.4 mm) nominal wall thickness. It should be noted that insulation system V-CG1 was tested three times during the validation phase, but in the previous section, this thesis only reported the experimental results from the second test. In order to make a better explanation, I named these three tests on cellular glass pipe insulation system V-CG1 as test A, B

and C. According to the measurements during tests B and C on cellular glass pipe insulation system V-CG1, the OD of the sample, which was calculated around 5.22-in (132.6 mm) in the test A, increased from 5.375 to 5.6-in (136.5 to 142.2 mm) due to the application of extra joint sealant on the longitudinal joints (the ODs were measured from the exterior perimeter of the pipe insulation system when it was installed on the PIT). For test B, the thickness of joint sealant was about 1/16-in (1.6 mm), but the measured thermal conductivity in this case was assumed to be representative of the thermal conductivity of cellular glass pipe insulation. This means I assume the joint sealant thickness was 0 in the test B. In the test C, the joint sealant thickness was assumed at 1/8-in (3.175 mm) by comparing the diameter difference of the pipe insulation systems in the test B and C. Then the pipe insulation system was modeled as shown in Equation (5.1) to predict an equivalent overall thermal resistance that combines the thermal resistances from pipe insulation, joint sealant, and air gap. The thermal conductivity of the joint sealant was assumed between 0.7 and 7.0 Btu-in/hr-ft^2-F (0.1 to 1.0 W/m-K). Figure 5.8 shows the impact of the joint sealant thickness on the pipe insulation thermal conductivity of cellular glass. Joint sealant thickness was varied from 1/16-in (1.6 mm) to 3/16-in (4.8 mm), with a constant thermal conductivity of 3.12 Btu-in/hr-ft^2-F (0.45 W/m-K). With this value as the joint sealant thermal conductivity, the joint sealant can potentially increases the overall thermal conductivity of the cellular glass pipe insulation system by up to 6% with respect to the case of without any joint sealant. It was also observed that a thicker layer of joint sealant would lead the pipe insulation system to behave more conductive. The insulation mean temperature is also important when evaluating the joint thickness effect on the longitudinal joints. Figure 5.9 shows the difference in thermal conductivity for cellular glass pipe insulation having a joint sealant thickness of 0.1-in (2.54 mm) and for reasonable range of joint sealant thermal conductivity from 2.4 to 6.9 Btu-in/hr-ft^2-F (0.35~1.0 W/m-K). The augmentation of the apparent thermal conductivity of the cellular glass pipe insulation system with the highest joint sealant thermal conductivity was up 13% with respect to the case with the lowest joint sealant thermal conductivity. It should be noted

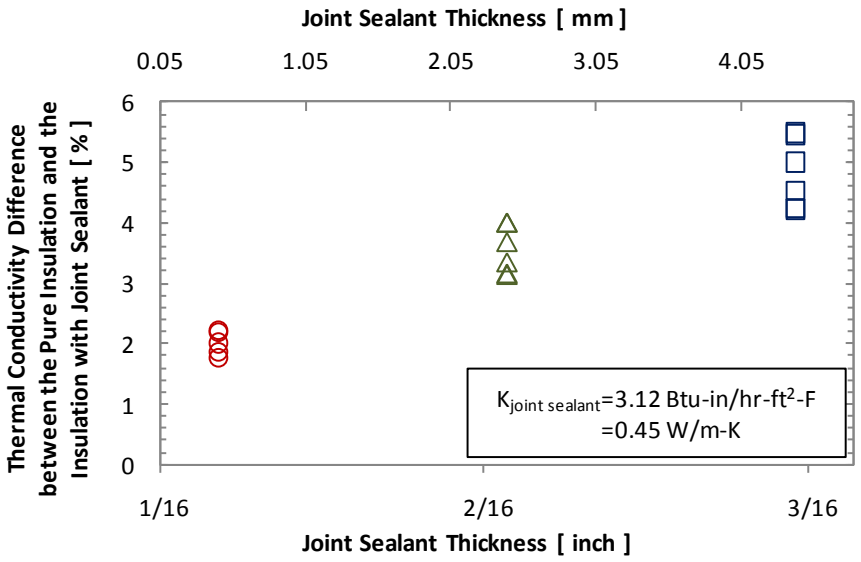

Figure 5.8: Sensitivity study of varying the joint sealant layer thickness on thermal conductivity of the pipe insulation test specimen

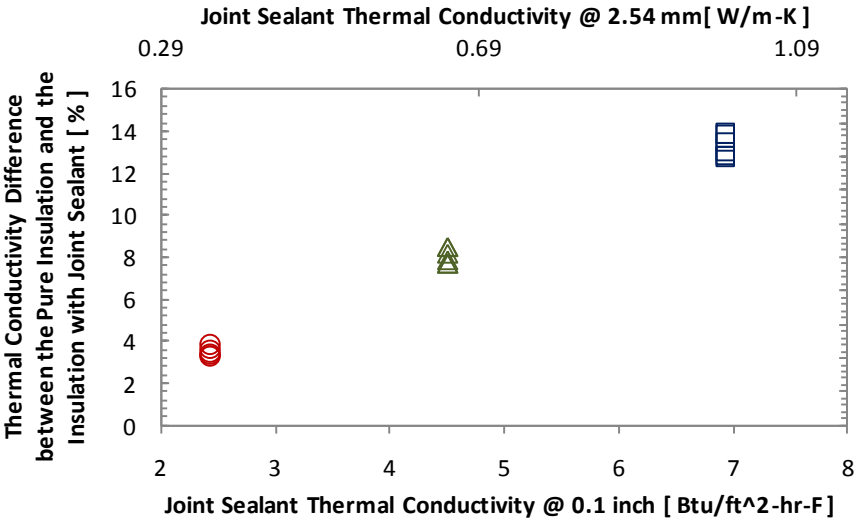

Figure 5.9: Sensitivity study of varying the joint sealant thermal conductivity on the thermal conductivity of the pipe insulation test specimen

that a similar increase was recorded with the experimental data for phenolic pipe insulation discussed previously. For example in Figure 5.7 at 60 ℉ (15.6 ℃) the thermal conductivity of

phenolic pipe insulation with joint sealant was 0.224 Btu-in/hr-ft^2-F (0.0323 W/m-K) while the thermal conductivity of phenolic pipe insulation without joint sealant was 0.194 Btu-in/hr-ft^2-F (0.028 W/m-K). The difference was about 15%, and it was attributed to the presence of joint sealant on the longitudinal joints.

5.4 Thermal conductivity tests results under dry non-condensing conditions in the second stage

Ten pipe insulation systems, including both closed-cell and fibrous types, were tested in the second stage of this research project. The detailed information on each system is listed in Table 5.7. It should be noted that for system P2-FG5 and P2-CG, both pipe insulation systems were tested twice, one on the bare aluminum pipe, and the other one was on the aluminum pipe painted with flat black, as shown in Figure 3.10. In the following description, the systems tested on the bare pipe were referred as pipe insulation systems P2-FG5A and P2-CGA, while the systems tested on the black pipe were referred as pipe insulation systems P2-FG5B and P2-CGB.

Table 5.7: Pipe insulation systems tested under dry conditions (in the second stage)

Test Samples (Ref. No.)	Thickness in (mm)	Joint Sealant	Edge Seal	Vapor Retarder / Insulation Jacketing
Fiberglass (P2-FG1)	2 (50.8)	N/A	Foster 90-66	N/A
Fiberglass (P2-FG2)	1.5 (38.1)	N/A	Foster 90-66	ASJ vapor retarder
Fiberglass (P2-FG3)	1.5 (38.1)	N/A	Foster 90-66	ASJ vapor retarder with 20 mil thick PVC jacketing
Fiberglass (P2-FG4)[1]	1.5 (38.1)	N/A	Chil-Perm CP-30	ASJ vapor retarder
Fiberglass (P2-FG5)[2]	2 (50.8)	N/A	Chil-Perm CP-30	N/A
Cellular Glass (P2-CG)[2,3]	1.5 (38.1)	Boss 368	Boss 368	N/A
Elastomeric Rubber (P2-ER1)	1.5 (38.1)	Stay-Seal with Protape	Aeroseal	N/A
Elastomeric Rubber (P2-ER2)	2 (50.8)	Stay-Seal with Protape	Aeroseal	N/A
Polyisocyanurate (P2-PIR1)	1 (25.4)	Chil-Joint CP-70	Chil-Joint CP-70	Saran 540CX vapor retarder
Polyisocyanurate (P2-PIR2)	1.5 (38.1)	Chil-Joint CP-70	Chil-Joint CP-70	N/A
Phenolic (P2-P)[4]	2 (50.8)	Chil-Joint CP-70	Chil-Joint CP-70	N/A

[1]: There is one butt joint in the center of the 3-ft (0.9 m) test section;
[2]: The same pipe insulation systems were tested twice on the bare pipe and the black pipe. The system tested on the bare pipe was referred as –A, and the system tested on the black pipe was referred as –B.
[3]: There is one staggered joint in the center 3-ft (0.9 m) test section;
[4]: This system was not tested under dry condition, and the information was provided here as a reference for the comparison in the wet condition

5.4.1 Fiberglass pipe insulation system

Fiberglass, the typical fibrous material, was tested in five pipe insulation systems, with different thicknesses and vapor barriers. The results on the apparent thermal conductivity of each pipe insulation system are plotted in Figure 5.10. During the measurement, the radial heat flux varied from 9.9 to 14.1 Btu/hr-ft (9.5 to 13.6 W/m-K), and the uncertainty was between ±4.1 to ±7.0%.

In both systems P2-FG1 and P2-FG5A, fiberglass pipe insulation was tested at 2-in (50.8 mm) nominal wall thickness without any vapor retarder. It was observed that the system thermal conductivity measured on P2-FG5A, shown as the diamond symbol in Figure 5.10 was around 7% higher than the values measured on the similar insulation system P2-FG1, shown as the red circles. This increasing is possibly caused by a temporary change we made to the PIT system. In order to seal the thermocouple grooves completely, an extra layer of aluminum foil tape was added between the pipe insulation interior surface and the test pipe, as shown in the previous section, Figure 3.6. Compared to the aluminum pipe surface, this highly polished film has a lower emissivity and led a shift to the values measured on the effective sand thermal conductivity. This systematic error was conducted to the thermal conductivity measurement on the test system P2-FG5A. After this test, the aluminum pipe that sealed with the aluminum foil was painted to flat black. The diamond symbols, shown in Figure 5.10, represent the measured thermal conductivity of the same pipe insulation system after the surface of the aluminum foil was painted black. The system thermal conductivity values decreased and matched with the results derived on system P2-FG1 within 2%. Wilkes *et al.* did similar tests on both bare pipe and black pipe, but they found that blackening the tube resulted in an increase in the measured thermal conductivity of the pipe insulation by 4 to 5%. This discrepancy may come from the fact that in our case, the thermocouples used for the surface temperature measurement were embedded in the grooves along the test pipe and below the aluminum foil, and the aluminum foil was blackened on the exterior surface. Compared to the case that the thermocouples were directly attached to the exterior surface of the black pipe, the change on the emissivity would result in a reversed impact on the surface temperature measurement. P2-FG2 (shown as the triangle symbols) and P2-FG4 (shown as the cross symbols) were another two similar systems with different edge seals. Both systems were tested at 1 ½ -in (38.1 mm) nominal wall thickness with ASJ vapor retarder. In the system of P2-FG2, the fiberglass was installed as full length sample in the center 3-ft (0.9 m) test section, and for the system P2-FG4, the fiberglass was installed as two detached pieces with one

insulation joint in the middle. Results showed that the apparent thermal conductivity in system P2-FG2 was around 4% higher that the values derived from system P2-FG4. The difference on the measured exterior diameters of the pipe insulation is a main reason to explain the shift on the thermal conductivity values between these two systems. From the experimental results, it seems that both ASJ vapor barrier and PVC jacketing would not affect the system thermal conductivity. Although the values demonstrate some differences among each system, they are within the system uncertainty range.

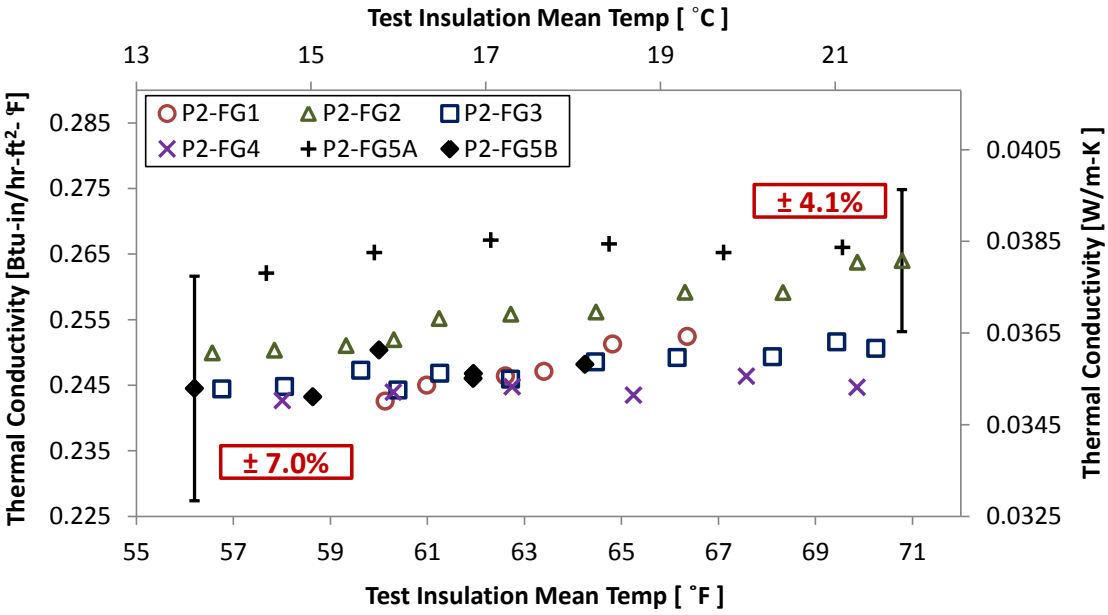

Figure 5.10: The apparent thermal conductivities of five fiberglass pipe insulation systems

5.4.2 Cellular glass pipe insulation system

Cellular glass is one of the closed-cell materials. In the second stage, pipe insulation system P2-CG was tested on cellular glass with 1 ½-in (38.1) nominal wall thickness. During the measurement, the radial heat flux varied from 11.8 to 15.3 Btu/hr-ft (11.3 to 14.7 W/m-K), and the uncertainty was between ±3.9 to ±5.2%. This pipe insulation system was tested twice both on

the bare pipe and the black pipe, referred as system P2-CGA and P2-CGB, respectively. The test results between these two measurements are shown in Figure 5.11. The values derived from the black pipe were about 6% lower than the thermal conductivity measured at the bare pipe, and the differences were caused by a variation on the actual exterior diameter of the pipe insulation systems. The actual diameter for system P2-CGA was measured at 6.8-in (172.7 mm), and the system P2-CGB was measured with a smaller exterior diameter, at 6.6-in (167.6 mm). The results on the thermal conductivity of pipe insulation system P2-CGA and P2-CGB were also compared to the other system V-CG1 that was tested during the validation phase at 1-in (25.4 mm) nominal wall thickness. Results demonstrate that the thermal conductivity measured in system P2-CG (shown as the hollow and solid circles) was around 17% higher than the values provided in system V-CG (shown as the triangle symbols). This is because in the previous stage (validation phase and the first stage of dry tests), instead of considering actual diameters of the pipe insulation systems, the nominal diameters were used in the data reduction. With the used of nominal diameters, the effect of joint sealant was not included, and the measured thermal conductivity was lower than the actual case. To further investigate the impact of the exterior diameter, the thermal conductivity of system P2-CG was recomputed with a nominal diameter, and the results were shown as the rectangle symbols in Figure 5.11. By varying the exterior diameter from 6.8-in (172.7 mm) to 6.375-in (161.9 mm), the system thermal conductivity decreased by almost 10%, and matched with the results of system V-CG1 within the uncertainty range. Another possibility that may also cause this systematic shift is the difference from the calibration methods that applied under these two scenarios. During the first stage, the sand thermal conductivity was calibrated at one single ambient condition, while in the second stage, the sand thermal conductivity was developed as a function of both sand mean temperature and the exterior temperature difference between the aluminum surface temperature and the ambient, as described in section 4.4.1. These two methodologies would bring in a difference on the sand

thermal conductivity and resulted in a shift on the apparent thermal conductivity of the pipe insulation systems.

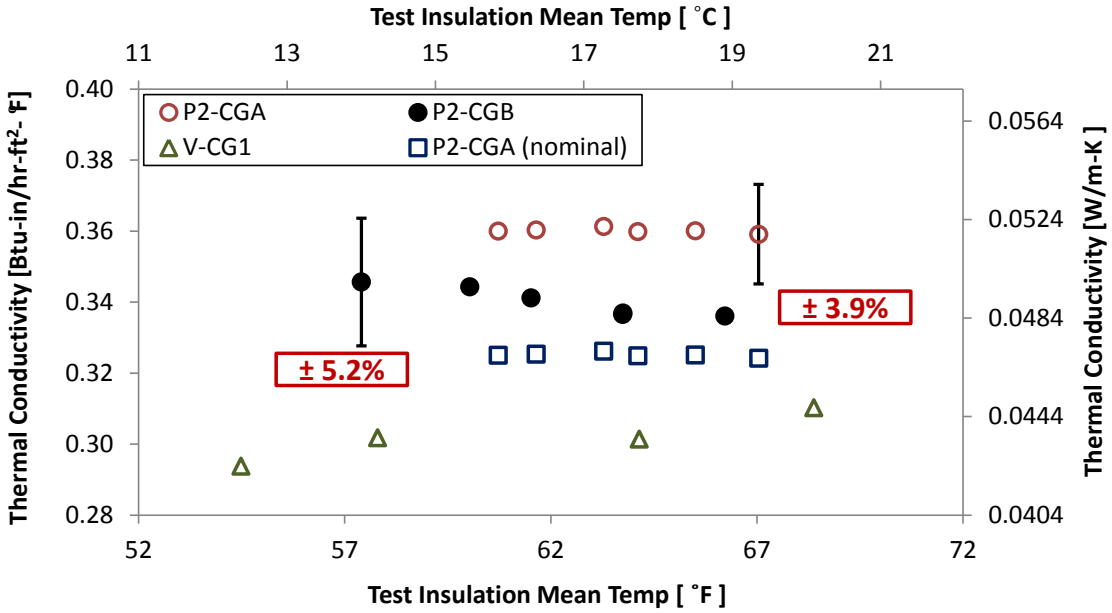

Figure 5.11: Thermal conductivities of cellular glass pipe insulation systems

5.4.3 Elastomeric rubber pipe insulation system

In the second stage, elastomeric rubber was tested in two pipe insulation systems: P2-ER1 with 1-in (25.4 mm) nominal wall thickness and P2-ER2 with 2-in (50.8 mm) nominal wall thickness. During the measurement, the radial heat flux through the test sample varied from 7.5 to 12.6 Btu/hr-ft (7.2 to 12.1 W/m-K) for system P2-ER1, and from 6.0 to 10.1 Btu/hr-ft (5.8 to 9.7 W/m-K) for system P2-ER2. The uncertainties for both systems were between ±4.4 to ±7.2%, as shown in Figure 5.12. By comparing these two systems with system P1-ER, which was tested in the first stage on the elastomeric rubber sleeve with 2-in (50.8 mm) wall thickness, all the three systems showed a similar trend on the thermal conductivity with insulation mean temperature. Although the values of the thermal conductivity in these three systems matched within the uncertainty

range, the following two facts should still be carefully considered. First, for system P1-ER, the data reduction was based on the nominal diameter of the pipe insulation system and a different calibration procedure for the measurement of sand thermal conductivity. Thus, the actual thermal conductivity in system P1-ER might be higher than the values shown in the plot. Second, different types of elastomeric rubber pipe insulation were selected in these systems. The material tested in P1-ER was manufactured as one piece of the unslit sleeve, and it was required for joint sealant during the installation. The test samples in system P2-ER1 and P2-ER2 were manufactured as insulation split with adhesive strip, as listed in Table 5.7. This type of insulation does not have any requirement on the joint sealant during pipe insulation system installation.

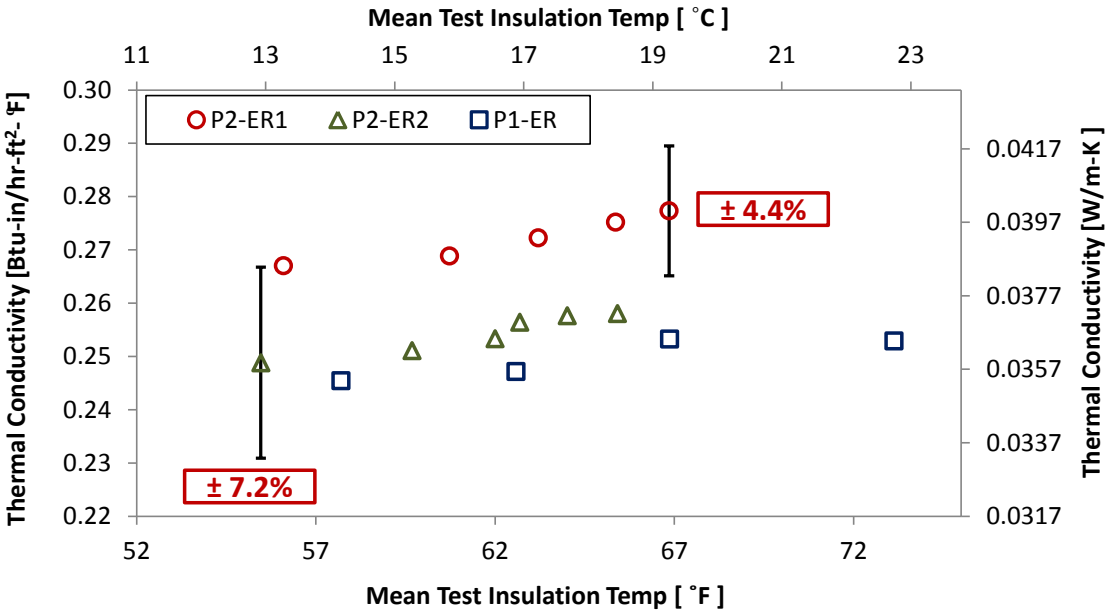

Figure 5.12: Thermal conductivities of elastomeric rubber pipe insulation systems

5.4.4 Polyisocyanurate (PIR) pipe insulation system

Figure 5.13 shows the test results of the thermal conductivity measurement on polyisocyanurate (PIR) pipe insulation systems P2-PIR1 and P2-PIR2. The insulation system P2-PIR was tested at 1-in (25.4 mm) nominal wall thickness and with Saran 540CX vapor retarder. During the

experiment, the radial heat flux was between 9.4 to 16.2 Btu/hr-ft (9.0 to 15.6 W/m-K), with an uncertainty between ±3.7 to ±5.4%. The other system, P2-PIR2 was tested at 1 ½-in (38.1 mm) nominal wall thickness without any vapor retarder. The radial heat flux through the system was between 7.5 to 13.1 Btu/hr-ft (7.2 to 12.6 W/m-K), and the uncertainty was from ±4.3 to ±6.2%. It seems that system P2-PIR1 with vapor retarder performs better than the other system P2-PIR2, and the system thermal conductivity does not change with insulation mean temperature. When compared to the other system V-PIR1, which was tested in the validation phase on the 1-in (25.4 mm) thick PIR without insulation jacketing, the measured thermal conductivity of V-PIR was nearly 20% lower than the other two systems tested in the second stage. Besides the two possible reasons that mentioned in previous sections: the application of nominal diameter during data reduction and the different calibration procedure on the determination of the sand thermal conductivity, "aging" effect is another issue that need to be considered for PIR pipe insulation systems.

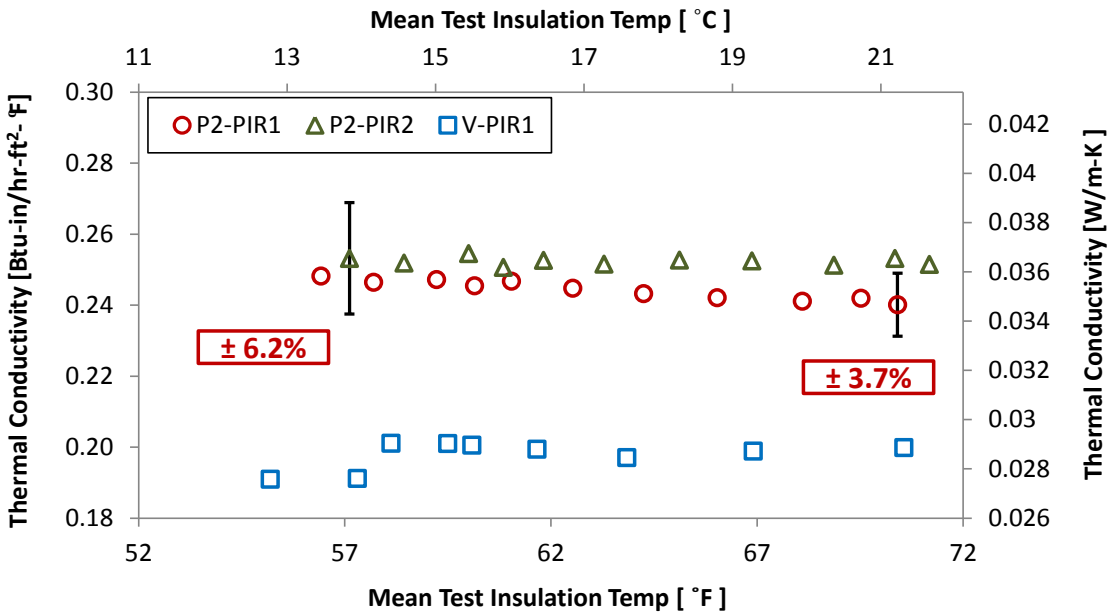

Figure 5.13: Thermal conductivities of polyisocyanurate (PIR) pipe insulation systems

Table 5.8: Pipe insulation systems tested under dry conditions (Phase 2)

Test Samples (Ref. No.)	Actual Diameter in (mm)	$^{*}k_{pipe,insulation} = a \cdot T + b$ Btu-in/hr- ft^2-F (W/m-K) a	b	Heat flux per unit length Btu/hr-ft (W/m)
Fiberglass (P2-FG1)	7.6 (193.0)	0.0016 (0.00041)	0.1475 (0.0286)	8.44
Fiberglass (P2-FG2)	6.7 (170.2)	0.0010 (0.00026)	0.1918 (0.0323)	10.68
Fiberglass (P2-FG3)	6.8 (172.7)	0.0005 (0.00013)	0.2156 (0.0334)	10.03
Fiberglass (P2-FG4)	6.6 (167.6)	0.0002 (0.00005)	0.2322 (0.0344)	9.40
Fiberglass (P2-FG5A)	7.6 (193.0)	0.0002 (0.00006)	0.2511 (0.0373)	8.63
Fiberglass (P2-FG5B)	7.6 (193.0)	0.0005 (0.00012)	0.2184 (0.0336)	8.31
Cellular Glass (P2-CGA)	6.8 (172.7)	-0.0001 (-0.00004)	0.3694 (0.0526)	13.42
Cellular Glass (P2-CGB)	6.6 (167.6)	-0.0013 (-0.00033)	0.4201 (0.0546)	12.80
Elastomeric Rubber (P2-ER1)	6.8 (172.7)	0.0010 (0.00025)	0.2112 (0.0350)	10.40
Elastomeric Rubber (P2-ER2)	7.7 (195.6)	0.0010 (0.00027)	0.1913 (0.0323)	8.45
Polyisocyanurate (P2-PIR1)	5.7 (144.8)	-0.0005 (-0.00014)	0.2789 (0.0377)	12.74
Polyisocyanurate (P2-PIR2)	6.8 (172.7)	-0.00005 (-0.00001)	0.2558 (0.0366)	10.30

*: T is in ℉ or ℃

Linear correlations were developed based on the measured thermal conductivity and test insulation mean temperature of the ten pipe insulation systems, listed in Table 5.8. Fiberglass pipe insulation system P2-FG5 and cellular glass pipe insulation system P2-CG were provided with two data sets by considering test on both bare pipe (P2-FG5A and P2-CGA) and black pipe (P2-FG5B and P2-CGB. The actual diameter measured from the insulation systems and the average heat fluxes per unit length are also provided in the table. From the previous section, it is found that during data reduction, replacing nominal diameter with the actual diameter measured from the insulation system would be more reasonable, and the changes will cause a difference on the system thermal conductivity around 6 to 10%. For all the nine pipe insulation systems, the

average heat flux per unit length were higher or close to the lower limit of the calibration range, and this helped maintain the system uncertainty within ±7.2%.

5.5 Thermal conductivity of pipe insulation systems under wet condensing conditions with moisture ingress

Eight pipe insulation systems were selected from previous dry tests to measure the system thermal conductivity under wet conditions with moisture ingress.

5.5.1 Fiberglass Pipe Insulation

According to the literature, fiberglass is a typical fibrous insulation material that allows water vapor pass through the gaps among the strands of fibers if a vapor repellent jacketing is not present (McFadden, 1988). The condensate can be easily accumulated and filled in the void spaces inside the material due to the loose and fibrous interior structure. In this thesis, fiberglass was tested in three pipe insulation systems under four different experimental conditions, as shown in Table 5.9. Pipe insulation system P2-FG5 was tested on both bare test pipe and black pipe, referred as P2-FG5A and P2-FG5B.

Table 5.9: Fiberglass pipe insulation systems tested under wet conditions

Test Samples (Ref. No.)	Test Pipe Temperature ˚F (˚C)	Ambient Temperature ˚F (˚C)	Relative Humidity %	Test Length Days	Actual Diameter inch (mm)	Vapor Retarder or Jacketing
Fiberglass (P1-FG)	41.6 (5.33)	107.6 (42.0)	81	12	*7.5(190.5)	N/A
Fiberglass (P2-FG4)	38.4 (3.6)	78.1 (25.6)	54.8	55	6.6 (167.6)	ASJ Vapor Retarder
Fiberglass (P2-FG5A)	40.6 (4.8)	78.1 (25.6)	54.8	55	7.6 (193.0)	N/A
Fiberglass (P2-FG5B)[1]	41.9 (5.5)	90.1 (32.3)	84	54	7.7 (195.6)	N/A

[1]: The pipe insulation system was tested on a black pipe
*: Actual diameter is not available. Use nominal diameter instead.

In systems P1-FG and P2-FG5, there was no vapor barrier around the exterior surface of fiberglass and the installation of fiberglass pipe insulation is shown in Figure 5.14 and Figure 5.16. Although in the industry field, fiberglass pipe insulation is normally applied with vapor retarder, in this project, the fiberglass pipe insulation was first tested without vapor jacketing due to the following reasons. (i) The project aimed to develop a method for the thermal conductivity measurement under wet conditions. Without vapor jacketing, the procedure for moisture accumulation would be accelerated and the moisture content would be measured more accurately with better uncertainty. (ii) Before further considering the impact of vapor jacketing, it would be very helpful to investigate the thermal performance of insulation materials with different moisture content under wet conditions. Once we are clear about how the thermal conductivity of the pipe insulation material varies with moisture content, the vapor jacketing is added to the system for further investigation. In both systems P1-FG and P2-FG5, the first PIT was used for the thermal conductivity measurement, and the second PIT was installed with the 6-in (152.4 mm) sectioned pieces to determine the moisture content. Due to the fibrous structure and light-weight of the material, fiberglass test samples were installed around the PITs by simply tightening plastic zip ties around the outer shell and no joint sealant was used. It should be noted that in the system P1-FG, both edges of the second PIT were sealed with Foster 90-66, but there was only plastic films applied between each 6-in (152.4 mm) section at the beginning of the moisture test. These plastic film sheets aimed to prevent longitudinal moisture diffusion from one sample to the adjacent one. However, I found that these plastic films also created preferential paths for moisture radial transfer in and out of the fiberglass insulation. Therefore, for the system P2-FG5A and P2-FG5B, the plastic films were replaced with vapor sealant Chil-Perm CP-30, which was the same sealant that applied to seal both edges of the second PIT, as shown in Figure 5.16.

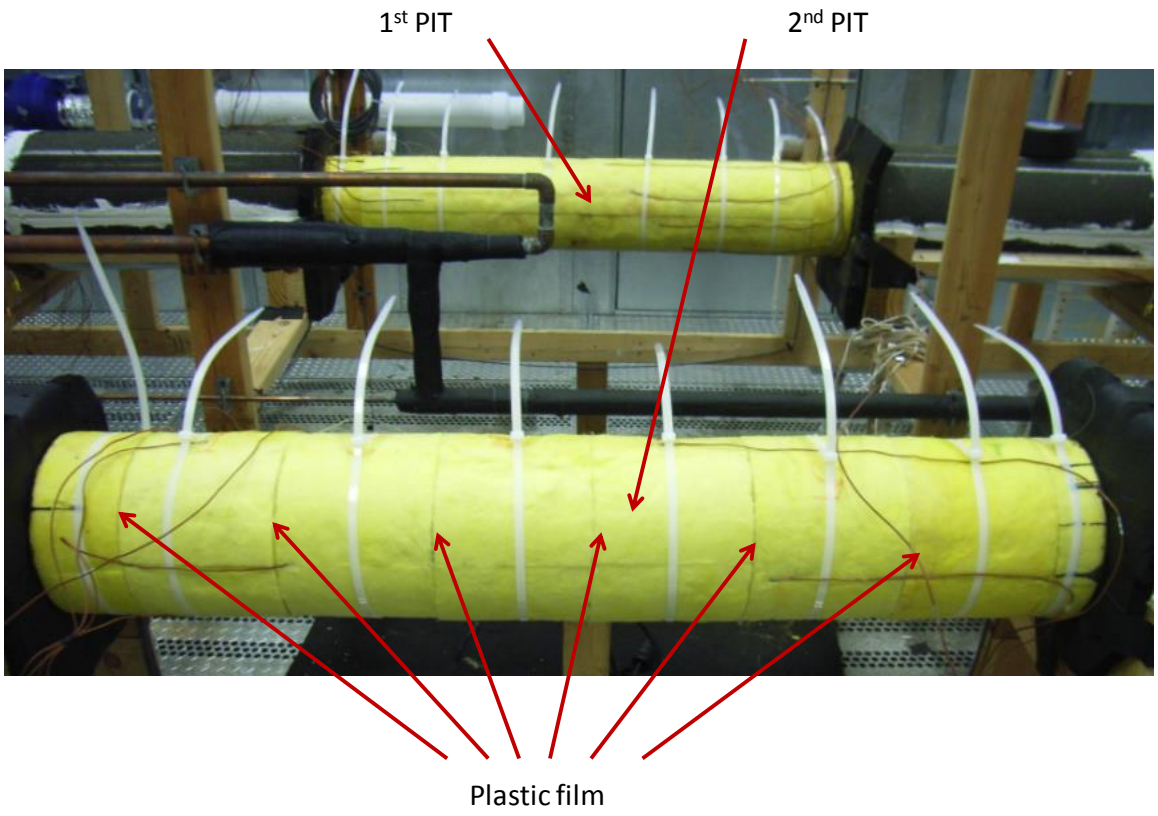

Figure 5.14: Photos of the pipe insulations P1-FG for the wet test

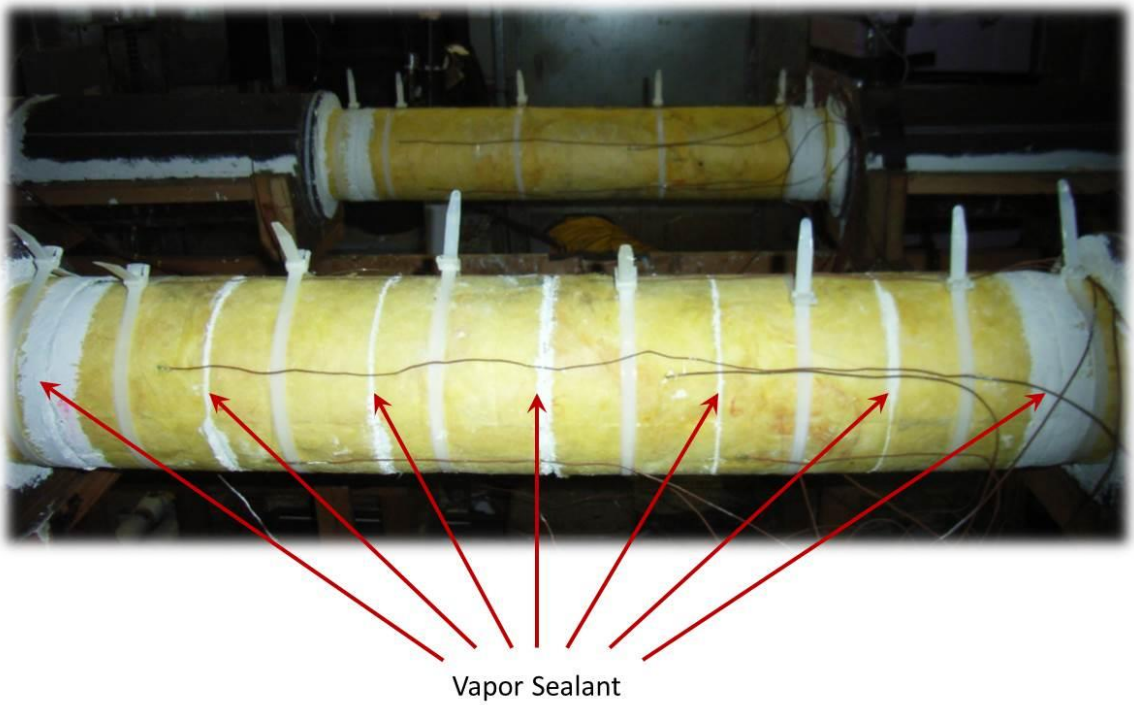

Figure 5.15: Photos of the pipe insulation system P2-FG5 for the wet test

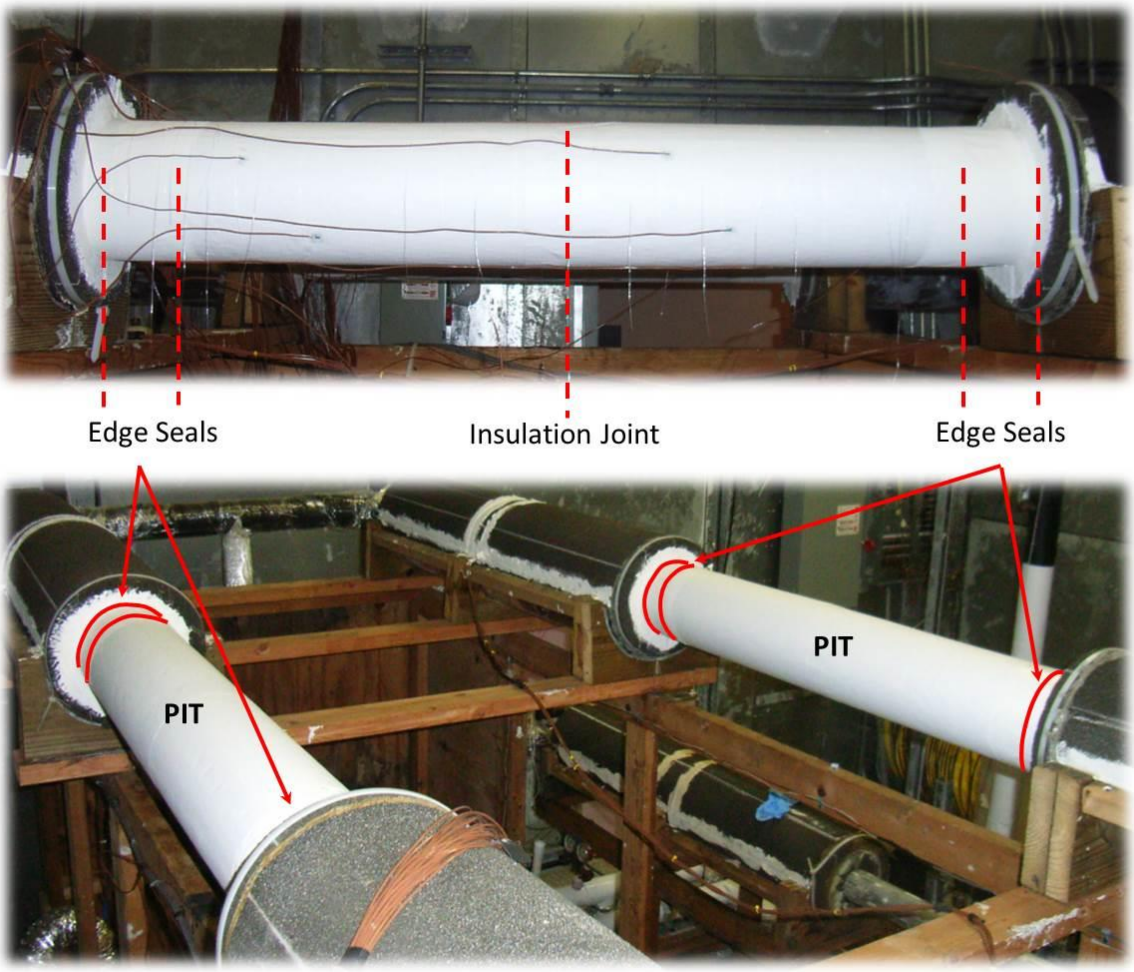

Figure 5.16: Photos of the pipe insulation system P2-FG4 for the wet test

In the system P2-FG4, the fiberglass pipe insulation was tested with ASJ vapor barrier applied on the exterior surface, and the material was installed with one insulation joint in the center of the 3-ft (0.9 m) test section, as shown in Figure 5.16. Considering the low water vapor permeability in the ASJ jacketing, the moisture content was only measured at the end of the moisture test, and both PITs were used for the thermal conductivity measurement. Two test samples of system P2-FG4 were installed simultaneously on the PITs with the same edge seals. These three fiberglass pipe insulation systems were tested under both acceleration condition and ambient conditions, as listed in Table 5.9. In order to accelerate the water condensation in the insulation, the ambient was required to maintain as hot and humid environment, and the most severe condition for testing

fiberglass pipe insulation system was at 107.6 ℉ (42 ℃) and 81% relative humidity, which resulted in an air dew point of about 100.4 ℉ (38 ℃).

Fiberglass pipe insulation system P1-FG

For a better description on the observations and findings I got from the experiment, the following discussion will be focused on one specific case, system P1-FG, which was tested under the most severe condition, 107.6 ℉ (42 ℃) and 81% RH. This test lasted for 12 days. Figure 5.17 shows the cross-section view of a fiberglass insulation sample which was taken out from the second PIT after 5 days test. The dark yellow region, circled in the middle of the bottom shell, was considered as a preferential path which was created due to a less dense area in the fiberglass material, partially unsealed seams and the gravity effect. The gravity effect would also cause portion of the water condensate come out from the insulation. Compared to the bottom shell, the top section remained quite dry at the outer surface. Only small amount of water droplets were observed on the interior surface of the pipe insulation. Considering the fact that each section on the second PIT represents one test specimen installed on the first PIT, the phenomenon observed from the sectional pieces was assumed to be a replicate of what happed in the full length insulation sample.

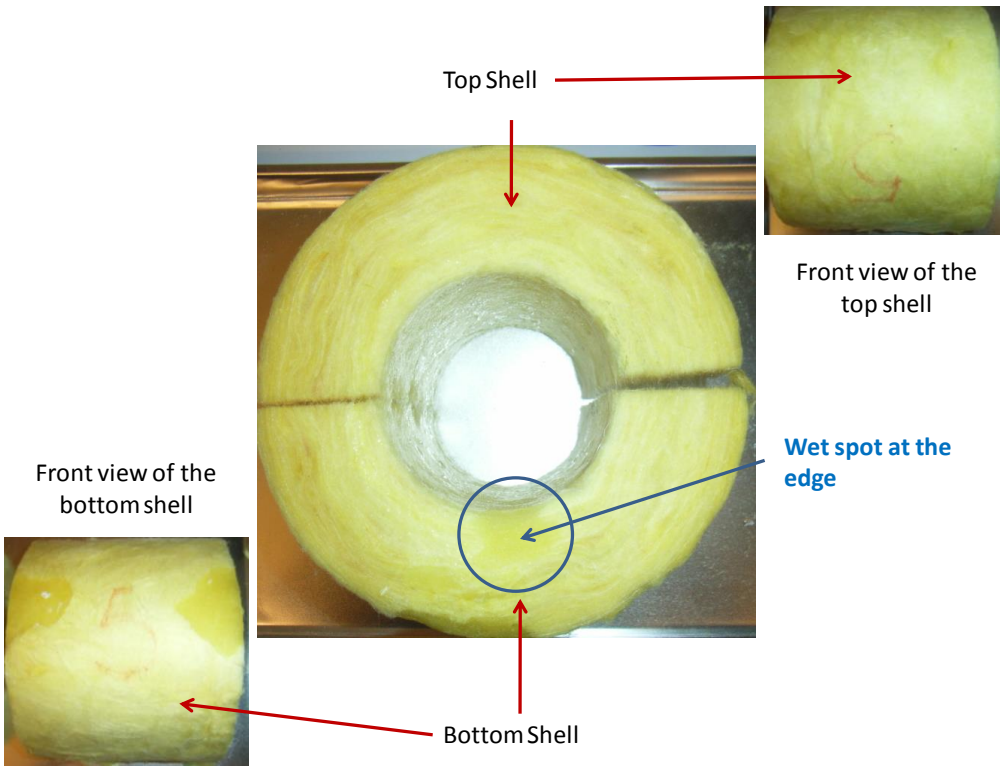

Figure 5.17: Photos of the wet regions of moisture accumulation on the pipe insulation 6-in (152.4) long sample removed from the second PIT

Figure 5.18 shows the development of the wet regions in the fiberglass pipe insulation system P1-FG. Two wet spots occurred at the surface of the bottom shell during the first day of the wet test, and the area of these regions increased obviously in the following three days. From the 4th day to the end of the test, that is day 12, although there was no significant change observed on the area of these wet regions, the moisture was accumulated inside the insulation system because the weight of the moist samples kept increasing. According to the literature, when the moisture content exceeds the critical volume available for the liquid, condensate becomes mobile and will be propelled by surface tension and diffuses towards drier regions (Wijeysundera *et al*., 1996). Therefore, the procedures of moisture accumulation in the current system can be explained as follows. First, the water vapor penetrated preferentially via less dense sections in the fiberglass insulation system. It was diffused until reaching the inner layer with temperature below the dew

point and the water vapor condensed. The water condensate transferred to the bottom shell due to the gravity effect and accumulated at the exterior layer, as the visible wet spots shown in Figure 5.19a. From the way the area of the wet region developed on the bottom shell (Figure 5.19a to b), I postulate that the moisture kept coating horizontally from wet to dry areas through the layers of fiber strands that were aligned in the longitudinal direction until a quasi-steady state equilibrium was achieved. Then the moisture spread through the radial direction and diffused from the exterior to the inner layers of the insulation (Motakef & El-Masri, 1985). This second mechanism is difficult to be observed with current test apparatus since there was no visual access along the radial direction of the pipe insulation test specimen. From day 4 to day 9 (Figure 5.19b to c), the area of the wet region on the exterior surface of the pipe insulation continued increasing but the rate was visibly lower than the one at the beginning of the wet test. For the top shell, the observation on the wet regions showed quite a different situation. There was no wet region formed on the top shell, but the weight augmented during the wet test. This is because the water vapor that transmitted through the top shell condensed at the low temperature region and filled the air gaps among the fiber strands. But this amount of water only stayed next to the inner layer due to the gravity effect.

The test on the fiberglass pipe insulation system P1-FG terminated at day 12 when visible droplets were observed dripping onto the floor. The pipe insulation thermal conductivity kept increasing, and the experimental apparatus was not able to maintain the test pipe surface temperature at 40°F (4.5°C). The aluminum surface temperature exceeded 45°F (7.2°C) and large wet regions were visually observed on the exterior surface of the pipe insulation at the termination of the wet test.

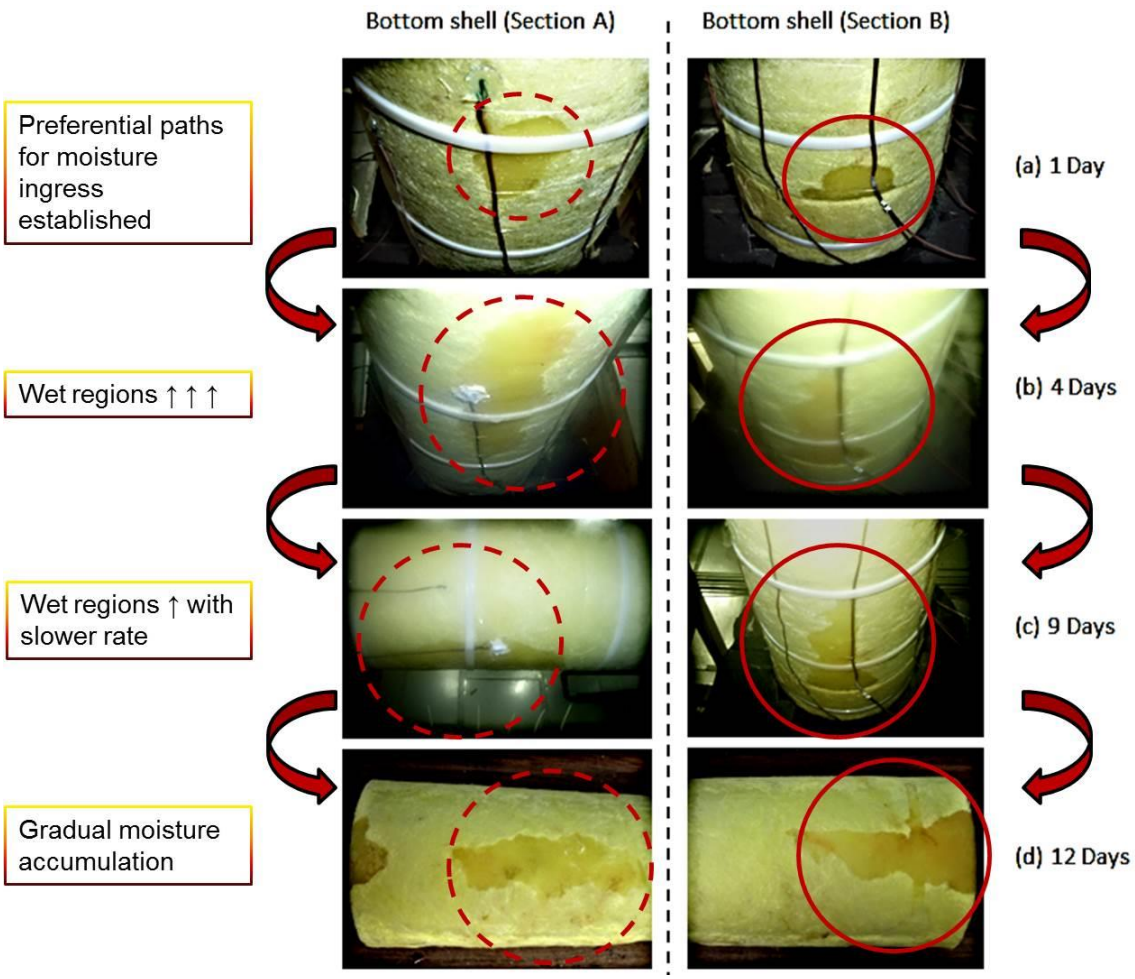

Figure 5.18: Photos of the development of the wet region on the exterior surface of the fiberglass pipe insulation system P1-FG

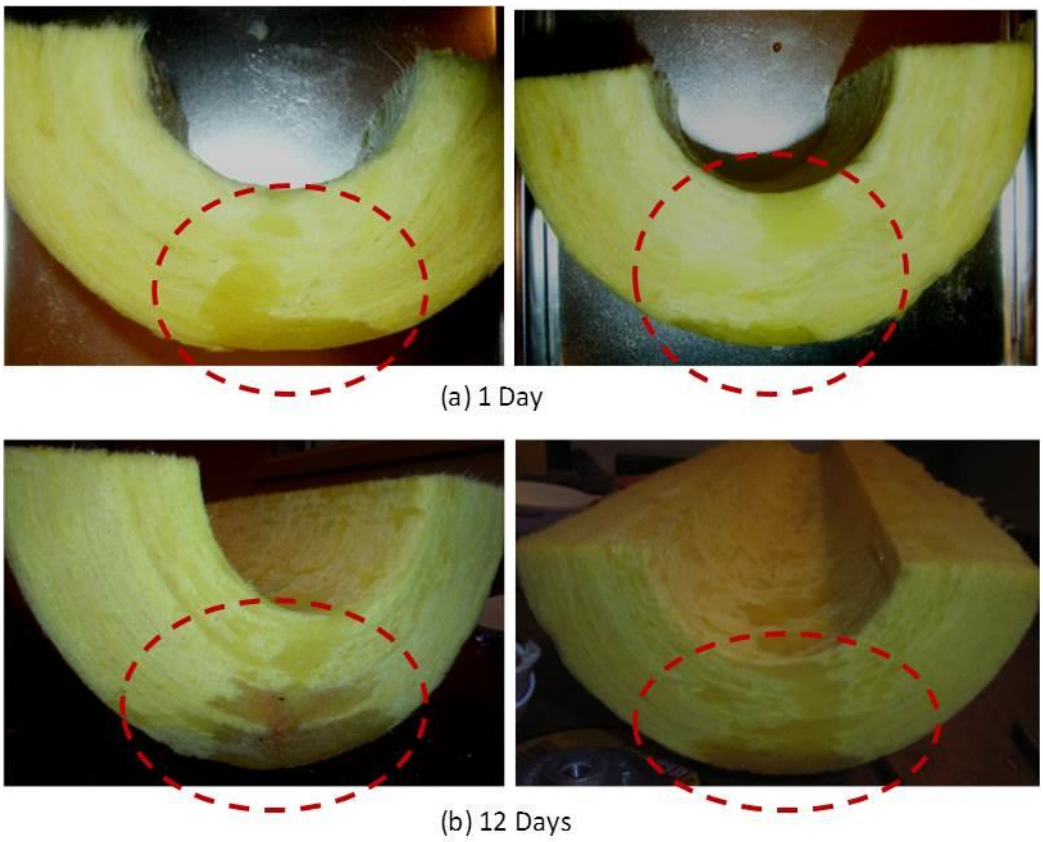

Figure 5.19: Moisture absorption in the cross-sections of the fiberglass pipe insulation system P1-FG between the first and last day of the wet test

During the 12 days test, a sample of the 6-in (152.4 mm) section was taken from the second PIT every two to three days. Each time, the wet sample was replaced with another dry piece of fiberglass pipe insulation of exactly the same dimensions. The wet sample taken out from the second PIT was weighed directly in the scale within five minutes, and then conditioned in the oven by following the baking procedures provided in the section 4.2.3. It should be noted that in order to determine the initial moisture content in the test sample, an additional piece of fiberglass was conditioned in the oven at about 160 to 170 ℉ (71 to 77 ℃) for eight hours. After the baking procedure, the weight of the sample decreased less than 0.0022 lbm (1 gram), which was the sensitivity of the scale. Therefore, I considered the test sample as completely dry at the beginning of the test, and the initial moisture content was zero.

Figure 5.20 shows the experimental results on the variation of thermal conductivity and moisture content in the fiberglass pipe insulation systems P1-FG. In these figures, each point of the thermal conductivity ratio is based on an average value of the system thermal conductivity during a 24 hour long period. The sensors were sampled every one to two seconds for a total of 3600 data points every 12 hours, and the recording procedure was repeated twice per day. In order to measure the moisture content, the 6-in (152.4 mm) sectioned samples need to be removed periodically during the moisture test. This sampling procedure proceeded right after the data recording so that the measurements on the moisture content and the system thermal conductivity can be considered as simultaneous measurements. The data recording and sampling procedures remain the same for the measurements on the other systems. By the end of the moisture tests on pipe insulation system P1-FG, the system thermal conductivity increased by more than 3 times of the dry reference value, and the moisture content was about 12% by volume. The moisture content was computed based on the volume of water that trapped in the system over the total volume of the insulation, and the upper limit of the moisture content would be equal to the porosity of the material. It should be noted that for system P1-FG, the reference value for the thermal conductivity ratio was estimated based on the correlation developed between system thermal conductivity and insulation mean temperature under dry condition. As shown in the *Figure 5.20*a and c, the thermal conductivity ratio followed a two-step variation during the moisture test. In the first three days, the system thermal conductivity increased dramatically with the moisture content lower than 2% by volume. From day 3 to day 12, the system thermal conductivity kept increasing with the moisture content, but the increasing rate was much lower when compared to the first step. Figure 5.20b provides the data of the moisture content in the top C-shell (circle data points), bottom C-shell (triangle data points), and the overall cylindrical section (cross data points). Due to the gravity effect, the moisture content in the bottom shell of system P1-FG was always higher than the one in the top shell. Water accumulated in the bowl

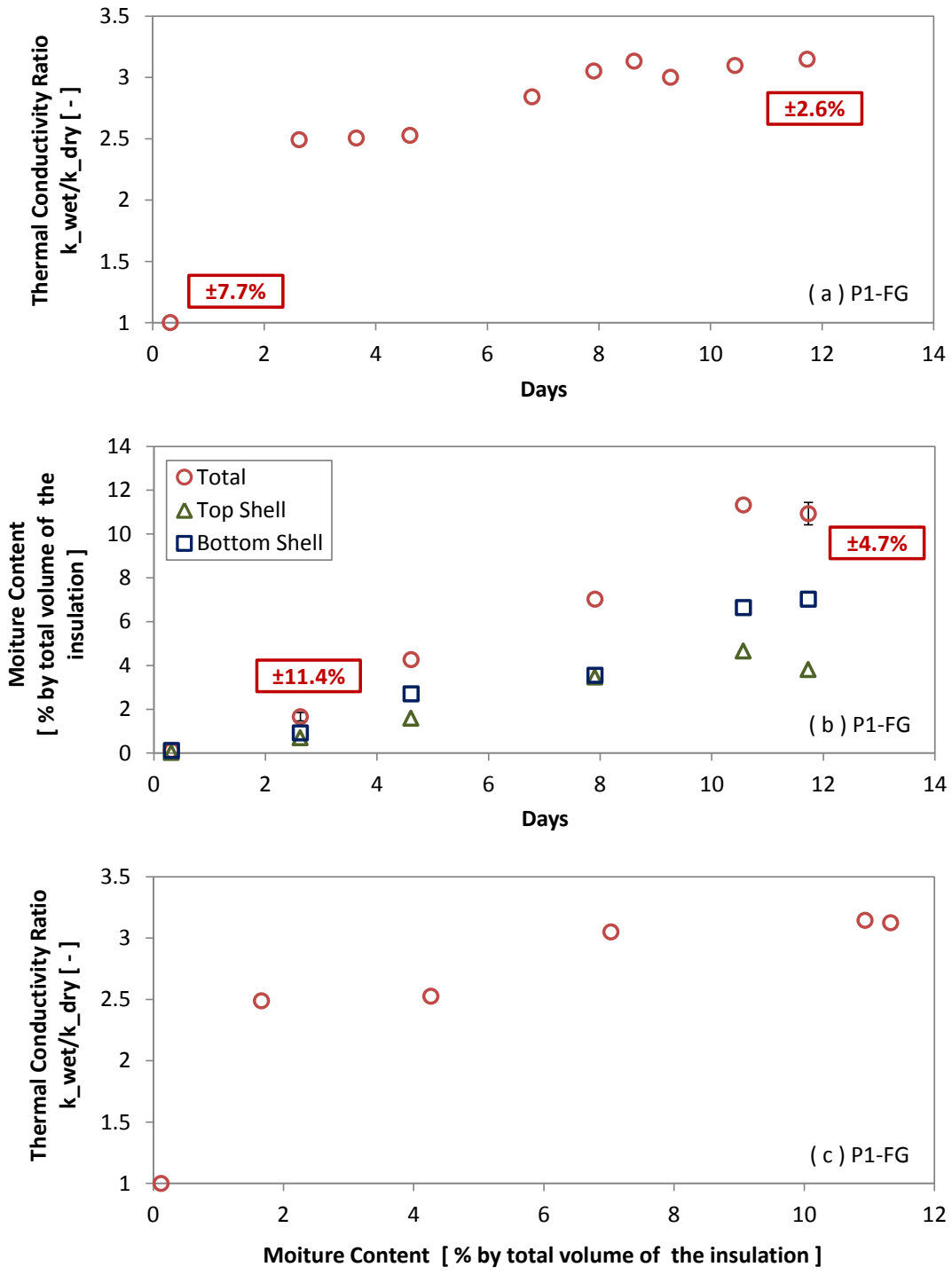

Figure 5.20: Experimental results on pipe insulation system P1-FG: (a) System thermal conductivity in real time during wet test period; (b) Moisture accumulation during wet test; (c) Effect of moisture content on the pipe insulation system thermal conductivity ratio

shape of the bottom C-shell and large wet regions were visually observed at the bottom surface of the pipe insulation.

For the moisture measurement, it should be noted that only the initial and final values of the moisture content were measured for the test specimen from the first PIT (used for thermal conductivity measurement) while the intermediate values of moisture content in the pipe insulation were extrapolated from the measurements of the test specimen around the second PIT (used for moisture measurement with sectional pieces). Due to the presence of more butt joints on the test samples installed on the second PIT, it was quite possible that the total amount of water measured from the second PIT would be higher than the first one. However, the second PIT would only be used for scaling the intermediate moisture content in the first PIT by considering the same increasing rate of moisture with time. The method used for determining the moisture profile on the first PIT was explained in detail as follows:

Take pipe insulation system P1-FG as an example. Figure 5.21 shows a comparison of the moisture content measured in the fiberglass pipe insulation on both first and second PITs. After 12 days in the wet condition, the insulation on the first PIT reached a moisture content of about 11% while the insulation on the second PIT was only about 8.0%. This behavior was consistent with the observation that some amount of water condensate dripped out from the second PIT, via the preferential radial cuts in the pipe insulation test specimen, while more water condensate was trapped in the pipe insulation system on the first PIT. By the end of the moisture test which is day 12, the ratio between the moisture content of the insulation specimen on the first PIT, $V_{moisture,1}$, and the moisture content of the insulation specimen on the second PIT, $V_{moisture,2}$ was:

$$\frac{V_{moisture,1}}{V_{moisture,2}} = \frac{V_{moisture,1,end\ test,fiberglass}}{V_{moisture,2,end\ test,fiberglass}} = \frac{11}{8.0} = 1.4\ (day\ 12) \tag{5.2}$$

At the beginning of the moisture test, $V_{moisture,1}$ was the same amount as $V_{moisture,2}$ and the initial moisture content on both insulation specimens was 0, that is,

$$\frac{V_{moisture,1}}{V_{moisture,2}} = 1 \ (day\ 0) \tag{5.3}$$

Considering a linear increase of the ratio of moisture content in the first and second PITs with time, the corrections on the moisture content absorbed in the fiberglass test specimen on the first PIT was determined as follows:

$$\frac{V_{moisture,1}}{V_{moisture,2}} = a \times day + b = 0.0325 \times day + 1 = CF_{moisture} \tag{5.4}$$

where the interpolating coefficients *a* and *b* were derived by using the conditions (5.2) and (5.3). The variable $CF_{moisture}$ is referred as the Correction Factor for the moisture content between the first and second PITs. At the beginning of the wet test, $CF_{moisture}$ =1, and at the end of the wet test, $CF_{moisture}$ =1.4. $CF_{moisture}$ was assumed to be linearly increasing during the wet test period. The moisture content $V_{moisture,1}$ during the wet tests was calculated as follows:

$$V_{moisture,1} = CF_{moisture} \times V_{moisture,2} \tag{5.5}$$

Where $V_{moisture,1}$ represents the moisture content in pipe insulation system that installed on the first PIT, and $V_{moisture,2}$ represents the moisture content measured form the sectional pieces on the second PIT.

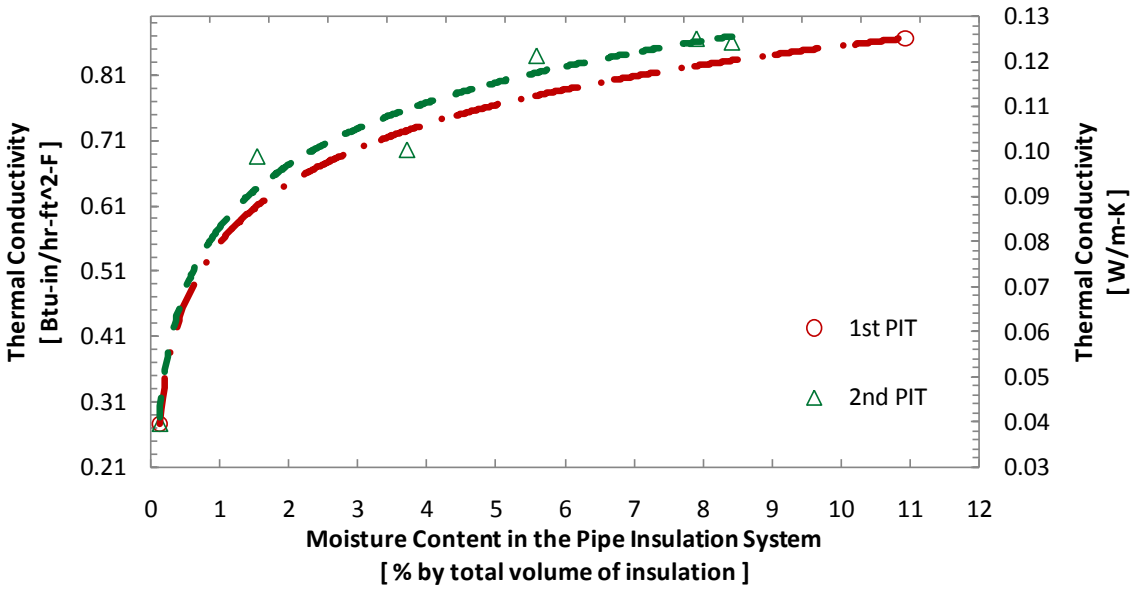

Figure 5.21: Thermal conductivity change with Moisture content in the fiberglass pipe insulation system P1-FG on the first and second PITs

Fiberglass pipe insulation system P2-FG5A

System P2-FG5 was tested twice under different ambient conditions. The first test, referred as P2-FG5A was on the bare pipe when the room temperature was maintained at 78.1 ˚F (25.6 ˚C), and the relative humidity was 54.8%. The test lasted for 55 days and the photos of the development of the wet region were shown in Figure 5.22. By the end of the moisture test, only two small wet spots were observed at the exterior surface of the bottom shell and next to the insulation ends of the test sample. Figure 5.22 shows the development of one wet region during the 55 days test. The wet spot, circled by the red dash line, was found during the first five days of the moisture test, and the wet area remained almost the same till the end of the test. The cross section of the test sample, as shown in Figure 5.22e demonstrates that a large amount of water was trapped next to the exterior layer of the fiberglass pipe insulation, and the possible reason for this phenomenon is the presence of preferential paths next to the insulation end. Figure 5.22g shows the interior

surface of the fiberglass insulation wrap that tested in the system. The interior surface of the top shell was almost dry, with only several water droplets attached to the surface layer of the fibers. On the bottom shell, larger wet spots were present next to the insulation edges, which were assumed to be around the preferential paths. The experimental results on the system thermal conductivity and moisture content are shown in *Figure 5.23*. By the end of the moisture test, the system thermal conductivity increased by 1.5 times of the dry reference value with the maximum moisture content around 1.66% by volume. Different from the previous system P1-FG, in the tests of current system, and the following systems P2-FG5A, P2-FG5B and P2-FG4, the reference values were derived from the mapping procedure (discussed in section 4.2.3) that considered the variations on the surface temperature of the aluminum pipe. From *Figure 5.23*a, it is found that the system thermal conductivity also followed a two-step variation with time, and the system thermal conductivity ratio increased to 1.5 with the moisture content less than 0.3% by volume at the beginning of the test, *Figure 5.23*c. Then the thermal conductivity ratio maintained around 1.5 when the moisture content increased from 0.3% to 1.66% by volume. It should be noted that between day 18 and day 25, the experiment stopped for 7 days due to the maintenance on the refrigeration loop, but the ambient condition was preserved to reduce moisture loss in the pipe insulation system. There was no certain pattern between the moisture content measured from the top and bottom shells of this insulation system, see Figure 5.23b. This can be explained by two possible reasons. First, the uncertainty during the moisture measurement increased significantly when the amount of water is small. From previous analysis, the uncertainty may increase above 20% if the moisture content is below 2% by volume. Second, the gravity effect might have a less impact on the water redistribution between the top and bottom shells when the total amount of moisture is small in the fiberglass insulation system.

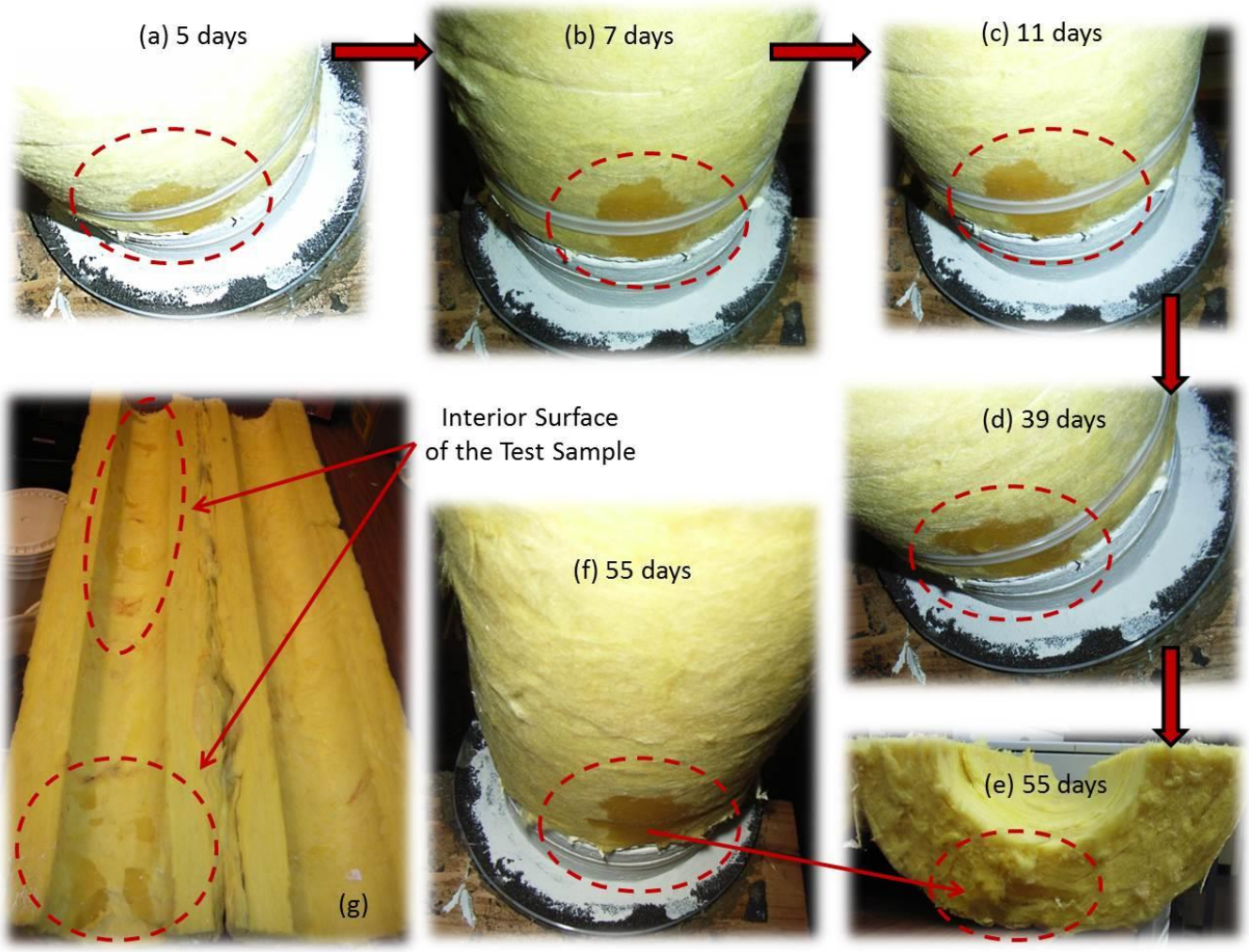

Figure 5.22: Moisture absorption on the bottom shell of pipe insulation system P2-FG5A

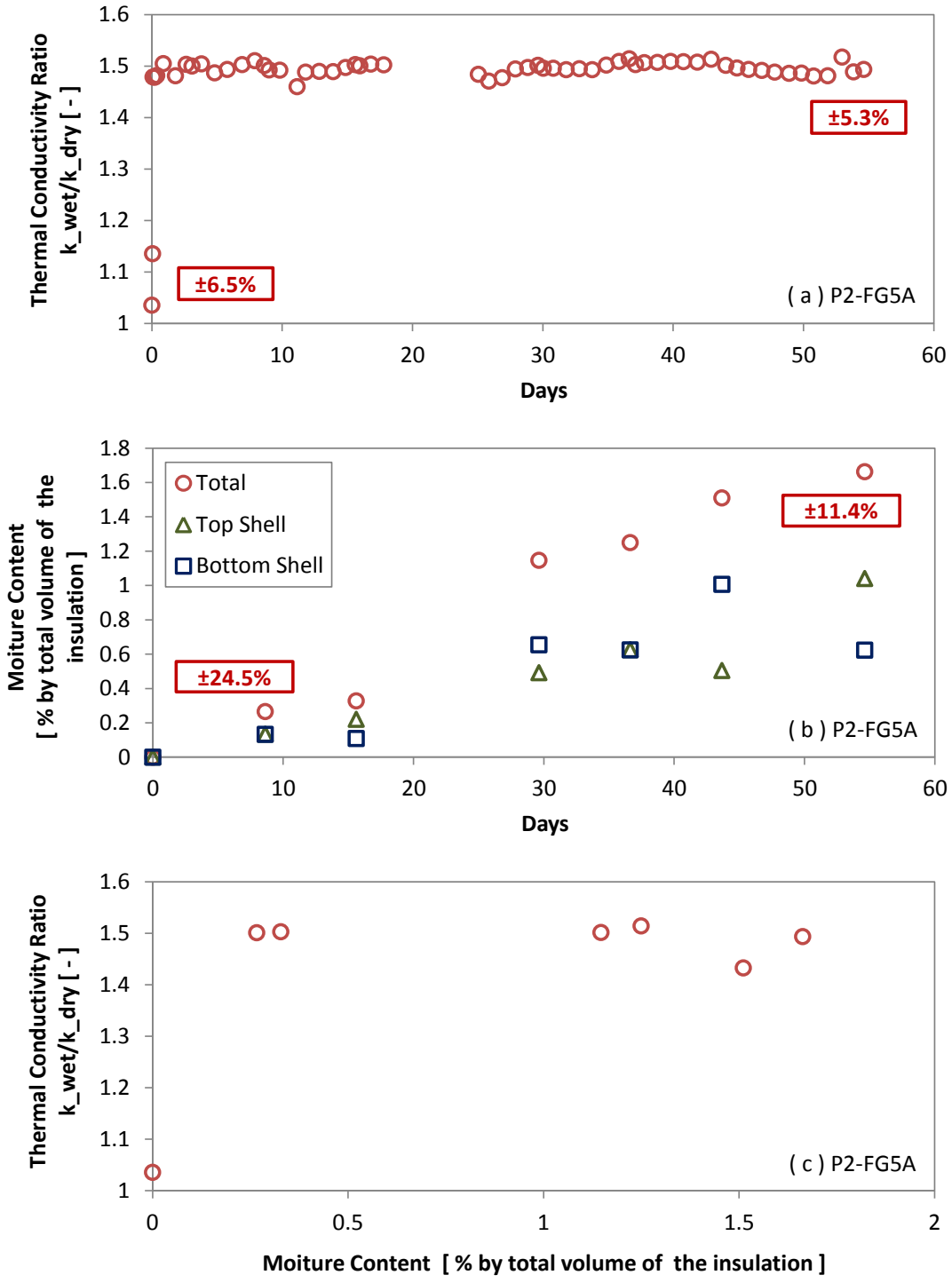

Figure 5.23: Experimental results on pipe insulation system P2-FG5A: (a) System thermal conductivity in real time during wet test period; (b) Moisture accumulation during wet test; (c) Effect of moisture content on the pipe insulation system thermal conductivity ratio

Fiberglass pipe insulation system P2-FG5B

Instead of testing on the bare pipe, the fiberglass pipe insulation system P2-FG5 was also tested on the black pipe (referred as P2-FG5B) under severe acceleration condition with high temperature and humidity, 90.1 ˚F (32.3 ˚C), 84%RH. This test lasted for 54 days. Compared to the large wet area that observed in system P1-FG, only one small wet spot was observed at the exterior surface of the bottom shell, and this wet region almost maintained the same during the entire test, as shown in Figure 5.24. One possible explanation for the formation of the much smaller wet region is the better edge seal in the current system. These better sealed edges affect the water vapor distribution in the insulation system, and led to a different quasi-steady state equilibrium in the longitudinal direction. A denser surface might be another possible reason to explain the smaller wet area that formed on the exterior surface of this system. Figure 5.24e shows the interior surface of both top and bottom shell of the fiberglass test sample in the system P2-FG5B. No obvious water marks were observed on the top shell, and the water droplets only covered the surface layer of the fibers. For the bottom shell, a large area of water mark was found at the location that circled out in the Figure 5.24a to d. This location might be a less dense region and led more water pass through the insulation system. The experimental results on the system thermal conductivity and moisture content were plotted in *Figure 5.25*. After 54 days test, the system thermal conductivity ratio increased up to 3.5 with the total moisture content around 15% by volume. The performance on the system thermal conductivity was similar to the results derived from the previous systems P1-FG and P2-FG5A, and demonstrates a two-step variation. The system thermal conductivity changed almost simultaneously with the ambient condition at the beginning of the moisture test. *Figure 5.25*b shows the moisture difference between the top and bottom shells, and similar to system P1-FG, more water was trapped in the bottom shell, and the moisture content was almost twice of the amount in the top shell.

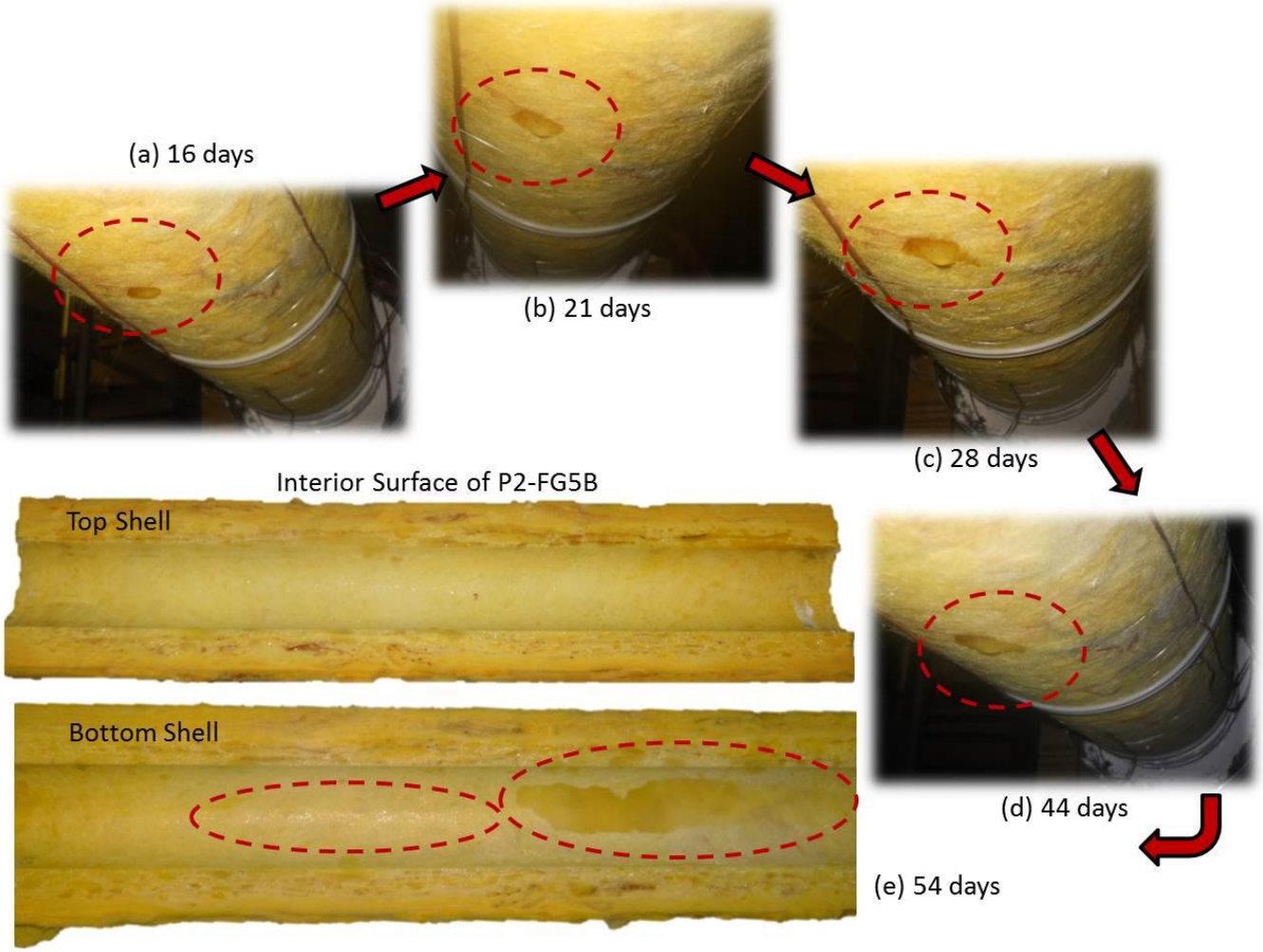

Figure 5.24: Moisture absorption on the bottom shell of pipe insulation system P2-FG5B

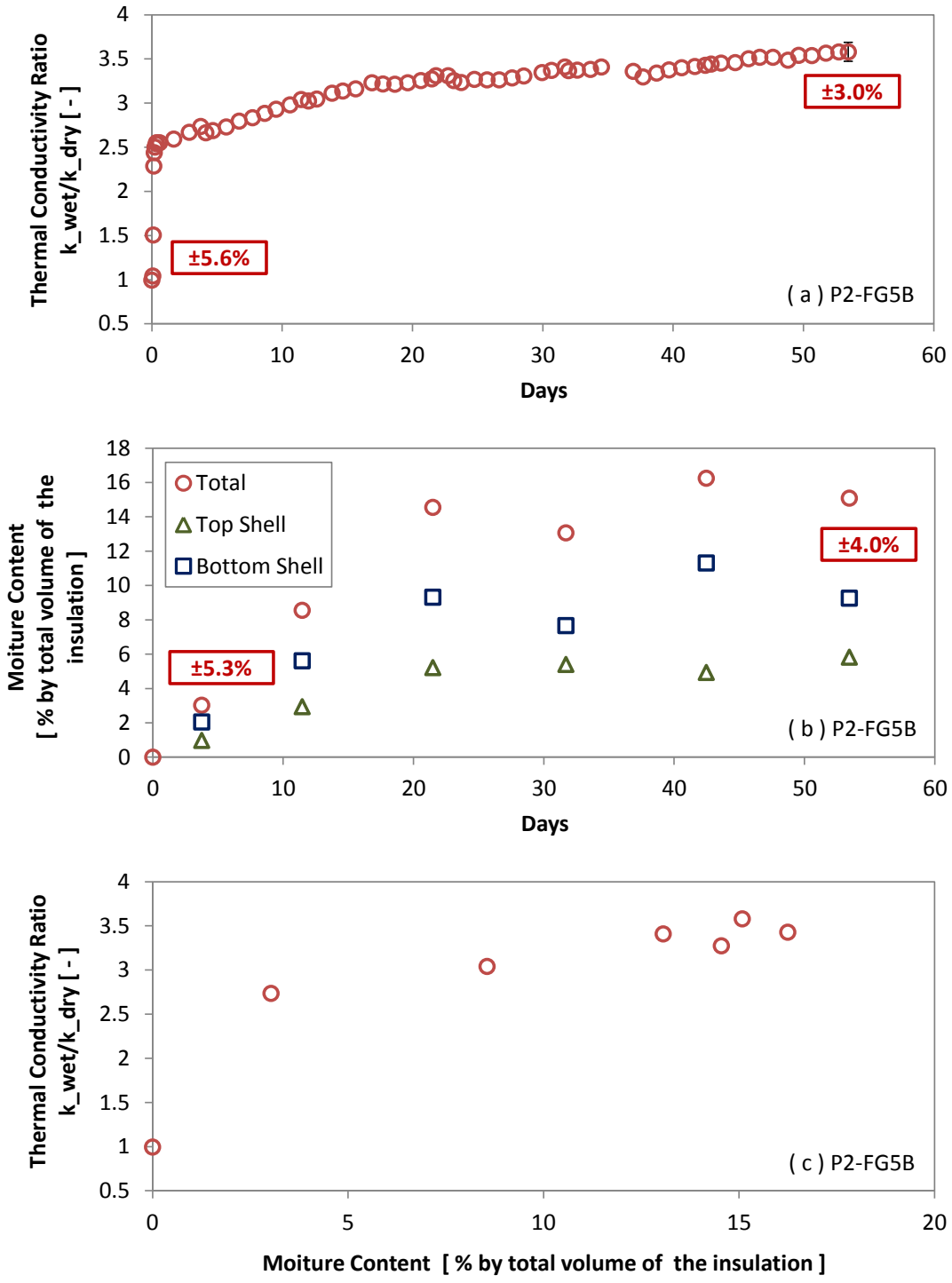

Figure 5.25: Experimental results on pipe insulation system P2-FG5B: (a) System thermal conductivity in real time during wet test period; (b) Moisture accumulation during wet test; (c) Effect of moisture content on the pipe insulation system thermal conductivity ratio

Fiberglass pipe insulation system P2-FG4

Different from previous three systems, pipe insulation system P2-FG4 was tested with water vapor barrier on the exterior surface of the fiberglass pipe insulation. This pipe insulation system was tested at 78.1 ˚F (25.6 ˚C), 54.8% relative humidity and the test lasted for 55 days. This ambient condition was very similar to the test condition provided in system P2-FG5A, and it was at a much lower temperature and humidity when compared to the other cases. Due to the presence of ASJ vapor retarder, no wet spot was observed during the moisture test. Figure 5.26 gives a comparison on the interior surface condition between the fiberglass pipe insulation that tested in system P2-FG4 and system P2-FG5A. In the pipe insulation system P2-FG4, there was no water droplet observed on the fibers, and the insulation interior surface appeared to be completely dry, as shown in Figure 5.26a. Figure 5.26b demonstrates the fiberglass interior surface of system P2-FG5A. There were several wet regions appeared along the interior surface of the bottom shell and larger wet areas were found next to the insulation end. Results showed the vapor retarder in the pipe insulation system would help prevent water vapor migration through the insulation material and the formation of the preferential paths.

The experimental results for system P2-FG4 was plotted in Figure 5.27. From Figure 5.27a, it indicates that the system thermal conductivity ratio increased slightly at the beginning of the moisture test, but in the second step, different from the previous three systems, the thermal conductivity ratio gradually decreased back to 1.0. The moisture content in the system was measured on two test samples, and both samples showed total moisture content around 0.25 to 0.26% by volume after 55 days test, *Figure 5.27*b. Due to this small amount of water, gravity effect become negligible for the water redistribution between the top and bottom shells, and the moisture content in both half shells were very similar.

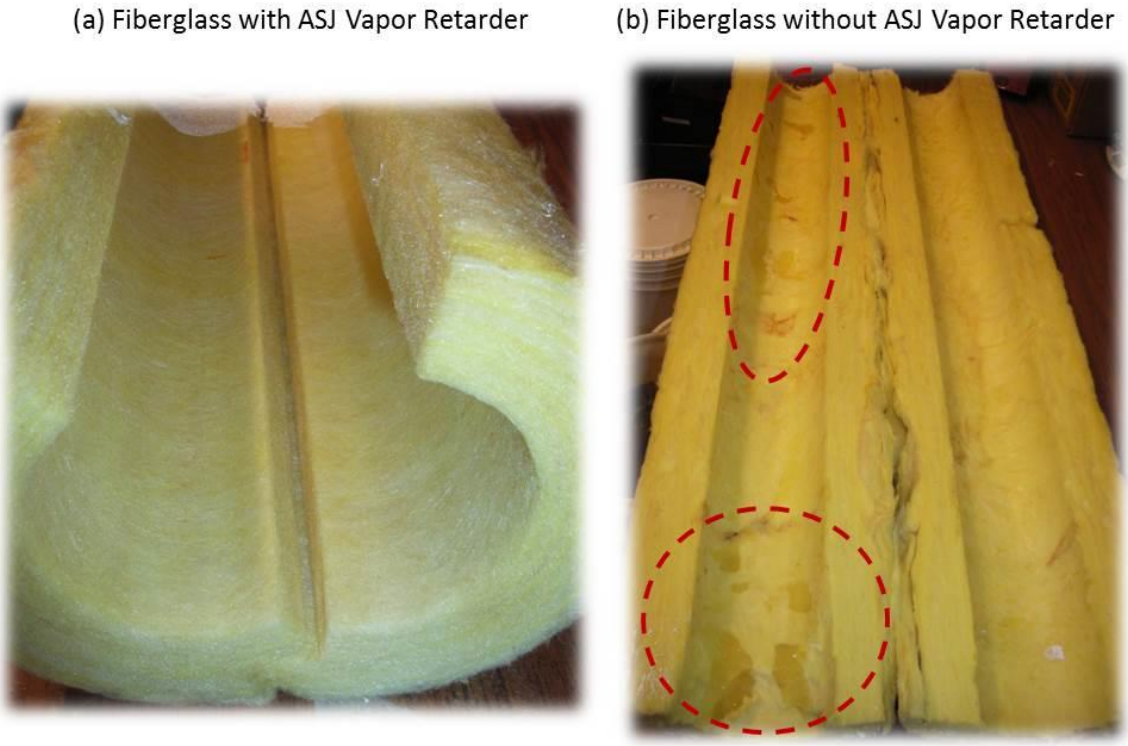

Figure 5.26: Comparison of the interior surface of pipe insulation systems P2-FG5A and P2-FG4: (a) P2-FG5A; (b) P2-FG4

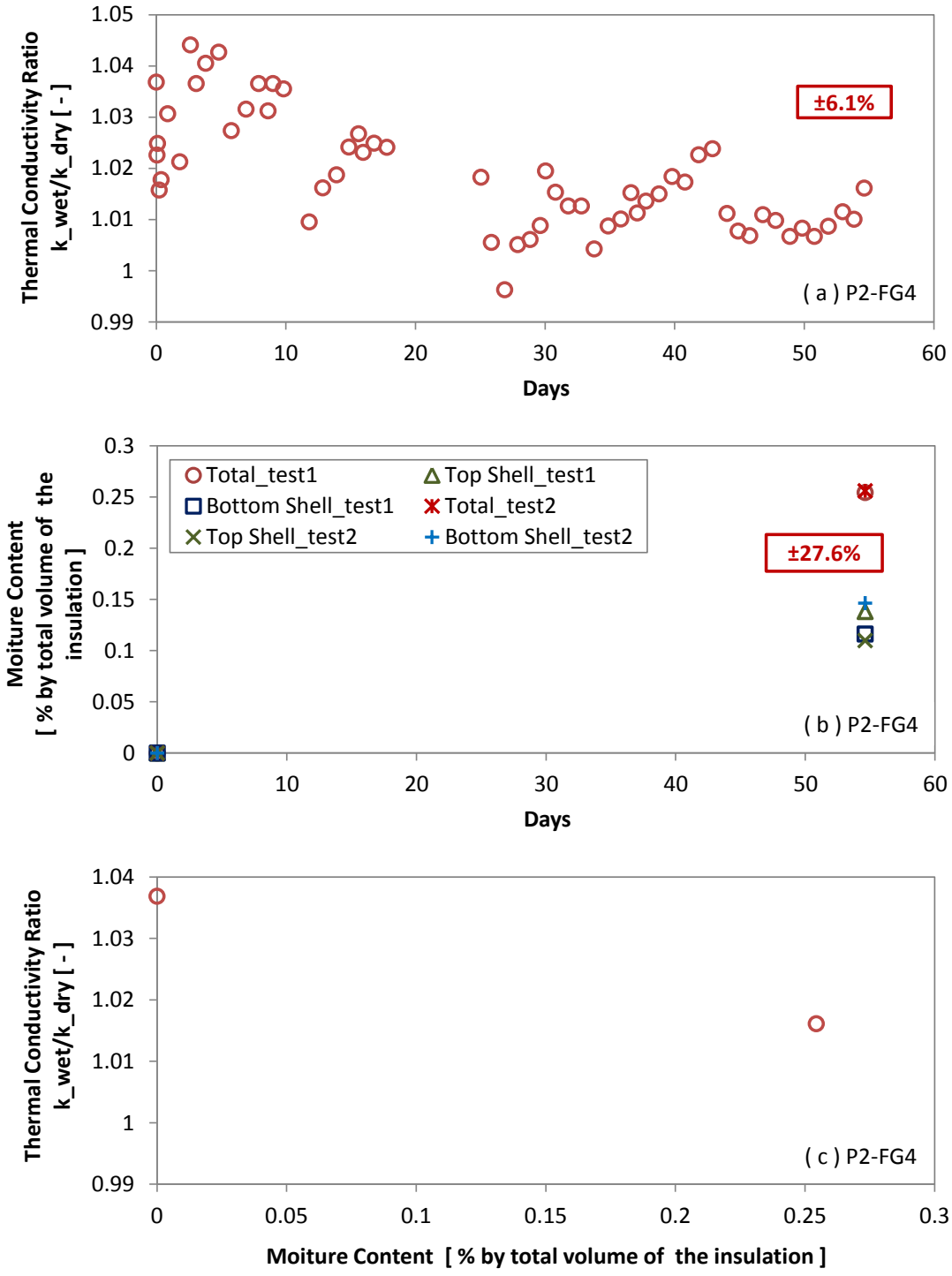

Figure 5.27: Experimental results on pipe insulation system P2-FG4: (a) System thermal conductivity in real time during wet test period; (b) Moisture accumulation during wet test; (c) Effect of moisture content on the pipe insulation system thermal conductivity ratio

In all the three cases on the pipe insulation system without vapor retarder, it is observed that the thermal conductivity ratio increased by 1.5 to 2.5 times of the dry reference value at the beginning of the moisture test. One possible reason for these dramatic increases on the system thermal conductivity is explained as follows. When the water vapor diffuses through the fibrous insulation and condensed in the regions with temperatures lower than the dew point, the water condensate would first accumulate at the points of the contact between fibers. The fibers were aligned perpendicular to the heat flow direction, and these beads of moisture enhanced the radial heat transfer immediately by providing preferential paths in the radial direction (McFadden, 1988). The presence of these preferential paths led to higher thermal bridging phenomenon that promoted larger heat losses and increased the thermal conductivity of the pipe insulation systems. It was also found that after this significant change, the system started to behave more stable. Although the system thermal conductivity continued rising, the rate was much lower than the previous step. This continuous increasing on the system thermal conductivity can be explained by the enlarged areas of the preferential paths and the fact that more regions of air gaps were replaced with water. Because of the constant water vapor pressure gradient across the pipe insulation, water vapor kept permeating into the insulation system. This amount of water condensate started coating along the fiber strands and gradually filled in the voids between the fibers (Ogniewicz and Tien, 1981). However, the impact of this step was not that severe as the one happed at the beginning of the test, because the direction of the heat flow would not be varied with the amount of water. The water amount was postulate to affect the moisture diffusion based on the diffusion mechanism discussed in the previous paragraph. After the formation of the preferential paths, the water condensate started accumulating on the exterior surface of the bottom shell due to surface tension and gravity effects (Modi and Benner, 1985). Water gradually coated the exterior fiber surfaces and increased the intersect areas among the strands until a quasi-steady state equilibrium was achieved in the longitudinal direction. Then the water started diffusing towards the adjacent inner layer of the fibers at a lower rate because of a lower local temperature

and water vapor permeability. However, for system P2-FG5B with black pipe, the thermal conductivity remained constant during the second step, and the moisture content was measured increasing from 0.3 to 1.66%. This discrepancy might be explained by the small amount of moisture that accumulated in the system and resulted in a minor change on the system thermal conductivity.

In the system P2-FG4, which was tested with ASJ vapor retarder, the thermal conductivity ratio also increased slightly in the first step. Although the vapor barrier around the exterior surface of the pipe insulation prevented water vapor transmission because of the low permeability, the water vapor that trapped in the insulation system would still condense in the low temperature region and formed the moisture beads at the contact points of the fibers. Due to the presence of the vapor barrier, the water vapor transmitted through system P2-FG4 at a much lower rate when compared to the water vapor transmission in the systems without vapor barrier. As a result, less preferential paths were formed during the first step, and the system thermal conductivity increased in a small range. In the second step, instead of coating the fibers and filling in the voids, the small amount of moisture might be redistributed in the system, and some of the moisture beads were shifted from the contact points of the fibers. This moisture redistribution procedure impacts the heat flow paths and result in a reducing on the system thermal conductivity.

In industry, the surface of the fibers may be manufactured either as hydrophobic or hydrophilic. According to the literature (Ge *et al.*, 2006), the water layer was found to be in a higher density near hydrophilic surfaces than in the bulk, while a thin layer of low density of water has been observed near hydrophobic surfaces. It seems that hydrophilic surfaces would accelerate the formation of thermal bridging by contacting two layers of fiber strands in the radial direction. However, with hydrophobic surfaces, more water condensate would drip out of the insulation system, and the convection heat transfer might be enhanced to decrease the system thermal

performance. Till now, the impact of insulation material surface tension still need to be further investigated.

5.5.2 Closed-cell pipe insulation

For closed-cell insulation, conduction, convection, and radiation heat losses are inhibited from the thin cell walls, which decrease the cross-sectional flow path areas, and by micro air pockets that surround the cells (McFadden, 1988). Four types of closed-cell materials, phenolic, cellular glass, elastomeric rubber and polyisocyanurate (PIR) were tested in six different pipe insulation systems under moisture condition. The test conditions are shown in Table 5.10.

Table 5.10: Fiberglass pipe insulation systems tested under wet conditions

Test Samples (Ref. No.)	**Test Pipe Temperature ˚F (˚C)**	**Ambient Temperature ˚F (˚C)**	**Relative Humidity %**	**Test Length Days**	**Actual Diameter inch (mm)**	**Vapor Retarder or Jacketing**
Phenolic (P1-P2)	40.7 (4.9)	96.4 (35.8)	87	24	*7.5(190.5)	N/A
Phenolic (P2-P)	40.7 (4.9)	107.7 (42.0)	82	45	7.7 (195.6)	N/A
Polyisocyanurate (P2-PIR2)	40.7 (4.8)	107.4 (41.9)	82	45	6.8 (172.7)	N/A
Cellular Glass (P2-CGA)	38.0 (3.4)	90.6 (32.6)	83	57	6.8 (172.7)	N/A
Cellular Glass (P2-CGB)[1]	37.7 (3.2)	89.8 (32.1)	83	64	6.6 (167.6)	N/A
Elastomeric Rubber(P2-ER1)	36.8 (2.7)	90.6 (32.6)	83	57	6.8 (172.7)	N/A

[1]: The pipe insulation system was tested on a black pipe
*: Actual diameter is not available. Use nominal diameter instead.

An overview of the closed-cell pipe insulation system around the first PIT and around the second PIT is shown in Figure 5.28. The first PIT was used for the system thermal conductivity measurement by installing a full length of test sample, and the second PIT was aimed to measure the moisture content by installing six sectioned pieces of the same insulation sample. For both PITs, the end sections were sealed with vapor sealant. Based on different pipe insulation systems, either joint sealant or vapor sealant were applied between each 6-in (152.4 mm) long section. Highly adhesive vapor sealant is not recommended because they may damage the insulation

samples during the sampling procedure. Water-based sealant also need to be carefully used because the moisture in the sealant might transport into the insulation and affect the test results.

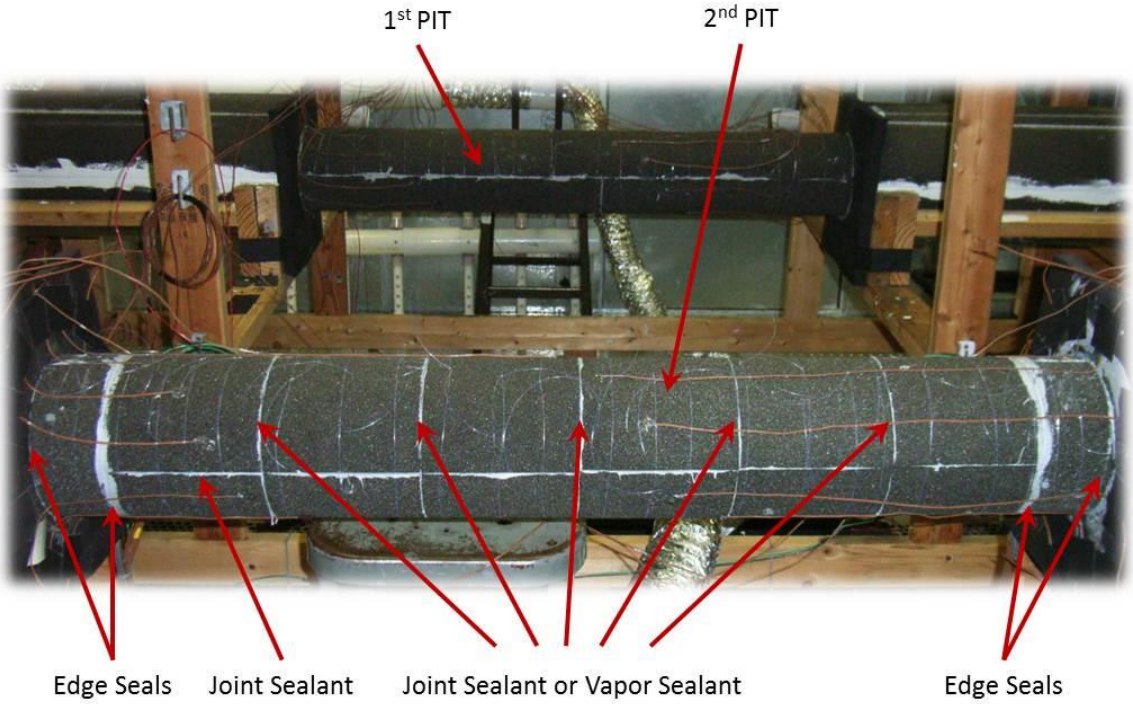

Figure 5.28: Photo of the closed-cell pipe insulation system installation for the wet test

Phenolic pipe insulation systems P1-P2 and P2-P

Phenolic pipe insulation was tested in two systems, P1-P2 and P2-P under different ambient conditions, as shown in Table 5.10. For system P1-P2, the ambient temperature was controlled at 96.3 ℉ (35.7 ℃) and the relative humidity was set to 87.1%. In these psychrometric conditions, the air dew point temperature was about 91.8 ℉ (33.2 ℃). Boss 368 butyl rubber sealant was applied along the longitudinal joints of the C-shells during the installation of phenolic pipe insulation. Foster 90-66 was applied at the two end sides of the insulation system as edge seals. An easy-to-peel off vapor sealant, Foster 30-80, was applied as 1/8-in (3.175 mm) thickness layer on the entire cross sectional surface of the insulation samples on the second PIT. Pipe insulation system P2-P was tested at a more severe condition. The ambient temperature was 107.7 ℉ (42

℃), and the relative humidity was 82%. A different type of the vapor sealant, Chil-Perm CP 70 was applied on all longitudinal and butt joints in the system on the first PIT, and between each 6-in (152.4 mm) sections on the second PIT.

Phenolic pipe insulation system P1-P2 was tested for 24 days. During the moisture test, there were no visible regions of moisture accumulation on the outer surface of the insulation system. At day 24, a small wet spot was observed at the bottom surface next to the end section of the insulation system, as shown in Figure 5.29.

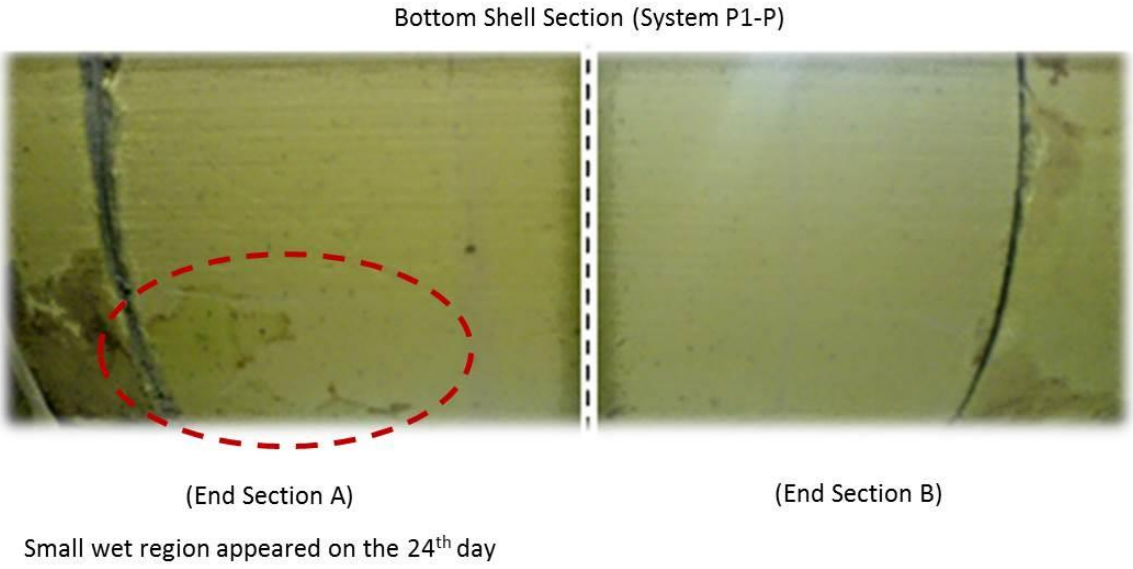

Figure 5.29: Photos of the wet regions at the bottom surface of the phenolic pipe insulation system P1-P2 at the day 24 since the wet test

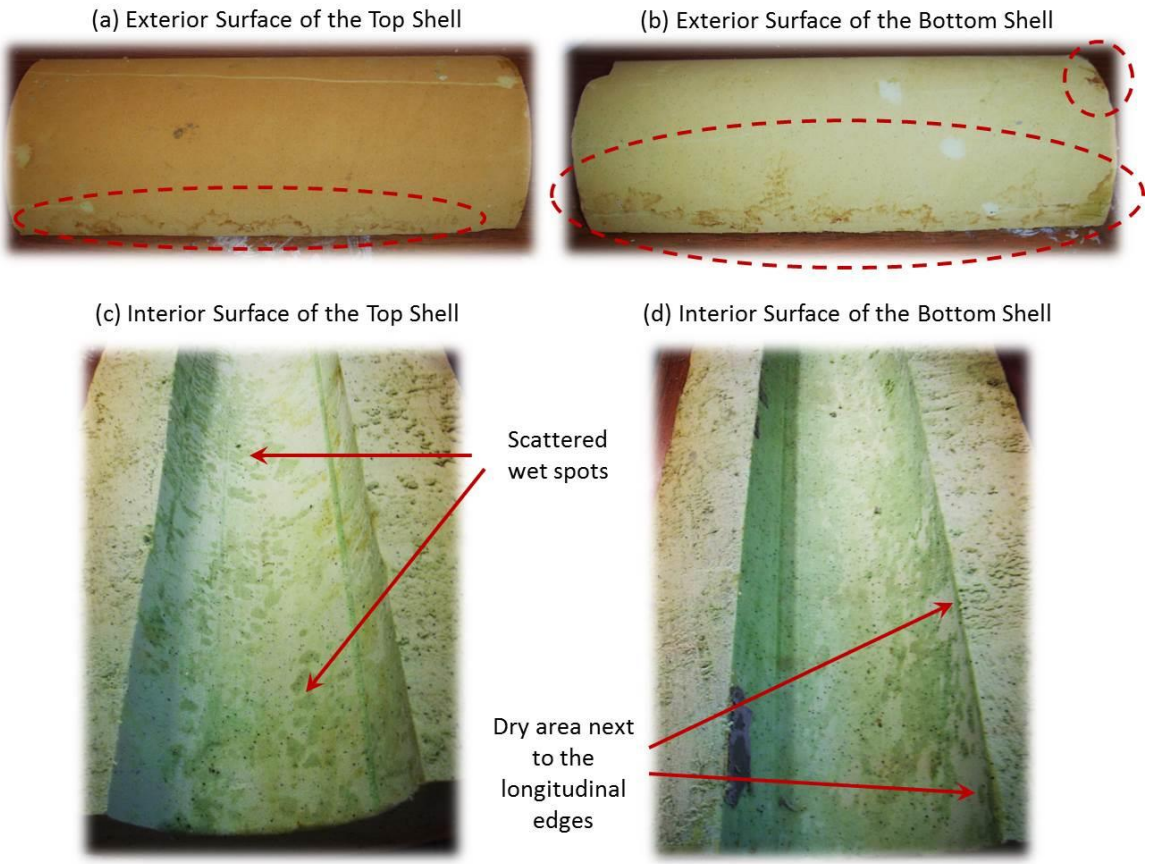

Figure 5.30: Photos of the wet regions at the top and bottom surfaces of the phenolic pipe insulation system P2-P at the day 45 since the wet test

Phenolic pipe insulation system P2-P was tested for 45 days. Figure 5.30 shows the wet regions that observed on both top and bottom shells by the end of the test. Similar to the system P1-P, no visible regions of moisture accumulation were observed on the exterior surface. However, several water marks were found next to the longitudinal joint on both top and bottom shells, see Figure 5.30a and b. These water marks were probably caused by the water condensed on the joint sealant surface. Compared to the insulation material, joint sealant was a more conductive layer, and the surface temperature would be lower than the insulation exterior surface temperature. In order to determine the joint sealant impact, an infrared camera was used to provide a surface temperature distribution profile in the pipe insulation system. This sample file was shown in Figure 5.31. The

green/blue lines represent longitudinal and butt joints sealed with joint sealant, and these local temperatures were almost 3˚F (1.7˚C) lower than the insulation surface temperature. Therefore, with the presence of the joint sealant, water vapor would condense first on the surface of the joint sealant layer, and then drip along the exterior surface of the pipe insulation. Figure 5.30c and d demonstrate the interior surface conditions at the end of the test. A large amount of scattered wet spots (in the dark green color) were found at the inner surface of the top shell. Due to the bowl shape of the bottom C-shell, water condensate would be collected in the small gaps between the test pipe and the insulation interior surface. Because of a continuous immersion in the water, the entire inner surface of the bottom shell was almost wet and only several dry areas left next to the longitudinal edges.

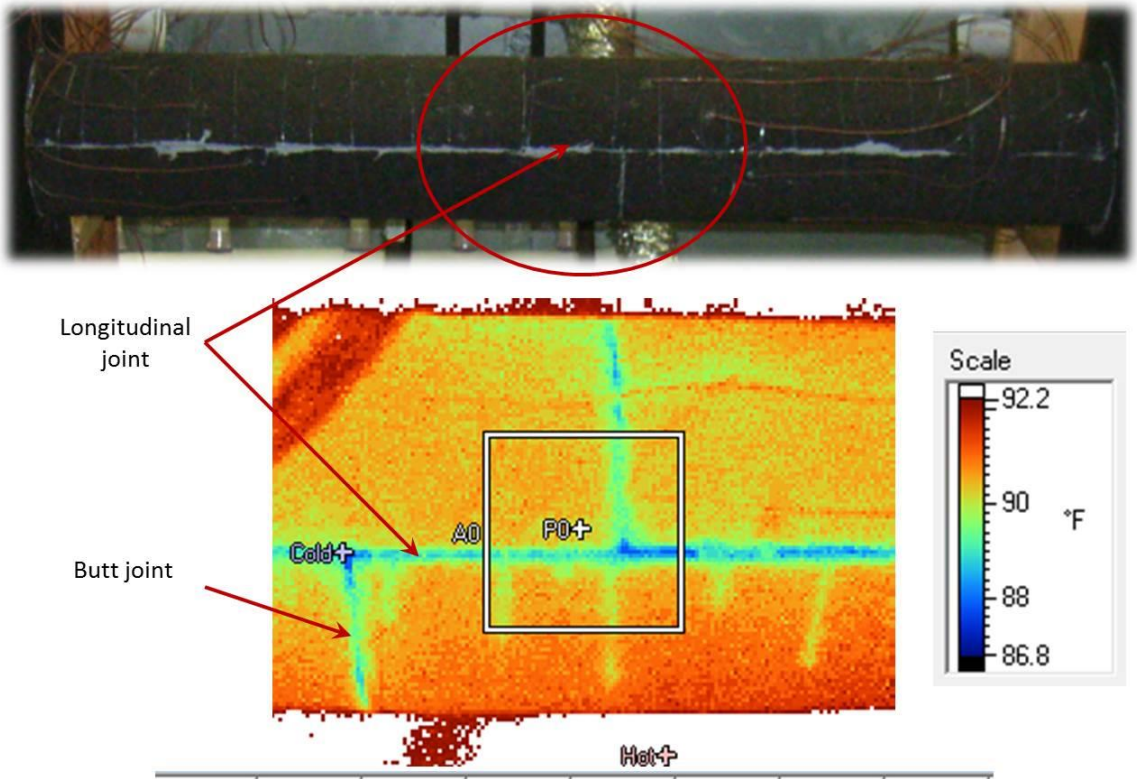

Label	Emis	BG	Ave	SD	Max	Min	Unit
A0	0.95	68.0	90.21	0.50	91.4	87.8	F
Cold	0.95	68.0	87.58	0.00	87.6	87.6	F
Hot	0.95	68.0	93.88	0.00	93.9	93.9	F
P0	0.95	68.0	90.28	0.00	90.3	90.3	F

Figure 5.31: Temperature distribution sample in the pipe insulation system with joint sealant

The diffusion mechanism was studied in Figure 5.32. Figure 5.32a to d are the photos of the cross sections of the phenolic test samples that were removed periodically from the second PIT, and Figure 5.32e to f show the cross section of the full length test sample removed from the first PIT. An extra piece of insulation, ¼ to ½-in (6.4 to 12.7 mm) thick, was cut off from the sample to eliminate edge effect, which was caused by the vapor sealant applied between each 6-in (152.4 mm) section and the insulation ends. According to the material characteristics, this type of light green phenolic will turn into a dark green color if the material becomes wet. On the 10^{th} day of the moisture test, the cross section of both top and bottom shells almost maintained a light green color, and only several water droplets were found next to the interior surfaces. After 17 days test, a very thin layer of dark green area started to form on the bottom shell as shown by the red arrow in Figure 5.32b. No obvious changes were observed on the top shell. On the 24^{th} day of the wet test, dark green regions were found next to the interior surface of both top and bottom shells, see the red arrows in Figure 5.32c. When cutting off the extra piece of insulation, the surfaces of the cross sections became wet because of the water coming out from the open pores. The piece of paper that prepared below the insulation sample started to become wet, as the region circled out by the dash line. After 31 days test, the dark green area increased in both two C-shells and larger water marks were found on the piece of paper below the insulation samples. By the end of this moisture test, it seems that the dark green region kept increasing, as shown in Figure 5.32e and f. Based on these observations, the diffusion mechanism in this closed-cell pipe insulation system seems to be different from the fiberglass insulation system. Due to the closed-cell structure, much less preferential paths were formed in the phenolic pipe insulation. Water condensate filled in the voids among each cell and diffused into closed pores gradually from the interior surface to the exterior. The only possibility for the formation of the preferential paths is the joints existed in the pipe insulation system. These joints include longitudinal joints between two half C-shells, butt joints between two full length pieces of pipe insulation, and the material joints that factory-made during pipe insulation fabrication. This would explain the fact that only small wet regions were

observed next to the edges on the pipe insulation exterior surfaces, Figure 5.29 and Figure 5.30a and b. It is also found that the appearance on the cross section of the top and bottom shells were very similar. The possible reason is explained as follows. The gas trapped in the closed-cell will be replaced by the water vapor when there is a large water vapor pressure difference across the pipe insulation system. When water vapor condenses, the portion of water condensate remains in the pores because the cell walls prevent water redistribution. Under this circumstance, gravity effect becomes a less important factor during the moisture distribution between top and bottom shells. However, it still needs to be considered because it will affect the liquid water distribution in the gaps between the test pipe and insulation inner surface. It leads more water to accumulate in the bottom shell of this annular space. This explains the scattered wet spots found on the interior surface of the top shell, and the larger wet region on the inner surface of the bottom shell.

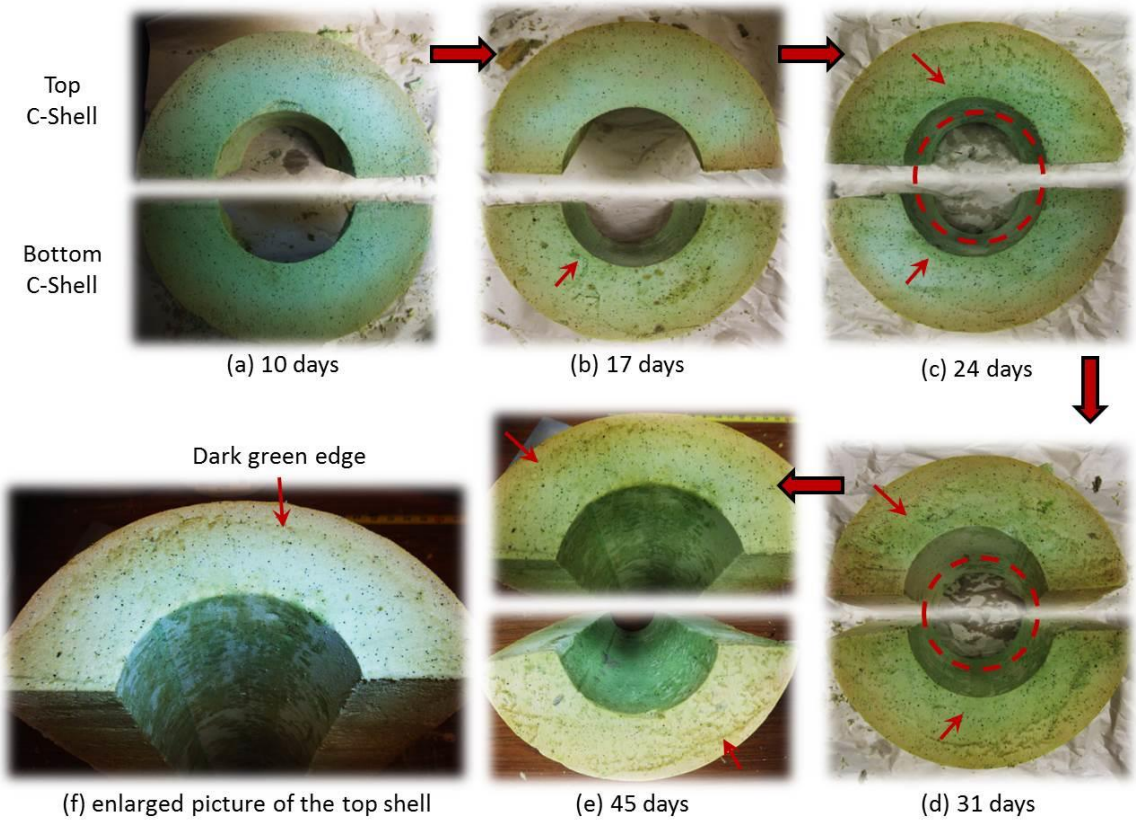

Figure 5.32: Photos of the cross section of phenolic pipe insulation during moisture test

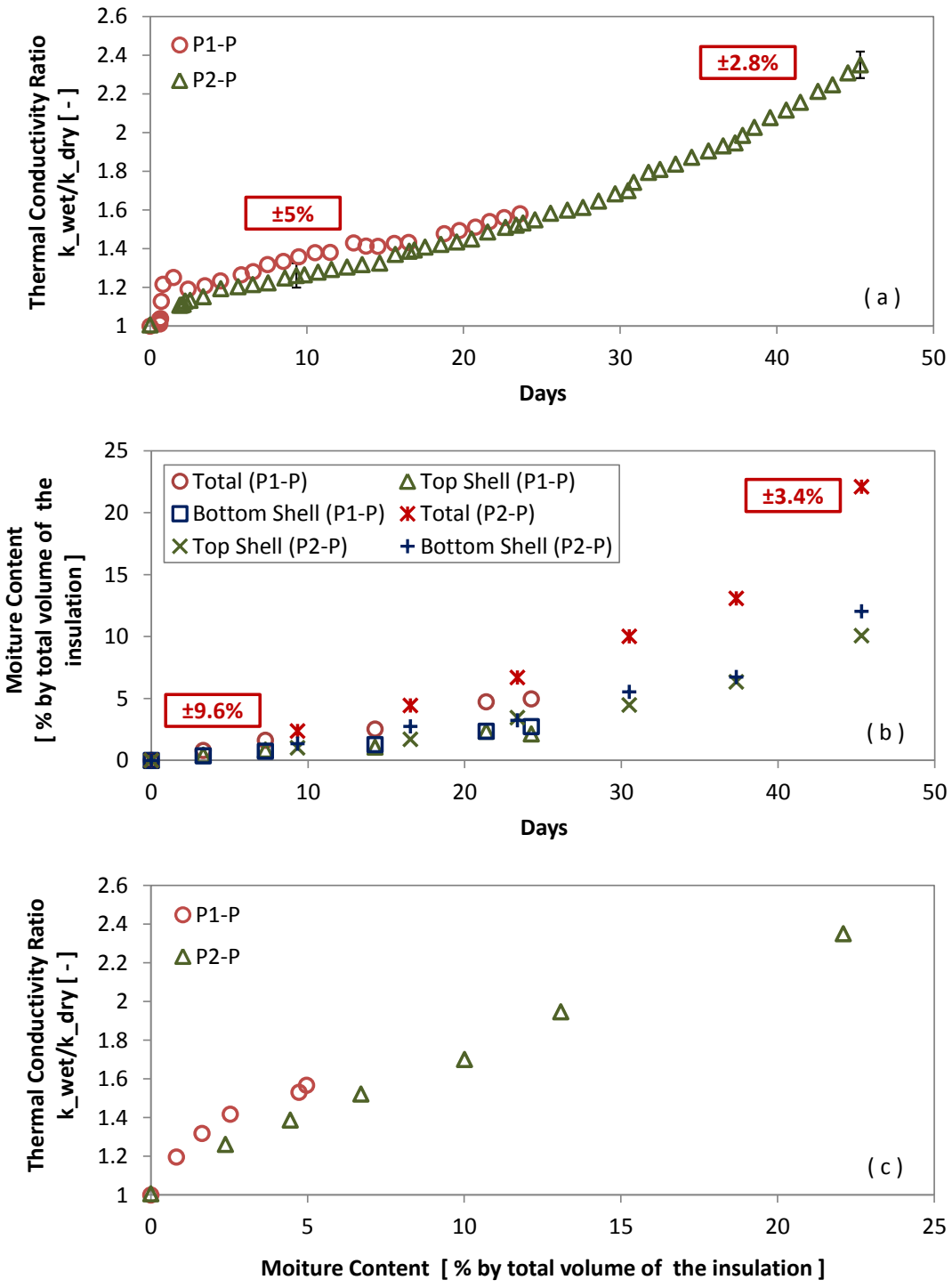

Figure 5.33: Experimental results on pipe insulation system P1-P2 and P2-P: (a) System thermal conductivity in real time during wet test period; (b) Moisture accumulation during wet test; (c) Effect of moisture content on the pipe insulation system thermal conductivity ratio

The experimental results on the variation of thermal conductivity and moisture content in phenolic pipe insulation systems P1-P2 and P2-P are given in Figure 5.33. Figure 5.33a shows the phenolic pipe insulation thermal conductivity at below ambient temperature in wet condensing conditions and with moisture ingress. In system P1-P2, the thermal conductivity ratio was derived from the thermal conductivity in wet conditions, k_{wet}, to the corresponding thermal conductivity in dry condition, k_{dry}. In system P2-P, the reference value under dry condition was updated based on the test pipe surface temperature by applying the correlation developed from the mapping test, as described in section 4.2.3. After 24 days test on system P1-P2, the thermal conductivity ratio increased to 1.57 with total moisture content around 5% by volume. System P2-P was tested under a more severe condition for 45 days, and the thermal conductivity ratio increased to 2.35 when the moisture content was around 22%. It seems that there is a slightly increase on the system thermal conductivity at the beginning of the moisture test, but the increasing range was much lower than fiberglass pipe insulation systems. Figure 5.33b shows the moisture content in the phenolic pipe insulation at below ambient temperature and in wet (condensing) conditions. In system P1-P2, the moisture content reached 5% by volume of the pipe insulation system, and the moisture content increased to 22% by volume in the system P2-P. For both phenolic pipe insulation systems, the moisture content was fairly uniform between the top C-shell sections and the bottom C-shell sections. According to the literature, the maximum moisture absorption for flat cubic specimen of phenolic insulation is expected to be between 3 to 8% by volume depending on actual density of the specimen (ASTM_C1126, 2009). However, this value was derived based on a two hour immersion test under ambient condition with temperature at 73±1˚F (23±2˚C) and relative humidity around 50±5% (ASTM_C209, 2007). This test might underestimate the moisture content that can trap in the insulation systems applied in the field because it neglect the impact of water vapor pressure difference between the cold surface and the ambient conditions. The water pressure gradient will be the key for the moisture migration in pipe insulation system. Figure 5.33c plotted the thermal conductivity ratio versus the moisture content, and it shows that

for both cases, the system thermal conductivity increased almost linearly with the moisture content in the pipe insulation system.

Polyisocyanurate (PIR) pipe insulation system P2-PIR

The test sample selected in the system P2-PIR has a nominal thickness of 1 ½ -in (38.1 mm) without any vapor retarder on the exterior surface, see Table 5.7. Similar to system P2-P, P2-PIR was also tested under a most severe condition with the ambient temperature at 107.4 ℉ (41.9 ℃), and the relative humidity around 82%. At this condition, the dew point was around 100.7 ℉ (38.1 ℃). Chil-Perm CP 70 was the vapor sealant applied on all longitudinal and butt joints in the system on the first PIT, and also between each 6-in (152.4 mm) sections on the second PIT. The moisture test lasted for 45 days. By the end of the test, no wet regions were observed on the exterior surface of the pipe insulation system, as shown in Figure 5.34. The water marks circled out by the red dash line were caused by the movement of the water that condensed on the joint sealant surface.

The experimental results on the variation of thermal conductivity and moisture content in the pipe insulation system P2-PIR are shown in Figure 5.35. Figure 5.35a shows the PIR pipe insulation thermal conductivity at below ambient temperature in wet condensing conditions and with moisture ingress. By the end of the moisture test, that is, the 45^{th} day, the system thermal conductivity increased to 1.51 times of the dry reference value, which was determined from the mapping procedure. At the beginning of the test, the humidifier was on for two hours, and it was off for 24 hour due to technical problems. When the humidifier was back to work, I immediately started data recording procedure, and the experimental results from both transient and steady-state conditions showed that there was a 10% increase on the system thermal conductivity. The total moisture content accumulated in the insulation system was measured around 16% by volume, and the difference between the top and bottom C-shells were small and within the uncertainty range,

see Figure 5.35b. Figure 5.35c shows the variation on thermal conductivity ratio with different moisture content in the insulation system, and a linear correlation seems to fit the data set.

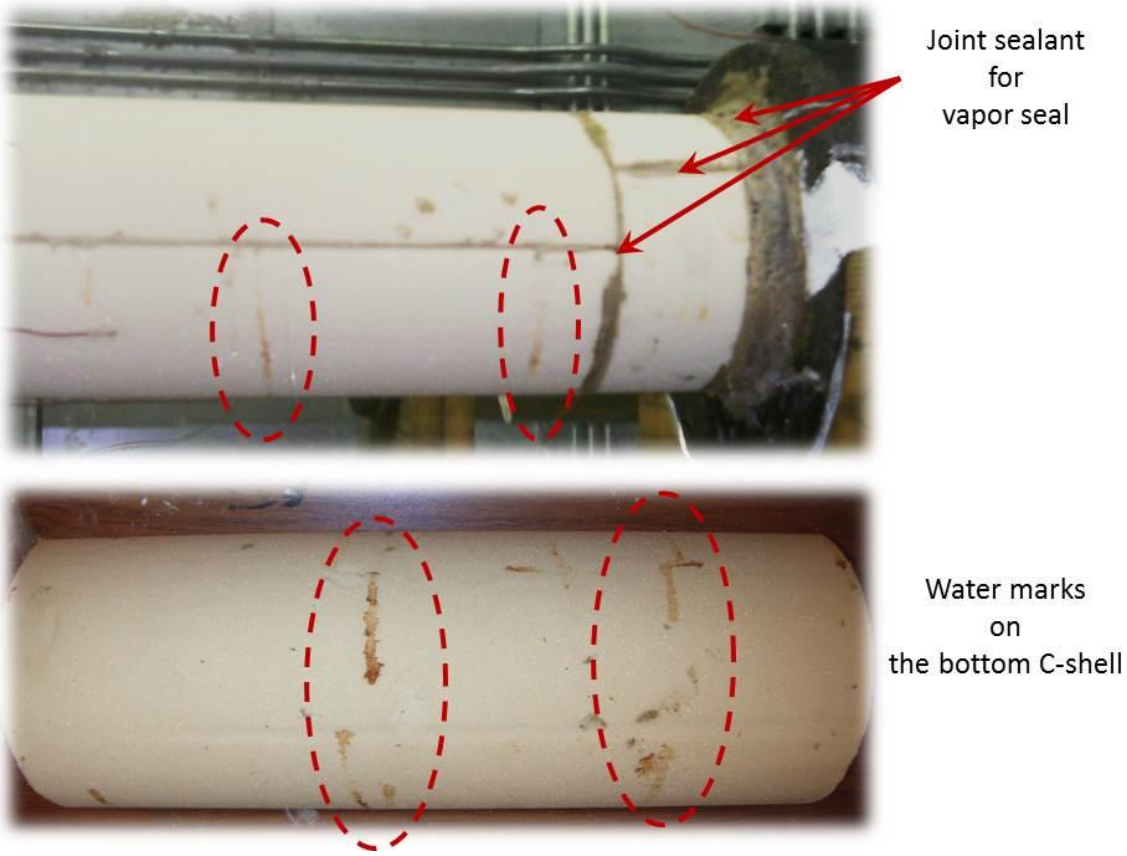

Figure 5.34: Photos of the water marks in PIR pipe insulation system P2-PIR

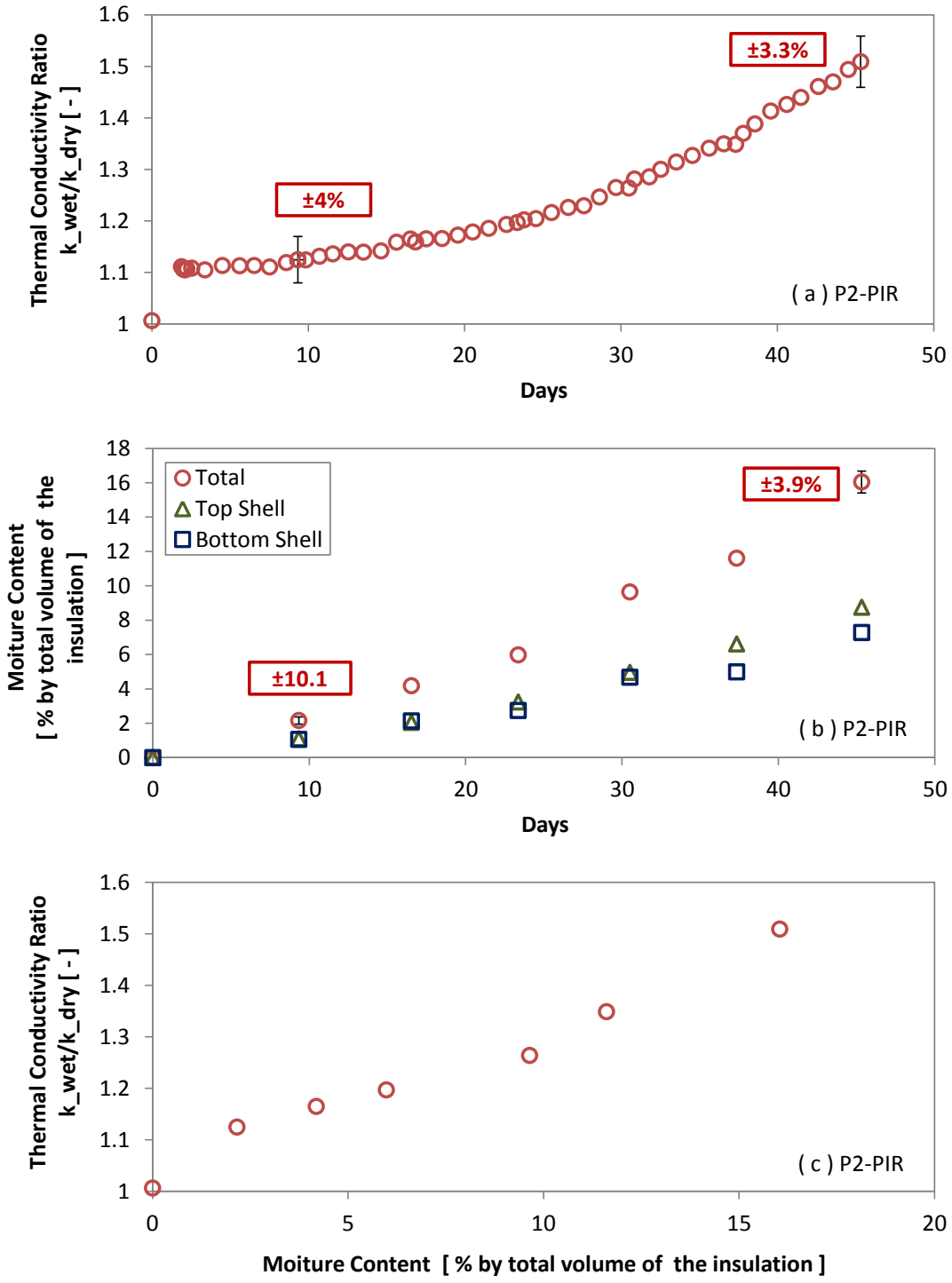

Figure 5.35: Experimental results on pipe insulation system P2-PIR: (a) System thermal conductivity in real time during wet test period; (b) Moisture accumulation during wet test; (c) Effect of moisture content on the pipe insulation system thermal conductivity ratio

Cellular glass pipe insulation systems P2-CGA and P2-CGB

Cellular glass pipe insulation was tested twice in the similar ambient condition. The difference between system P2-CGA and P2-CGB is the test pipe. In the system P2-CGA, cellular glass pipe insulation was installed around the bare pipe with thermocouple grooved exposed to the interior surface of the test sample, and in the system P2-CGB, the test pipe was sealed with aluminum tape and painted as black to avoid radiation impact. The test samples in both systems has a nominal wall thickness of 1 ½ -in (38.1 mm). Boss 368 butyl rubber sealant was applied as the joint sealant, and also used for edge seals on both PITs. System P2-CGA was tested at an ambient temperature around 90.6 ℉ (32.6 ℃), and the relative humidity at 83%. At this condition, the dew point was around 84.8 ℉ (29.3 ℃). System P2-CGA was tested with ambient temperature at 89.8 ℉ (32.1 ℃), relative humidity at 83%, and the dew point was around 83.9 ℉ (28.8 ℃). The test length for system P2-CGA and P2-CGB are 57 and 64 days, respectively.

For both cellular glass pipe insulation systems, no wet spots were observed on the insulation surface, but large amount of water condensate occurred on the joint sealant surface, and dripped along the exterior surface of the bottom C-shell, as shown in Figure 5.36 and Figure 5.37. By the end of the moisture test, more water was found to accumulate in the bottom C-shell, and formed larger wet area at the interior surface. For the top shell, the wet region only formed next to the insulation ends, as circled out in Figure 5.38a. In pipe insulation system P2-CGA, one piece of the test sample, which used as the bottom shell, was manufactured with material joint and wet regions appeared next to the material joints on both interior and exterior surfaces. The material joints and wet regions are shown in Figure 5.38b.

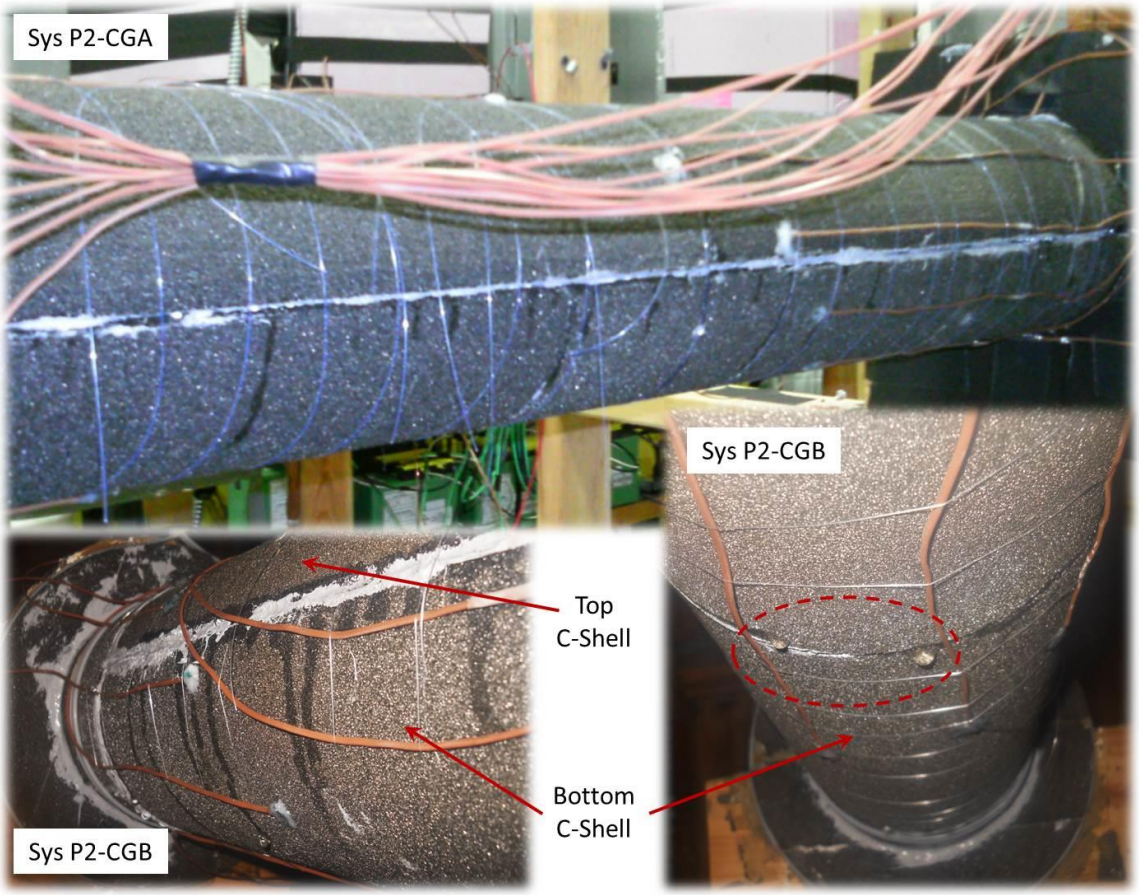

Figure 5.36: Photos of the exterior appearance on cellular glass pipe insulation system P2-CGA and P2-CGB

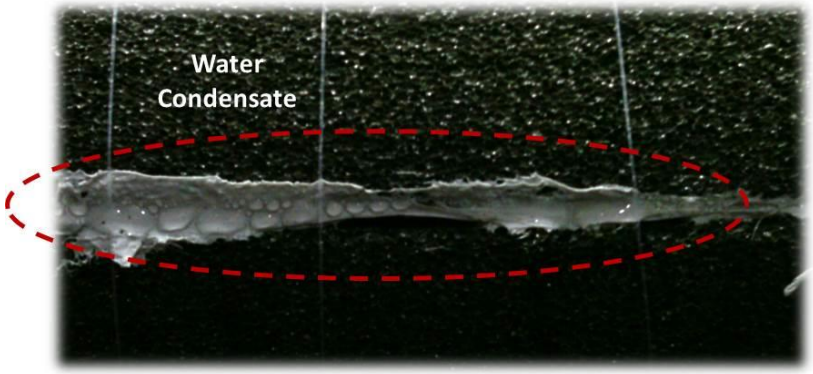

Figure 5.37: Photos of the wet regions at the top and bottom surfaces of the phenolic pipe insulation system P2-P at the day 45 since the wet test

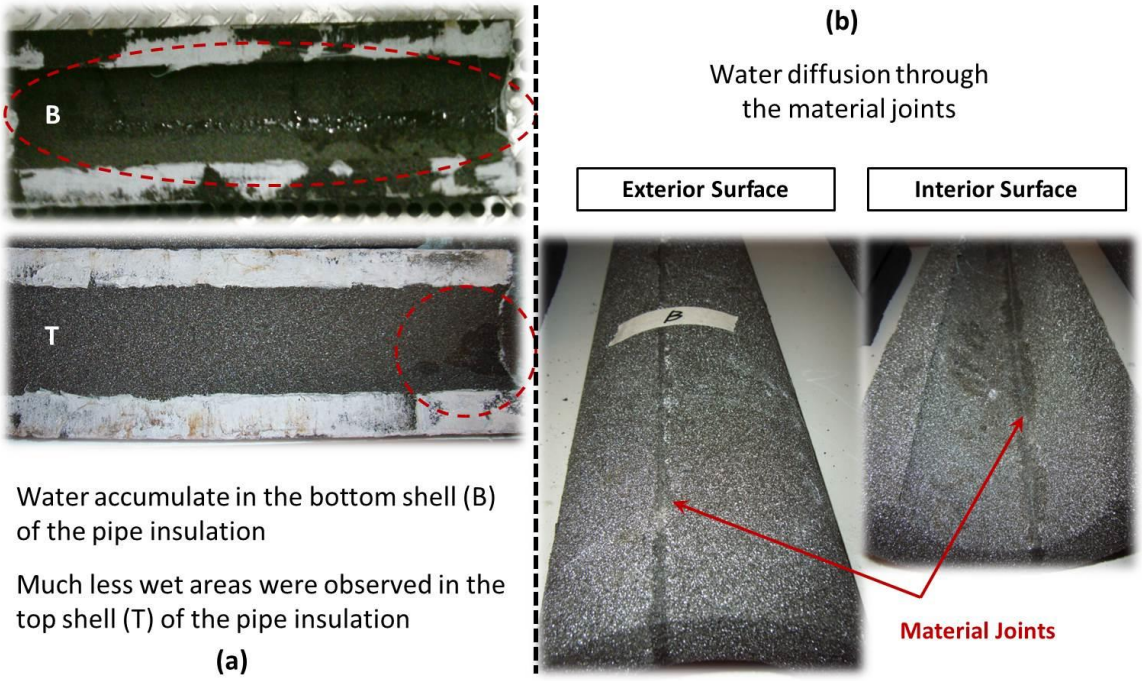

Figure 5.38: Wet regions in cellular glass pipe insulation system P2-CGA

The experimental results on the variation of thermal conductivity and moisture content in pipe insulation systems P2-CGA and P2-CGB are shown in Figure 5.39. In both systems, the thermal conductivity increased slightly at the beginning of the moisture test. In system P2-CGA, the system thermal conductivity increased by 7% on the 15^{th} day, and maintained almost constant until the end of the moisture test. The system thermal conductivity in P2-CGB increased slower than the thermal conductivity in system P2-CGA, and showed a continuous rising till the last day of the moisture test. For the moisture measurement, due to the small amount of water being collected in the insulation system, the uncertainties in both pipe insulation systems exceed ±15%. In system P2-CGA, the total moisture content was 0.32% by volume after 57 days test, and for in system P2-CGB, the total moisture content reached 0.27% by volume after 64 days test. One possible reason for the fact that system P2-CGA was found at higher thermal conductivity and

moisture content is the presence of the material joint. It should be noted that the difference on the results between these two systems were within the uncertainty range. Because of the small amount of water content, there was no certain pattern of correlation suitable between the system thermal conductivity ratio and moisture content, as shown in Figure 5.39c.

Elastomeric rubber pipe insulation system

Different from previous three pipe insulation systems, elastomeric rubber pipe insulation is usually manufactured as un-slit sleeves, or as an insulation wrap, and normally joint sealant is not a requirement during system installation. In this moisture test, elastomeric rubber pipe insulation system P2-ER was tested as an insulation wrap with adhesive tape along the longitudinal joint. The test sample has a nominal wall thickness of 1 ½ -in (38.1 mm) and the test sample was installed as one piece around the whole test pipe on both 1st and 2nd PITs. The seam with the adhesive tape must be installed as face-up on the top of the insulation system. During sampling procedure, one 6-in (152.4 mm) section need to be directly cut out from the entire piece on the 2nd PIT. Then the void was replaced by another dry sample. Plastic film and joint sealant are required between the newly installed sample and the adjacent pieces. Aeroseal was the sealant used in the edge seals and between each 6-in (152.4 mm) sample. Elastomeric rubber pipe insulation system P2-ER was tested at 90.6 ℉ (32.6 ℃), with relative humidity at 83%, and the dew point was around 84.8 ℉ (29.3 ℃). The moisture test lasted for 57 days. Similar to the other closed-cell pipe insulation systems, no visible wet regions were observed on the exterior surface of the pipe insulation during the moisture test. Two wet regions were found on the interior surface, as shown in Figure 5.41. It seems that the water condensate only stayed on the interior surface because the water droplet could still move along the surface.

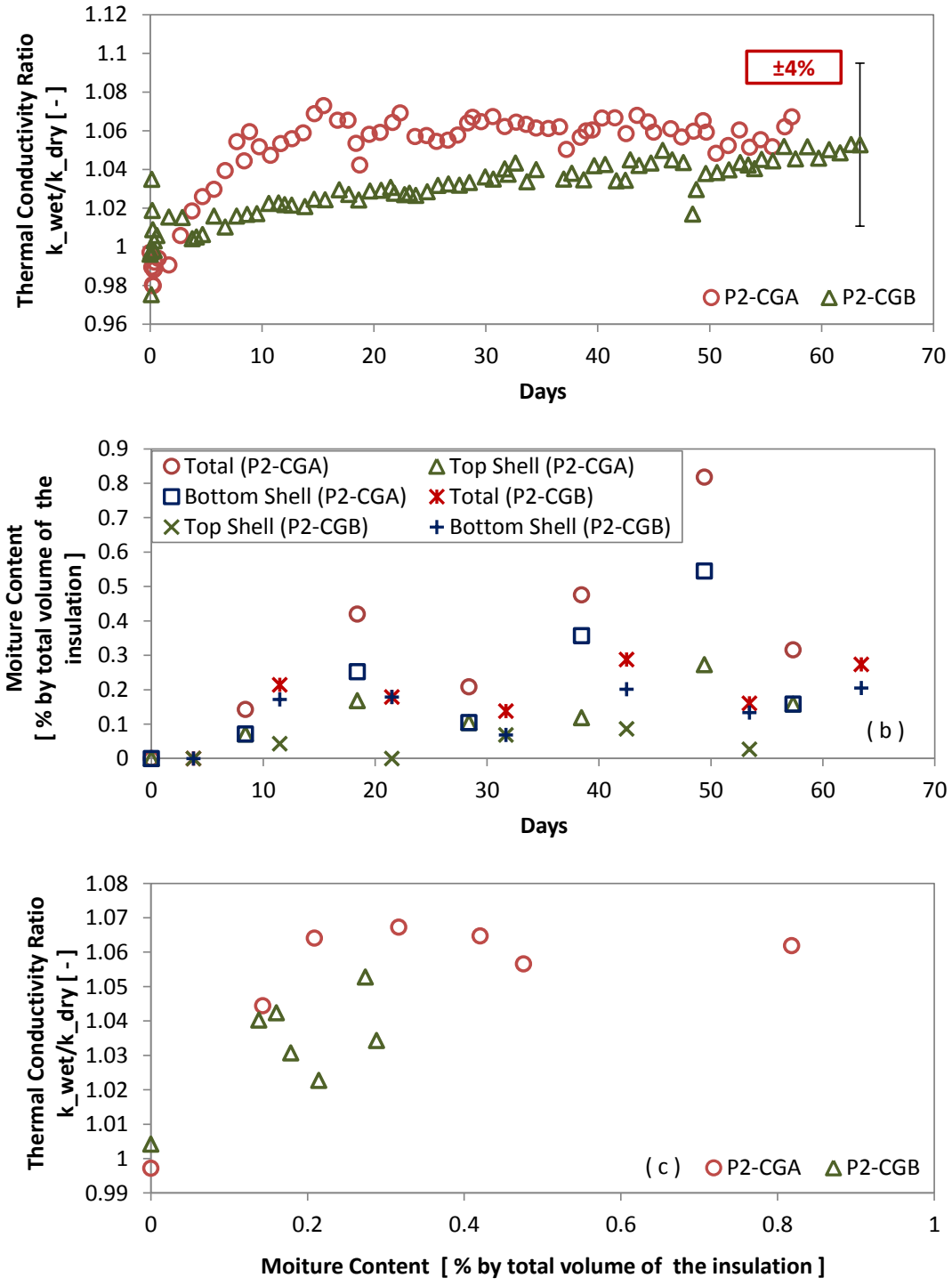

Figure 5.39: Experimental results on pipe insulation system P2-CGA and P2-CGB: (a) System thermal conductivity in real time during wet test period; (b) Moisture accumulation during wet test; (c) Effect of moisture content on the pipe insulation system thermal conductivity ratio

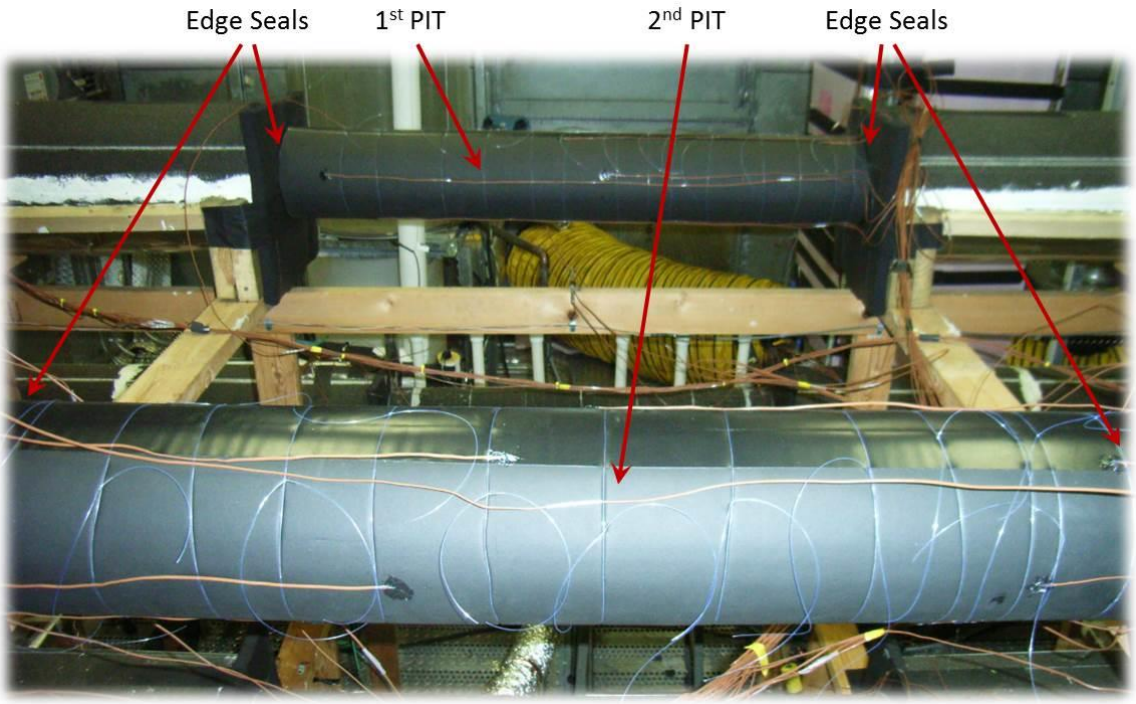

Figure 5.40: Photo of the elastomeric rubber pipe insulation system installation for the wet test

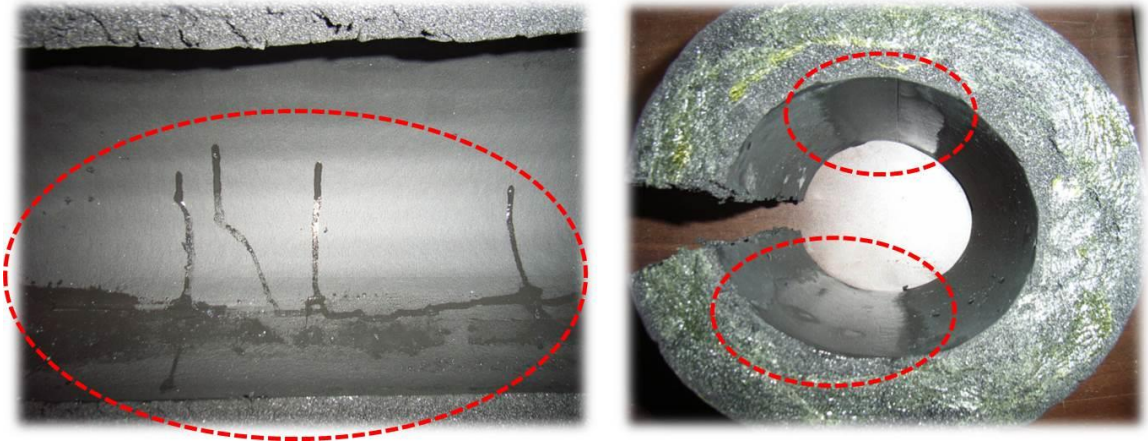

Figure 5.41: Photo of the interior surface of the elastomeric rubber pipe insulation

The experimental results on the variation of thermal conductivity and moisture content in the pipe insulation system P2-ER are shown in Figure 5.41. In Figure 5.41a, a slightly increase on the system thermal conductivity was observed at the beginning of the moisture test, then the system thermal conductivity dropped back, and followed by a gradually increase until the end of the test.

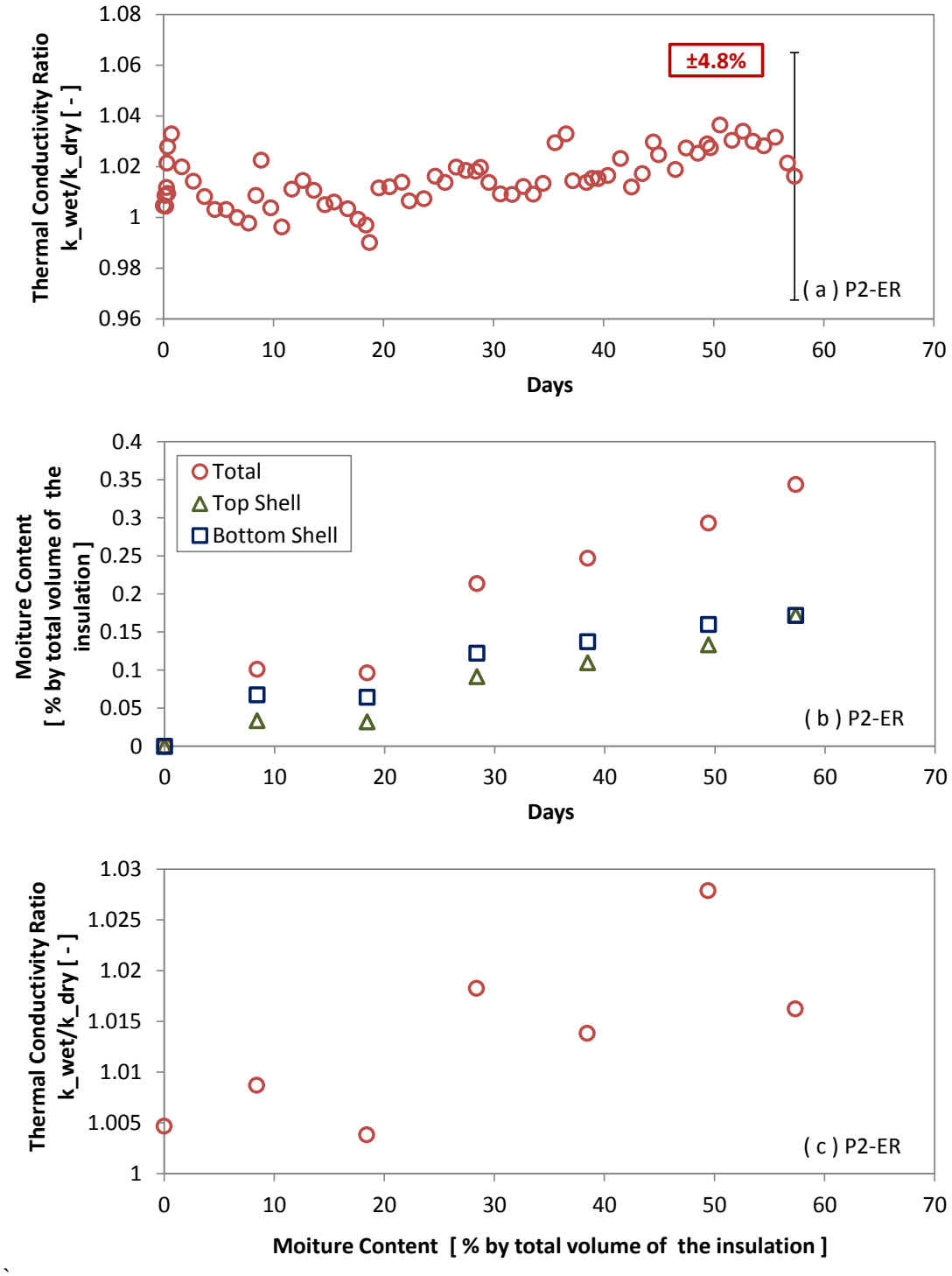

Figure 5.42: Experimental results on pipe insulation system P2-ER: (a) System thermal conductivity in real time during wet test period; (b) Moisture accumulation during wet test; (c) Effect of moisture content on the pipe insulation system thermal conductivity ratio

After 57 days of the continuous moisture test, the system thermal conductivity increased by 2% when compared to the dry reference value, which was derived from the mapping test. Figure 5.41b demonstrates the moisture profile with time. By the end of the moisture test, the total water content was around 0.34% by volume, and it showed a linear increase with time. The amount of water trapped in the bottom shell was slightly higher than the one in the top shell. From the plot in Figure 5.41c, it seems that the system thermal conductivity follows a linear correlation with the water content.

For all these closed-cell pipe insulation systems, a slightly increase on the thermal conductivity was observed at the beginning of the moisture test. This phenomenon was happened almost simultaneously with the ambient varied from dry condition to wet condition. The increasing rate on the system thermal conductivity ranged from 5% to 20%. This increasing might be caused by an unsteady-state measurement when the ambient condition was stabilizing. Another possible reason is explained as follows. During the fabrication procedure, a certain amount of water vapor was trapped in the closed-cell insulation, especial in the materials with "aging" phenomenon, PIR and phenolic for example. When the ambient changed to wet conditions, this amount of water vapor started condensing in the pores. However, due to the closed-cell structure, instead of redistributing among different cells, the water droplets was trapped in the small enclosures and started coating the cell walls. With an enhanced heat transfer along the cell walls, the system thermal conductivity slightly increased during this procedure. Compared to the moisture bead on the contact points between each fiber, the thermal bridging effect is much lower in the closed-cell insulation.

By comparing the thermal conductivity ratio and moisture content between fibrous and closed-cell pipe insulation systems, results show that moisture has a more significant impact on the apparent thermal conductivity of fibrous pipe insulation systems, and closed-cell pipe insulation was observed less dependent on the moisture content. For example, in fiberglass, when the

moisture content was around 10.9% by volume, the system thermal conductivity increased up to more than 3 times of the dry reference value. However, in phenolic, the thermal conductivity ratio increased to 2.35 by the end of the moisture test when the water content reached 22.1% by volume, which was almost twice of the amount of water trapped in the fiberglass. This phenomenon can also be explained by the different diffusion mechanisms between the fibers and the closed cells. McFadden's (1988) experiments on the fibrous and closed-cell insulation foams also showed similar results. During the thermal conductivity measurement on the fiberglass batt, McFadden found that there was a transition region when the moisture content was between 2~3% by volume, and the thermal conductivity increased almost by 4 times of the value under the dry condition. By the end of the test, the maximum thermal conductivity ratio increased to about 3.7 when the moisture content was around 8% by volume. McFadden also measured other close-cell insulation boards, such as polyurethane/polyisocyanurate foam, extruded and molded polystyrene board. Slight increase was found in the polyurethane foam at the beginning of the test, when the moisture content was less than 1% by volume. The thermal conductivity ratio was estimated to increase upto 2.3 with moisture content around 7% by volume. Extruded and molded polystyrene foams showed almost linear increase between the insulation thermal conductivity and moisture content. For extruded polystyrene, the thermal conductivity ratio increased to 2.0 when the moisture content was 22% by volume. For molded polystyrene foam, the maximum moisture content was measured around 10%, the thermal conductivity increased to 1.2 times of the original value that measured under the dry condition. The comparison results were provided in Table 5.11. All these values showed that fibrous insulation degraded more on the insulation thermal conductivity with moisture when compared to the closed-cell insulation foam.

Table 5.11: Comparison between the experimental results and literature values on fiberglass and PIR insulation

	Moisture content (% by volume)		Thermal conductivity ratio (k_{wet}/k_{dry})	
	[1]Experiment	[2]Literature	[1]Experiment	[2]Literature
Fiberglass	4.00	4.00	2.80	3.30
	15.08	8.00	3.58	3.69
Polyisocyanurate (PIR)	4.00	4.00	1.14	2.06
	16.04	7.00	1.51	2.31
Extruded polystyrene	-	10	-	1.19
Expanded polystyrene	-	22	-	2.0

[1]: Experimental results were based on pipe insulation systems
[2]: Literature values were based on flat slabs, from the work presented by (McFadden, 1988)

Therefore, it is concluded that due to the difference in the moisture diffusion mechanism, the fibrous pipe insulation performs more sensitive to the moisture content. The thermal conductivity may follow a two-step variation and increases dramatically at the beginning of the test because of the formation of the thermal bridging and preferential paths. For closed-cell pipe insulation systems, the presence of water condensate would not change the heat transfer patterns, and the apparent thermal conductivity is not sensitive on the moisture content as that of the fibrous pipe insulation systems. The apparent thermal conductivity increases gradually with the amount of water that trapped in the system.

The test ambient conditions, insulation system specification and experimental results for both dry and wet conditions are documented in Table 5.12 to 5.14.

Table 5.12: Summary of the test conditions and experimental results on fiberglass pipe insulation systems under both dry and moisture conditions

Insulation Systems		**Fiberglass**						
Ref No.	Units	P1-FG	P2-FG1	P2-FG2	P2-FG3	P2-FG4	P2-FG5A	P2-FG5B
Density	kg/m^3 (lbm/ft^3)	70 (4.4)	70 (4.4)	56 (3.5)	56 (3.5)	56 (3.5)	70 (4.4)	70 (4.4)
Nominal Wall Thickness	in (mm)	*2 (50.8)	2 (50.8)	1 1/2 (38.1)	1 1/2 (38.1)	1 1/2 (38.1)	2 (50.8)	2 (50.8)
Actual Diameter	in (mm)	7.5(190.5)*	7.6 (193.0)	6.7 (170.2)	6.8 (172.7)	6.6 (167.6)	7.6 (193.0)	7.7 (195.6)
Test Pipe (bare or black)	-	bare	bare	bare	bare	bare w/ Al tape	bare	black
Insulation joint[1]	-	N/A	N/A	N/A	N/A	1	N/A	N/A
Joint Sealant	-	N/A	N/A	N/A	N/A	N/A	N/A	N/A
Edge Seal	-	Foster 90-66 and Foster 30-80	Foster 90-66	Foster 90-66	Foster 90-66	Chil-Perm CP-30	Chil-Perm CP-30	Chil-Perm CP-30
Vapor retarder	-	N/A	N/A	ASJ	ASJ and PVC jacketing	ASJ	N/A	N/A
Calibration Method on k_{eff}[2]	-	1	2	2	2	2	2	2
Dry test Condition								
Ambient Temp	˚F (˚C)	77.2 ~ 110.8 (25.1 ~ 43.8)	75.5 ~ 99.1 (24.2 ~ 37.3)	77.1 ~ 107.2 (25.1 ~ 41.8)	77.0 ~ 106.2 (25 ~ 41.2)	77.0 ~ 101.5 (25 ~ 38.6)	76.9 ~ 101.8 (24.9 ~ 38.8	76.9 ~ 96.3 (24.9 ~ 35.7)
Test Pipe Temp	˚F (˚C)	40.9 (4.9)	36.7 (2.6)	37.7 (3.2)	37.7 (3.2)	40.7 (4.8)	39.5 (4.2)	35.1 (1.7)
Relative Humidity		20.6 ~ 14.2	11.2 ~ 7.0	21.1 ~ 5.8	21.1 ~ 5.8	15.6 ~ 7.3	15.6 ~ 7.3	14.7 ~ 8.0
Dew Point Temp	˚F (˚C)	33.8 ~ 51.2 (1.0 ~ 10.7)	19.4 ~ 25.2 (-7 ~ -3.8)	26.4 ~ 34.3 (-3.1 ~ 1.3)	25.7 ~ 34.1 (-3.5 ~ 1.2)	27.4 ~ 27.7 (-2.6 ~ -2.4)	27.4 ~ 27.9 (-2.6 ~ -2.3)	26.1 ~ 26.3 (-3.3 ~ -3.2)

Table 5.12 (*Continued*): Summary of the test conditions and experimental results on fiberglass pipe insulation systems under both dry and moisture conditions

Insulation Systems		**Fiberglass**						
Ref No.	Units	P1-FG	P2-FG1	P2-FG2	P2-FG3	P2-FG4	P2-FG5A	P2-FG5B
Dry Test Results								
a[3]	-	0.0016 (0.00041)	0.0016 (0.00041)	0.0010 (0.00026)	0.0005 (0.00013)	0.0002 (0.00005)	0.0002 (0.00006)	0.0005 (0.00012)
b[3]	-	0.1475 (0.0286)	0.1475 (0.0286)	0.1918 (0.0323)	0.2156 (0.0334)	0.2322 (0.0344)	0.2511 (0.0373)	0.2184 (0.0336)
Heat Flux	Btu/hr-ft (W/m)	8.44 (8.12)	8.44 (8.12)	10.68 (10.27)	10.03 (9.64)	9.4 (9.04)	8.63 (8.30)	8.31 (7.99)
Uncertainty	%	5.8	5.8	4.9	5.1	5.4	5.7	5.8
Wet Test Condition								
Ambient Temp	˚F (˚C)	107.6 (42.0)	N/A	N/A	N/A	78.1 (25.6)	78.1 (25.6)	90.1 (32.3)
Test Pipe Temp	˚F (˚C)	41.6 (5.33)	N/A	N/A	N/A	38.4 (3.6)	40.6 (4.8)	41.9 (5.5)
Relative Humidity	%	81	N/A	N/A	N/A	54.8	54.8	84
Dew Point	˚F (˚C)	100.4 (38.0)	N/A	N/A	N/A	60.6 (15.9)	60.6 (15.9)	84.6 (29.2)
Test Length	Days	12	N/A	N/A	N/A	55	55	54
Wet Test Results								
Thermal Conductivity Ratio	-	3.15	N/A	N/A	N/A	1.02	1.49	1.16
Moisture Content	% by volume	10.93	N/A	N/A	N/A	0.26	1.66	15.08

[1]: Numbers of insulation butt joints in the 3-ft (0.9 m) test section;
[2]: Calibration under one ambient temperature (1); Calibration under different ambient temperatures (2);
[3]: Pipe insulation system thermal conductivity $k_{pipe,insulation} = a \cdot T + b$
[*]: Actual diameter is not available, use nominal diameter instead.

Table 5.13 Summary of the test conditions and experimental results on closed-cell pipe insulation systems under both dry and moisture conditions (Part I)

Insulation Systems		**Phenolic**			**Elastomeric Rubber**		
Ref No.	Units	P1-P1	P1-P2	P2-P	P1-ER	P2-ER1	P2-ER2
Density	kg/m^3 (lbm/ft^3)	37	37	37	50	40	40
Nominal Wall Thickness	in (mm)	1 (25.4)	2 (50.8)	2 (50.8)	2 (50.8)	1 1/2 (38.1)	2 (50.8)
Actual Diameter	in (mm)	*5.5 (139.7)	*7.5 (190.5)	7.7 (195.6)	*7.5 (190.5)	6.8 (172.7)	7.7 (195.6)
Test Pipe (bare or black)	-	bare	bare	bare	bare	bare	bare
Insulation joint[1]	-	N/A	N/A	N/A	N/A	N/A	N/A
Joint Sealant	-	Boss 368	Boss 368	Chil-Joint CP-70	Aeroseal	Self-adhesive Tape and Aeroseal	Self-adhesive Tape and Aeroseal
Edge Seal	-	Boss 368	Foster 90-66 and Foster 30-80	Chil-Joint CP-70	Aeroseal	Aeroseal	Aeroseal
Vapor retarder	-	N/A	N/A	N/A	N/A	N/A	N/A
Calibration Method on k_{eff}[2]	-	1	1	2	1	2	2
Dry test Condition							
Ambient Temp	˚F (˚C)	75.6 ~ 101.8 (24.2 ~ 38.8)	80 ~ 110 (26.7 ~ 43.3)	N/A	77.3 ~ 110.1 (25.2 ~ 43.4)	75.5 ~ 96.9 (24.2 ~ 36.1)	74.9 ~ 97.2 (23.8 ~ 36.2)
Test Pipe Temp	˚F (˚C)	40.3 (4.6)	40.4 (4.7)	N/A	40.7 (4.8)	38.3 (3.5)	36.6 (2.6)
Relative Humidity		19.1 ~ 13.9	17.7 ~ 14.9	N/A	18.3 ~ 14.0	11.2 ~ 7	11.2 ~ 7
Dew Point Temp	˚F (˚C)	36.5 ~ 43.6 (2.5 ~ 6.4)	32.3 ~ 51.8 (0.15 ~ 11.1)	N/A	31.1 ~ 50.2 (-0.5 ~ 10.1)	19.4 ~ 23.8 (-7.1 ~ -4.5)	19.0 ~ 24.0 (-7.2 ~ -4.4)

Table 5.13 *(Continued)*: Summary of the test conditions and experimental results on closed-cell pipe insulation systems under both dry and moisture conditions (Part I)

Insulation Systems		**Phenolic**			**Elastomeric Rubber**		
Ref No.	Units	P1-P1	P1-P2	P2-P	P1-ER	P2-ER1	P2-ER2
Dry Test Results				N/A			
a^3	-	0.0007 (0.00018)	0.0012 (0.00032)	N/A	0.0005 (0.00014)	0.0010 (0.00025)	0.0010 (0.00027)
b^3	-	0.1821 (0.0297)	0.1217 (0.0233)	N/A	0.2144 (0.0334)	0.2112 (0.0350)	0.1913 (0.0323)
Heat Flux	Btu/hr-ft	13.20	7.13	N/A	8.38	10.40	8.45
	W/m	12.69	6.86	N/A	8.06	10.00	8.13
Uncertainty	%	4.3	6.5	N/A	5.8	5.0	5.8
Wet Test Condition							
Ambient Temp	˚F (˚C)	N/A	96.4 (35.8)	107.7 (42.0)	N/A	90.6 (32.6)	N/A
Test Pipe Temp	˚F (˚C)	N/A	40.7 (4.9)	40.7 (4.9)	N/A	36.8 (2.7)	N/A
Relative Humidity	%	N/A	87.1	82	N/A	83	N/A
Dew Point	˚F (˚C)	N/A	91.9 (33.3)	100.9 (38.3)	N/A	84.7 (29.3)	N/A
Test Length	Days	N/A	24	45	N/A	57	N/A
Wet Test Results							
Thermal Conductivity Ratio	-	N/A	1.57	2.35	N/A	1.02	N/A
Moisture Content	% by volume	N/A	4.87	22.1	N/A	0.34	N/A

[1]: Numbers of insulation butt joints in the 3-ft (0.9 m) test section;
[2]: Calibration under one ambient temperature (1); Calibration under different ambient temperatures (2);
[3]: Pipe insulation system thermal conductivity $k_{pipe,insulation} = a \cdot T + b$
[*]: Actual diameter is not available, use nominal diameter instead.

Table 5.14: Summary of the test conditions and experimental results on closed-cell pipe insulation systems under both dry and moisture conditions (Part II)

Insulation Systems		**Cellular Glass**		**PIR**	
Ref No.	Units	P2-CGA	P2-CGB	P2-PIR1	P2-PIR2
Density	kg/m^3 (lbm/ft^3)	115	115	32	32
Nominal Wall Thickness	in (mm)	1 1/2 (38.1)	1 1/2 (38.1)	1 (25.4)	1 1/2 (38.1)
Actual Diameter	in (mm)	6.8 (172.7)	6.6 (167.6)	5.7 (144.8)	6.8 (172.7)
Test Pipe (bare or black)	-	bare	black	bare	bare w/ Al tape
Insulation joint[1]	-	1	1	N/A	N/A
Joint Sealant	-	Boss 368	Boss 368	Boss 368	Chil-Joint CP-70
Edge Seal	-	Boss 368	Boss 368	Boss 368	Chil-Joint CP-70
Vapor retarder	-	N/A	N/A	Saran CX 540	N/A
Calibration Method on k_{eff}[2]	-	2	2	2	2
Dry test Condition					
Ambient Temp	˚F (˚C)	84 ~ 97.1 (28.9 ~ 36.2)	77.0 ~ 96.9 (25 ~ 36.1)	77.1 ~ 107.5 (25.1 ~ 41.9)	77.1 ~ 106.5 (25.1 ~ 41.4)
Test Pipe Temp	˚F (˚C)	40.1 (4.5)	39.3 (4.1)	38.9 (3.8)	38.1 (3.4)
Relative Humidity		9.0 ~7.0	14.7 ~ 8.0	21.1 ~ 5.8	21.1 ~ 5.8
Dew Point Temp	˚F (˚C)	20.6 ~ 24 (-6.3 ~ -4.5)	26.2 ~ 26.7 (-3.2 ~ -3.0)	26.6 ~ 34.3 (-3.0 ~ 1.3)	25.9 ~ 34.3 (-3.4 ~ 1.3)

Table 5.14 *(Continued)*: Summary of the test conditions and experimental results on closed-cell pipe insulation systems under both dry and moisture conditions (Part II)

Insulation Systems		**Cellular Glass**		**PIR**	
Ref No.	Units	P2-CGA	P2-CGB	P2-PIR1	P2-PIR2
Dry Test Results					
a[3]	-	-0.0001 (-0.00004)	-0.0013 (-0.00033)	-0.0005 (-0.00014)	-0.00005 (-0.00001)
b[3]	-	0.3694 (0.0526)	0.4201 (0.0546)	0.2789 (0.0377)	0.2558 (0.0366)
Heat Flux	Btu/hr-ft (W/m)	13.42 (12.90)	12.80 (12.31)	12.74 (12.25)	10.30 (9.90)
Uncertainty	%	4.2	4.4	4.4	5.0
Wet Test Condition					
Ambient Temp	˚F (˚C)	90.6 (32.6)	89.8 (32.1)	N/A	107.4 (41.9)
Test Pipe Temp	˚F (˚C)	38.0 (3.4)	37.7 (3.2)	N/A	40.7 (4.8)
Relative Humidity	%	83	83	N/A	82
Dew Point	˚F (˚C)	84.7 (29.3)	83.9 (28.8)	N/A	100.7 (38.1)
Test Length	Days	57	64	N/A	45
Wet Test Results					
Thermal Conductivity Ratio	-	1.07	1.05	N/A	1.51
Moisture Content	% by volume	0.32	0.27	N/A	16.04

[1]: Numbers of insulation butt joints in the 3-ft (0.9 m) test section;
[2]: Calibration under one ambient temperature (1); Calibration under different ambient temperatures (2);
[3]: Pipe insulation system thermal conductivity $k_{pipe,insulation} = a \cdot T + b$

CHAPTER VI

6. SIMULATION MODEL

6.1 Introduction

In current literature, the common methods for predicting the variation of pipe insulation thermal conductivity and moisture accumulation are summarized as these three types: (1) curve-fitting correalations (Abdou & Budaiwi, 2005; Adams, 1974), (2) semi-empirical methods, and (3) numerical simulation.

Generally, the correlations generated from the experiments are confined to the methodological conditions. They are case-specific and prone to errors when apply the correlations to a different ambient conditions, or on the same materials but with different physical properties. Semi-empirical methods on the other hand are fast and simply to use. Usually these methods start with analytical model first, and use experimental data set to generate the profile of the coefficients in the model. These coefficients are normally considered as constant among different cases according to specific assumptions made in the analytical model. These methods mainly deal with steady or quasi-steady phase of the heat and mass transfer processes. They are able to give approximations and can be applied to a wide range of test conditions and different type of test samples. However, they might be failed to provide detailed information especially through transient conditions, such as the variation on the local thermal conductivity, and moisture distribution in the pipe insulation. Numerical simulation is one of the most commonly used methods for the investigation of transient heat and mass transfer through insulation materials.

Computational fluid dynamics (CFD) model will provide a detailed investigation on the thermal performance of insulation materials during the transfer processes. However, the simulations are often complex and time consuming. In order to investigate in detail on the moisture diffusion in different types of pipe insulation systems, a dedicate geometry is required for specific internal structure of the insulation material. For example, the geometries of fibrous pipe insulation might need to consist of single fiber, regular arrays of uniform fibers assumed to be parallel with gas flow. Different diameters and orientation of the fibers may also need to be considered, which will lead to some difficulties in the determination of appropriate boundary conditions. In order to provide detailed information on the moisture distribution, a three-dimensional CFD model is very useful for a complete simulation, but the complex 3-D geometries demand powerful computing resources and a large amount of time.

In my PhD research work, one of the research objectives is to develop an applicable model that can be utilized in the field of mechanical engineering for a prediction on the thermal behavior of pipe insulation systems, and this model should be able to help the mechanical engineers make an optimization in the design between economy cost and system efficiency. Therefore, the model is required to be general and applicable to a wide range of insulation systems and materials with different physical properties. Considering the advantages and disadvantages among these three approaches, together with the research goals in this study, the semi-empirical methods were selected, and a lumped model will be discussed in detail in this chapter.

6.2 Literature review of the existing models for insulation thermal conductivity

For porous type of insulation, Luikov (1966) proposed that the apparent thermal conductivity (k_{app}) is equal to the summation of the conductive (k_{cond}), convection (k_{conv}) and radiative (k_{rad}) components of thermal conductivity, shown in Equation as follows:

$$k_{app} = k_{cond} + k_{conv} + k_{rad} \quad (6.1)$$

Bankvall, referred by Batty *et al*. (1981), proposed four different physical distribution models for glass fiber insulation: series arrangement, parallel arrangement, bead arrangement, and foam arrangement. Wijeysundera *et al.* (1996) agreed that the apparent thermal conductivity of moist insulation depends on the manner that the liquid distribute in the insulation, and considered the three patterns be: bead arrangement, series arrangement and parallel arrangement in porous insulation. However, both researches did not consider a combination of different moisture distribution patterns. Ochs *et al.* (2008) developed a model to predict effective thermal conductivity of moistened porous insulation based on flat slab. The conductive component of the apparent thermal conductivity was considered as a combination of series and parallel arrangement, and the radiation effect was considered with pore specifications, while the convection effect was ignored due to the low Rayleigh number. Based on Equation (6.1), Karamanos *et al*. (2008) developed an analytical model for the impact of temperature and moisture on the thermal performance of stone wool. By neglecting the small convection term, the conductive and radiative components of thermal conductivity are still need to be determined from further specification of the fiber, such as the diameter, density, and orientation factor of the fibers. Compared to Bankvall's (Batty *et al.*, 1981) model, Karamanos *et al*.'s model is not specifying the shape of fibrous insulation since most of the parameters required for are independent from the material geometry.

There are also several other analytical methods for computing thermal conductivity under dry and moist conditions. Mar *et al.* (2008) considered the heat barrier resistances in the conductive term of the apparent thermal conductivity. However, the determination for this resistance is so complicated due to the absence of reliable method for the contact areas between grains, especially within microcracks, and grain boundaries. Wijeysundera *et al.* (1993) proposed analytical solution for the effective thermal conductivity of flat-slab and round-pipe insulations in the

presence of condensation. This model considers the temperature and vapor pressure gradient within the insulation, and it can be further developed for computing the effective thermal conductivity in the pipe insulation systems by combing joint sealant and air gap effects.

6.3 Model for closed-cell pipe insulation systems

A 2-D analytical model for closed-cell pipe insulation was originally developed by Ochs *et al.* (2008), and a similar approach was used in the present work. This approach was considered as a lumped model to predict the system apparent thermal conductivity with the total amount of moisture trapped in the system. The overall thermal resistance was considered as a combination of the thermal resistances from insulation material, air gaps and joint sealant, as shown in Figure 6.1.

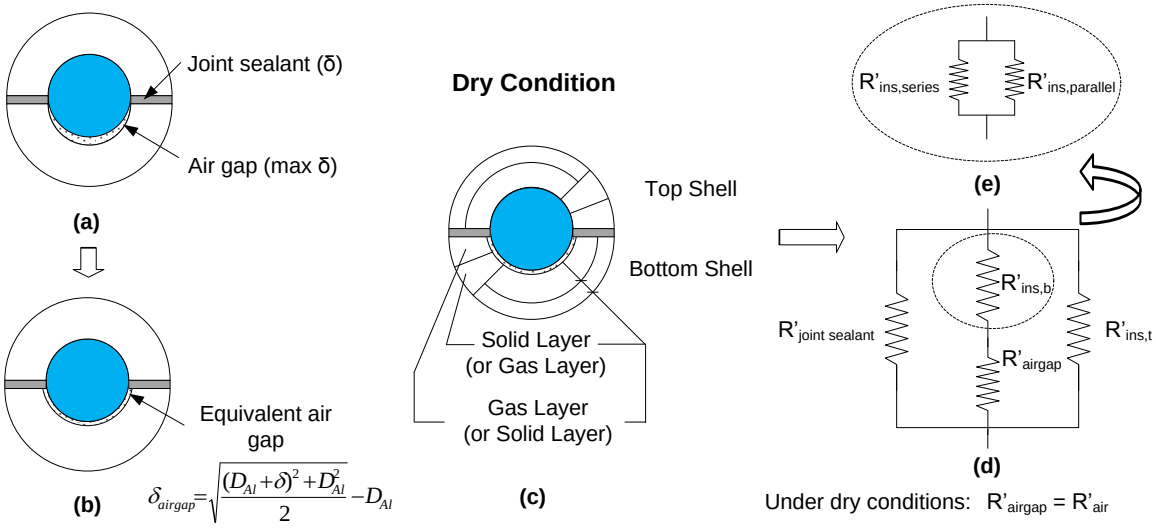

Figure 6.1: Sketch of combined thermal resistance of cellular pipe insulation under dry condition

The actual configuration of the pipe insulation system as installed on a cold pipe is illustrated in Figure 6.1a. The assumptions for the present model are as follows: 1) the convection term is neglected due to the low Rayleigh number (<<1708, a sample computation on the convection term will be shown in the section 6.4); 2) the insulation materials are essentially composed of solid and gas layers, plus liquid layer if in wet condition, and only two arrangements of the cells

are taken into consideration: series and parallel, as shown in Figure 6.1c to e. The arrangement in Figure 1c, for dry conditions, represents a limiting case for the resistance to the heat flow through the materials. Under wet conditions, the solid layer remained the same as in dry condition, but the gas layer is affected by water vapor and condensate and it has to be divided further to include water layer, moist pores layer and the residual gas layer. Additional underlying assumptions of the present model are 3) the insulation materials are homogeneous; 4) the fraction of series and parallel configuration remain constant for the same type of pipe insulation under dry condition; and 5) the air gap exists only at the interface between the bottom pipe wall surface and the bottom interior surface of the insulation system and the thickness of the air gap was assumed uniform within the 180° angle of the bottom shell, as shown in Figure 6.1b. An important parameter *a* was introduced in the model, and it represents the volume fraction of the poor conductive layer with different phases positioned in series configuration, as shown in Figure 6.1c. Therefore, *(1-a)* represents the fraction of resistances in parallel. Considering the fact that the value of thermal resistances in parallel would always be lower that the value of thermal resistance in series, parameter *(1-a)* could also be considered as the amount of thermal bridging that existed in the system. However, the parameter *a* could not be measured according to the physical procedures. Based on the above mentioned assumptions, the thermal resistance and thermal conductivity for the insulation material become as follows:

$$1/\mathrm{R}'_{\mathrm{ins}} = \mathrm{a}/\mathrm{R}'_{\mathrm{series}} + (1-\mathrm{a})/\mathrm{R}'_{\mathrm{parallel}} \qquad (6.2)$$

$$\mathrm{k}_{\mathrm{ins}} = \mathrm{a}\mathrm{k}_{\mathrm{series}} + (1-\mathrm{a})\mathrm{k}_{\mathrm{parallel}} \qquad (6.3)$$

where k_{series} represents the lowest thermal conductivity component of the insulation, while $k_{parallel}$ represents the maximum. It should be noted that the formulations of k_{series} and $k_{parallel}$ are different when the insulation system is considered dry (i.e., no water vapor and condensate) or wet (that is, water vapor and water condensate present). The sealant on the longitudinal joints behaves as a

resistance in parallel to the insulation material and can create a thermal bridge effects based on its thermal conductivity and sealant thickness. These additional variables due to the presence of joint sealant and air gaps in cylindrical insulation configuration are considered in the present model for the first time.

In dry conditions, the combined thermal resistance and the overall thermal conductivity of the pipe insulation system are expressed by the thermal resistance of the join sealant, $R'_{joint,sealant}$, the thermal resistance of the top shell of insulation, $R'_{ins,t}$, the thermal resistance of the bottom shell of insulation, $R'_{ins,b}$, and the thermal resistance from the air gap, R'_{airgap}:

$$R'_{combined} = \frac{1}{\frac{1}{R'_{joint\ sealant}} + \frac{1}{R'_{ins,t}} + \frac{1}{R'_{ins,b} + R'_{airgap}}} = \frac{\ln(\frac{D_{exterior,ins}}{D_{exterior,Al,pipe}})}{2\pi k_{tot} L} \quad (6.4)$$

Where

$$R'_{joint\ sealant} = \frac{D_{exterior,ins} - D_{exterior,Al,pipe}}{4k_{joint\ sealant}\delta_{joint\ sealant} L} \quad (6.5)$$

$$R'_{airgap} = \frac{\ln(\frac{D_{exterior,Al,pipe} + \delta_{airgap}}{D_{exterior,Al,pipe}})}{\pi k_{airgap} L} \quad (6.6)$$

$$R'_{ins,t} = \frac{\ln(\frac{D_{exterior,ins}}{D_{exterior,Al,pipe}})}{\pi k_{ins,t} L} \quad (6.7)$$

$$R'_{ins,b} = \frac{\ln(\frac{D_{exterior,ins}}{D_{exterior,Al,pipe}})}{\pi k_{ins,b} L} \quad (6.8)$$

And in terms of thermal conductivity, Eq. (6.4) yields to

$$k_{tot} = \ln\left(\frac{D_{exp}}{D_{exterior,Al,pipe}}\right)\left(\frac{2k_{joint\ sealant}\delta_{joint\ sealant}}{\pi(D_{exterior,ins} - D_{exterior,Al,pipe})} + \frac{k_{ins,t}}{\ln\left(\frac{D_{exterior,ins}}{D_{exterior,Al,pipe}}\right)}\right.$$

$$\left. + \frac{1}{\frac{\ln\left(\frac{D_{exterior,ins}}{D_{exterior,Al,pipe}}\right)}{k_{ins,b}} + \frac{\ln\left(\frac{D_{exterior,Al,pipe} + \delta_{airgap}}{D_{exterior,Al,pipe}}\right)}{k_{airgap}}}\right) \quad (6.9)$$

Where $D_{exterior,ins}$ is the exterior diameter of the pipe insulation; $D_{exterior,Al,pipe}$ is the exterior diameter of test pipe; L is the length of test section; k_{airgap} is the thermal conductivity of the air gap: at dry condition, $k_{airgap} = k_{air}$, and at wet condition, $k_{airgap} = k_{water}$; $k_{jointsealant}$ is the thermal conductivity of the joint sealant; $\delta_{jointsealant}$ is the thickness of the joint sealant; δ_{airgap} is the thickness of the air gap, and an equivalent air gap dimension was calculated as annular shape around the bottom half of the tested aluminum pipe surface.

$$Vol_{airgap} = {}^{\pi L}/_{8}\left[(D_{exterior,Al,pipe} + \delta_{airgap})^2 - D^2_{exterior,Al,pipe}\right] \quad (6.10)$$

Where Vol_{airgap} is the volume of the air gap, m3 (in3), and $\delta_{airgap} = \sqrt{\frac{(D_{Al}+\delta_{jointsealant})^2 + D_{Al}^2}{2}} - D_{Al}$.

6.3.1 Sub-model of thermal conductivity for dry pipe insulation systems (closed-cell)

The series thermal conductivity factor k_{series} can be calculated from the series thermal resistance, R'_{series}, which is determined with either gas phase or solid phase in the interior, as shown in Figure 6.1c. Since series configuration represents the case of the highest thermal resistance, R'_{series} can be determined by comparing these two scenarios:

$$R'_{series,dry} = R'_{s,series,dry} + R'_{g,series,dry} = \max(R'_{series,dry,1}, R'_{series,dry,2}) \quad (6.11)$$

Where $R'_{s,series}$ and $R'_{g,series}$ are the thermal resistances of solid and gas phases in series configuration. $R'_{series,dry,1}$ represents the thermal resistance when solid phase is in the exterior, and

$R'_{series,dry,2}$ represents the one with solid phase in the interior. In terms of thermal conductivity it becomes Equation (6.12) if the maximum resistance is $R'_{series,dry,1}$, or the thermal conductivity is calculated as Equation (6.13) if the maximum resistance is $R'_{series,dry,2}$.

$$k_{series} = \frac{\ln\left(\frac{D_{exterior,ins}}{D_{exterior,Al,pipe}}\right)}{\frac{\ln\left(\frac{D_{exterior,ins}}{D_{x1}}\right)}{k_s} + \frac{\ln\left(\frac{D_{x1}}{D_{exterior,Al,pipe}}\right)}{k_p}} \quad (6.12)$$

$$k_{series} = \frac{\ln\left(\frac{D_{exterior,ins}}{D_{exterior,Al,pipe}}\right)}{\frac{\ln\left(\frac{D_{exterior,ins}}{D_{x2}}\right)}{k_p} + \frac{\ln\left(\frac{D_{x2}}{D_{exterior,Al,pipe}}\right)}{k_s}} \quad (6.13)$$

Where k_s is the thermal conductivity of the solid particles; k_p is the thermal conductivity of the pores in closed-cell insulation. The diameters D_{x1} and D_{x2} are calculated as follows:

$D_{x1} = \sqrt{n\left(D^2_{exterior,ins} - D^2_{exterior,Al,pipe}\right) + D^2_{exterior,Al,pipe}}$ (interior: gas, exterior: solid)

$D_{x2} = \sqrt{D^2_{exterior,Al,pipe} - n\left(D^2_{exterior,ins} - D^2_{exterior,Al,pipe}\right)}$ (interior: solid, exterior: gas)

The maximum thermal resistance is normally derived when the gas phase is next to the interior surface ($R'_{series,dry,1}$). Take a 3 ½-in × 2-in (88.9 × 50.8 mm) thickness fiberglass pipe insulation as an example, $R'_{series,dry,1}$ will be smaller than $R'_{series,dry,2}$ only if the solid thermal conductivity decreases to a similar value as the air. In most cases, the thermal conductivity of the solid phase is much higher than that of the gas phase. The porosity also indicates that the volume of the gas is much higher than the solid. Therefore, the maximum thermal resistance in the pipe insulation system is normally determined by the thermal resistance with the gas phase at the interior layer ($R'_{series,dry,1}$).

In order to consider the radiation effects in the cells, the relations originally proposed by Ochs *et*

al. (2008) are applied for this system and the results are as follows:

$$k_p = k_{pg} + k_{rad} \quad (6.14)$$

$$k_{rad} = \frac{4\sigma_s d_m}{\frac{2}{\varepsilon} - 1} T_k^3 = c_{rad} T_k^3 \quad (6.15)$$

Where k_{pg} is the gas thermal conductivity; k_{rad} is the effect of radiation; d_m is the pore diameter, ε is the particle surface emissivity and σ_s is the blackbody radiation constant. As suggested by Ochs *et al.* (2008), due to the fact that the coefficient of emission is not available in most cases, the parameters can be lumped to the radiation constant c_{rad}, and k_{rad} can be expressed as a function of c_{rad} and the absolute temperature, T_k. In the present model, c_{rad} was determined from Nelder-Mead optimization based on experimental data.

The parallel thermal resistance, $R'_{parallel}$, represents the lowest thermal conductivity when the resistances of solid and gas are in parallel arrangement. Based on the assumption that the porosity is homogenous throughout the entire insulation materials, the parallel thermal resistance and thermal conductivity are calculated as follows:

$$R'_{parallel} = R'_{s,parallel}/(1-n) + R'_{g,parallel}/n \quad (6.16)$$

$$k_{parallel} = nk_s + (1-n)k_p \quad (6.17)$$

Where n is the porosity of the insulation materials; $R'_{s,parllel}$ and $R'_{g,parallel}$ are the thermal resistances of solid and gas phases in parallel arrangement.

It should be noted that the combined thermal conductivity of the insulation material collapses to the solid or to the gas thermal conductivity in the limiting case of no porosity ($n \rightarrow 0$) or gas filling completely the annular space ($n \rightarrow 1$), that is:

$$\lim_{n\to 0} k_{ins} = ak_s + (1-a)k_s = k_s \quad (6.18)$$

$$\lim_{n\to 1} k_{ins} = ak_p + (1-a)k_p = k_p \quad (6.19)$$

6.3.2 Sub-model of water content accumulated in wet pipe insulation systems with moisture ingress (closed-cell)

Closed-cell insulation systems are normally more resistant to the water and water vapor transport compared to fibrous and open-cell insulation. However, there are studies reported that some closed-cell insulation systems are not completely impermeable to water vapor. It is acknowledged that the apparent thermal conductivity depends on the water content accumulated in the insulation, and thus it is important to determine the moisture content in the pipe insulation systems with moisture ingress. Considering the vapor pressure differences between the two conditions at the interior and exterior surfaces, I modified the correlations for mass flow rate of the water vapor ($\dot{m}_v$) through the pipe insulation and the total amount of water that accumulated in the insulation (m_w) as follows:

$$\dot{m}_v = 2\pi L \cdot \mathcal{P} \frac{P_{v,exterior,ins} - P_{v,exterior,Al,pipe}}{ln \left. D_{exterior,ins} \right/ D_{exterior,Al,pipe}} \quad (6.20)$$

$$m_{w(t)} = f_1 f_2 \dot{m}_{v(t)} t \quad (6.21)$$

Where $\mathcal{P}$ is the water vapor permeability of the material; $P_{v,exterior,ins}$ *and* $P_{v,exterior,Al,pipe}$ represent the partial vapor pressures at the exterior and interior surfaces of the pipe insulation; m_w is the total amount of water accumulated in the insulation; n is the material porosity and ρ_w is the water density; t is the time length for the moisture test in days. f_1 *and* f_2 are the two correction coefficients I added to the amount of water that is trapped in the pipe insulation. f_1 is defined as a condensation coefficient to represent for the portion of the water vapor that condensed to liquid water. Theoretically, f_1 results the volume ratio of the space with temperatures lower than the dew

point over the total volume of the test sample. This definition of f_1 assumes that water vapor condenses if the local temperature is below the air dew point temperature. The detailed procedures to determine f_1 will be discussed in detail in the section 6.5.1. f_2 is considered as a correction factor on the insulation water vapor permeability. Due to the variation of the ambient conditions at the pipe insulation surface, both temperatures and humidity are different from the standard condition that this property being tested for, and this may require a correction on the water vapor permeability through the insulation systems. The presence of joint sealant will also cause a deviation on the system permeability from the reported value in the standard because of a different behavior between the sealant and the insulation materials. Both these impacts will be included by the coefficient f_2. To summarize, two new correction factors must be included in the modeling of wet pipe insulation systems: f_1 is the coefficient that considers the effect of temperature distribution on the water vapor condensing rate in the pipe insulation, and f_2 is the coefficient that includes the impacts of different ambient conditions and the presence of joint sealant on the water vapor permeability of pipe insulation systems with respect to the data originally derived from the test at standard room conditions.

6.3.3 Sub-Model of Thermal Conductivity of Wet Pipe Insulation Systems with Moisture Ingress (Closed-cell)

For wet insulation in addition to solid and gas phases, layers of liquid phase and moistened pores (i.e. pores with water vapor) are added in the model as described next. Logically the water layer and water vapor in the pores layer takes place in the air-only filled regions, and they are modeled as shown in Figure 6.2b and 2c.

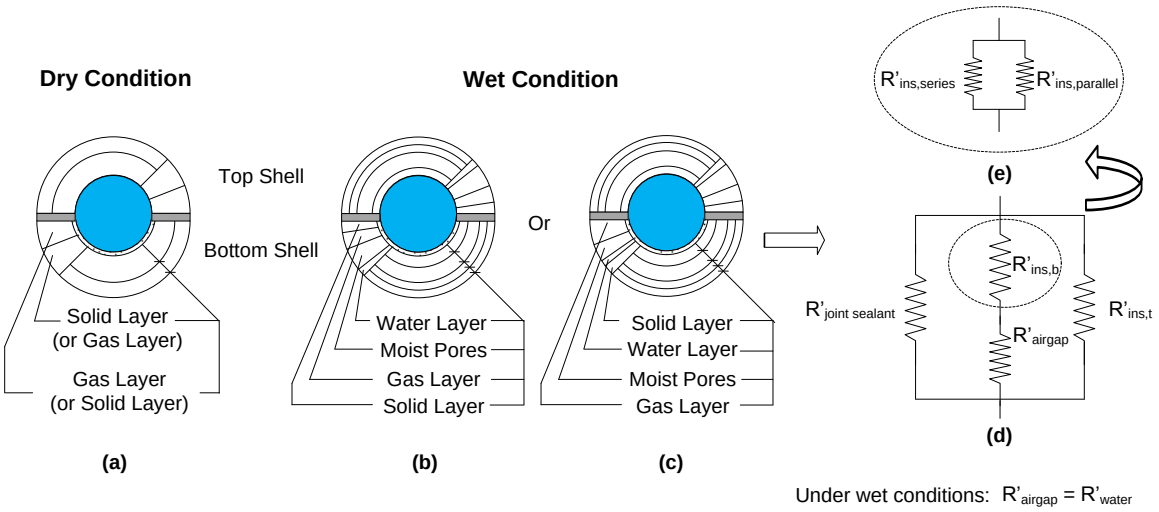

Figure 6.2: Sketch of combined thermal resistance of cellular pipe insulation

Depending on the solid material thermal conductivity and gas trapped in the insulation material, the thermal resistance of these two configurations was computed, and the configuration that had highest thermal resistance was selected. For the water vapor diffusion in the moistened pores, the effective thermal conductivity (k_{pd}) is determined from the thermal conductivity due to water vapor diffusion (k_{diff}), which takes into consideration the heat transfer due to the evaporation occurring at the warm side of the pore, and condensation at the cold side. The expressions are as follows:

$$k_{pd} = k_p + k_{diff} \qquad (6.22) \qquad k_{diff} = \frac{D_v}{R_v^2 T_k^2} \cdot \frac{P_{amb}}{P_{amb} - P_{sat}} \Delta h_v^2 \qquad (6.23)$$

Where $D_v = 23.4 \cdot 10^{-6} (\frac{T_k}{273})^{2.3}$, is the water vapor diffusion coefficient; $P_{sat} = 610.8 \cdot \exp(\frac{17.08085 \cdot T}{234.175+T})$, saturation vapor pressure; P_{amb} is the ambient pressure; h_v is the latent heat of evaporation; R_v is the gas constant. More details for computing diffusion thermal conductivity factor are reported in the work by Ochs *et al.* (2008). By assuming that the portion of the pores involved in the vapor diffusion (V_{pd}) is proportional to the pores with gas in them, the fraction of moistened pores in the cells (b) is calculated as follows:

$$V_{pd} = b(n - V_w) \qquad (6.24) \qquad b = 1 - (1 - {V_w}/{V_{fs}})^9 \qquad (6.25)$$

Where V_w is the volume fraction of water per volume of the test sample; V_{pd} is the volume fraction of the cells involved with the vapor diffusion per volume of the test sample; and V_{fs} is the volume fraction of water condensate in free saturation conditions per volume of the test sample.

The series thermal resistance ($R'_{serial,wet}$) was calculated from equation (6.11) to (6.13) by adding water and pore diffusion layers.

$$R'_{serial,wet} = R'_{w,serial,wet} + R'_{pd,serial,wet} + R'_{s,serial,wet} + R'_{g,serial,wet} \qquad (6.26)$$

The parallel thermal resistance ($R'_{parallel,wet}$) was calculated as follow:

$$R'_{parallel,wet} = \frac{R'_{w,parallel,wet}}{V_w} + \frac{R'_{pd,parallel,wet}}{V_{pd}} + \frac{R'_{s,parallel,wet}}{1-n} + \frac{R'_{g,parallel,wet}}{(n - V_w - V_{pd})} \qquad (6.27)$$

And, in terms of overall apparent thermal conductivity of the wet pipe insulation systems ($k_{parallel,wet}$) results:

$$k_{parallel,wet} = V_w k_w + V_w k_{pd} + (n - V_w - V_{pd})k_p + (1-n)k_s \qquad (6.28)$$

Based on the experimental observation that moisture content of the bottom shells was typically higher than the moisture content measured on the top C-shell, the equations (6.11) to (6.28) were solved independently for the half shells at the top and bottom, yielding to two values of the apparent thermal resistance $R'_{series,wet,t}$ and $R'_{series,wet,b}$, respectively.

6.4 Model for fibrous pipe insulation systems

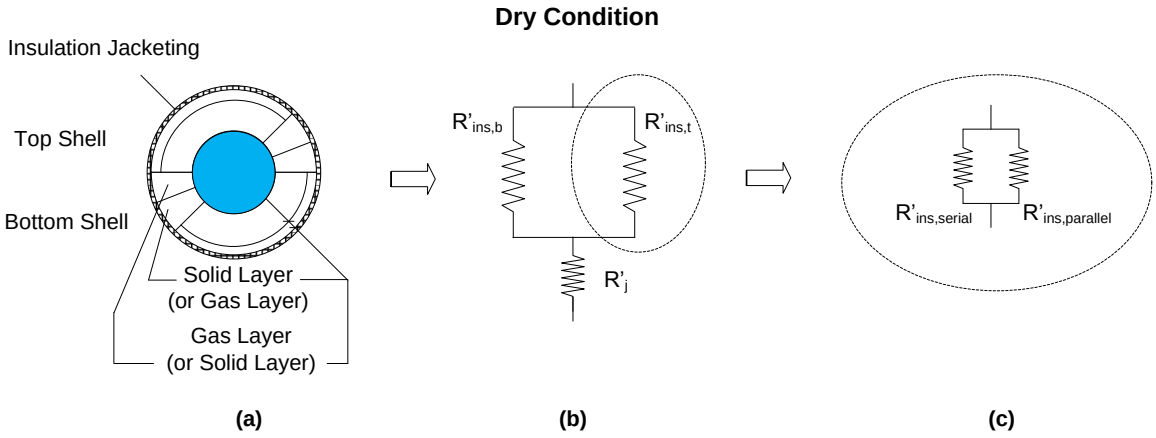

Figure 6.3: Sketch of combined thermal resistance of fibrous pipe insulation under dry condition

According to the literature, it is quite common to develop models specific to either cellular or fibrous insulation since these two types of insulation have different internal structure and physical properties. However, it would be very promising if there is a general method for any type of the insulation materials. In Karamanos's (2008) model, although it is independent from the shape of insulation, most of the parameters, such as the fibers diameter, the coefficient of fibers orientation, are specific for fibrous material and cannot be expanded easily to porous materials. Compared to Karamanos's model, the methodology proposed by Batty *et al.* (1981) was developed based on the assumption that the insulation thermal resistance was composed with a combination of serial and parallel layers of solid and gas, which shared the same theory as the one applied for closed-cell insulation. Therefore, for fibrous pipe insulation under dry condition, the thermal conductivity will be computed from the similar dry model as cellular pipe insulation. Considering the fact that instead of applying joint sealant between the two half shells, jacketing is normally manufactured on the exterior surface of the insulation, as shown in Figure 6.3, the thermal resistance and effective thermal conductivity are expressed as:

$$R'_{combined} = \frac{1}{\frac{1}{R'_{ins,t}} + \frac{1}{R'_{ins,b}}} + R'_{jacketing} \quad (6.29)$$

$$k_{tot} = \ln\left(\frac{D_{exp}}{D_{exterior,Al,pipe}}\right) \Bigg/ \left(\frac{\ln\left(\frac{D_{exterior,ins}}{D_{exterior,Al,pipe}}\right)}{k_{ins,t}+k_{ins,b}} + \frac{\ln\left(\frac{D_{exp}}{D_{exterior,ins}}\right)}{k_{jacketing}}\right) \quad (6.30)$$

Where $R'_{jacketing}$ is the thermal resistance of the vapor jacketing.

Similar to close-cell pipe insulation, the convection term was neglected in the model due to a trival value. In the following section, the convection term was computed in fiberglass pipe insulation. For fibrous pipe insulation, the fibers are alighned in horizontal direction, and the natual convection can be considered as in horizontal rectangular enclosures. By assuming the fiber diameter around 6×10^{-7}-in (15nm), as suggested by Karamanos *et al*. (2008), and 0.2 ℉ (0.1 ℃) diffference between the fiber surface and the air in the gap, the Rayleigh number (*Ra*) is around 4.57E-07, and the Nussult number (*Nu*) is 1:

$$Nu = 1 + 1.44\left[1 - \frac{1708}{Ra_D}\right]^+ + \left[\frac{Ra_D^{\frac{1}{3}}}{18} - 1\right]^+ \quad (6.31)$$

Where $[\ \ ]^+$indicates that if the quantity in the bracket is negative, it should be equal to zero (Holland *et al.*, 1976).

Therefore, it can be treated that there is no convection current in the fiberglass and other fibrous pipe insulation systems.

6.4.1 Sub-model of thermal conductivity for dry pipe insulation systems (fibrous)

Under dry conditions, the fibrous insulation are composed of solid and gas phases, and the simulation theory would be the same as the one previously described for closed-cell pipe insulation, Equation (6.11) to (6.19).

6.4.2 Sub-model of water content accumulated in pipe insulation systems with moisture ingress (fibrous)

Moisture migration in the fibrous insulation can be considered as a serious problem for degrading insulation thermal performances. Similar to the closed-cell pipe insulation, the transmitted mass flow rate of water vapor ($\dot{m}_v$) through the pipe insulation is computed from the vapor partial pressure differences between the two conditions at the interior and exterior surfaces, Equation (6.20).

According to the literature, the permeability is correlated with material porosity for fibrous pipe insulation. Take fiberglass insulation for example (Golestanian, 2007). There is:

$$\text{‘P} = 3 \times 10^{-13} e^{8.6643n} \qquad (6.32)$$

It should be noted that this correlation was derived from the experimental data under one ambient condition, and the value might be systematically shifted due to a variation on the test conditions, such as higher temperature and humidity. This impact will be considered by the permeability correction factor f_2, which will be discussed in detail in section 6.5.2.

Fibrous pipe insulation systems are normally applied with insulation jacketing or vapor retarder which has much lower water vapor permeability. With the presence of vapor retarder, the total vapor resistance (*Rp'*) in the pipe insulation systems is:

$$Rp'_{tot} = Rp'_v + Rp'_p \qquad (6.33)$$

$$Rp'_v = \frac{\ln[\left(D_{exterior,ins} + 2\delta_{jacketing}\right)/D_{exterior,ins}]}{2\pi\text{‘P}_{jacketing}\text{L}} \qquad (6.34)$$

$$Rp'_p = \frac{\ln(\frac{D_{exterior,ins}}{D_{exterior,Al,pipe}})}{2\pi\text{‘PL}} \qquad (6.35)$$

Where Rp'_v is the vapor resistance of the insulation jacketing; $P_{jacketing}$ represents the water vapor permeability of the insulation jacketing, and Rp'_p is the vapor resistance through the pipe insulation.

Therefore, for the pipe insulation with insulation jacketing or vapor retarder, the effective water vapor permeability is modified as:

$$P_{tot} = \frac{\ln\left(\frac{D_{exterior,ins} + 2\delta_{jacketing}}{D_{exterior,Al,pipe}}\right)}{2\pi R p'_{tot} L} = \frac{\ln\left(\frac{D_{exterior,ins} + 2\delta_{jacketing}}{D_{exterior,Al,pipe}}\right)}{\frac{\ln\left(\frac{D_{exterior,ins} + 2\delta_{jacketing}}{D_{exterior,ins}}\right)}{P_{jacketing}} + \frac{\ln\left(\frac{D_{exterior,ins}}{D_{exterior,Al,pipe}}\right)}{P}} \quad (6.36)$$

With more water condensate filling in the air gaps among the fibers, the fraction of the voids over the total volume decreases, and the differences come from the spaces occupied by the water condensate. Therefore, the water vapor permeability would not maintain constant in the wet conditions, and I developed the procedure for computing the water accumulation as shown in Equations (6.37) to (6.39).

$$n_{(t)}V = n_{(t-1)}V - m_{w(t-1)}/\rho_w \quad (6.37)$$

$$m_{w(t)} = m_{w(t-1)} + f_1 f_2 f_3 \dot{m_{v(t)}}[t-(t-1)] = m_{w(t-1)} + f_1 f_2 f_3 \dot{m}_{v(t)} \Delta t \quad (6.38)$$

$$\frac{\dot{m_{v(t)}}}{\dot{m_{v(t-1)}}} = \frac{P_{(t)}}{P_{(t-1)}} = \exp\left[8.6643\left(n_{(t)} - n_{(t-1)}\right)\right] = \exp\left(-\frac{8.6643 m_{w(t-1)}}{\rho_w}\right) \quad (6.39)$$

Where t is the time length for the moisture test in days; Δt is the time interval, and in this case. Δt =1; V is the volume of the entire test sample; m_w is the total amount of water accumulated in the

insulation; n is the material porosity and ρ_w is the water density. Similar to closed-cell pipe insulation systems, f_1 *and* f_2 are the two coefficients that will modify the amount of water trapped in the pipe insulation. f_1 is the condensation coefficient that represents for the portion of the water vapor condensed to liquid water, and f_2 is the correction factor on the water vapor permeability due to different ambient conditions and installation method. In fibrous pipe insulation, correction factor f_2 is assumed to be 1, which will be explained in the section 6.5.2. Another coefficient, f_3, is defined as water retention factor and represents the portion of water condensate that will remain trapped in the pipe insulation. Due to the presence of preferential paths, a small amount of water condensate drips out of the insulation. Although the total amount is small, it is non-negligible when compared to the closed-cell pipe insulation, and should not be counted in as the moisture content remained in the insulation. However, till now there is not enough data to provide a correlation to predict how the ambient conditions affect the water dripping rate out of the pipe insulation. The coefficient f_3 is derived based on the experimental data from one specific case and assumed to be constant among the same material in fibrous pipe insulation systems. For closed-cell pipe insulation, very few amount of water drips out from the insulation because of its low water absorption and the compact gas-filled cellular structure. The portion of water trapped in the insulation is almost the same as the total amount of water condensed in the insulation materials, and this coefficient does not need to be considered in the modeling.

Based on the iterations among equations (6.37) to (6.39), the mass flow rate of water vapor transmitted into the insulation can be updated with a varied water vapor permeability, and the profile of the water amount accumulated in the insulation can be predicted from the days being tested for. The procedures for computing the water content in fiberglass test samples are summarized in detail in the flow chart shown in Figure 6.4.

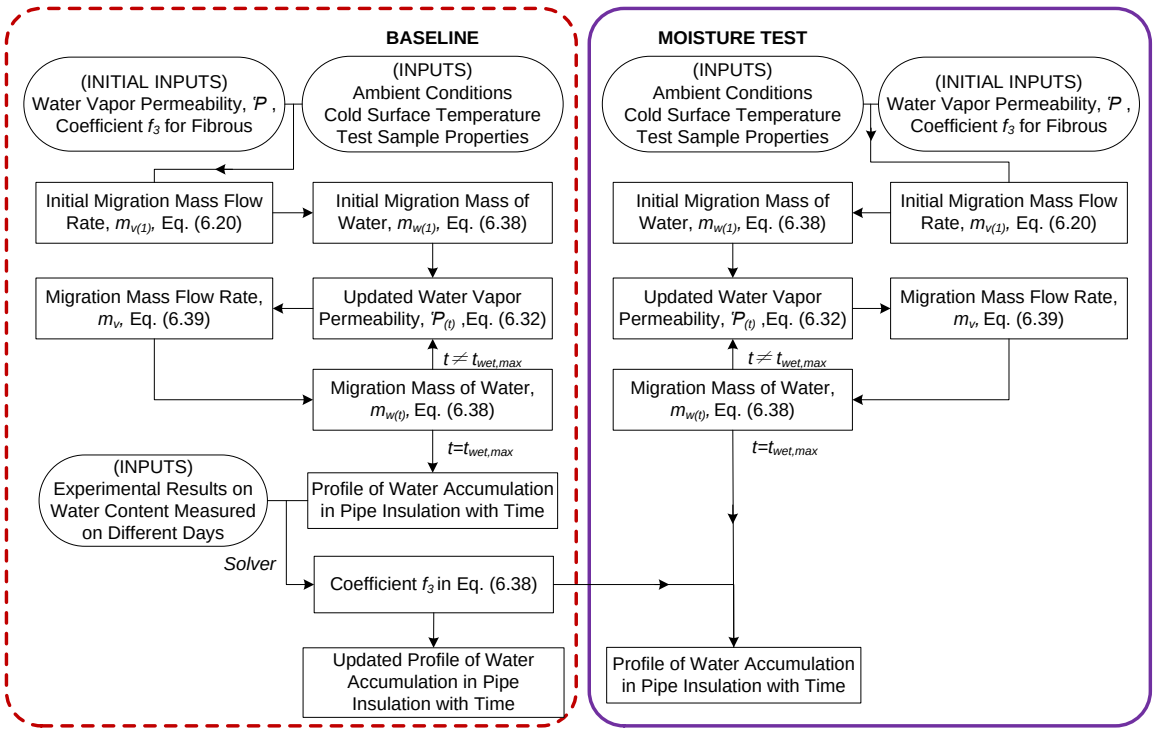

Figure 6.4: Flow chart of the procedures for the profile moisture content in the pipe insulation systems

The simulation starts from considering the ambient conditions and the cold surface temperatures provided in the baseline experimental data. The initial water vapor permeability is derived from the empirical correlations in the current literature. Based on the permeability and water vapor pressure computed from the given conditions, the initial mass migration rate of water vapor can be determined from Equation (6.20). On Day 1, the mass of water vapor migrated into the insulation is the migration rate multiple by the day, as shown in Equation (6.38) when *t* is equal to 1. From Day 2, the permeability of water vapor in fibrous insulation starts to decrease due to a lower porosity in the material. For different types of pipe insulation, the correlations between permeability and porosity might be different. Equation (6.32) shows a curve-fitting correlation based on the data reported on fiberglass mat (Golestanian, 2007), and this material porosity will be updated by the total amount of water accumulated in Day 1, Equation (6.37). The water vapor

permeability and the water vapor migration rate on day 2 will also be varied with the updated porosity according to Equations (6.32), (6.38) and (6.39). The same procedures are repeated in the following days to generate a profile of water accumulation in the pipe insulation systems with time. This moisture profile will be compared to the baseline experimental data to determine the coefficients f_3, which is assumed to be a constant value for the same insulation material. Therefore, the moisture content accumulated in the pipe insulation systems with the same insulation material can be predicted from the initial testing conditions.

6.4.3 Sub-model of thermal conductivity of wet pipe insulation systems with moisture ingress (fibrous)

Similar to closed-cell pipe insulation, under wet condition, the serial arrangement of fibrous pipe insulation is composed of water layer, gas layer and solid layer. Water layer is part of the gas layer under dry condition and is closer to the cold surface when compared to the gas layer, as shown in Figure 6.5(b). Considering the fact that water condensate on the cold surface transfers to the exterior surface through the preferential paths due to the gravity affect, and accumulate on the exterior surface because the surface tension effect, the assumption that made for closed-cell pipe insulation, "the fraction of series and parallel configuration remain constant for the same type of pipe insulation under both dry and wet conditions", is not valid any more for fibrous pipe insulation. Since more water will accumulate at certain region of the pipe insulation, and the preferential paths are almost filled with water through the interior to the exterior surface, parallel configuration will weigh more for fibrous pipe insulation under wet condition. Therefore, the parameter *a* will be varied from the value derived in dry condition, as the sketch shown in Figure 6.5b and c. The method used for updating the values of parameter a will be discussed in the section 6.5.3.

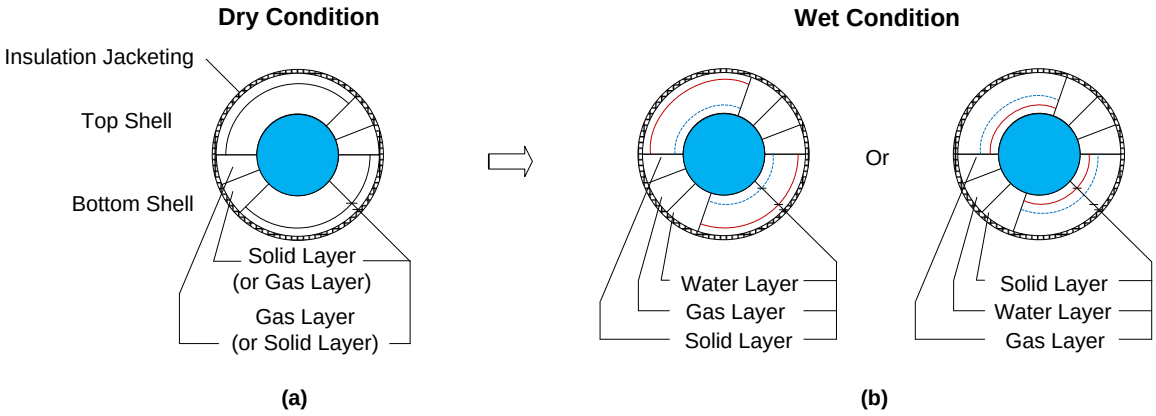

Figure 6.5: Sketch of combined thermal resistance of fibrous pipe insulation under wet condition

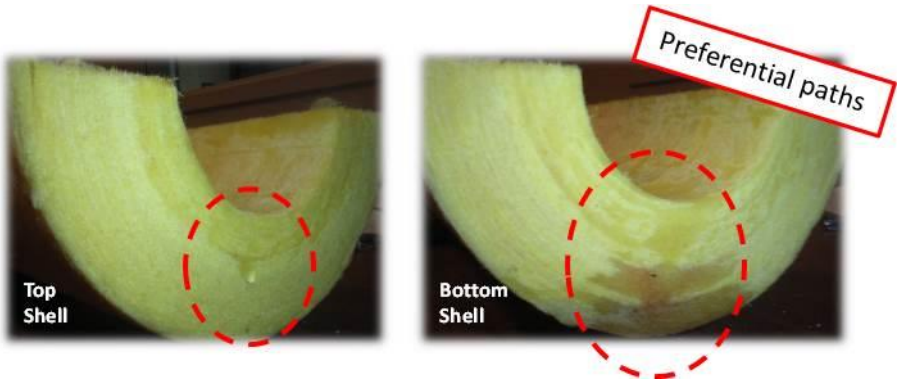

Figure 6.6: Fiberglass pipe insulation with moisture ingress

Similar to closed-cell pipe insulation, the thermal resistances in fibrous pipe insulation is also composed of the thermal resistances in the parallel and series layers. The thermal resistance ($R'_{series,wet}$) and the effective thermal conductivity ($k_{series,wet}$) of the serial layer are:

$$R'_{series,wet} = R'_{s,series,wet} + R'_{g,series,wet} + R'_{w,series,wet} = \max(R'_{series,wet,1}, R'_{series,wet,2}) \quad (6.40)$$

$$k_{serial,wet} = \frac{ln\left(\frac{D_{exterior,ins}}{D_{exterior,Al,pipe}}\right)}{\frac{ln\left(\frac{D_{exterior,ins}}{D_{x1}}\right)}{k_s} + \frac{ln\left(\frac{D_{x1}}{D_{w1}}\right)}{k_{gr}} + \frac{ln\left(\frac{D_{w1}}{D_{exterior,Al,pipe}}\right)}{k_w}}$$

(Exterior: solid; Interior: gas)

(6.41)

or

$$\frac{ln\left(\frac{D_{exterior,ins}}{D_{exterior,Al,pipe}}\right)}{\frac{ln\left(\frac{D_{exterior,ins}}{D_{w2}}\right)}{k_{gr}} + \frac{ln\left(\frac{D_{w2}}{D_{x2}}\right)}{k_w} + \frac{ln\left(\frac{D_{x2}}{D_{exterior,Al,pipe}}\right)}{k_s}}$$

(Exterior: gas; Interior: solid)

where k_{gr} is the gas phase thermal conductivity with radiation effect.

The parallel thermal resistance ($R'_{parallel,wet}$) is calculated similarly to the closed-cell pipe insulation, except that the pore diffusion layer does not exist anymore in the fibrous pipe insulation. Then there is:

$$R'_{parallel,wet} = \frac{R'_{w,parallel,wet}}{V_w} + \frac{R'_{s,parallel,wet}}{1-n} + \frac{R'_{g,parallel,wet}}{(n-V_w)} \quad (6.42)$$

And, in terms of overall apparent thermal conductivity of the wet pipe insulation systems ($k_{parallel,wet}$) results:

$$k_{parallel,wet} = V_w k_w + (n - V_w)k_{gr} + (1 - n)k_s \quad (6.43)$$

Equation (6.40) to (6.43) also need to be modified for the half shell geometry.

As discussed in previous section, parameter *a* would not be remained the same as in dry condition due to the formation of more preferential paths in fibrous pipe insulation. The thermal resistance and apparent thermal conductivity should be computed with an updated a_{wet}, as shown in Equations (6.44) and (6.45).

$$R'_{ins,wet} = R'_{series,wet}/(1 - a_{wet}) + R'_{parallel,wet}/a_{wet} \quad (6.44)$$

$$k_{wet} = a_{wet}k_{series,wet} + (1 - a_{wet})k_{parallel,wet} \quad (6.45)$$

The system thermal resistance and thermal conductivity are computed by combing the thermal resistance and conductivity under wet conditions in equations (6.29) and (6.30)

6.5 Determination of the coefficients

6.5.1 Condensing coefficient f_1

Condensing coefficient f_1 represents the volume fraction of the space with temperature lower than the dew point over the total volume of the test sample, shown as Equation (6.42). This definition assumes that water vapor condenses if the local temperature is below the air dew point temperature. The region of temperatures lower than the dew point is determined from the temperature distribution derived based a steady-state, one dimensional heat conduction equation, Equation (6.47). The radius of the region that water condensate appears is computed from Equation (6.49).

$$f_1 = V_{dp}/V \quad (6.46)$$

$$\frac{d}{dr}\left(r\frac{dT}{dr}\right) = 0 \quad (6.47)$$

Boundary conditions: $r = r_1 \rightarrow T(r_1) = T_{Al}$;

$$r = r_2 \rightarrow k_{tot}\frac{dT(r_2)}{dr} = h[T_{amb} - T(r_2)]$$

$$T(r) = J_1 lnr + J_2 \quad (6.48)$$

And $J_1 = \frac{T_{Al} - T_{amb}}{lnr_1 - lnr_2 - \frac{k_{tot}}{hr_2}}$ $J_2 = T_{Al} - \frac{T_{Al} - T_{amb}}{lnr_1 - lnr_2 - \frac{k_{tot}}{hr_2}}$

$$r = \mathrm{e}^{\frac{T_r - J_2}{J_1}} = r_1 \exp[\frac{T_r - T_{Al}}{T_{Al} - T_{amb}}\left(lnr_1 - lnr_2 - \frac{k_{tot}}{hr_2}\right)] \quad (6.49)$$

Where V_{dp} represents the volume of the region with temperature below dew point; k_{tot} is the apparent thermal conductivity of the pipe insulation system; h is the convection heat transfer coefficient; J_1 and J_2 are the arbitrary constants; r is the radius of the condensation region; r_1 is the interior radius of the pipe insulation system and r_2 represents the exterior radius.

It should be noted that the coefficient f_1 might not be constant during the wet test because the temperature distribution inside the pipe insulation would be varied with insulation thermal conductivity. However, in the model presented in this report, coefficient f_1 is assumed to be a function of the initial temperature distribution in the pipe insulation systems.

6.5.2 Permeability correction factor f_2

The correction factor f_2 considers the impact of different ambient conditions and the presence of joint sealant on the of water vapor permeability through the insulation systems. According to the standard (ASTM_C209, 2007; ASTM_C272, 2007), the values of water vapor permeability provided for most closed-cell materials are tested under room conditions, around 24˚C (75˚F) with 50% RH. From current literature, it is not clear on how this parameter changes under severe conditions, for example, 42˚C (107˚F) and 83% RH. One acknowledged correlation is shown in Equation (6.50), but two parameters: the permeability constant (P_0) and the energy of activation for permeation (E) depend on the compositions in the insulation materials, and are difficult to be determined based on current research. However, it can still be concluded that the water vapor permeability increases with higher ambient temperature.

$$P = P_0 e^{-E/RT_k} \quad (6.50)$$

Where P_0 represents the permeability constant at absolute zero; E is the energy of activation for permeation; R is the gas constant; and T_k is the absolute temperature.

Joint sealant is another impact factor in most closed-cell pipe insulation systems. For a better estimation, the water vapor permeability should be corrected by the joint sealant property and the amount applied in the system. Assume the vapor resistance of joint sealant (Rp'_{js}) is in parallel to the vapor resistance of the pipe insulation (Rp'_p), the total water vapor permeability (P_{tot}) can be corrected based on Equation (6.51) to (6.54). Result shows that the system water vapor permeability increases with the presence of the joint sealant, but more specific information, such as the water vapor permeability and thicknesses of the joint sealant is required to further quantify the sealant impact. Such information is lacked in some cases.

$$\frac{1}{Rp'_{tot}} = \frac{1}{Rp'_p} + \frac{1}{Rp'_{js}} \quad (6.51)$$

$$Rp'_p = \frac{\ln(\frac{D_{exterior,ins}}{D_{exterior,Al,pipe}})}{2\pi P L} \quad (6.52)$$

$$Rp'_{js} = \frac{D_{exterior,ins} - D_{exterior,Al,pipe}}{4 P_{js} \delta_{js} L} \quad (6.53)$$

$$P_{tot} = P + \frac{P_{js} \delta_{js} \ln(\frac{D_{exterior,ins}}{D_{exterior,Al,pipe}})}{2\pi(D_{exterior,ins} - D_{exterior,Al,pipe})} \quad (6.54)$$

Considering the difficulties to quantify these two impacts, in currently model for closed-cell pipe insulation, the correction f_2 is determined from the experiment data in one specific case, and assume to be constant in the same type of materials.

For fibrous pipe insulation, the water vapor permeability is measured based on the procedures issued in ASTM C1104 (2006). In order to provide a maximum value on the water transmission in the standard, the test sample is conditioned in an ambient with temperature at 49 ± 2˚C (120 ± 3.6˚F), 90% ± 3% RH for 96 ± 4 hours, which is close to the ambient conditions during the

moisture tests. Instead of two half shells, fibrous pipe insulation is usually manufactured as an a wrap with adhesive vapor retarder around the exterior surface. Joint sealant is not required during the installation. Therefore, f_2 is assumed to be 1 in the model of fibrous pipe insulation system.

6.5.3 Parameters *a* and c_{rad}

Parameters *a* and c_{rad} perform differently under dry and wet conditions.

At dry non-condensing conditions, the parameters *a* and c_{rad} of the present model were derived by regression of data from material samples tested in radial configuration. In order to apply this method, a baseline experiment is needed for the determination of these two parameters of the pipe insulation. Then, the parameter c_{rad} is adjusted based on the porosity difference between the insulation samples tested in the baseline experiment and the other cases, see equation (6.55).

$$\frac{c_{rad1}}{c_{rad2}} = \frac{d_{m1}}{d_{m2}} = \sqrt[3]{\frac{V_{m1}}{V_{m2}}} = \sqrt[3]{\frac{n_1}{n_2}} \qquad (6.55)$$

The material porosity can be correlated the material density, which is easier to be determined through measurements:

$$\frac{\rho_1}{\rho_2} = \frac{n_1\rho_g + (1-n_1)\rho_s}{n_2\rho_g + (1-n_2)\rho_s} = \frac{n_1\frac{\rho_g}{\rho_s} + (1-n_1)}{n_2\frac{\rho_g}{\rho_s} + (1-n_2)} \qquad (6.56)$$

Where, d_m is the density of the gas in the pores; *n* is the porosity of the material; V_m is the volume of the gas in the pores; ρ_g is the density of the gas in the pores; ρ_s is the density of the solid particles.

The solid density is expected to be in the order of 10^2 higher than the gas density, thus Equation (6.56) can be simplified:

$$\frac{\rho_1}{\rho_2} \approx \frac{1-n_1}{1-n_2} \quad (6.57)$$

By combining Equation (6.55) and (6.57), the parameter c_{rad} can be updated as follow:

$$c_{rad2} = c_{rad1} \sqrt[3]{[1-\frac{\rho_1}{\rho_2}(1-n_1)]/n_1} \quad (6.58)$$

Therefore, for the same type of materials but with different grade or manufacturer, less dense materials have larger pore diameter, and lead to a larger c_{rad}. The parameter, a, was assumed to be dependent only on the type of insulation material and thus it was assumed constant for the same insulation material with various wall thicknesses and various densities.

Under wet condition, the variation on parameter c_{rad} follows the same rule as described in dry condition. However, parameter a behaves differently in closed-cell and fibrous pipe insulation with moisture ingress. In closed-cell pipe insulation, it is assumed that the fraction of series and parallel configuration remain constant for the same type of pipe insulation under both dry and wet conditions. However, in fibrous pipe insulation, this assumption becomes weak because of the presence of preferential paths. Parallel configuration weights more in the total thermal resistances, and the parameter a decreases when compared to value derived under dry condition.

During the experiment, it is noted that the thermal conductivity of fiberglass pipe insulation increased dramatically at the beginning of the test, and then gradually reach an asymptotic value. This phenomenon is assumed to happen by following a similar change on parameter a. In order to include a similar variation on parameter a as happened to the pipe insulation thermal conductivity, the function developed for parameter a is modified from the sigmoidal function (Figure 6.7), which is defined as:

$$Y = A_b - \frac{A_t - A_b}{1 + exp[-(x - x_0)/w]} \quad (6.59)$$

Where A_b and A_t are two asymptotic values; w is the width of the region of x values where the curve crosses between these two asymptotic values and x_0 is the center point of these x region.

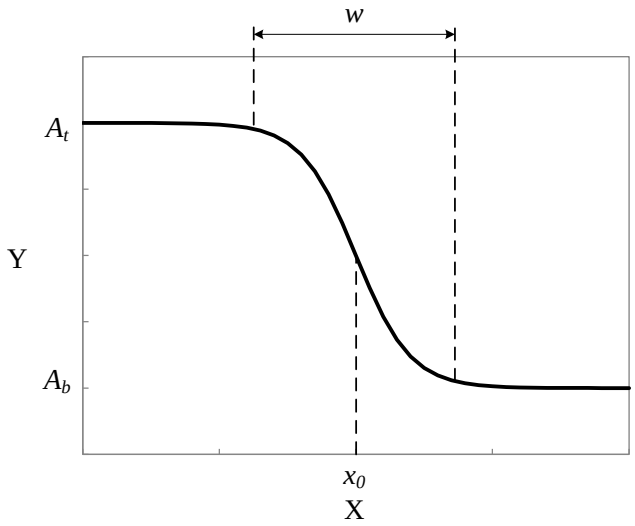

Figure 6.7: Sigmoidal function in nonlinear curve-fitting

Modified from the sigmoidal function, I developed the correlation for parameter *a* as:

$$a_{wet} = a_{dry} - \frac{\Delta a}{1 + exp[-(t - t_0)/\Delta t]} \quad (6.60)$$

Where Δa represents the difference between two asymptotic values of parameter *a*, *t* represents the days being tested for; Δt represents the time length for transient condition, and t_0 is the center point during the transient condition. It should be noted that the transient condition would not affect the asymptotic values, but will have an impact on the decreasing rate of parameter *a*. With a larger transient region, it takes longer time for parameter *a* to reach the asymptotic value.

Two impact factors, the water vapor pressure differences and the moisture content in the insulation, promote the formation of preferential paths, and both of them should be included in

the function of parameter *a*. The function of parameter *a* is further defined as Equation (6.61) and (6.62).

$$\Delta a = a_{dry} - C_1 \Delta P_v \quad (6.61)$$

$$a_{wet} = a_{dry} - \frac{C_1 \Delta P_v}{1 + exp\left[-\frac{t - t_0}{\Delta t}\right]} - C_2 m_w \quad (6.62)$$

Where C_1 *and* C_2 are the coefficients represent the sensitivity of water vapor pressure difference and moisture content on the variation of parameter *a*. These two coefficients are derived from the experimental data in one specific case, and it is assumed that the coefficient C_1 depends on the surface water permeability of different pipe insulation systems, while C_2 only depends on the type of pipe insulation materials. If there is a vapor retarder around the exterior surface of the fibrous pipe insulation, C_1 is assumed to be 0 due to the low water vapor permeability on the surface and a minor reaction to the instant changes from the ambient conditions. This correlation is developed due to the observation of a dramatic increase on the pipe insulation thermal conductivity at the beginning of the test and the fact that the area of preferential paths would increase with larger amount of water accumulated in the pipe insulation. Therefore, the profile of parameter *a* is composed of two steps. In the first step, the ambient starts to be humidified, and the vapor partial pressure difference across the pipe insulation system increases. This promotes the water vapor transmission and the formation of preferential paths, such as condensate cover the intersection area between two parallel fibers. The presence of liquid phase significantly changes the internal structure of the fibrous pipe insulation, and it is considered as a dominant impact on the variation of parameter *a*. This procedure is represented by the sigmoidal function, and the decreasing rate depends on how fast the water condensate finishes covering the intersection areas. The time length of the transient region (Δt) can be derived from the temperature profile measured at the exterior surface of the pipe insulation system. In step 2, water condensate starts accumulate in the insulation and coating the fibers. The areas of preferential paths will continue increasing with the

moisture content and further decrease the value of parameter *a*. However, this is a secondary impact, and it is assumed that the decreasing rate on parameter *a* is much slower than the previous step.

6.6 Model implementation

The model was implemented in Excel spreadsheet with dedicated VBA code.

6.6.1 Implement of thermal conductivity model under dry conditions

Under dry conditions, both closed-cell and fibrous pipe insulation share the same thermal conductivity model. The procedures for the model under dry conditions are shown in Figure 6.8. Two steps were needed in the dry model. First, a baseline experimental data set is required to determine parameters *a* and c_{rad}. In the second step, these two parameters will be updated based on the dry test sample properties, and apply to the thermal conductivity model. The sample input and output files in the first step are shown in Figure 6.9. The inputs for the baseline case are as follows: interior diameter of the pipe insulation (D_i), actual exterior diameter of the pipe insulation (D_exp), joint sealant thickness (delta_js_ip), test sample length (L), solid thermal conductivity (k_s), joint sealant thermal conductivity (k_js), porosity (n), number of measuremnts (N_measrured), type of blowing agent, material density, and experimental results on the insulation mean temperature (T_ins) and the apparent thermal conductivity (k_exp). The outputs are: pipe insulation exterior diameter (without joint sealant effect, D_o), parameter *a* and c_{rad}, the apparent thermal conductivity of the pipe insulation system (k_tot), and the thermal conductivities in both serial and parallel configurations of the two half shells..

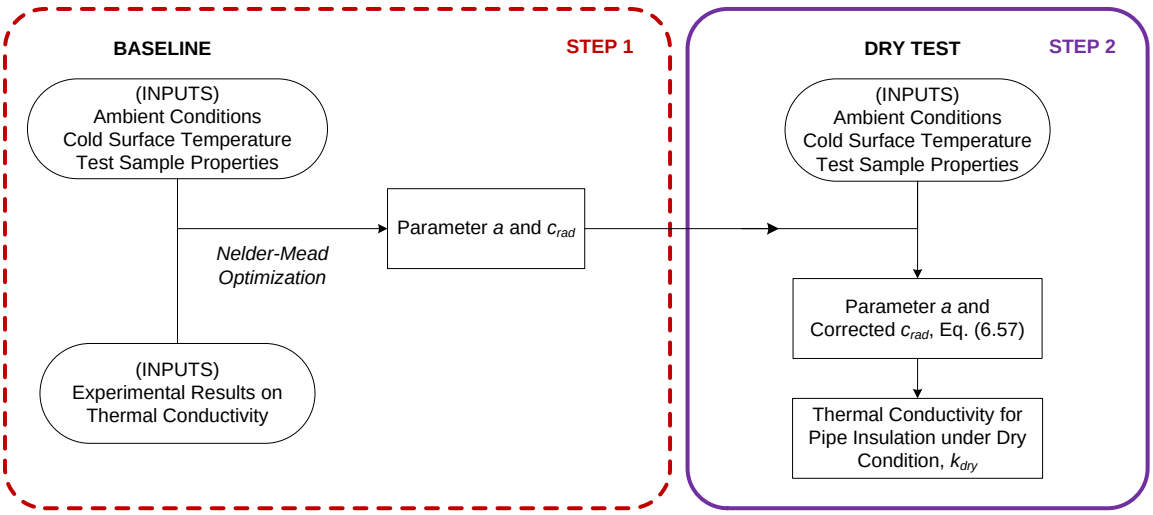

Figure 6.8: Flow chart of the procedures for computing thermal conductivity of the pipe insulation systems under dry conditions

INPUTS			
D_i (inch)	3.5	T_ins	k_exp
D_exp (inch)	7.5	C	W/m-K
delta_js_ip (inch)	1.00E-10	14.03	0.0334
L (inch)	36	17.01	0.0337
k_s (W/m-K)	2.6	19.63	0.0340
k_js (W/m-K)	1.00E-10	23.27	0.0343
n	0.91		
N_measured	4		
Blowing agent	Air		
Density	70		

"Air", "CO2", or "C2H5"

Sample input file in Step 1

OUTPUTS									
D_o	a	c_rad	k_tot	k_ins_t	k_ins_b	k_series_t	k_series_b	k_parallel_t	k_parallel_b
inch	-	×10^(-10)	W/m-K	W/m-K	W/m-K	W/m-K	W/m-K	W/m-K	W/m-K
7.5	0.97828925	0.70207812	0.0334	0.0334	0.0334	0.0284	0.0284	0.2586	0.2586
			0.0337	0.0337	0.0337	0.0287	0.0287	0.2589	0.2589
			0.0340	0.0340	0.0340	0.0290	0.0290	0.2591	0.2591
			0.0343	0.0343	0.0343	0.0293	0.0293	0.2594	0.2594

Use "Nelder-Mead" to determine *a* and c_{rad}

Sample output file of Step 1

Figure 6.9: Sample input and output files of the baseline case under dry condition

The sample input file of the thermal conductivity model is shown in Figure 6.10. The inputs are almost the same as the baseline case, and two more parameters are added for the jacketing impact. It should be noted that the baseline case aims to determine the parameters regarding to the internal structure of the pure insulation material, and it is not recommended to choose any pipe insulation systems with vapor barriers or insulation jacketing. The parameters highlighted as bold represent the inputs from the baseline case. Parameter a and c_{rad} will be automatically updated in the inputs file by following Equations (6.55) and (6.56). The outputs file is almost the same as the baseline case, but without parameters a and c_{rad}.

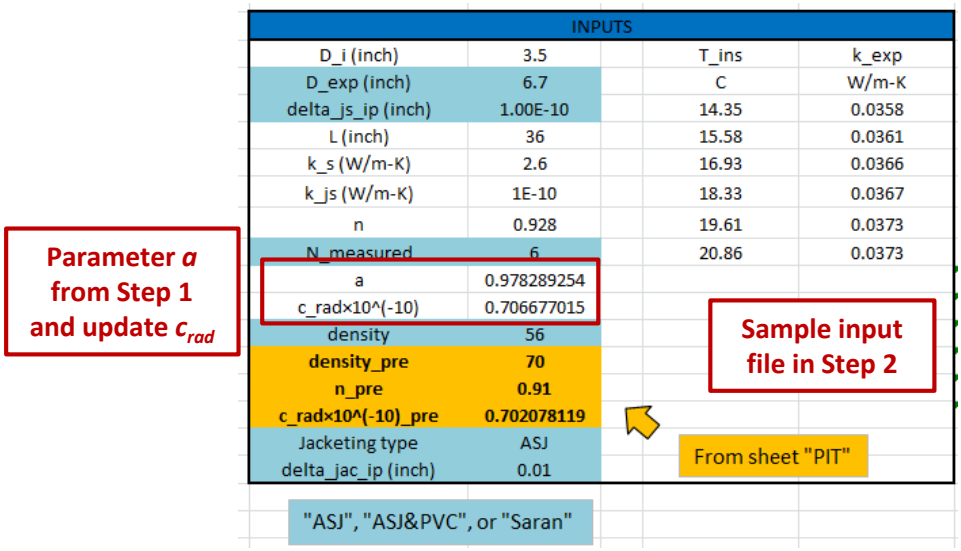

Figure 6.10: Sample input file of thermal conductivity model under dry condition

6.6.2 Implement of thermal conductivity model under wet conditions with moisture ingress

The parameters that must be provided to the program depend on the type of insulation. For closed-cell pipe insulation, the parameters are water vapor permeability $\mathcal{P}$, and the correction factor f_2, while for fiberglass insulation the parameter to the simulation program are water vapor

permeability P, water retention coefficient f_3, and sensitivity coefficients C_1 and C_2. These parameters are obtained from specific heat transfer tests in the current work, and they are generalizable to other systems and operational conditions as will be explained in detail in the model validation section later.

Closed-cell pipe insulation systems

In closed-cell pipe insulation systems, the first step is to determine the correction factor f_2 from a specific case by comparing the water content (by volume) between simulation and experimental results. The sample inputs file of closed-cell pipe insulation is shown in Figure 6.12. The correction factor f_2 will be optimized based on the "Solver" function provided in the Excel spreadsheet. The outputs of step 2 will be f_2 and the updated moisture profile, as shown in Figure 6.12 and Figure 6.13. A correlation between the moisture content in the pipe insulation systems and the testing time length can be derived from the moisture profile. In step 2, this correlation will be used to predict the moisture content that accumulated in the pipe insulation, and these values are the inputs to the thermal conductivity model to simulate how the thermal conductivity varies with the moisture content and with time. The sample input file in step 2 is shown in Figure 6.14.

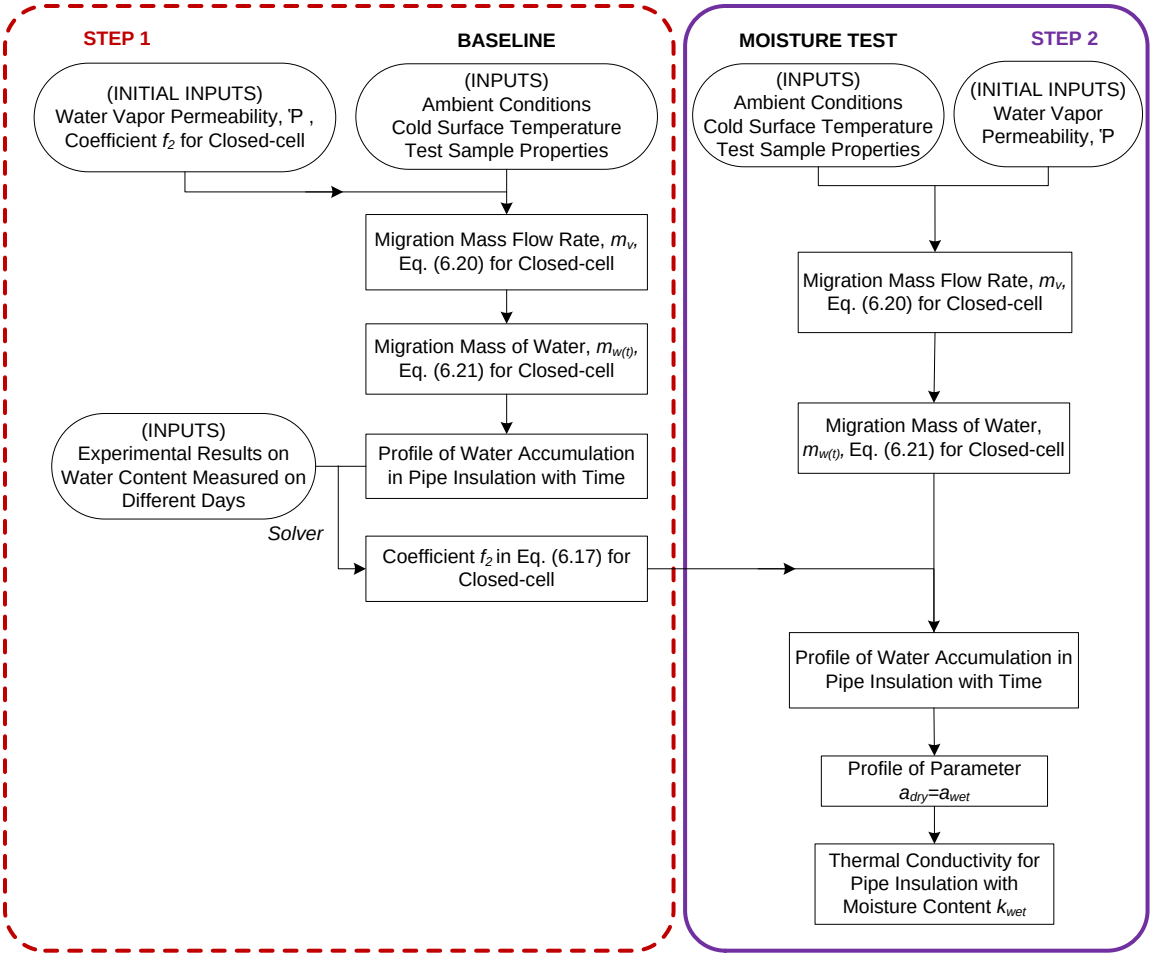

Figure 6.11: Flow chart of the procedures for computing moisture content and thermal conductivity in closed-cell pipe insulation with moisture content

Sample input file in Step 1

1	**INPUTS**	Elastomeric Rubber (2012 Wet 1_PIT3)				
2	**Tempearture Profiles**					
3	Amb temp	T_amb	F	90.59	C	32.55
4	R.H.	RH_amb	%	83.00	%	83.00
5	Outins temp	T_outins	F	88.034	C	31.13
6	Cold pipe temp	T_al	F	36.77	C	2.65
7	Dew point	T_dp	F	84.56	C	29.20
8	**Test Sample Geometries**					
9	Test length	L	in	36	m	0.9144
10	Insulation exterior diameter	D_o	in	6.5	m	0.1651
11	Insulation interior diameter	D_i	in	3.5	m	0.0889
12	**Properties**					
13	Dry thermal conductivity	k_dry	tu-in/hr-ft^2-	0.28	W/m-K	0.0401
14	Permeability	P	US perms	2.52E-15	m^2/s	1.44E-13
15	Water density	rho	lbm/ft^3	62.4	kg/m^3	1000
16	Convection heat transfer coefficient	h	Btu/hr-ft^2-F	1.63	W/m^2-C	9.26
17						
18	**OUTPUTS**					
19	Partial vapor pressure (cold pipe=dp)	P_v1	in. Hg	0.25	Pa	739.4
20	Partial vapor pressure	P_v2	in. Hg	1.96	Pa	4047
21	Atmosphere pressure	P_amb	in. Hg	29.9	Pa	101325
22	Diameter at dew point	D_dp	in	6.353384719	m	0.161375972
23	Insulation volume	V	ft^3	4.91E-01	m^3	0.013899999
24	Condensate volume	V_cond	ft^3	4.60E-01	m^3	0.013026846
25	Coefficient f1	f1	**Use "Solver" to determine f_2**			0.937183246
26	**Coefficient f2**	f2				**2.437242036**
27	Condensate mass flow rate	m_w_dot	lbm/hr	8.0137E-05	kg/s	1.00971E-08
28			lbm/day	6.923840831	kg/day	0.000872389
29	**Optimization (Solver)**	**m_w_dot (exp)**			**kg/day**	**0.000872389**
30		**SQE**				**0**
31		**SSQE**				**0.00E+00**

	1	2	3	4	5	6	7	8
1	Elastomeric Rubber							
2	**m_w_dot**		V	**Days**	V%	**V% exp**	SQE	SSQE
3	**kg/day**		m^3		%	**%**		
4	**0.000872389**		0.0139	**0**	0	**0.00001**	1E-10	0.004791
5				**8**	0.050209457	**0.10**	0.002605933	
6				**18**	0.112971278	**0.10**	0.00027429	
7				**28**	0.175733099	**0.21**	0.001440557	
8				**38**	0.23849492	**0.25**	7.1702E-05	
9				**49**	0.307532923	**0.29**	0.000203231	
10				**57**	0.35774238	**0.34**	0.000195136	

Figure 6.12: Sample input file for predicting moisture content under wet conditions (closed-cell)

	1	2	3	4	5	6	7	8
1				Elastomeric Rubber				
2	m_w_dot		V	Days	V%	V% exp	SQE	SSQE
3	kg/day		m^3		%	%		
4	0.000872389		0.0139	0	0	0.00001	1E-10	0.004791
5				8	0.050209457	0.10	0.002605933	
6				18	0.112971278	0.10	0.00027429	
7				28	0.175733099	0.21	0.001440557	
8				38	0.23849492	0.25	7.1702E-05	
9				49	0.307532923	0.29	0.000203231	
10				57	0.35774238	0.34	0.000195136	
11								
12								
13	m_per		V	Days	m_w	V_w	V%	V% exp
14	kg/day		m^3		kg	m^3	%	%
15	0.000872389		0.0139	0	0	0	0	
16	0.000872389			1	0.000872389	8.72389E-07	0.006276182	
17	0.000872389			2	0.001744779	1.74478E-06	0.012552364	
18	0.000872389			3	0.002617168	2.61717E-06	0.018828546	
19	0.000872389			4	0.003489557	3.48956E-06	0.025104728	
20	0.000872389			5	0.004361946	4.36195E-06	0.031380911	
21	0.000872389			6	0.005234336	5.23434E-06	0.037657093	
22	0.000872389			7	0.006106725	6.10672E-06	0.043933275	
23	0.000872389			8	0.006979114	6.97911E-06	0.050209457	
24	0.000872389			9	0.007851503	7.8515E-06	0.056485639	
25	0.000872389			10	0.008723893	8.72389E-06	0.062761821	
26	0.000872389			11	0.009596282	9.59628E-06	0.069038003	
27	0.000872389			12	0.010468671	1.04687E-05	0.075314185	
28	0.000872389			13	0.011341061	1.13411E-05	0.081590367	
29	0.000872389			14	0.01221345	1.22134E-05	0.087866549	
30	0.000872389			15	0.013085839	1.30858E-05	0.094142732	
				16	0.013958228	1.39582E-05	0.100418914	
				17	0.014830618	1.48306E-05	0.106695096	
				18	0.015703007	1.5703E-05	0.112971278	
				19	0.016575396	1.65754E-05	0.11924746	
				20	0.017447785	1.74478E-05	0.125523642	

Sample output file in Step 1: Moisture profile in the first 20 days

Figure 6.13: Sample output file of moisture content (by volume) in step 1 (closed-cell)

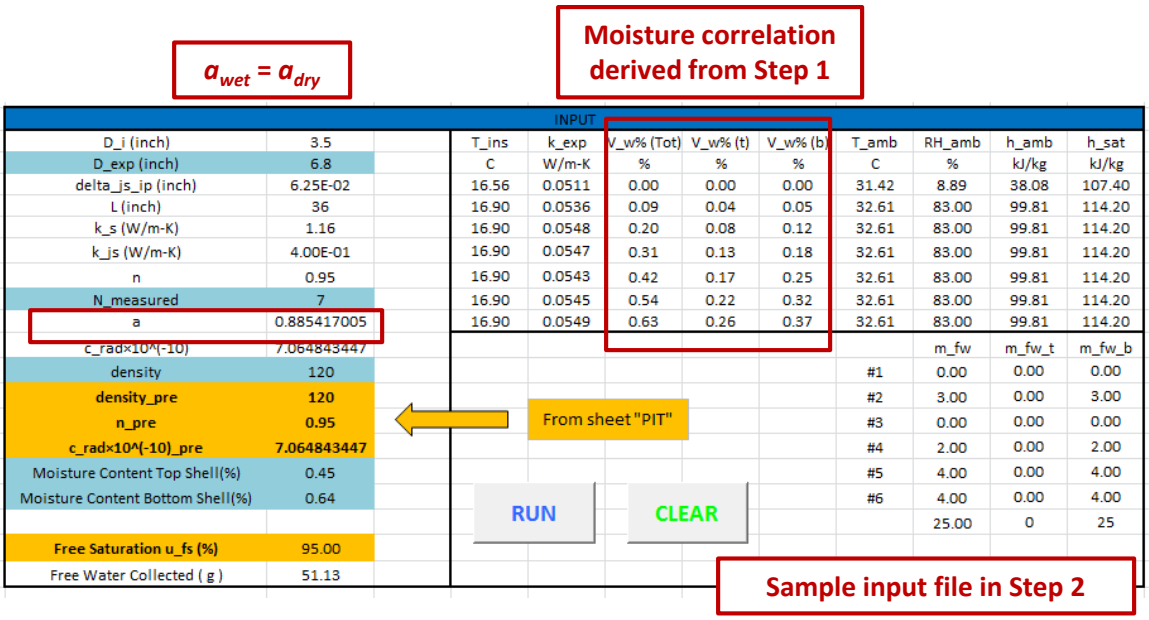

Figure 6.14: Sample input file to the thermal conductivity model in step 2 (closed-cell)

Fibrous pipe insulation systems

The procedures for computing the water content in fiberglass test samples and the system thermal conductivity are summarized in detail in the flow chart shown in Figure 6.15. There are three steps to generate the profiles of moisture content and thermal conductivity in the pipe insulation systems. Similar to the closed-cell pipe insulation systems, a specific case (baseline experimental data) is required at the beginning of the simulation to determine the water retention coefficient f_3 by comparing experimental results on the moisture content with the simulation values, as shown in Figure 6.16. This coefficient can be used directly on other cases to provide the moisture profiles in the same insulation systems.

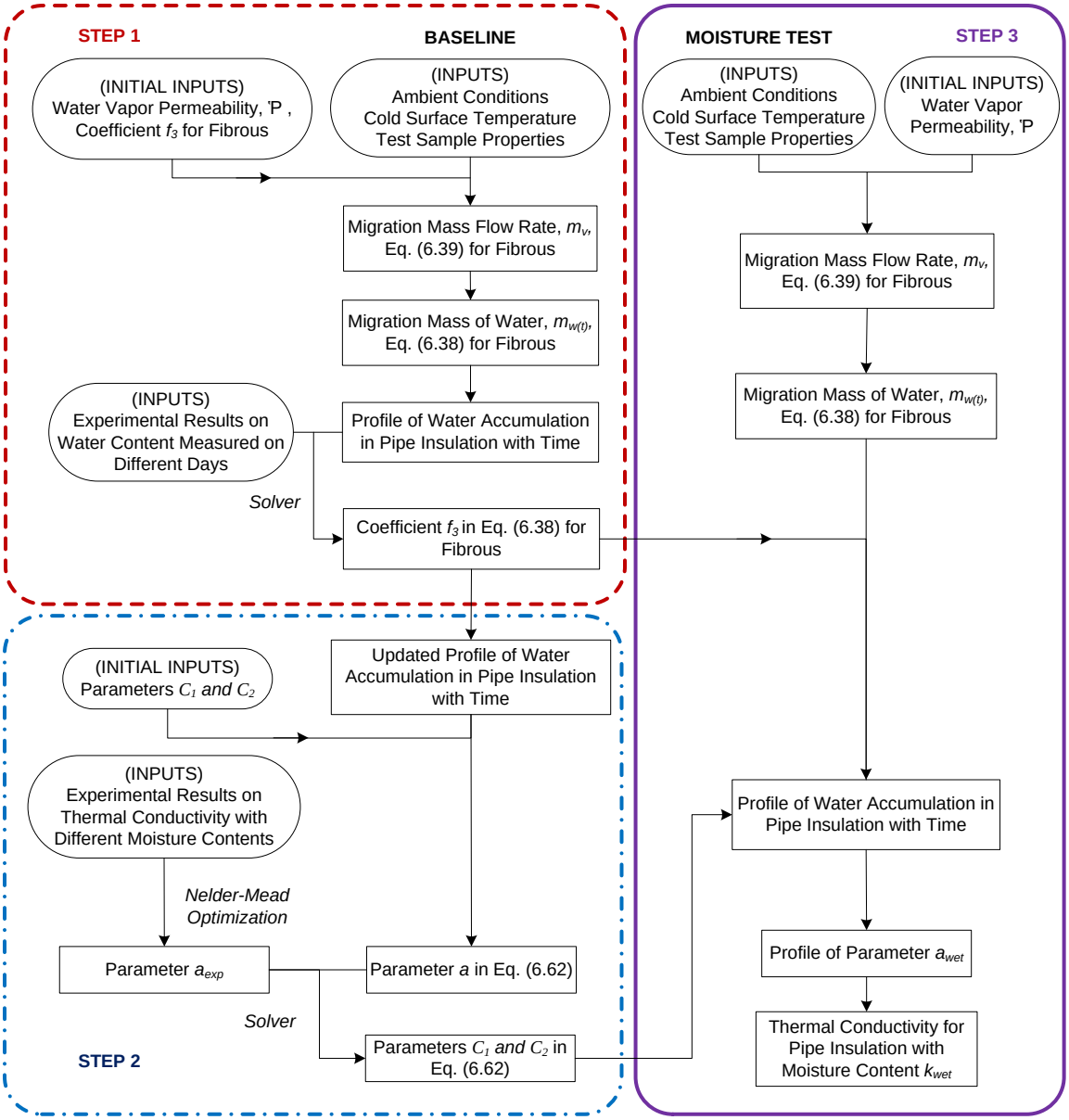

Figure 6.15: Flow chart of the procedures for computing moisture content and thermal conductivity in fibrous pipe insulation with moisture content

Sample input file in Step 1

	1			4	5	6
1	**INPUTS**	**Fiberglass (Baseline)**				
2	**Tempearture Profiles**		IP Units		SI Units	
3	Amb temp	T_amb	F	107.60	C	42.00
4	R.H.	RH_amb	%	81.00	%	81.00
5	Outins temp	T_outins	F	103.98	C	39.99
6	Cold pipe temp	T_al	F	41.60	C	5.33
7	Dew point	T_dp	F	100.44	C	38.02
8	**Test Sample Geometries**					
9	Test length	L	in	36	m	0.9144
10	Insulation exterior diameter	D_o	in	7.5	m	0.1905
11	Insulation interior diameter	D_i	in	3.5	m	0.0889
12	**Properties**					
13	Dry thermal conductivity	k_dry	Btu-in/hr-ft^2-K	0.24	W/m-K	0.0343
14	Permeability	P	US perms	1.39E-11	ng/s-m-Pa	7.97E-10
15	Water density	rho	lbm/ft^3	62.4	kg/m^3	1000
16	Convection heat transfer coefficient	h	Btu/hr-ft^2-F	1.63	W/m^2-C	9.26
17						
18	**OUTPUTS**					
19	Partial vapor pressure (cold pipe=dp)	P_v1	in. Hg	0.25	Pa	892.8
20	Partial vapor pressure	P_v2	in. Hg	1.96	Pa	6648.4
21	Atmosphere pressure	P_amb	in. Hg	29.9	Pa	101325
22	Diameter at dew point	D_dp	in	7.147831857	m	0.181554929
23	Insulation volume	V	ft^3	7.20E-01	m^3	0.020386666
24	Condensate volume	V_cond	ft^3	6.36E-01	m^3	0.017996561
25	Coefficient f1	f1		0.882761369		0.882761369
26	Coefficient f2	f2		1		1
27	**Coefficient f3**	**f3**		**0.068425603**		**0.068425603**
28	Condensate mass flow rate	m_w_dot	lbm/hr	0.016572665	kg/s	2.08812E-06
29			lbm/day	1431.878269	kg/day	0.180413627
30	**Optimization (Solver)**	**m_w_dot (exp)**			**kg/day**	**0.180340723**
31		**SQE**				**5.31501E-09**
32		**SSQE**				**5.32E-09**

	1	2	3	4	5	6	7	8	9	10	11
1	Fiberglass at 107F (2010)_PIT1										
2	**m_w_dot**	deltaPv	V		**t0**	**Days**	V%	**V% exp**	SQE	SSQE	
3	**kg/day**		m^3				%	**%**			
4	**0.180340723**	5755.6	0.0204		**0.083333333**	**0**	0	**0.12**	0.01414	5.062189	
5						**3**	2.65	**1.66**	0.975236		
6						**5**	4.40	**4.26**	0.017532		
7						**8**	6.96	**7.03**	0.004239		
8						**11**	9.44	**11.33**	3.565003		
9						**12**	10.24	**10.93**	0.486038		

Use "Solver" to determine f_3

Figure 6.16: Sample input file for predicting moisture content under wet conditions (fibrous)

Step 2 is to determine coefficients C_1 and C_2 in the function of parameter a. Based on the experimental results, the expected values of parameter a (a_{exp}) can be computed from the measured thermal conductivity and the moisture content in the specific case. The sample input file of step 2 is shown in Figure 6.17. According to Equation (6.62), the parameter a can be simulated with initial inputs of C_1 and C_2, as shown in Figure 6.18, and an optimization study will

be applied between the simulation results and a_{exp} to determine coefficients C_1 and C_2. These coefficients will behave as constants during the other groups of tests on the same type of pipe insulation materials, and provide a profile on the variation of parameter a, which will be used in the thermal conductivity model.

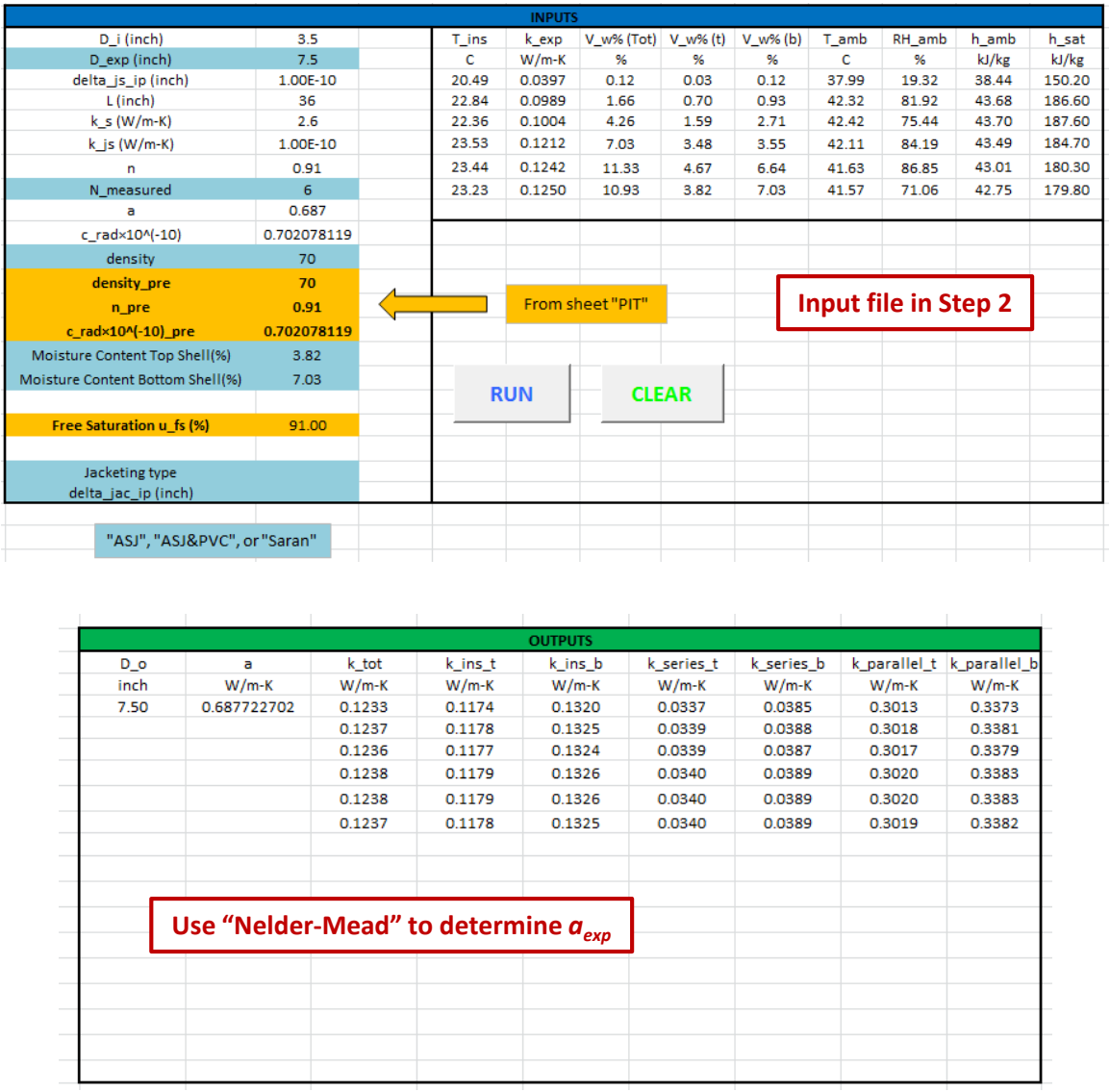

Figure 6.17: Input and output files for the baseline case (fibrous)

	1	2	3	4	5	6	7	8	9	10	11
1	Fiberglass at 107F (2010)_PIT1										
2	m_w_dot	deltaPv	V		t0	Days	V%	V% exp	SQE	SSQE	
3	kg/day		m^3				%	%			
4	0.180340723	5755.6	0.0204		0.083333333	0	0	0.12	0.01414	5.062189	
5						3	2.65	1.66	0.975236		
6						5	4.40	4.26	0.017532		
7						8	6.96	7.03	0.004239		
8						11	9.44	11.33	3.565003		
9						12	10.24	10.93	0.486038		
10											
11											
12	m_w_dot	deltaPv	C1	C2	t0	Days	a1	a2_exp	a2	SQE	SSQE
13	kg/day										
14	0.180340723	5755.6	4.50E-05	0.019	0.083333333	0	0.98	0.9508717	0.98	0.000848	0.002088
15						3	0.98	0.7092192	0.71	2.31E-06	
16						5	0.98	0.7258476	0.70	0.000479	
17						8	0.98	0.6691881	0.69	0.000617	
18						11	0.98	0.694503	0.68	0.000101	
19						12	0.98	0.6877227	0.68	4.07E-05	
20											
21											
22	Fiberglass at 107F (2010)_PIT1										
23	m_w_dot	rate	V		t0	Days	m_diff	V_diff	V%	a1	a2
24	kg/day		m^3				kg	m^3	%		0.651494
25	0.180340723		0.0204		40	0	0	0	0	0.98	0.98
26	0.1803	0.0000				1	0.1803407	0.0001803	0.884601	0.98	0.71864
27	0.180059156	0.0003				2	0.3603999	0.0003604	1.767822	0.98	0.714153
28	0.179497778	0.0006				3	0.5398977	0.0005399	2.648288	0.98	0.71074
29	0.178660078	0.0008				4	0.7185577	0.0007186	3.524646	0.98	0.707345
30	0.177551231	0.0011				5	0.896109	0.0008961	4.395564	0.98	0.703972
31	0.176178033	0.0014				6	1.072287	0.0010723	5.259747	0.98	0.700625
32	0.174548811	0.0016				7	1.2468358	0.0012468	6.115938	0.98	0.697308
33						8	1.4195091	0.0014195	6.962929	0.98	0.694027
34						9	1.5900717	0.0015901	7.799567	0.98	0.690787
35						10	1.7583006	0.0017583	8.624758	0.98	0.68759
36						11	1.9239861	0.001924	9.437473	0.98	0.684442
37	0.162946367	0.0027				12	2.0869324	0.0020869	10.23675	0.98	0.681346
38	0.16002648	0.0029				13	2.2469589	0.002247	11.02171	0.98	0.678306
39	0.156941163	0.0031				14	2.4039001	0.0024039	11.79153	0.98	0.675324
40	0.153706181	0.0032				15	2.5576063	0.0025576	12.54549	0.98	0.672403

Sample output file in Step 2:
Use "Solver" to determine C_1 and C_2

Sample output file in Step 1:
Moisture profile in the first 15 days

Figure 6.18: Sample output files of moisture content and parameter a (fibrous)

With the water retention coefficient derived from step 1, and the two coefficients, C_1 and C_2 in the function of parameter *a*, determined from step 2, both profiles on the moisture content and the parameter *a* can be provided in other cases that test with the same type of pipe insulation materials. These two groups of data are the inputs to the thermal conductivity model, and used for the prediction on the thermal conductivity of the pipe insulation systems with moisture ingress. The sample input file in step 3 is shown in Figure 6.19.

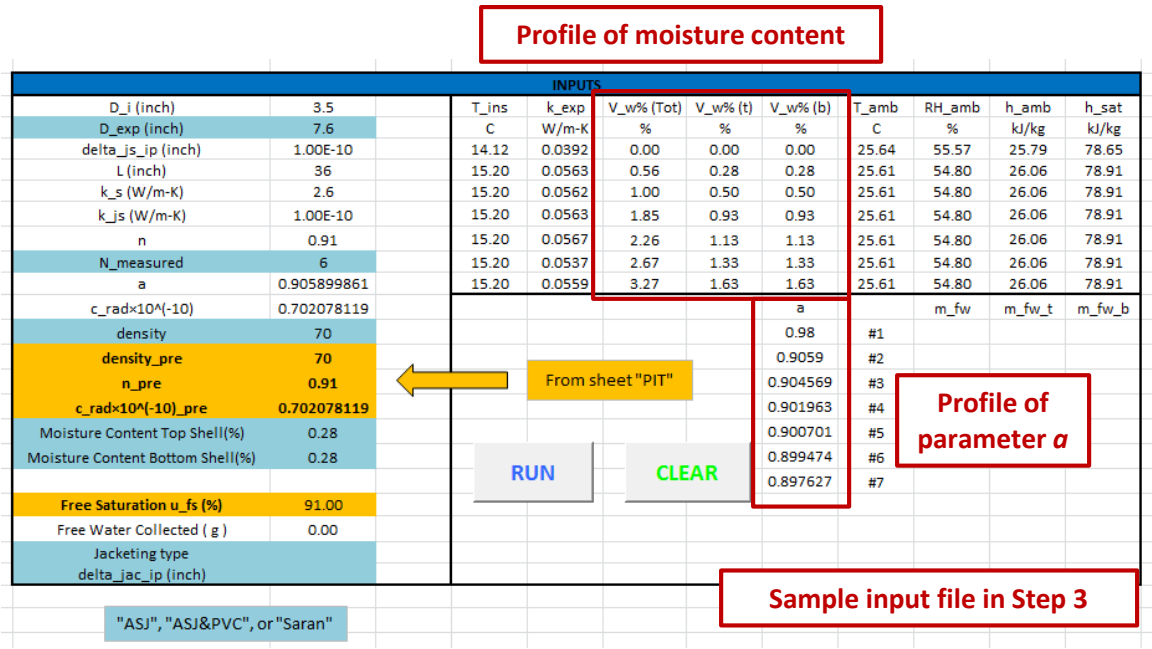

Figure 6.19: Sample input files in step 3 (fibrous)

6.7 Model validation for dry conditions at below ambient temperatures

6.7.1 Closed-cell pipe insulation

The experimental data of thermal conductivity of closed-cell pipe insulation system, including cellular glass, phenolic and elastomeric pipe insulation systems reported in the chapter 5, were used as benchmark for the simulation results during a preliminary sensitivity study of the thermal conductivity for the parameters a and c_{rad}. The pipe insulation systems were selected from previous test results. They are include: 1) cellular glass pipe insulation systems V-CG1, V-CG2, and P2-CGA; 2) phenolic pipe insulation systems P1-P1 and P1-P2; 3) elastomeric rubber pipe insulation systems P1-ER, P2-ER1 and P2-ER2. The specifications of the systems in the baseline and in the actual experiments are listed in Table 6.1, and the results of the comparison are shown in Figure 6.20. As an example, let's consider the cellular glass pipe insulation. First the experimental data of cellular glass pipe insulation system V-CG1 with 1-in (25.4) wall thickness was used as a baseline case to derive the two parameters, a and c_{rad}, based on the Nelder-Mead

regression optimization approach (Nelder & Mead, 1965). Then for the same type pipe insulation systems with different insulation wall thickness, the parameters a and c_{rad} were kept constant.

Table 6.1: Parameters of the systems in the tests and literature

Experiment System (Ref No.)	**Thickness** in (mm)	**Density** lb/ft^3 (kg/m^3)	**Joint Sealant Thickness** in (mm)	**Joint Sealant Thermal Conductivity** Btu-in/hr-ft^2-F (W/m-K)	**Porosity**	***a**	***c_{rad}** $\times10^{-10}$
V-CG1(baseline)	1 (25.4)	7.5 (120)	1/16 (1.6)	2.77 (0.4)	0.95	0.8854	7.0648
V-CGB	2 (50.8)	7.5 (120)	1/16 (1.6)	2.77 (0.4)	0.95	0.8854	7.0648
P2-CGA	1.5 (38.1)	7.5 (120)	1/16 (1.6)	2.77 (0.4)	0.95	0.8854	7.0648
CG (literature)[1]	2 (50.8)	8.5 (136.2)	-	-	0.94	0.8854	7.0481
P1-P1 (baseline)	1 (25.4)	2.3 (37)	1/12 (2.2)	2.77 (0.4)	0.95	0.6887	4.1155
P1-P2	2 (50.8)	2.3 (37)	1/12 (2.2)	2.77 (0.4)			
Phenolic (literature)[2]	0.9 (22)	2.9-4.2 (46-67)	-	-	0.94	0.6887	4.0979
P1-ER (baseline)	2 (50.8)	3.1 (50)	-	-	0.91	0.7590	2.5576
P2-ER1	1.5 (38.1)	2.5 (40)	-	-	0.93	0.7590	2.5744
P2-ER2	2 (50.8)	2.5 (40)	-	-	0.93	0.7590	2.5744
ER (literature)[3]	1 (25.4)	4.1 (66)	-	-	0.88	0.7590	2.5390

*: Pararmeter a and c_{rad} were determined by SI unit
[1]: Specifications from literature, by Whitakar and Yarbrough (2002);
[2]: Specifications from literature, by Tseng and Kuo(2002);
[3]: Specifications from literature, by Wilkes (2002)

The thermal conductivity for the other cellular glass pipe insulation systems V-CG2 and P2-CGA were predicted with a 5% and 17% deviation with respect to the experimental data. It should be noted that P2-CGA showed a higher thermal conductivity and a slightly flatten trend of the thermal conductivity with temperature with respect to V-CG2. However, the difference was due to the test methodology used to measure the thermal conductivity of these two samples. If the data reduction procedure used to analyze the experimental data is the same for both cases, the effective thermal conductivity of P2-CGA decreases from group 3 to 4, and the data of P2-CGA and V-CG2 become within the experimental uncertainty. For the purpose of model validation both groups can still be considered, as shown in Figure 6.20a. The joint sealant effect was also

considered in the simulation. By varying the thickness of joint sealant from 1/16 in (1.6 mm) to 1/12-in (2.1 mm) on V-CG2, the difference on the thermal conductivity computed from model to the experimental results decreased from 17% to 10% (dash-dot line 1 to 2, Figure 6.20a). Phenolic pipe insulation system was validated with two systems, system P1-P1 at 1-in (25.4 mm) nominal wall thickness, and system P1-P2 are 2-in (50.8 mm) nominal wall thickness. System P1-P1 with 1-in (25.4 mm) wall thickness was considered as the baseline and the simulation results for P1-P2 was about 10% higher than the experimental results. By decreasing the thickness of joint sealant from 1/12-in (2.1 mm) to 1/16-in (1.6 mm), the difference decreased to 6% (see Figure 6.20b). The simulation was also applied on elastomeric rubber pipe insulation system. The baseline case was taken from the data of system P1-ER with 2-in (50.8 mm) nominal wall thickness. The other two test samples, P2-ER1 and P2-ER2, had about 20% density difference, most likely because the sample were from a different batch. Thus an adjustment of the c_{rad} parameter was made as previously discussed in this section. Using the same parameter a and the adjusted c_{rad}, the simulation results matched well with the experimental values on P2-ER1 and P2-ER2 and the deviation was 12% and 7%, respectively, as shown in Figure 6.20c.

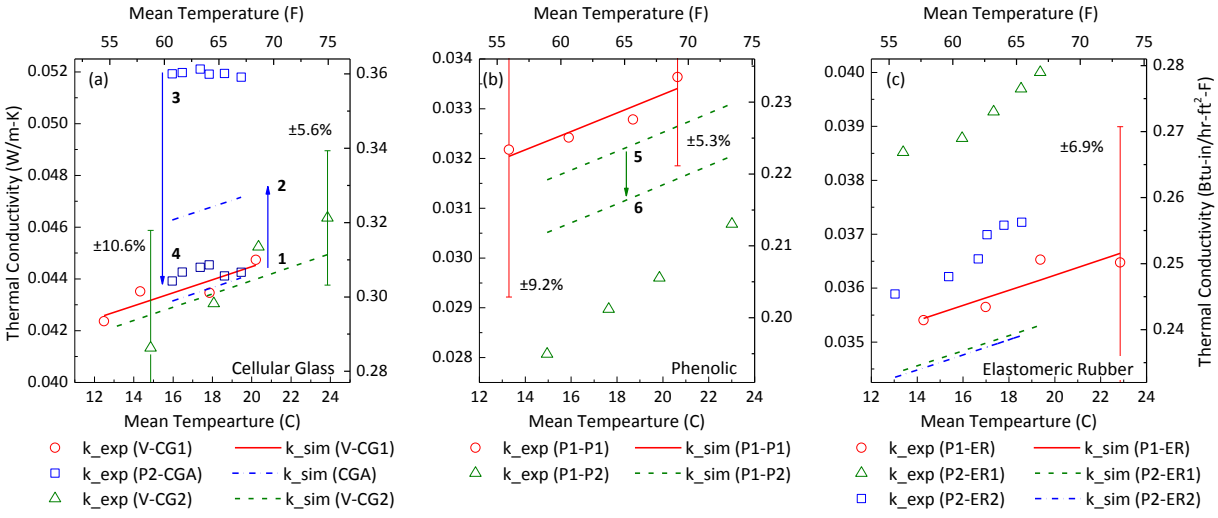

Figure 6.20: Comparison between the experimental and simulation results under dry condition

The simulation results were also compared with published values of thermal conductivity of pipe insulation systems in the literature, as shown in Figure 6.21. Due to the fact that for cellular glass and phenolic pipe insulation systems there was no information provided on the joint sealant applied between the two pipe insulation half shells, the model was applied without joint sealant, and then compared to the cases with the same joint sealant as used in the baseline samples. Without joint sealant, the simulation results matched the reported values with average differences of 25% for cellular glass, and 25% for phenolic pipe insulation. By considering the joint sealant effects, the differences decreased to 21% on cellular glass insulation system with a 1/16-in (1.6 mm) thickness of joint sealant, but the difference increased to 32% on phenolic with a 1/12-in (2.2 mm) thickness, shown in Figure 6.21a and b. For cellular glass, the literature values might be obtained based on the test specimens with joint sealant applied between the two half shells, and the specifications of the joint sealant were not clearly identified. Thus, the thermal conductivity and thickness of the joint sealant selected in the model can be different from the one used in the experimental measurement. The simulation model over-predicted phenolic pipe insulation when compared to the literature values because less conductive or a thinner layer of joint sealant might have been present during experimental measurements. Aging effect on phenolic is also another source of uncertainty that might cause the simulation results to deviate from the experimental data in the literature. Elastomeric rubber was not affected by the joint sealant, since it is usually installed as one piece around the pipe, or pre-slimed with a very thin layer of adhesive factory applied. The differences between the simulation results and the values in the literature were within 4%, as shown in Figure 6.21c.

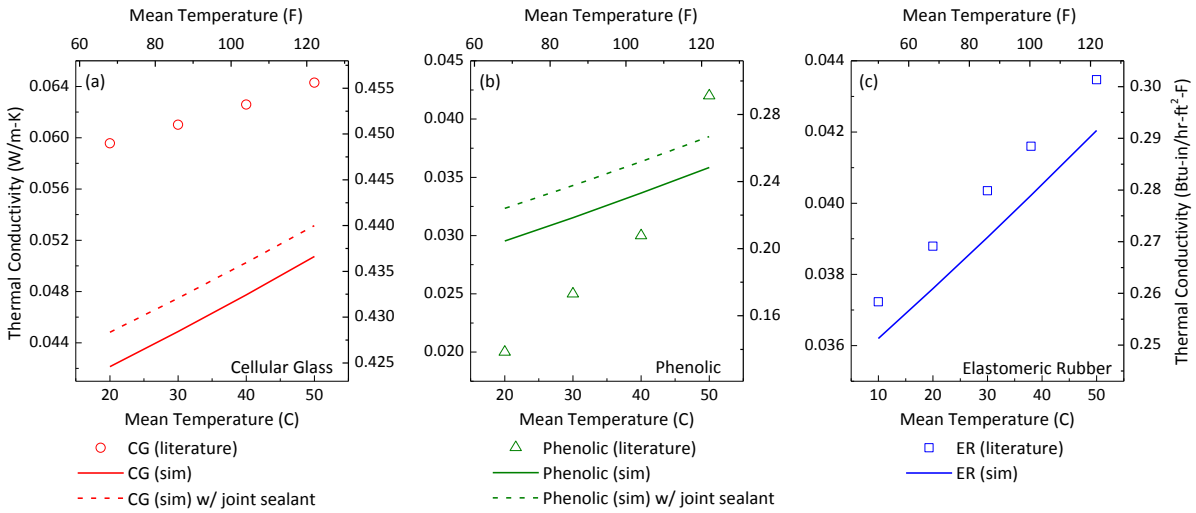

Figure 6.21: Comparison between the literature and simulation results under dry condition

6.7.2 Fibrous pipe insulation

Fiberglass is one of the most commonly used fibrous materials and is selected as the validation sample for fibrous pipe insulation. By applying a similar methodology as the cellular pipe insulation, the computed thermal conductivity of fiberglass pipe insulation was compared to the experimental results and published values from the literature. The test on fiberglass pipe insulation system P1-FG, with 2-in (50.8 mm) nominal wall thickness was considered as the baseline to determine the parameters a and c_{rad}. Since another similar insulation system was tested two years later, system P2-FG1, two groups of parameters were determined from these two baseline results, shown as baseline 1 and baseline 2. The following simulations were computed by applying the parameters from baseline 2, which was tested after baseline 1 and before the other experiments with jacketing. The other systems included in this validation phase are: system P2-FG2 with ASJ vapor retarder and P2-FG3 with ASJ vapor retarder and PVC jacketing. Compared to the baseline sample, the test samples in the other two systems were from different manufacturer with lower density and different vapor barriers, as listed in Table 6.2.

Table 6.2: Parameters of the systems in the tests and literature

Experiment System (Ref No.)	**Thickness** in (mm)	**Jacketing Thickness** in (mm)	**Density** lb/ft^3 (kg/m^3)	**Porosity**	***a**	***c_{rad}** ×10^{-10}
P1-FG (baseline 1)	2 (50.8)	-	4.4 (70)	0.91	0.98	0.8187
P2-FG1 (baseline 2)	2 (50.8)	-	4.4 (70)	0.91	0.99	3.7138
P2-FG2 (w/ ASJ)	1.5 (38.1)	0.01 (0.254)	3.5 (56)	0.93	0.99	3.7324
P2-FG3 (w/ ASJ&PVC)	1.5 (38.1)	0.03 (0.762)	3.5 (56)	0.93	0.99	3.7324
Fiberglass[1] (L1)	2.125 (54)	-	2.1 (33)	0.96	0.99	3.7774
Fiberglass[2] (L2)	2 (50.8)	-	5.4 (86.5)	0.89	0.99	3.6847

*: Pararmeter a and c_{rad} were determined by SI unit
[1]: Specifications from literature, Wilkes at al.(2002);
2: Specifications from literature, Whitaker and Yabrough (2002)

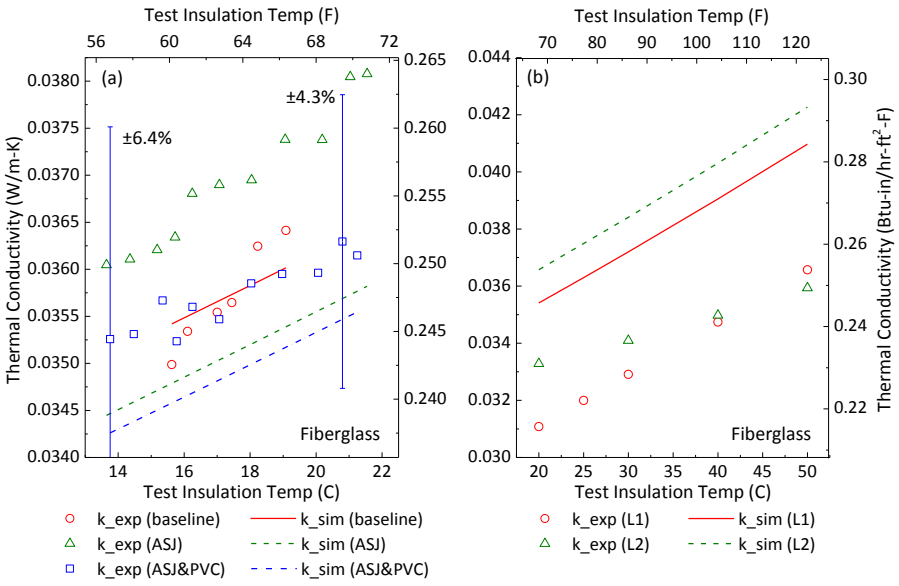

Figure 6.22: Validation of the simulation results under dry condition (fibrous pipe insulation)

The comparison is plotted in Figure 6.22a. For the fiberglass pipe insulation system P2-FG2 with ASJ vapor retarder, the difference between the experimental and simulation results are within 7%, and for the insulation system P2-FG3 with ASJ and PVC jacketing, it is within 4%. Both the experimental and simulation results show that the thermal performance of fiberglass with PVC jacketing is better than the one with only ASJ jacketing. From current literature, two different

types of fiberglass pipe insulation with various density and thicknesses are selected and applied to the simulation model. The updated parameters are listed in Table 6.2, and the comparison is shown in Figure 6.22b. The simulation curve showed a similar trend to the experimental results, except one case on the literature review data (triangle data points), and the average differences are around 11% and 10% respectively.

6.8 Model validation under wet conditions with moisture ingress

6.8.1 Closed-cell pipe insulation systems

Four types of closed-cell pipe insulation systems, without any vapor retarder or barrier, were tested under wet conditions with moisture ingress. These systems are cellular glass (P2-CGA and P2-CGB), elastomeric rubber (P2-ER1), phenolic (P1-P and P2-P) and polyisoyanurate (P2-PIR). The specifications of the test samples and test ambient conditions are summarized in Table 6.3. Cellular glass pipe insulation system was tested twice, one was on the bare pipe (P2-CGA), and the other one was on the black pipe (P2-CGB). Two phenolic pipe insulation systems with different sealant, P1-P1 and P2-P were tested under two ambient conditions.

Table 6.3: Specifications of systems and ambient conditions in moisture tests

Experiment System Ref No.	**Thickness**	**Density**	**Porosity**	**Ambient Temp**	**Al pipe surfaces Temp**	**RH**
	in (mm)	lb/ft^3(g/m^3)		˚F (˚C)	˚F (˚C)	%
P2-CGA	1.5 (38.1)	115 (7.2)	0.95	90.6 (32.6)	38.0 (3.4)	83
P2-CGB				89.8 (32.1)	37.7(3.2)	83
P2-ER	1.5 (38.1)	40 (2.5)	0.91	90.6 (32.6)	36.8 (2.7)	83
P1-P2	50.8 (2)	37 (2.3)	0.95	96.4 (35.8)	40.7 (4.9)	87
P2-P				107.7 (42.0)	40.7 (4.9)	82
P2-PIR	1.5 (38.1)	40 (2.0)	0.95	107.4 (41.9)	40.7 (4.9)	82

Validation on the mass of water accumulated in closed-cell pipe insulation system

The moisture accumulated in the closed-cell insulation system is computed by following the procedures discussed in section 6.2.2, from Equations (6.20) to (6.49). Due to the fact that in

ASTM standard, the published water vapor permeability is almost constant regarding to the materials with different densities, it is assumed that for all closed-cell pipe insulation, water vapor permeability is not sensitive to the material porosity and would maintain constant under the same ambient conditions. Therefore, the moisture accumulation is a linear correlation with time, shown in Figure 6.23a to d. According to the standards, the water vapor permeability is given based on the normal temperature range for room conditions. For example, rigid cellular phenolic is tested by submission in water at 73.2±3.6˚F (23±2˚C), 50RH±5% for 2 hours, and cellular glass is tested by immersion on blocks, at 70±5˚F (21±2.8˚C), 50RH±10% for 2 hours. All these conditions are quite different from the severe conditions required during the moisture tests. Besides, different types and amount of joint sealant were applied in each insulation system. This sealant behaves differently to the water vapor transmission and would have an impact on the system water vapor permeability. Therefore, the system water vapor permeability for these four types of pipe insulation systems were corrected by adjusting the coefficient f_2, as listed in Table 6.4.

Table 6.4: Simulation results on coefficient f_2 and correlations between moisture content with time

Experiment System Ref No.	**Coefficient f_1**	**Coefficient f_2**	**Correlations[1]**
Cellular Glass (P2-CGA)	0.98	84.1	V_w%=0.0110t
Cellular Glass (P2-CGB)	0.97	84.1	V_w%=0.0106t
Elastomeric Rubber (P2-ER1)	0.94	2.4	V_w%=0.0062t
Phenolic (P1-P)	0.93	11.6	V_w%=0.2107t
Phenolic (P2-P)	0.89	11.6	V_w%=0.2533t
PIR (P2-PIR)	0.83	2.0	V_w%=0.3195t

[1]: The correlations are given based on moisture content (% by volume) and time (days).

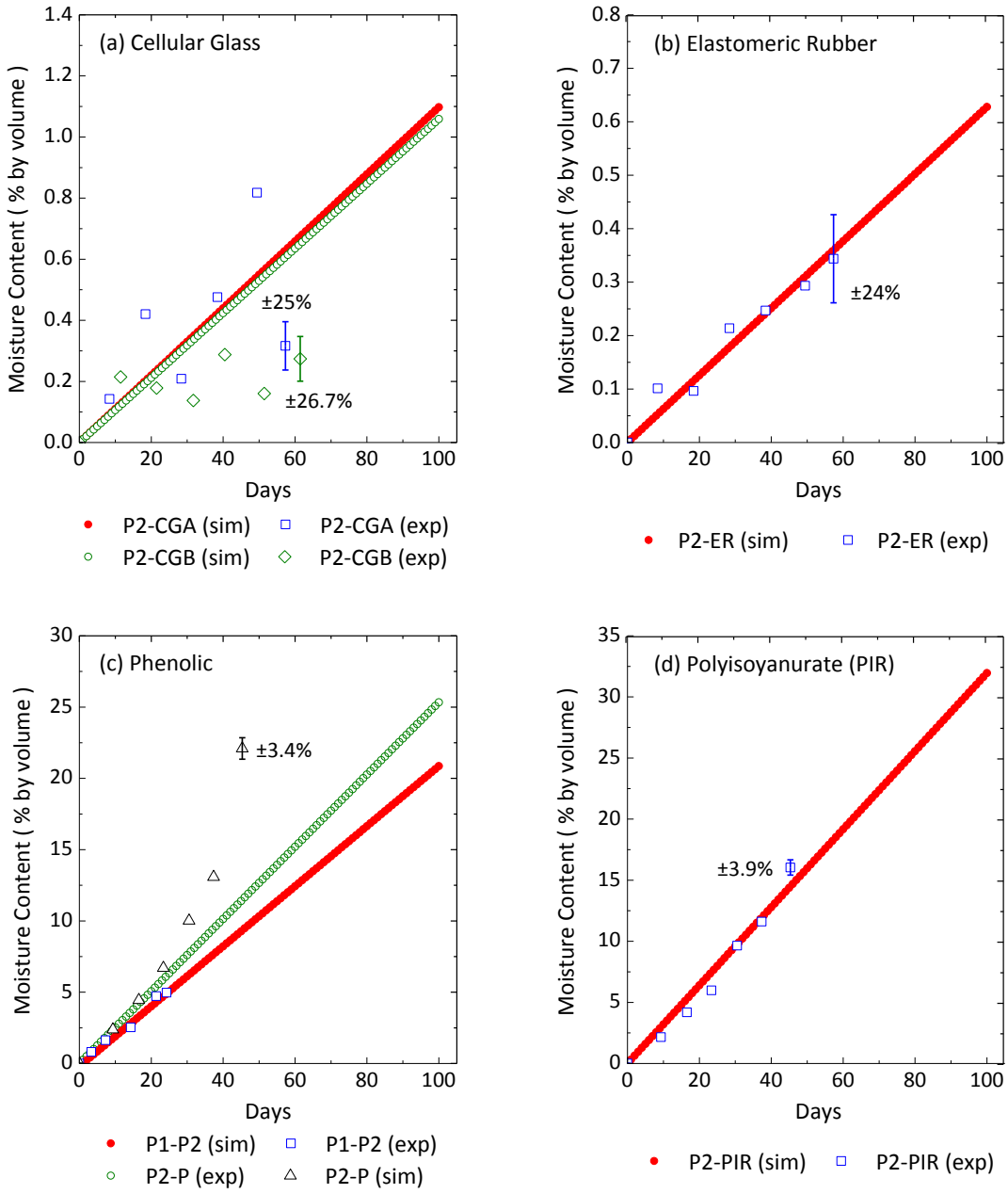

Figure 6.23: Comparison between experimental and simulation results four types of closed-cell pipe insulation systems

There are several findings from the simulation results on the moisture content in the insulation system:

Phenolic pipe insulation systems P1-P2 and P2-P were tested under different ambient conditions. The water vapor permeability correction factor f_2 was computed from the experimental results on the moisture profile provided in system P1-P2. For system P2-P, by maintaining the same correction factor f_2, and updating condensation coefficient f_1 according to the ambient conditions, the simulation results on the moisture content in system P2-P matched with the experimental results in 30%. The last point was obviously out of the simulation range, and the difference increased to 48%. By maintaining the same coefficient f_2 in the cellular glass pipe insulation system P2-CGB, although the simulation results over predicted the moisture content by 30~40%, the total amount of water was very low, and this resulted in a large uncertainty during the measurement. From these comparisons, it seems that with current assumptions, the simulation results did not quite follow the experimental results and there are two possible reasons. First, the water vapor permeability of closed-cell pipe insulation may not be constant and it will be varies with insulation mean temperature and the volume of water. In this case, the moisture profile would not follow a linear correlation. The second possible reason is that the water vapor permeability is sensitive to the ambient temperature and the system joint sealant, the coefficient f_2 may not be constant. However, more experimental data is required on the same type of the insulation systems to further validate the correlations of the moisture profile.

Second, it is found that there are large differences on the values of the coefficient f_2 among these four types of pipe insulation systems. These dissimilarities indicate that each type of the insulation might behave differently to the changes from the ambient conditions. Some of them are not sensitive to the water vapor pressure differences, and the water vapor permeability remains constant under varied temperatures and humidity, such as elastomeric rubber and PIR. However, some of them perform fairly sensitive when the ambient condition changes, such as cellular glass.

The application of joint sealant might be another reason to explain the variation on the coefficient f_2. Compared to other closed-cell materials, cellular glass has a very low water vapor permeance, 0.005 US perm (0.007 metric perm). Boss 368 was used on all the joints as both joint sealant and vapor sealant. However, this material is not recommended as a good vapor sealant, and the water vapor permeability might be much larger than cellular glass insulation. With the presence of this type of joint sealant, the system water permeability increased. In the PIR pipe insulation system P2-PIR, Chil-Joint CP-70 was applied on all the joints as vapor seal, and this material has very low water vapor permeability with the maximum permeance is 0.008 perm-inch (0.012 metric perm). For PIR insulation, the water permeance is reported at 4.0 perm-inch (5.8 metric perm). This large difference indicates that the water vapor permeability in PIR system may not be affected by the joint sealant. For the other pipe insulation systems, elastomeric rubber did not require joint sealant during installation, and f_2 was close to 1. Currently, further research is still needed for better explanations on why this coefficient is large than 1 and why the variations are large among different types of closed-cell pipe insulation systems.

The third finding is that for closed-cell pipe insulation system, the maximum moisture content might be reached when all the cells with temperatures below than the dew point are filled with water. A more specific water distribution profile will help predict how the moisture content in closed-cell pipe insulation reaches the asymptotic values. It seems that with moisture gradually filling in the cells from interior outward, the increase on the local thermal conductivity will lead to lower insulation temperatures and higher values on the coefficient f_1, which is assumed to maintain constant in current model. If the coefficient f_1 increases, the water condensate will be accumulated in the pipe insulation at a higher rate. This might be the reason to explain why the last points in the following three tests on cellular glass P2-CGA, phenolic P2-P and PIR P2-PIR, are slightly higher than the simulation results. However, considering the low permeability under severe test conditions, in current model, the moisture content was assumed to increase linearly

with time for the first 100 days of test. The linear correlations for the moisture content in the pipe insulation are derived based on the optimization between the simulation and experimental results and documented in Table 6.4. These correlations will be applied next to the thermal conductivity model.

Validation on the thermal conductivity of closed-cell pipe insulation with moisture ingress

The variation on the thermal conductivity of the pipe insulation with moisture ingress are predicted with the present model and validated with the experimental data from the present work. The experimental data were gathered according to the methodology described in details in chapter 3. All the required inputs on the ambient conditions are included in Table 6.3. The parameters a and c_{rad} were computed from one specific case on the same type of insulation tested under dry conditions, and c_{rad} was adjusted based on the material porosity. The values of parameter a and c_{rad} used in the simulation are documented in Table 6.5.

Table 6.5: Test samples specifications in moisture tests

Experiment System Ref No.	**Joint Sealant Thickness** in (mm)	**Joint Sealant Thermal Conductivity** Btu-in/hr-ft^2-F (W/m-K)	**Water Vapor Permeability** perm-in. (ng/s-m^2-Pa)	***a**	***c_{rad}** $\times 10^{-10}$
Cellular Glass (P2-CGA) Cellular Glass (P2-CGB)	1/16 (1.6)	2.77 (0.4)	0.005 (0.007)	0.4159	0.000088
Elastomeric Rubber (P2-ER)	-	-	0.1 (0.0144)	0.9999	5.2052
Phenolic (P1-P1) Phenolic (P1-P2)	1/12 (2.1)	2.77 (0.4)	0.9 (1.3)	0.6887	4.1155
Polyisocyanurate (P2-PIR)	1/12 (2.1)	2.77 (0.4)	4.0 (5.8)	0.7503	0.00002

*: Pararmeter a and c_{rad} were determined by SI unit

Both cellular glass and elastomeric rubber have very low water vapor permeability, and the thermal conductivity ratio increased in the similar trends as predicted by the model. In these three cases (two tests on cellular glass and one test on elastomeric rubber), the thermal conductivity were better predicted with moisture content than with time. As shown in Figure 6.24a and c, the

simulated thermal conductivity ratio with moisture content matched the experimental values within the uncertainty range. The thermal conductivity ratio was also predicted with time, and the differences between the simulation and experimental results were within 5%. These differences were brought into the thermal conductivity model from the deviations in the simulated moisture profiles. It should be noted that cellular glass pipe insulation system was tested twice under the same ambient condition (Table 6.3), thus the simulation results on system P2-CGA and P2-CGB are almost the same. The thermal conductivity of phenolic pipe insulation systems P1-P2 and P2-P were measured under different ambient conditions, and the test specimens had same nominal wall thickness and density, as listed in Table 6.5. The simulation results on the thermal conductivity ratio were compared to the experimental values in Figure 6.24 e and f. It shows that the simulation results under-predicted the thermal conductivity of the phenolic pipe insulation by about 8 ~ 9% when considering different moisture content, and the simulation results would deviate from the experimental curve upto 36% when considering with time. These larger differences on the thermal conductivity ratio with time were from the inaccurate moisture profile developed for the closed-cell pipe insulation systems. For PIR pipe insulation system with no vapor retarder, the model over-predicted the thermal conductivity ratio within 12% when compared to the experimental results. These differences might be caused by a minor deviation on the parameter *a* during the wet condition. Take PIR pipe insulation system as an example, on day 45, the moisture content was 16.04% by volume, when parameter *a* increased from 0.75 to 0.8, the thermal conductivity ratio decreased from 1.78 to 1.64, with the difference between simulation and experimental result (with time) decreased from 12% to 7%. However, more data sets are required to prove this theory, and in the currently model, parameter *a* was considered as constant for all closed-cell pipe insulation systems. It should be noted that based on the assumption that moisture content is linearly increased with time during the first 100 days of moisture tests, the variation on the thermal conductivity ratio can only be predicted within these 100 days, and it might increase faster in the long run due a larger condensation region. This larger

region will increase the value of coefficient f_1, and increase the system water migration rate. The simulation results are documented in Table E1-5 in the Appendix E.

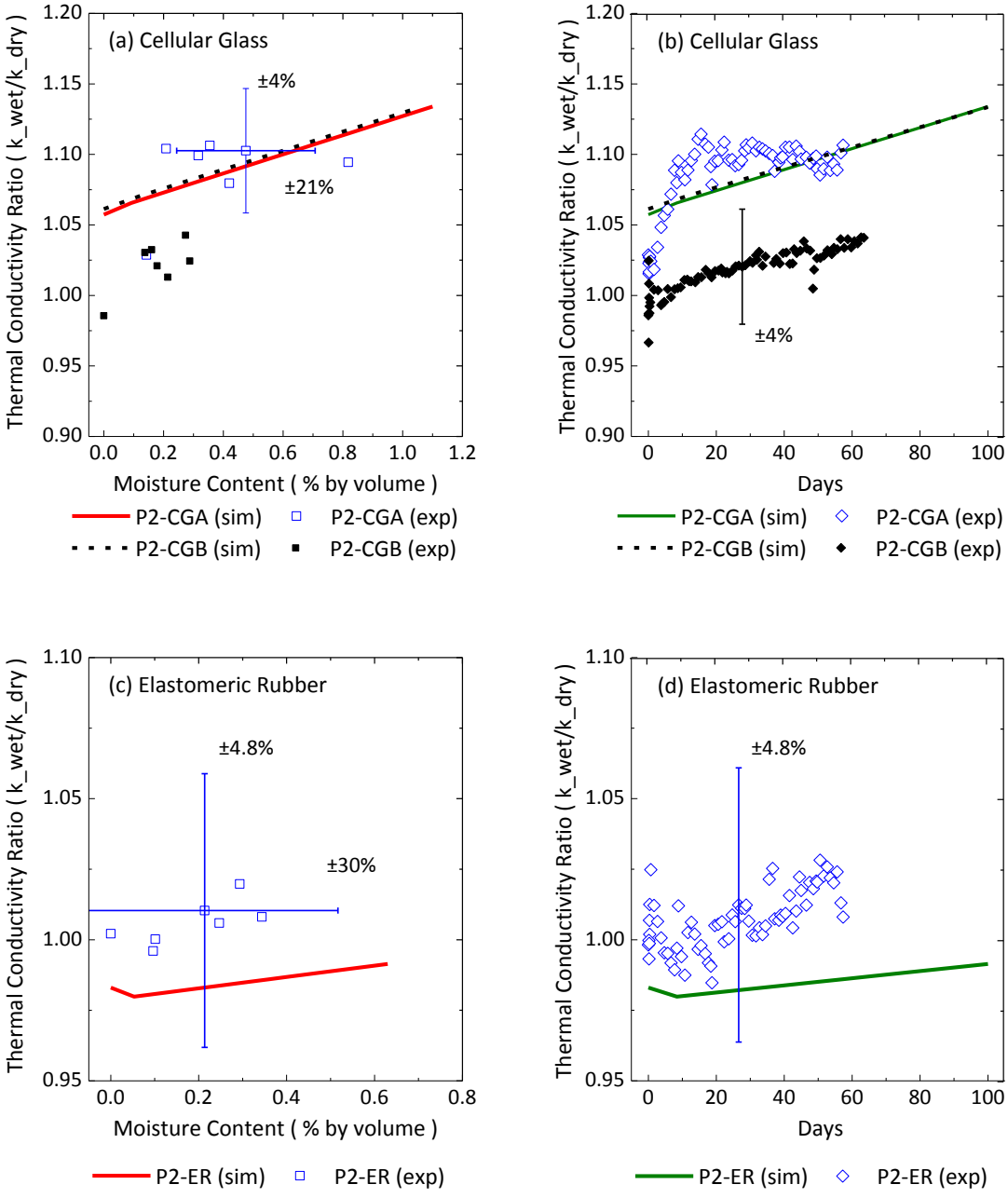

Figure 6.24: Comparison between experimental and simulation results on the thermal conductivity ratio between dry and wet closed-cell pipe insulation systems

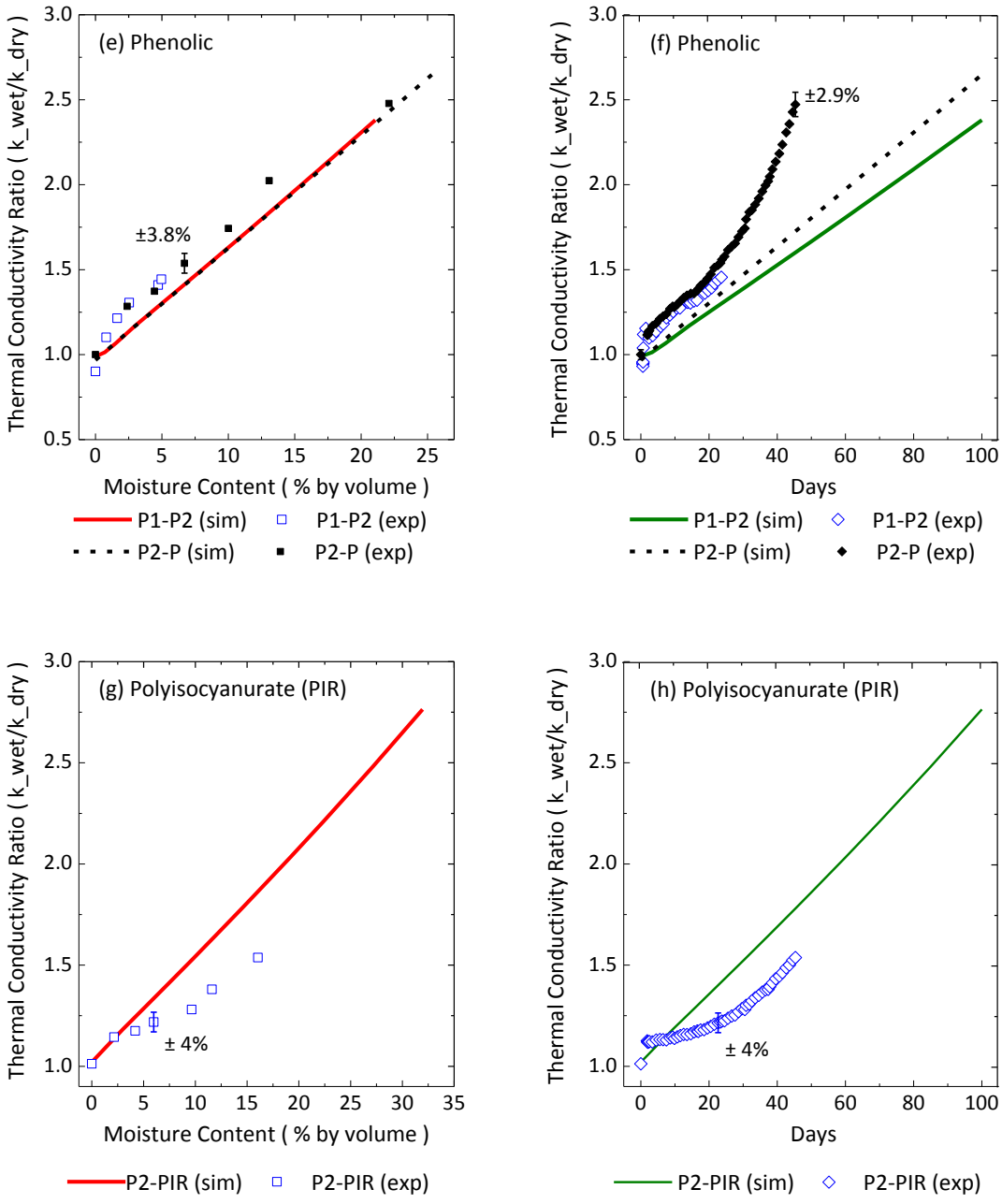

Figure 6.24(continued): Comparison between experimental and simulation results on the thermal conductivity ratio between dry and wet closed-cell pipe insulation systems

6.8.2 Fibrous pipe insulation system systems

Four groups of moisture tests were done on fiberglass pipe insulation in the past three years. The specifications of the test samples and tested ambient conditions are summarized in Table 6.6. Three groups of tests were applied on fiberglass pipe insulation without ASJ jacketing (system P1-FG, P2-FG5A and P2-FG5B), and one group was tested with the jacketing effect (P2-FG4).

Table 6.6: Specifications of test samples and ambient conditions in moisture tests

Experiment System Ref No.	**Thickness** in (mm)	**Density** lb/ft^3 (kg/m^3)	**Porosity**	**Ambient Temp** ˚F(˚C)	**Al pipe surfaces Temp** ˚F(˚C)	**RH** %
P1-FG	50.8 (2)	70 (4.4)	0.91	107.6 (42.0)	41.6 (5.33)	81
P2-FG5A	50.8 (2)	70 (4.4)	0.91	78.1 (25.6)	15.9 (4.8)	54.8
P2-FG5B	50.8 (2)	70 (3.5)	0.91	90.1 (32.3)	41.9 (5.5)	84
P2-FG4	38.1 (1.5)	56 (3.5)	0.93	78.1 (25.6)	38.4 (3.6)	54.8

Validation on the mass of water accumulated in fibrous pipe insulation

The comparison between experimental and simulation results of moisture content for three groups of test on fiberglass without ASJ jacketing are plotted in Figure 6.25a,c and e. The experimental data on the moisture content and system thermal conductivity that derived in the system P1-FG was used to generate the water retention coefficient f_3, coefficients C_1 and C_2, as shown in Equation (6.62). For the other fiberglass pipe insulation systems without vapor retarder, these three coefficients were considered as constant values and could be directly used as inputs. Based on different ambient conditions (Table 6.6), the moisture content in each pipe insulation system would reach asymptotic value differently. In the second case, which was tested on fiberglass pipe insulation system P2-FG5A, the transient conditions last for more than 200 days, and the maximum moisture content would be around 8% by volume. This is the ambient condition for system P2-FG5A was not very severe. The water vapor permeability decreases with water content at a slower rate, and it takes longer time to reach asymptotic values when compared to the other

systems. System P1-FG shows a higher value on the maximum moisture content and a faster reaction time than system P2-FG5B. It is reasonable because the ambient temperature in system P1-FG was much higher than the temperature setting in P2-FG5B, and the humidity in both cases were very similar. For system P1-FG, the fiberglass would reach maximum moisture content around 33% on the day 120; in system P2-FG5A, the fiberglass would reach maximum moisture content around 8.7% on the day 480, and in system P2-FG5B, the maximum moisture content would be around 24.2% by volume on the day 170. The variations on parameter *a* are plotted in Figure 6.25b, d and f. In all three cases, parameter *a* drops dramatically at the beginning of the moisture test due to the increase on the water vapor pressure difference between the ambient and the cold pipe surface. This humid condition promotes the formation of moisture beads on the contact points among each fiber, and this would change the heat flow paths by the presence of more thermal bridging. More thermal bridging can be considered as more parallel thermal resistances in the system, and this explains the decreasing on the parameter *a,* which represents the fraction of the poor conductive layer. Then parameter *a* continue decreases but at a much slower rate until it reaches the asymptotic values. This matches the observation during the experiments. Parameter *a* in system P1-FG dropped most in these three cases, from 0.98 to 0.61. This is compatible with the finding that system P1-FG would collect larger amount of water, and have more chances to form thermal bridging to further decrease parameter *a*. System P2-FG5B shows a higher *a* value than system P1-FG, from 0.98 to 0.75, and system P2-FG5A indicates the smallest difference between a_{dry} and a_{wet}, from 0.98 to 0.88, due to the lowest water content. All these results are summarized in Table 6.7.

Table 6.7: Simulation results on the required minimum test length, maximum moisture content and parameter a_{wet}

Experiment Systems (Ref No.)	Minimum Test Length Days	Max. Moisture Content % by volume	Coefficient f_3	Coefficient C_1	Coefficient C_2	Final a_{wet}
P1-FG	80	33.0				0.61
P2-FG5A	250	8.7	0.074	4.430E-05	0.018	0.88
P2-FG5B	100	24.2				0.75
P2-FG4	*N/A	*N/A	1	0	0.019	0.97

*: Haven't reached an asymptotic value after 1000 days.

It also needs to point out there that coefficient f_3 is much smaller than 1 due to the following two possible reasons. The first possible reason is that for fibrous pipe insulation, the water vapor permeability is measured based on the procedures issued in ASTM C1104 (2006). In order to provide a maximum value on the water transmission in the standard, the test sample is conditioned in an ambient with temperature at 120 ± 3.6˚F (49 ± 2˚C), 90% ± 3% RH for 96 ± 4 hours. Due to the fact that for fibrous insulation, the water vapor permeability is dependent on the ambient temperature, as shown in Equation (6.50), the water vapor permeability derived at such standard conditions is higher than the one in all three moisture tests reported in Table 6.4. For fibrous pipe insulation systems, I made the assumption that the water vapor permeability correction factor f_2 is equal to 1 because the temperature difference between the test condition in the standard and the ambient condition in the moisture test are smaller when compared to the closed-cell pipe insulation. However, the temperature difference might still have an impact on the insulation water vapor permeability, and the coefficient f_3 is lower than 1 due to the less severe conditions. The second reason is that according to the definition of f_3, this water retention coefficient considers the portion of water trapped in the pipe insulation. Because of the large air gaps among the fibers, more preferential paths would form in the fibrous pipe insulation and lead to a certain amount of water drip out of the system. In order to only consider the portion of water condensate trapped in the material, which is key on the variation of pipe insulation thermal conductivity, the coefficient f_3 should be less than 1. For system P2-FG5A, which was tested at a much lower temperature and humidity when compared to the other two cases, the coefficient f_3

needs to be corrected from 0.074 to 0.04 to get a better match between the simulation and experimental results, as shown in Figure 6.25c. This finding indicates two aspects that need to be further studied: 1) the water vapor permeability might still be affected by the ambient conditions, and the sensitivity depends on material internal structure and physical properties; 2) water dripping rate (out of the insulation) is restricted with surface tension, material density, water concentration, etc., and need a further investigation.

System P2-FG4 was applied on fiberglass pipe insulation with ASJ jacketing. Due to the presence of ASJ jacketing, the entire water vapor permeability is very low in the pipe insulation systems, and the value is in the same order as the closed-cell pipe insulation. Therefore, the coefficient f_3 was set at 1, and C_1, which is depended on the surface water vapor permeability, was input as 0. Since the pipe insulation is still fiberglass, the coefficient C_2, which only depends on insulation materials, is remained the same as the values applied in the other three systems. The simulation results on the moisture content and parameter *a* is plotted in Figure 6.25g and f. Comparing to the experimental result, which has only one point at day 55, the simulation curve matches with the point within an acceptable range. Parameter *a* remains almost the same value as the one in the dry condition after 1000 days of the moisture test.

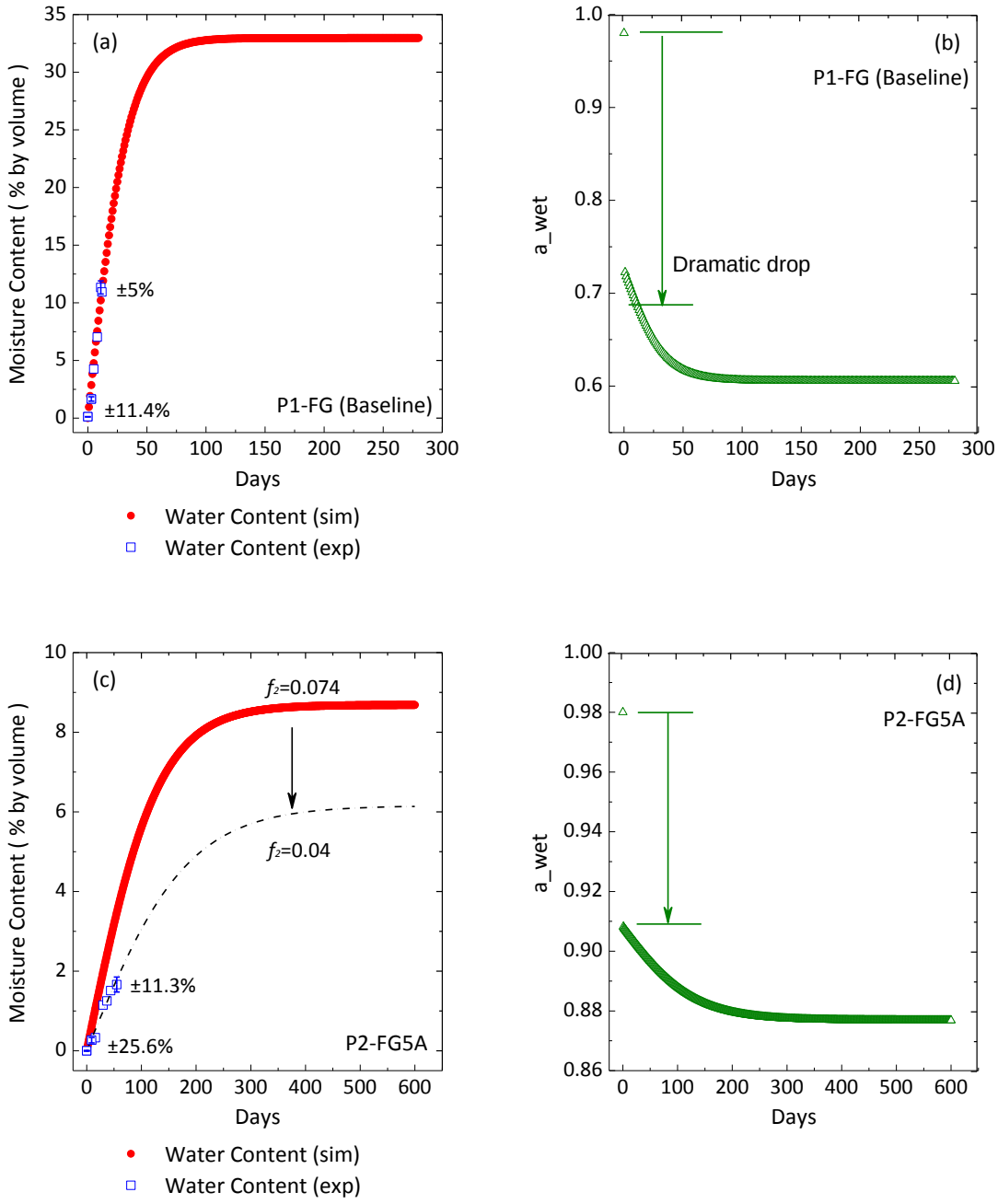

Figure 6.25: Comparison between experimental and simulation results on moisture content and the prediction of parameter a_{wet}

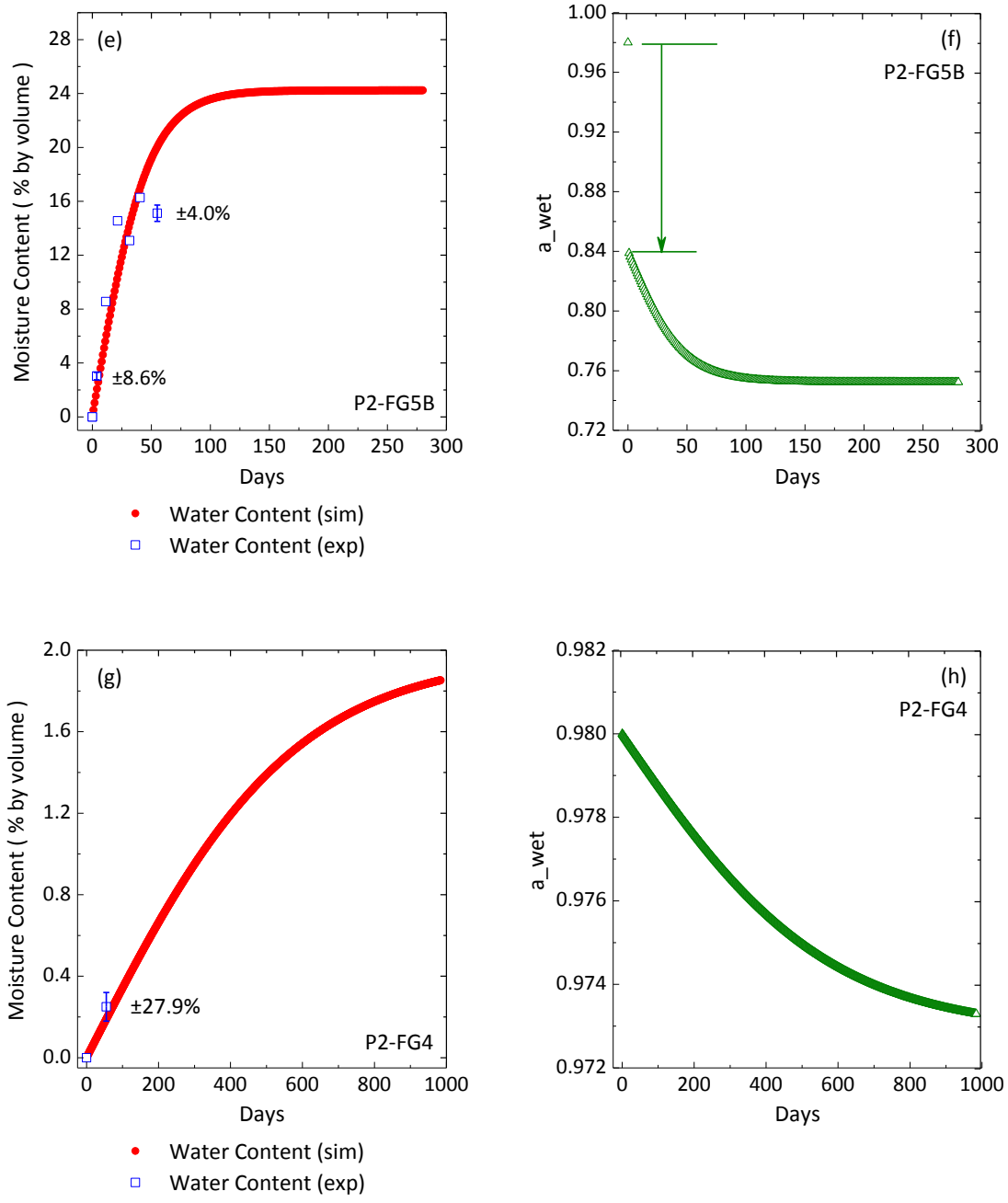

Figure 6.25 (Continued): Comparison between experimental and simulation results on moisture content and the prediction of parameter a_{wet}

Validation on the thermal conductivity of fibrous pipe insulation with moisture content

With the profiles of moisture and parameter *a* derived from previous section, the thermal conductivity of moist fiberglass pipe insulation could be predicted with water content and with time. It should be noted that from current model, the moisture profile would only be available on the total water content in the fiberglass pipe insulation system without considering the moisture difference between the top and bottom C-shells. In order to take into account for these differences, the ratio of the mass in the top shell to the total moisture in the test sample was estimated from each test. By considering the same ratio in the simulation, the moisture profile was then divided to two groups of inputs, one for the moisture content in the top shell and one for the bottom. The simulation results on the variation of thermal conductivity with moisture content and with time for four fiberglass pipe insulation systems are plotted in Figure 6.26a, c, e and g, with the values.

For systems P1-FG, P2-FG5A, and P2-FG5B, which were fiberglass pipe insulation without jacketing, the thermal conductivity ratio increased fast due to a dramatic drop on the value of parameter *a*, and parameter *a* was very sensitive to the water vapor pressure differences between the ambient and the cold pipe surface. Then the thermal conductivity ratio kept increasing but at a much slower rate. As explained in the previous section, the dramatic increase was due to the formation of more thermal bridging that changed the direction of the thermal paths; a slower increasing in the second step was caused by the large amount of high conductive liquid phase that introduced into the system. Similar to the profiles of moisture content and parameter *a*, the thermal conductivity would also reach an asymptotic value, and the pipe insulation system could be considered as saturated under such test conditions. These simulation results on the thermal conductivity ratio are also compared to the experimental values. For all three cases, the thermal conductivity ratio matched with the experimental results within 15%. The thermal conductivity ratio in system P1-FG would increase most. By the time the insulation system becomes saturated,

the system thermal conductivity would increase upto 5.5 times of the dry reference value. System P2-FG5A would increase by 1.8 times of the dry reference value when it reaches maximum moisture content. In system P2-FG5B, the final thermal conductivity ratio was predicted to be around 3.6 by the time the insulation system being saturated. It should be noted that two groups of dry reference values were considered in Figure 6.26f. One group was developed from the mapping test based on the test pipe surface temperature, as shown by the hollow diamond symbols. The other group of the dry reference data was derived from the correlation that developed under dry condition, and the values of the thermal conductivity ratio were shown by the solid symbols. Because the simulated thermal conductivity ratio was derived from the latter group of the dry reference data, by considering the latter group, the difference between the simulation and the experimental values was decreased to within 15%. Detailed simulation results on thermal conductivity ratio, moisture content and time are documented in Appendix Table E-7 to 9.

Figure 6.26g and h shows the results in the pipe insulation system P2-FG4 with ASJ jacketing. From the plots, it indicates that the thermal conductivity ratio changes slowly with moisture content and with time by increasing less than 10% in almost three years. The only point derived from the experiment was measured at the end of the moisture test, on the 55^{th} day, and this value matched with the simulation results within 15%. The thermal conductivity ratio was less than 1 and the explanation is as follows. During the moisture test, the initial value of parameter *a* should be the same as the one used in the dry model. In the dry model, parameter *a* was determined from one specific case and this value was assumed to be constant in all the other systems with the same pipe insulation. During this step, a systematic error will be included in the simulation results under both dry and wet conditions. Detailed simulation results in system P2-FG4 is documented in Appendix Table E-10.

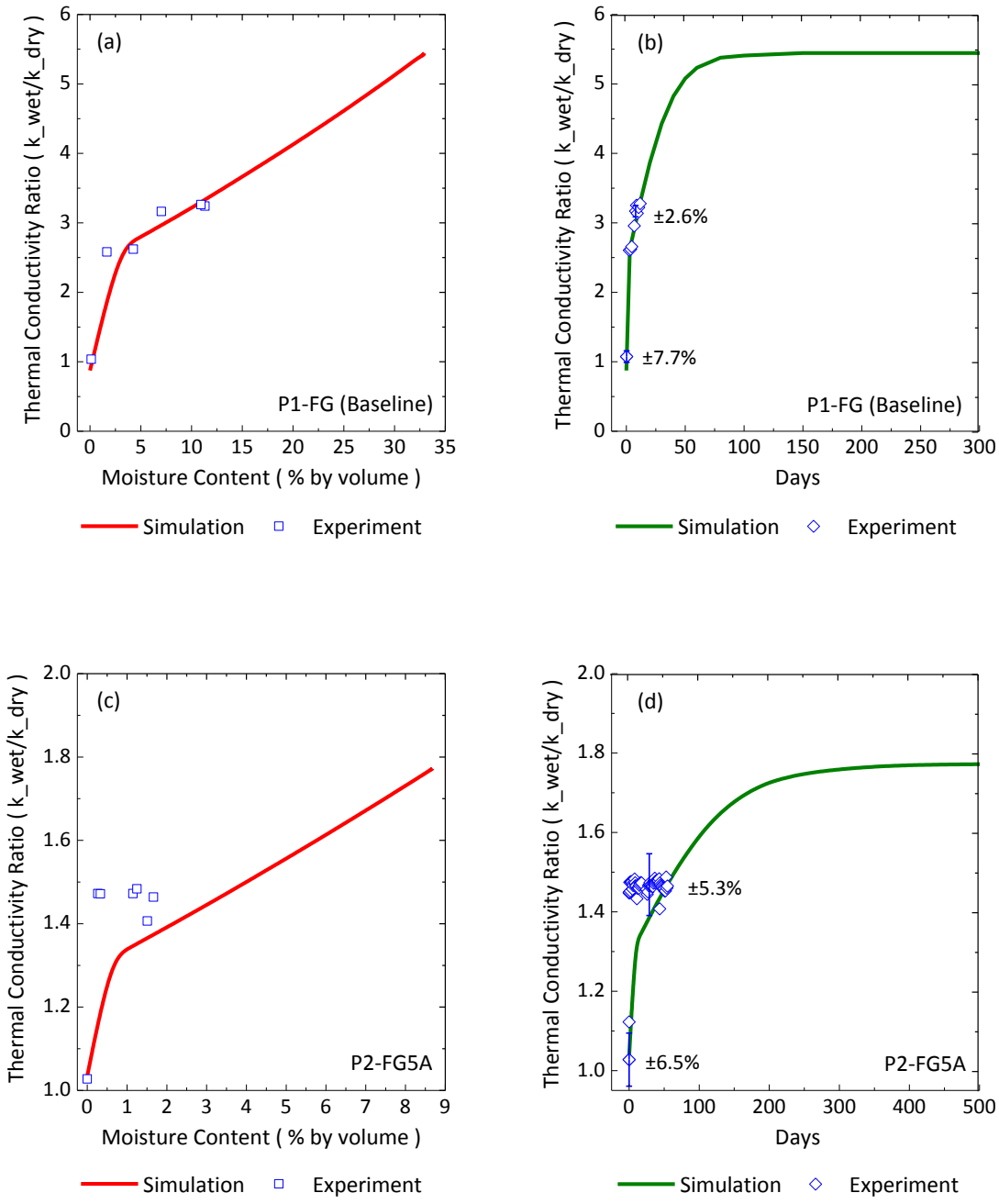

Figure 6.26: Comparison between experimental and simulation results on the thermal conductivity ratio between dry and wet fiberglass pipe insulation

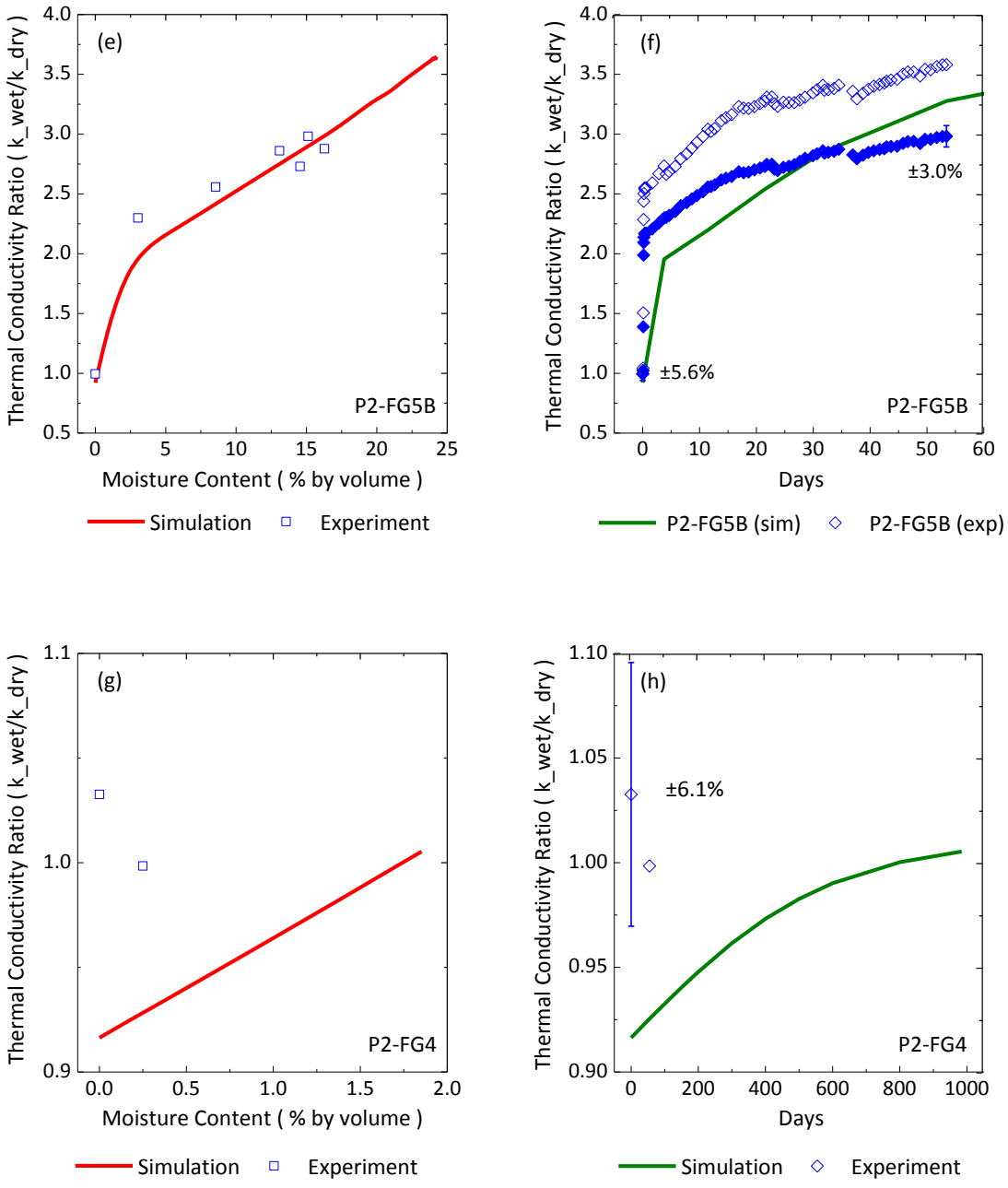

Figure 6.26 (Continued): Comparison between experimental and simulation results on the thermal conductivity ratio between dry and wet fiberglass pipe insulation

6.8.3 Validation with the results reported in the current literature

The model was also validated by the values from the literature on both fibrous and closed-cell insulation. Due to the fact that the data on the pipe insulation systems was very limited, the model was compared to the literature values on the flat slabs.

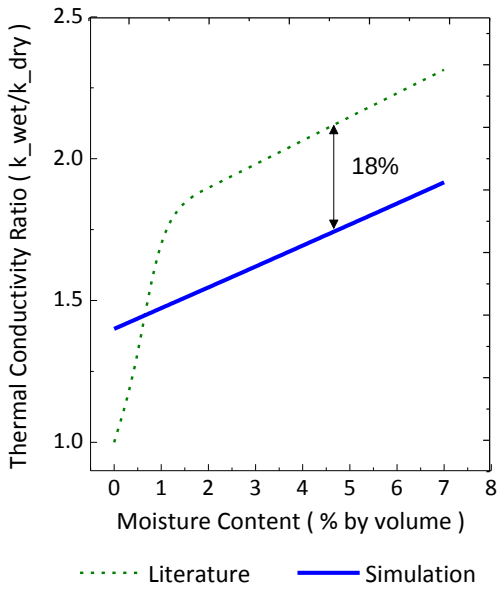

Figure 6.27: Model validation with the literature values on PIR insulation

Figure 6.27 shows the comparison on the thermal conductivity ratio with moisture content in the closed-cell pipe insulation systems. The literature values were derived from McFadden's (1988) previous work on the thermal conductivity measurement of polyurethane and polyisocyanurate foam insulation. In the simulation, the parameter *a* was assumed to be the same as the value derived from previous study on the PIR pipe insulation under dry condition. Considering the fact that no joint sealant was applied on the foam insulation, the thickness of joint sealant was input as zero in the model. The other inputs were provided in Table 6.8. Results showed that the differences between the simulation results and the literature values were within 18%. Because in the current model, it was assumed that there were no preferential paths in the closed-cell pipe insulation system, the thermal conductivity ratio increased gradually with moisture content in the

system. However, McFadden's experiment observed a slightly increase at the beginning of the test, and he proposed a two-step approach with different correlations applied when the moisture content was less than 1% by volume. The comparison results were demonstrated in Figure 6.27, and the correlations between system apparent thermal conductivity and moisture content were shown in Table 6.8.

Table 6.8: Input parameters to the simulation model in PIR insulation

	Unit	Literature (McFadden, 1988)	Simulation
Insulation system	-	PUR/PIR foam	PIR pipe insulation
Insulation mean temperature	℉ (℃)	-	59. 4 ℉ (15.2 ℃)
Thickness	in (mm)	-	1 (25.4)
Density	lbm/ft^3 (kg/m^3)	-	1.8 (29)
Parameter *a*	-	-	0.7503
Thermal conductivity	Btu-in/hr-ft^3-F	[1] $k = k_0+0.085(\%M)$ ($0 < \%M < 0.5\%$) [1] $k = 0.27+0.013(\%M)$ ($1\% < \%M < 7\%$)	[1] $k = 0.2191+0.0118(\%M)$ ($\%M < 7\%$)

[1]: The function of thermal conductivity (k) is given in IP units, and the moisture content ($\%M$) is the percentage of water by volume.

The model was further validated with fiberglass foam insulation, and the simulation results were compared to two sets of data reported in the literature.

McFadden's (1988) derived a two-step approach to predict the thermal conductivity with moisture content in the fiberglass batt. Based on the reported thermal conductivity of the fiberglass batt under dry condition, the physical properties of the test sample were calculated back in the pipe insulation model, and the values for the input parameters to the simulation model was documented in Table 6.9. The comparison results were shown in Figure 6.28 and Table 6.9. Different from the experimental results in the literature, the simulation showed that the thermal conductivity of fiberglass pipe insulation increased fast when the moisture content was lower than 1% by volume, while the literature values showed a dramatic increase with the moisture content around 2% by volume. In the second step, the simulation results were 11% higher than the

reported values in the literature. This is probably due to the fact that the preferential paths are formed faster and more in pipe insulation systems than the flat slabs because of the gravity effect.

Table 6.9: Input parameters to the simulation model in fiberglass insulation (case 1)

	Unit	Literature (McFadden, 1988)	Simulation
Insulation system	-	Fiberglass batt	Fiberglass pipe insulation
Insulation mean temperature	℉ (℃)	-	59. 4 ℉ (15.2 ℃)
Thickness	in (mm)	-	3 ½ (88.9)
Density	lbm/ft^3 (kg/m^3)	-	6.24 (100)
Parameter *a*	-	-	a = -0.2684(%M) + 0.98 (%M < 1%) a = -0.0036(%M) + 0.725 (%M ≥ 1%)
Thermal conductivity	Btu-in/hr-ft^3-F	$^1k = k_0$+0.03(%M) (0 < %M < 2%) ^1k = 0.73+0.024(%M) (3% < %M < 8%)	$^1k = k_0$+0.628(%M) (%M < 1%) ^1k = 0.822+0.025(%M) (1% < %M < 8%)

[1]: The function of thermal conductivity (k) is given in IP units, and the moisture content (%M) is the percentage of water by volume.

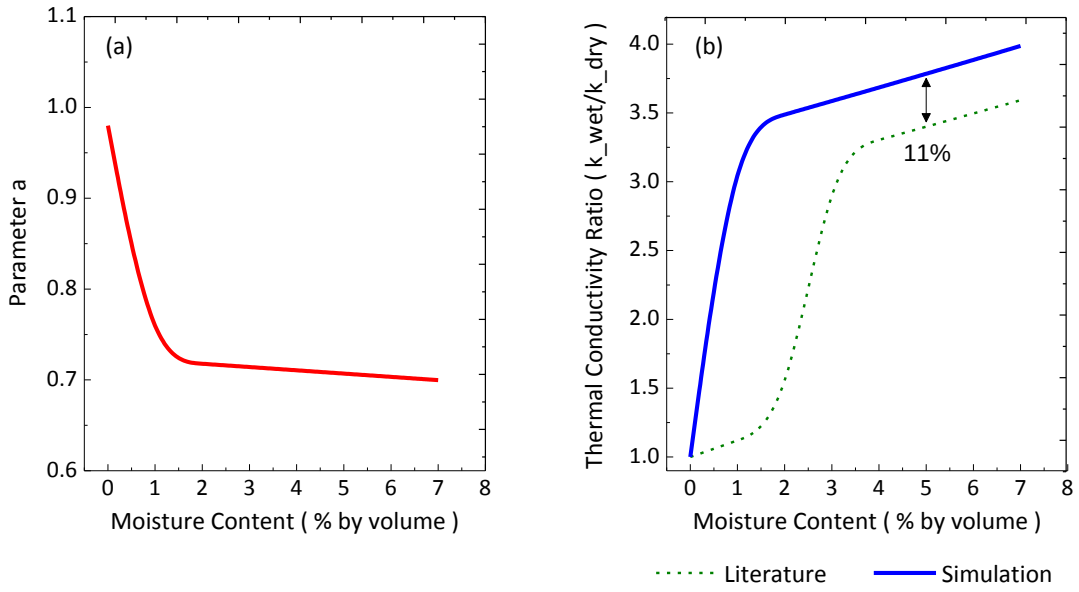

Figure 6.28: Model validation with the literature values on fiberglass insulation: (a) The profile of parameter a; (b) Comparison on the thermal conductivity ratio with moisture content (McFadden, 1988)

The second group of literature data was selected from Abdou and Budaiwa's (2013) work. The input parameters were provided in Table 6.10. Considering the fact that the test sample was prepared by conditioning in a container with high humidity, and then measured at room temperature, the parameter *a* was estimated by assuming the water vapor pressure difference to be zero, as shown in Equation (6.62). Without the pressure difference across the insulation, the parameter *a* gradually decreased with moisture accumulation, as indicated in Figure 6.29a. With this profile of parameter *a*, the computed thermal conductivity was plotted as the solid line shown in Figure 6.29b, and the difference between the simulation results and the reported data were within 10%.

Table 6.10: Input parameters to the simulation model in fiberglass insulation (case 2)

	Unit	Literature (Abdou & Budaiwi, 2013)	Simulation
Insulation system	-	Fiberglass foam	Fiberglass pipe insulation
Insulation mean temperature	℉ (℃)	61.7 ℉ (16.5 ℃)	61.7 ℉ (16.5 ℃)
Thickness	in (mm)	2 (50.8)	2 (50.8)
Density	lbm/ft^3 (kg/m^3)	5.24 (84)	5.24 (84)
Parameter *a*	-	-	$a = -0.0036(\%M) + 0.98$ (%M < 1%)
Thermal conductivity	Btu-in/hr-ft^3-F	[1] $k = 0.0001(\%MC)+0.0327$	[2] $k = 0.0018(\%M)+0.035$

[1]: The function of thermal conductivity (k) is given in SI units, and the moisture content (%MC) is the percentage of water by **weight**.
[2]: The function of thermal conductivity (k) is given in SI units, and the moisture content (%M) is the percentage of water by **volume**.

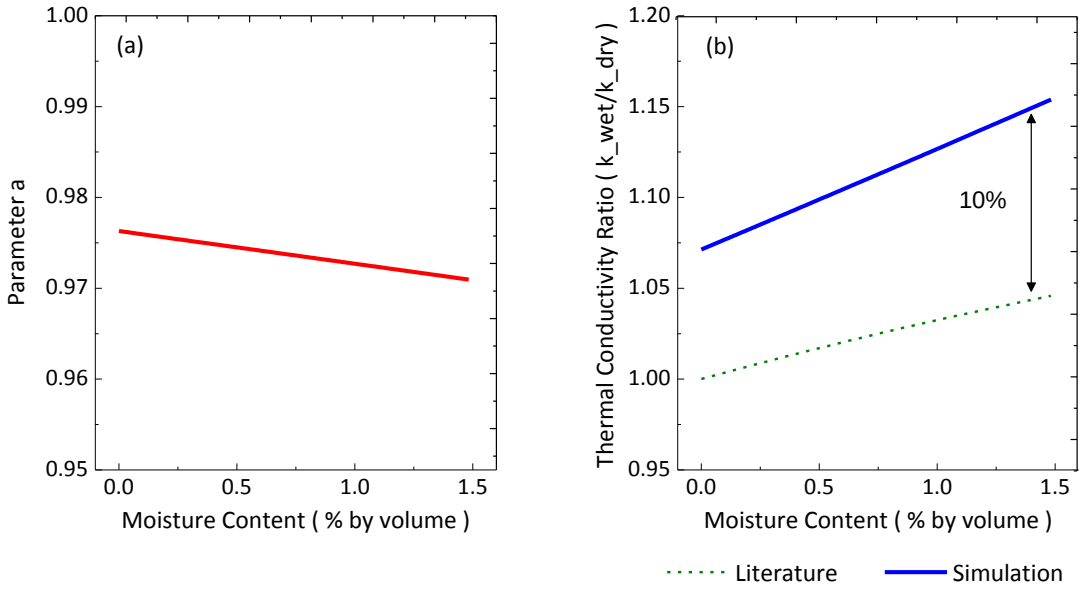

Figure 6.29: Model validation with the literature values on fiberglass insulation: (a) The profile of parameter a; (b) Comparison on the thermal conductivity ratio with moisture content (Abdou & Budaiwi, 2013)

6.8.4 Sensitivity analysis on the coefficients

A sensitivity analysis was conducted to investigate the impact of parameters f_1, f_2, f_3, C_1 and C_2 based on the experimental results. The coefficients f_1, f_2, and f_3 were applied for the profile of moisture accumulation, and each of them would weigh the same on the final results. A coefficient f, which was defined as a product of f_1, f_2 and f_3 was considered in the sensitivity analysis. Figure 6.30a indicated the differences between the experimental and simulation results when each coefficient varied by ±10%. In this case, the coefficient f was varied between -27.1% to 33.1%. Compared to the experimental results, the differences were within ±20%. The impact of each coefficient was indicated in Figure 6.30b, and the sensitivity study was based on coefficient f_1. By varying the coefficient f_1 by ±10%, the computed moisture accumulation would match with the experimental results and the deviation was around ±10%.

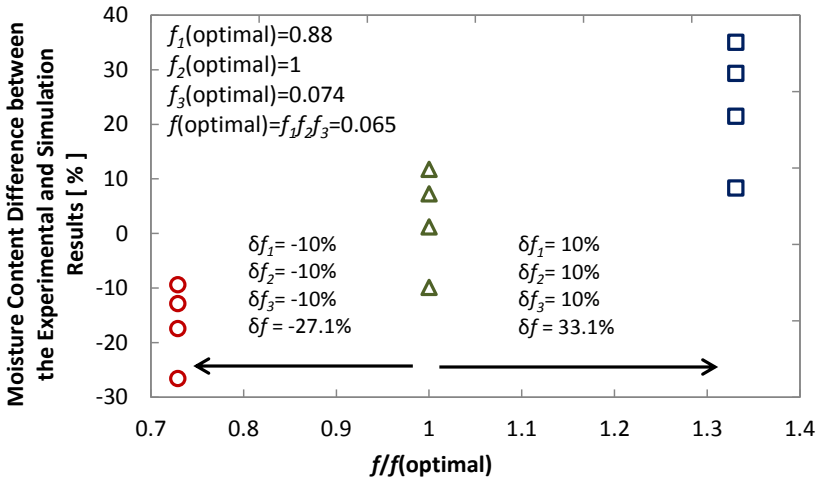

(a)

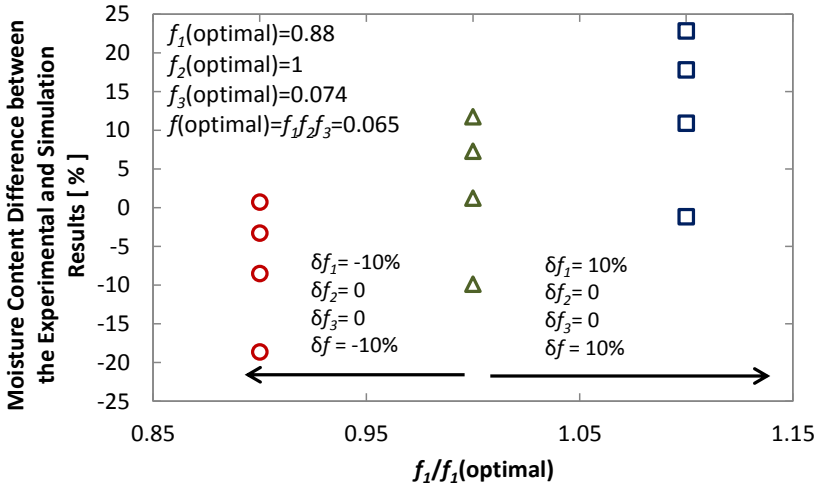

(b)

Figure 6.30: Sensitivity study of varying the coefficients f_1, f_2 and f_3 on the simulation of the moisture content in the pipe insulation systems: (a) the impact of the combined coefficient f ($f=f_1f_2f_3$); (b) the impact of each coefficient

Parameter C_1 and C_2 were used to determine parameter a, which was a key parameter for the system apparent thermal conducivity. The sensitivity study on parameters C_1 and C_2 was based on the experiemtnal results of fiberglass pipe insulation system P1-FG. The results were shown in

Figure 6.31 and Figure 6.32. Each symbol reprsents one group of data. As described in previous sections, parameter C_1 represents the impact of water vapor pressure on the value of parameter *a*. By varying C_1 of ±20%, the average difference on parameter *a* betweeen the experimental and simulation results were around ±7%.

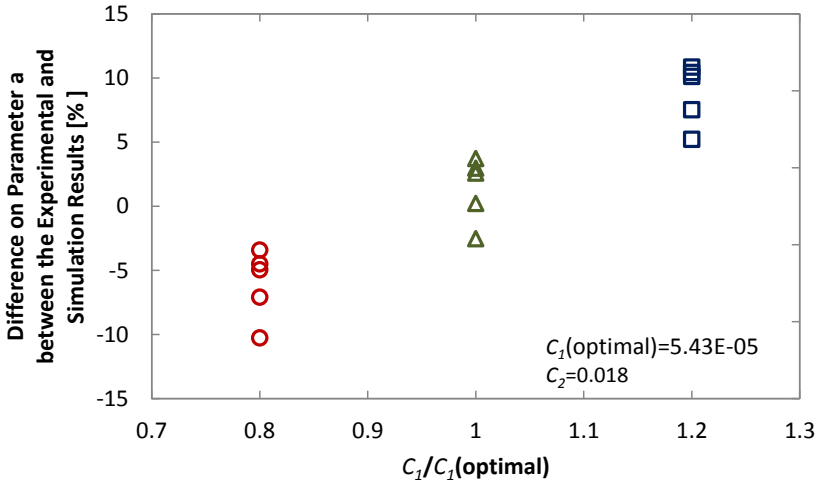

Figure 6.31: Sensitivity study of varying the parameter C_1 on the simulation of the parameter a in the pipe insulation systems

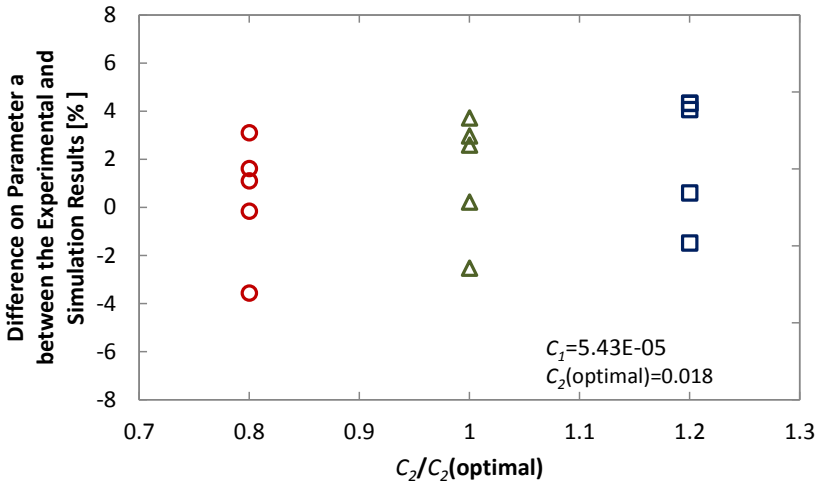

Figure 6.32: Sensitivity study of varying the parameter C_2 on the simulation of the parameter a in the pipe insulation systems

Parameter C_2 was defined to estimate the impact of moisture content on the value of parameter *a*. Compared to C_1, C_2 was not a sensitive factor to parameter *a*. With a ±20% variation on C_2, the difference on parameter *a* was only ±1%, as shown in Figure 6.32.

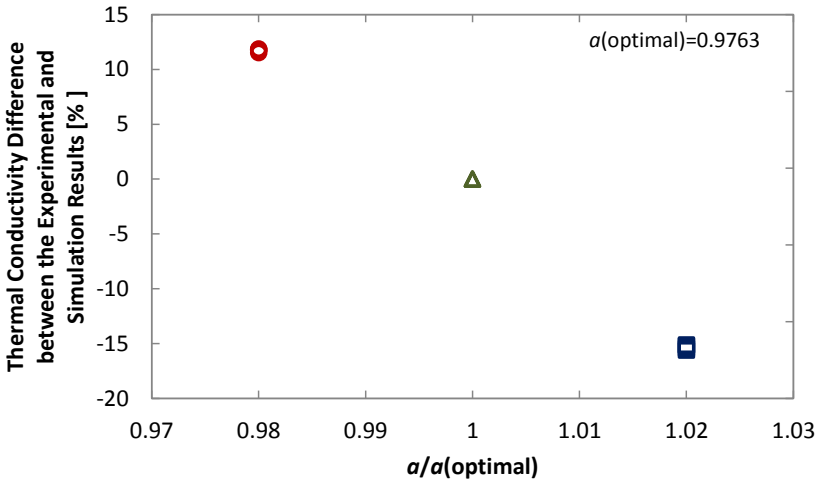

Figure 6.33: Sensitivity study of varying the parameter a on the thermal conductivity in the pipe insulation systems

As mentioned in previous sections, parameter *a* is a key factor on the apparent thermal conductivity of pipe insulation systems. The results of sensitivity study were shown in Figure 6.33. Results showed that the apparent thermal conductivity behaves very sensitive to the values of parameter *a*. A 2% variation on the parameter *a* would lead to a 15% difference on the final results of apparent thermal conductivity.

CHAPTER VII

7. CONLCUSIONS AND RECOMMENDATIONS

7.1 Conclusions on the current work

The main objective of this research was to investigate the effects of water vapor ingress on the thermal conductivity of pipe insulation systems. This thesis describes the work I conducted on this topic and the main findings from my research. The phenomenon of water vapor ingress in pipe insulation systems is a complex heat and mass transfer process with numerous variables that have to be considered. An objective of my Ph.D. research project was to develop a model for predicting the thermal performance of pipe insulation systems that are commonly used for indoor building space conditioning. The experimental validation of my model required to develop a new methodology to measure the thermal conductivity of pipe insulation system under wet operating conditions with water vapor moisture ingress. This is an interesting heat and mass transfer problem that the researchers have spent limited, if any, resources investigating. I believe this research is important, especially to the building space conditioning service because pipe insulation systems could lead to tremendous energy savings when properly designed, installed, and maintained. With my thesis, I believe I addressed all three aspects at some degree of closure.

Since the thesis is mainly divided in three stages, a conclusion for each stage of my research is summarized next.

Step 1 was to conduct a critical literate review to clarify the similarities and differences on the apparent thermal conductivity between pipe insulation systems and flat slabs. I started this review

by comparing different experimental methodologies for measuring the apparent thermal conductivity of pipe insulation and flat slab systems. Both transient and steady-state methodologies are proposed for the thermal conductivity measurement. Although the steady state methods have some disadvantages, such as , need a considerable amount of time to reach thermal equilibrium, large test sample size to eliminate edge effect, and a limited temperature range to prevent radiation, it is considered as an appropriate method for measuring the system apparent thermal conductivity. It is simpler and provides a more direct measurement than transient methods. Transient method can provide a fast measurement on the local thermal conductivity, but to determine a system behavior, this method is strongly depended on the number and locations of the probing sensors. The accuracy and repeatability of transient methods for pipe insulation systems are also not as well defined as steady-state methodologies. Therefore, a steady-state method was selected for the following experiments in this thesis. Under wet condition, different techniques are required during thermal conductivity measurement depending on how the test samples being prepared in the laboratory. Based on the current literature, I summarized four moisturizing strategies as flooded method, spray/injection method, laboratory pre-conditioning method, and conditioned ambience with cold surface/pipe method. It is concluded that only the last moisturizing strategy would provide similar boundary conditions as in the actual field. This technique can be combined with steady state methodologies to determine the system apparent thermal conductivity without the water redistribution impact. However, it should be noted that this technique requires a large investment for the equipment and control of the ambient conditions. A more compact test apparatus, or a novel technique that would solve current challenges, such as the non-uniform surface temperatures, and moisture redistribution in radial configuration, is required for further study. From the literature review, the methodology selected for the following tests is a radial heat flow meter with temperature and humidity controlled in a psychrometric chamber.

During the second stage of my research, a novel experimental apparatus, referred in this dissertation as pipe insulation tester, or PIT, was developed for the system thermal conductivity measurement. Pipe insulation systems were installed around the test pipe of these PITs. The test pipe surface temperature was maintained by a refrigeration system. The radial heat flux was calculated by surface temperature measurements on the inner refrigeration tubing and on the test pipe. The test apparatus kept improving based on what I learned from the experiments, and the current test apparatus was able to measure a low heat flux of about 8.2 Btu/hr-ft (7.9 W/m) with an uncertainty at ±5.7%. Up to now, seven fibrous and nine closed-cell pipe insulation systems were tested on the PITs under dry condition. The ambient temperature was controlled between 75 to 110 ℉ (~23.8 to 43.3 ℃), with the insulation mean temperature varied from 55 to 73 ℉ (~12.8 to 22.8 ℃). For both fibrous and closed-cell pipe insulation systems, the apparent thermal conductivity varies almost linearly with the insulation mean temperature. I also observed that the joint sealant seems to be a significant impact for the system thermal performance, and the presence of the joint sealant may increase the system apparent thermal conductivity by 15%. All the detailed information, including material properties and installation, are documented in Table 5.13. Four fibrous and six closed-cell pipe insulation systems were tested under wet, condensing conditions with moisture ingress. The ambient condition was set as a hot and humid environment to accelerate moisture ingress in the pipe insulation systems. In most cases, the temperature was controlled from 90 to 110 ℉ (32 to 43 ℃), with relative humidity between 81 to 84%. According to the observation during the experiment, I summarized the water diffusion mechanism and moisture impact on the system performance for both fibrous and closed-cell pipe insulation. In fibrous pipe insulation systems, moisture diffuses through the preferential paths and the system behaves fairly sensitive to the ambient at the beginning of the moisture test. This is because under condensing conditions, moisture bead would start forming at the contact point between each fiber and change the thermal path by creating more thermal bridging in the insulation systems. The thermal conductivity would increase dramatically during this process, even with a small amount

of water in the system. Closed-cell pipe insulation systems are less affected by the moisture during the initial stage. This is due to the enclosure structure of the cells in the material would have less possibility to form thermal bridging and the preferential paths. Moisture will diffuse gradually from the internal surface outward. These two mechanisms are important and would be used as the basic theory for model development. All the information regarding to the material installation, ambient conditions and test results under wet conditions are documented in detail in Table 5.14.

Based on the conclusions from the experiments, a semi-empirical analytical model was developed to predict the system thermal conductivity with different ambient conditions and with time. Considering the similarities between fibrous and closed-cell pipe insulation systems, a general model was developed for both cases. This model considered the insulation system as a combination of solid phase, gas phase and liquid phase in different configurations. A parameter, *a*, was introduced to represent the portion of each configuration, which would have a significant impact on the system thermal conductivity. This parameter *a* was assumed to be constant among the same type of insulation materials. For closed-cell pipe insulation systems, parameter *a* would remain constant between dry and wet conditions due to a steady variation observed on the system performance. For fibrous pipe insulation systems, parameter *a* was not a constant value with the presence of moisture, and this parameter was further correlated with the ambient condition and the moisture content in the system. Under wet conditions, parameter *a* would decrease by following a two-step variation, and gradually approach an asymptotic value. The system thermal conductivity would also reach a maximum when parameter *a* become stabilized. This model was validated with both experimental data and the reported values from the open domain literature. For closed-cell pipe insulation systems, the moisture profile with time need to be further investigated. The thermal conductivity ratio could be predicted with moisture content, and the difference between the simulation and experimental results were within 10%. For fibrous pipe

insulation systems, both moisture profile and thermal conductivity ratio with moisture content and with time matched well with the experimental results. The differences were within 15%.

7.2 Recommendations for future work

The following recommendations are mainly on the modelling part.

In the current model, coefficients f_1, f_2 and f_3 are used to generate moisture profiles. The method used for the determination of these three factors can be better improved in the future work. The coefficient f_1 is the condensation coefficient that represents the volume ratio of the region with temperature lower than the dew point to the total volume. In the current model, this coefficient was derived based on a 2-d steady-state conduction heat transfer equation, with a boundary condition from the beginning of the test. This value was assumed to be constant during the moisture test. However, this assumption is weak because the boundary condition keeps changing and the condensation region varies during the wet period. A detailed temperature distribution profile may help updating the condensation region, and the coefficient f_1. Functioned as a correction factor on the water vapor permeability, f_2 is an important coefficient since the water vapor permeability is a key parameter to predict the water content that accumulated in the insulation. According to the literature, it will be varied with ambient temperature and material porosity. However, currently I haven't found enough information to correlate the water vapor permeability with ambient temperature and material porosity for different types of pipe insulation systems. Either a deeper research in the literature, or another group of test on the same pipe insulation system, may help determine this correlation. By adding one additional group of test will help back out the parameter that is required in the current correlation between water vapor permeability and the ambient temperature. Coefficient f_3 is the water retention coefficient that represents the portion of the water condensate remains trapped in the insulation system. One additional step in the experiment may do some help in the determination of this coefficient. For

example, we can collect all the condensate that drips out from the insulation, and compare to the amount water trapped in the insulation system. This simple procedure will help us have a better understand on how this coefficient changes with time and with the total moisture content. Moisture redistribution is another important factor that need to be further considered in the model. Especially for fibrous pipe insulation systems, the moisture distributions in the top and bottom shells are different and it may lead to different internal structures that would be referred to in the model.

Parameter *a* is a factor that cannot be physically measured, and it was assumed to vary linearly with water vapor pressure difference across the insulation and the moisture content trapped in the insulation system. The only way validate this theory is from more experimental data on the moisture test under different ambient conditions.

Joint sealant seems to be an important factor to the thermal behavior of pipe insulation systems under both dry and wet conditions. Under dry condition, the high conductive layer would increase the system apparent thermal conductivity, and under wet condition, the high water vapor permeability might impact on the total water content in the insulation system. The high conductive layer also caused water accumulation on the joint sealant surface, and this may effect both temperate and moisture distribution in the pipe insulation systems. A parallel study on the joint sealant would be very helpful on the future research of pipe insulation systems.

At last, it should be noted that all the conclusions derived from both moisture test and simulation models are only considered the pipe insulation systems applied in the horizontal direction. For vertically installed pipe insulation systems, the findings that derived from the horizontal tests might still be applicable if it is under dry condition, but with the presence of moisture in the system, the results might be quite different due to the effect of gravity.

REFERENCES

Abdou, A., & Budaiwi, I. (2013). The variation of thermal conductivity of fibrous insulation materials under different levels of moisture content. *Construction and Building Materials, 43*, 533-544. doi: 10.1016/j.conbuildmat.2013.02.058

Abdou, A. A., & Budaiwi, I. M. (2005). Comparison of thermal conductivity measurements of building insulation materials under various operating temperatures. *Journal of Building Physics, 29*(2), 171-184.

Adams, L. (1974). Thermal conductivity of wet insulations. *ASHRAE Journal, 16*(10), 61-62.

Adl-Zarrabi, B. (2005). Determination of thermal conductivity: The IPS method for determining of insulation of pipes. *Euroheat and Power (English Edition)*(2), 40-42.

Al-Hammad, A.-M., Abdelrahman, M. A., Grondzik, W., & Hawari, A. (1994). Comparison between actual and published k-values for Saudi insulation materials. *Journal of Thermal Insulation and Building Envelopes, 17*, 378-385.

Albers, M. A. (2002). *A round robin interlaboratory comparison of thermal conductivity testing using the guarded hot plate up to 1000C*, Charleston, SC, USA.

ASTM C 585 - 09, Standard Practice for Inner and Outer Diameters of Thermal Insulation for Normal Sizes of Pipe and Tubing. (2009). ASTM International, West Conshohocken, PA. doi: 10.1520/C0585-10.

ASTM C518 - 10 Standard Test Method for Steady-State Thermal Transmission Properties by Means of the Heat Flow Meter Apparatus. (2010). ASTM International, West Conshohocken, PA. doi: 10.1520/C0518-10.

ASTM Standard C177-10. (2010). Standard test method for steady-state heat flux measurements and thermal transmission properties by means of the guarded-hot-plate apparatus, ASTM International, Philadelphia. doi: 10.1520/C0177-10.

ASTM Standard C209-07a. (2007). Standard Test Methods for Cellulosic Fiber Insulating Boar, ASTM International, Philadelphia. doi: 10.1520/C0209-07A.

ASTM Standard C272-01. (2007). Standard Test Method for Water Absorption of Core Materials for Structural Sandwich Construction, ASTM International, Philadelphia. doi: 10.1520/C0272-01R07.

ASTM Standard C335-05. (2005). Standard test bethod for steady-state heat transfer properties of pipe insulation, ASTM International, Philadelphia. doi: 10.1520/C0335-05.

ASTM Standard C518-10. (2010). Standard test method for steady-state thermal transmission properties by means of the heat flow meter apparatus, ASTM International, Philadelphia. doi: 10.1520/C0518-10.

ASTM Standard C552-12b. (2012). Standard Specification for Cellular Glass Thermal Insulation, ASTM International, Philadelphia. doi: 10.1520/C0552-12B.

ASTM Standard C1104/C1104M-00. (2006). Standard Test Method for Determining the Water Vapor Sorption of Unfaced Mineral Fiber Insulation, ASTM International, Philadelphia. doi: 10.1520/C1104_C1104M-00R06.

ASTM Standard C1114. (2006). Standard test method for steady-state thermal transmission properties by means of the thin-heater apparatus, ASTM International, Philadelphia. doi: 10.1520/C1114-06.

ASTM Standard C1126-04. (2009). Faced or unfaced rigid cellular phenolic thermal insulation, ASTM Interational, Pheladelphia. doi: 10.1520/C1126.

ASTM Standard C1363-11. (2011). Standard test method for thermal performance of building materials and envolop assemblies by means of a hot box apparatus, ASTM International, Philadelphia. doi: 10.1520/C1363-11.

Batty, W. J., O'Callaghan, P. W., & Probert, S. D. (1981). Apparent thermal conductivity of glass-fiber insulant: effects of compression and moisture content. *Applied energy, 9*(1), 55-76. doi: 10.1016/0306-2619(81)90042-8.

Batty, W. J., Probert, S. D., Ball, M., & O'Callaghan, P. W. (1984). Use of the thermal - probe technique for the measurement of the apparent thermal conductivities of moist materials. *Applied energy, 18*(4), 301-317.

Benner, S. M., & Modi, D. K. (1986). Moisture gain of spray - applied insulations and its effect on effective thermal conductivity - Part II. *Journal of thermal insulation, 9*, 211-223.

Bezjak, M., & Zvizdic, D. (2011). Dynamic measurements of the thermal conductivity of insulators. *International Journal of Thermophysics, 32*(7-8), 1467-1478. doi: 10.1007/s10765-011-1025-8.

Bhattacharjee, D., King, J. A., & Whitehead, K. N. (1991). Thermal conductivity of PU/PIR foams as a function of mean temperature. *Journal of Cellular Plastics, 27*(3), 240-251.

Biedermann, A., Kudoke, C., Merten, A., Minogue, E., Rotermund, U., Ebert, H. P., Heinemann, U., Fricke, J., & Seifert, H. (2001). Analysis of heat transfer mechanisms in polyurethane rigid foam. *Journal of Cellular Plastics, 37*(6), 467-483. doi: 10.1106/kemu-lh63-v9h2-kfa3

BS-EN 253. (2009). District heating pipes - Preinsulated bounded pipe systems for directly buried hot water networks - pipe assembly of steel service pipe, polyurethan thermal insulation and outer casing of polyethylene, British-Adopted European Standard.

BS-EN 12667. (2001). Thermal Resistance of Building Materials and Products - Determination of Thermal Resistance by Means of Guarded Hot Plate and Heat Flow Meter Methods - Products of High and Meduum Resistance, British-Adopted European Standard.

Budaiwi, I., Abdou, A., & Al-Homoud, M. (2002). Variations of thermal conductivity of insulation materials under different operating temperatures: Impact on envelope-induced cooling load. *Journal of Architectural Engineering, 8*(4), 125-132.

Chalumeau, A., & Felix-Henry, A. (2006). *Water absorption effect on syntactic foam thermal insulation of a flexible pipe*, Hamburg, Germany.

Christian, J. E., Desjarlais, A., Graves, R., & Smith, T. L. (1998). Five-year field study confirms accelerated thermal aging method for polyisocyanurate insulation. *Journal of Cellular Plastics, 34*(1), 39-64.

Chyu, M.-C., Zeng, X., & Ye, L. (1997a). *Effect of moisture content on the performance of polyurethane insulation used on a district heating and cooling pipe*, Philadelphia, PA, USA.

Chyu, M.-C., Zeng, X., & Ye, L. (1997b). *Performance of fibrous glass pipe insulation subjected to underground water attack*, Philadelphia, PA, USA.

Cremaschi, L., Cai, S., Ghajar, A., & Worthington, K. (2012a). ASHRAE RP 1356 final report: Methodology to measure thermal performance of pipe insulation at below ambient temperatures: ASHRAE, available by request to ASHRAE.

Cremaschi, L., Cai, S., Worthington, K., & Ghajar, A. (2012b). *Measurement of pipe insulation thermal conductivity at below ambient temperatures Part I: Experimental methodology and dry tests (ASHRAE RP-1356)*. Paper presented at the ASHRAE winter conference - Technical papers, January 21, 2012 - January 25, 2012, Chicago, IL, USA.

Eriksson, D., & Sunden, B. (1998). Heat and mass transfer in polyurethane insulated district cooling and heating pipes. *Journal of Thermal Envelope and Building Science, 22*, 49-71.

Freitas, V., Crausse, P., & Abrantes, V. (1991). *Moisture diffusion in thermal insulating materials*, Gatlinburg, TN, USA.

Ge, Z., Cahill, D. G., & Braun, P. V. (2006). Thermal conductance of hydrophilic and hydrophobic interfaces. *Physical Review Letters, 96*(18). doi: 10.1103/PhysRevLett.96.186101

Glazebrook, S. R. (1922). *A dictionary of applied physics, Volume 1* (Vol. 1): Macmillan and co.

Golestanian, H. (2007). Physical determination of permeability variation with porosity for composite performs (Vol. 18, pp. 67-73): IUST International Journal of Engineering Science (Special Issue).

Guldbrandsen, T., Kaplar, C. W., & Korsgaard, V. (2011). Analytical model of heat transfer in porous insulation around cold pipes. *International Journal of Heat and Mass Transfer, 54*(1-3), 288-292.

Gustafsson, M., Karawacki, E., & Gustavson, S. (1994). On the use of transient plane source sensors for studying materials with direction dependent properties. *Review of Scientific Instruments, 65*, 3856.

Gustafsson, S. E., Karawacki, E., & Khan, M. N. (1978). Transient hot - strip method for simultaneously measuring thermal conductivity and thermal diffusivity of solids and fluids. *Journal of Physics D: Applied Physics, 12*(9), 1411-1421.

Hay, B., Cortes, L., Doucey, B., Filtz, J. R., Hammerschmidt, U., Sokolov, N., Stacey, C., Zarr, R., & Zhang, J. (2009). *International comparison on thermal conductivity measurements of insulating materials by guarded hot plate-preliminary results*, Pittsburgh, PA, USA.

ISO 8301. (1991). Thermal insulation - Determination of steady-state thermal resistance and related properties - Heat flow meter apparatus.

ISO 8302. (1991). Thermal insulation - Determination of steady-state thermal resistance and related properties - Guarded hot plate apparatus.

ISO 8497. (1994). Thermal Insulation - Determination of steady-state thermal transmission properties if thermal insulation for circular pipes.

Jerman, M., & Cerny, R. (2012). Effect of moisture content on heat and moisture transport and storage properties of thermal insulation materials. *Energy and Buildings, 53*, 39-46. doi: 10.1016/j.enbuild.2012.07.002

Johns, W., & March, N. H. (1985). Theoretical solid state physics: Courier Dover Publications.

Johnson, A. B., Simonson, C. J., and Besant, R. W. (1998). *Uncertainty analysis in the testing of air-to-air heat/energy exchangers installed in buildings*. Paper presented at the ASHRAE Transactions, San Francisco, CA, USA.

Kaplar, C. W. (1974). Moisture and freeze - thaw effects on rigid thermal insulations. *United States Army, Corps of Engineers, Cold Regions Research & Engineering Laboratory, Hanover, N.H. Technical Report*(249).

Karamanos, A., Hadiarakou, S., & Papadopoulos, A. M. (2008). The impact of temperature and moisture on the thermal performance of stone wool. *Energy and Buildings, 40*(8), 1402-1411.

Kehrer, M., Kunzel, H. M., & Sedlbauer, K. (2002). Ecological insulation materials - Does sorption moisture affect their insulation performance? *Journal of Thermal Envelope and Building Science, 26*(3), 207-212. doi: 10.1177/109719603027869.

Kellner, J., & Dirckx, V. (1999). Change of thermal conductivity of polyurethane in pre-insulated pipes as a function of time. *Euroheat and Power/Fernwarme International, 28*(6), p 5-p 5.

Kimball, L. R. (1974). Thermal conductance of pipe insulation: a large-scale test apparatus. *American Society of Mechanical Engineers (Paper)*(74 -HT-48).

Klein, S. A. (2006). Engineering Equation Solver (Version V7.723-3D). Madison, WI, USA: F-Chart Software.

Korsgaard, V. (1993). *Innovative concept to prevent moisture formation and icing of cold pipe insulation*, Chicago, IL, USA.

Kulkarni, S. P., & Vipulanandan, C. (2006). Hot wire method to characterize the thermal conductivity of particle-filled polymer grouts used in pipe-in-pipe application. *Journal of Testing and Evaluation, 34*(3), 224-231.

Kumaran, M. K. (1987). Moisture transport through glass - fibre insulation in the presence of a thermal gradient. *Journal of thermal insulation, 10*, 243-255.

Kumaran, M. K. (2006). *A thermal and moisture property database for common building and insulation materials*, Quebec City, QC, Canada.

Lakatos, A., & Kalmar, F. (2012). Investigation of thickness and density dependence of thermal conductivity of expanded polystyrene insulation materials. 1-5. doi: 10.1617/s11527-012-9956-5

Langlais, C., Hyrien, M., & Klarsfeld, S. (1982). *Moisture migration in fibrous insulating material under the influence of a thermal gradient and its effect on thermal resistance*, Philadelphia, PA, USA.

Langlais, C., Hyrien, M., & Klarsfeld, S. (1983). *Influence of moisture on heat transfer through fibrous-insulating materials*, Clearwater Beach, FL, USA.

Langlais, C., & Klarsfeld, S. (1984). Heat and mass transfer in fibrous insulations. *Journal of thermal insulation, 8*, 49-80.

Litovsky, E., Issoupov, V., Kleiman, J., Latham, R., Kotrba, A., & Olivier, K. (2008). *Thermal conductivity of mechanically compressed fiber insulation materials in a wide temperature range: New test method and experimental results*, Birmingham, AL, USA.

Log, T. (1993). Transient hot-strip (THS) method for measuring thermal conductivity of thermally insulating materials. *Fire and Materials, 17*(3), 131-138.

Luikov, A. V. (1966). *Heat and mass transfer in apillary-porous bodies.* Oxford, New York: Pergamon Press.

Mar, J. D., Litovsky, E., & Kleiman, J. (2008). Modeling and database development of conductive and apparent thermal conductivity of moist insulation materials. *Journal of Building Physics, 32*(1), 9-31.

McCaa, D. J., & Smith, D. R. (1991). *Interlaboratory comparison of the apparent thermal conductivity of a fibrous batt and four loose-fill insulations*, Gatlinburg, TN, USA.

McFadden, T. (1986). *Moisture effects on extruded polystyene insulation*, Anchorage, AK, USA.

McFadden, T. (1988). Thermal performance degradation of wet insulations in cold regions. *Journal of Cold Regions Engineering, 2*(1), 25-34.

Miller, R. A., & Kuczmarski, M. A. (2009). Method for measuring thermal conductivity of small samples having very low thermal conductivity. Cleveland, Ohio: Glenn Research Center.

Modi, D. K., & Benner, S. M. (1985). Moisture gain of spray - applied insulations and its effect on effective thermal conductivity - Part I. *Journal of thermal insulation, 8*, 259-277.

Moore, J. P., McElroy, D. L., & Jury, S. H. (1985). Technique for measuring the apparent thernal conductivity of flat insulations. *Journal of thermal insulation, 9*, 102-110.

Motakef, S., & El-Masri, M. A. (1985). Liquid diffusion in fibrous insulation. *Journal of Heat Transfer, 107*(2), 299-306.

Mumaw, J. R. (2002). *A test protocol for comparison of the moisture absorption behavior of below-ambient piping insulation systems operating in hot-humid environments*, Charleston, SC, USA.

Musgrave, D. S. (1979). Thermal performance of urethane foam pipe insulation at cryogenic temperatures *Journal of thermal insulation* (Vol. 3, pp. 3-21).

Nelder, J. A., & Mead, R. (1965). A Simplex Method for Function Minimization. *The Compiter Journal, 7*(4), 308-313.

Ochs, F., Heidemann, W., & Muller-Steinhagen, H. (2008). Effective thermal conductivity of moistened insulation materials as a function of temperature. *International Journal of Heat and Mass Transfer, 51*(3-4), 539-552.

Ohmura, T. (2007). *Study on comparison of thermal conductivities of thermal insulations using different measurement methods in wide range of temperature*, Vancouver, BC, Canada.

Peuhkuri, R., Rode, C., & Hansen, K. K. (2008). Non-isothermal moisture transport through insulation materials. *Building and Environment, 43*(5), 811-822.

Ramsden, R. (1985). Insulation used on chilled water pipes in South Afican gold mines. *Journal of the Mine Ventilation Society of South Africa, 38*(5), 49-54.

Rawlins, A. (2005). Chilled water pipe insulation materials, their properties and application. *Journal of the Mine Ventilation Society of South Africa, 58*(2), 45-57.

Rides, M., Morikawa, J., Halldahl, L., Hay, B., Lobo, H., Dawson, A., & Allen, C. (2009). Intercomparison of thermal conductivity and thermal diffusivity methods for plastics. *Polymer Testing, 28*(5), 480-489. doi: 10.1016/j.polymertesting.2009.03.002.

Rywotycki, R. (2003). Electric sensor for prompt measurement of moisture content in solid food products. *Journal of Food Process Engineering, 25*(6), 473-483.

Sabuga, W., & Hammerschmidt, U. (1995). New method for the evaluation of thermal conductivity and thermal diffusivity from transient hot strip measurements. *International Journal of Thermophysics, 16*(2), 557-565.

Salmon, D. (2001). Thermal conductivity of insulations using guarded hot plates including recent developments and sources of reference materials. *Measurement Science and Technology, 12*(12), R89-R98. doi: 10.1088/0957-0233/12/12/201.

Salmon, D., & Tye, R. P. (2010). An inter-comparison of a steady-state and transient methods for measuring the thermal conductivity of thin specimens of masonry materials. *Journal of Building Physics, 34*(3), 247-261. doi: 10.1177/1744259109360060.

Sandberg, P. I. (1995). Thermal conductivity of moist masonry materials. *Journal of Thermal Insulation and Building Envelopes, 18*, 276-288.

Saxena, N. S., Gustafsson, S. E., Chohan, M. A., & Maqsood, A. (1989). Temperature dependence of thermal conductivities and thermal diffusivities of composites using transient hot-strip method. *International Journal of Energy Research, 13*(4), 411-417.

Simonson, C. J., Tao, Y. X., & Besant, R. W. (1996). Simultaneous heat and moisture transfer in fiberglass insulation with transient boundary conditions. *ASHRAE Transactions, 102*(1), 315-327.

Stovall, T. (2009). *Measuring the impact of experimental parameters upon the estimated thermal conductivity of closed-cell foam insulation subjected to an accelerated aging protocol: Two-year results*, Vancouver, BC, Canada.

Suleiman, B. M. (2006). Moisture effect on thermal conductivity of some major elements of a typical Libyan house envelope. *Journal of Physics D: Applied Physics, 39*(3), 547-551.

Taylor, J. R. (1997). An introduction to error analysis : the study of uncertainties in physical measurements (pp. xvii, 327 p.). Sausalito, Calif.: University Science Books.

Tritt, T. M. (2004). *Thermal conductivity : theory, properties, and applications*: New York : Kluwer Academic/Plenum Publishers.

Tseng, C.-J., & Kuo, K.-T. (2002). Thermal properties of phenolic foam insulation. *Journal of the Chinese Institute of Engineers, Transactions of the Chinese Institute of Engineers,Series A/Chung-kuo Kung Ch'eng Hsuch K'an, 25*(6), 753-758.

Tye, R. P. (1969). *Thermal Conductivity*. New York: Academic Press Inc.

Vrana, T., & Bjork, F. (2008). A laboratory equipment for the study of moisture processes in thermal insulation materials when placed in a temperature field. *Construction and Building Materials, 22*(12), 2335-2344.

Whitaker, T. E., & Yarbrough, D. W. (2002). *Review of thermal properties of a variety of commercial and industrial pipe insulation materials*, Charleston, SC, United states.

Wijeysundera, N. E., & Hawlader, M. N. A. (1988). Thermal transmittance property evaluation of insulation systems. *RERIC International Energy Journal, 10*(1), 45-65.

Wijeysundera, N. E., Zheng, B. F., Iqbal, M., & Hauptmann, E. G. (1993). Effective thermal conductivity of flat-slab and round-pipe insulations in the presence of condensation. *Journal of Thermal Insulation and Building Envelopes, 17*, 55-76.

Wijeysundera, N. E., Zheng, B. F., Iqbal, M., & Hauptmann, E. G. (1996). Numerical simulation of the transient moisture transfer through porous insulation. *International Journal of Heat and Mass Transfer, 39*(5), 995-1004.

Wilkes, K. E., Desjarlais, A. O., Stovall, T. K., McElroy, D. L., Childs, K. W., & Miller, W. A. (2002). *A pipe insulation test apparatus for use below room temperature*, Charleston, SC, USA.

Woodbury, K. A., & Thomas, W. C. (1985). *Measurement of moisture concentration in fibrous insulation using a microprocessor-based thermistor probe*, Washington, DC, USA.

Wulf, R., Barth, G., & Gross, U. (2007). Intercomparison of insulation thermal conductivities measured by various methods. *International Journal of Thermophysics, 28*(5), 1679-1692. doi: 10.1007/s10765-007-0278-8.

Yu, M., Sui, X., Peng, X., & Fang, Z. (2009). Influence of moisture content on measurement accuracy of porous media thermal conductivity. *Heat Transfer - Asian Research, 38*(8), 492-500.

Zarr, R. R., & Nguyen, T. (1994). Effects of humidity and elevated temperature on the density and thermal conductivity of a rigid polyisocyanurate foam co-blown with CCl3F and CO2. *Journal of Thermal Insulation and Building Envelopes, 17*, 330-350.

Zehendner, H. (1983). Thermal conductivity of thermal insulation materials on pipes. *Journal of thermal insulation, 7*, 52-68.

APPENDICES

Appendix A: Thermal conductivity of seven common insulation materials: fiberglass, polyurethane, polystyrene, cellular glass, polyisocyanurate (PIR), mineral wool and elastomeric rubber insulation reported in the open domain literature

Table A-1: Comparison among experimental methods and test results for fiberglass insulation (SI units)

Fiberglass							
Literature	Mean temperature	Thermal conductivity	Type	Method	Uncertainty /Deviation	Thickness	Description
	˚C	W/m-K			%	mm	
Modi and Benner (1985)	20	0.0310	board	GHP (sample between water and air space	-	50.8	density 45.8 kg/m^3
	27	0.0350	board			50.8	
Moore *et al.* (1985)	25	0.0342	board	GHP	1	15.9-36.3	density 26kg/m^3
	25	0.0435	pipe	-	-		density 15kg/m^3
Wijeysundera and Hawlader (1988)	30	0.0328	board	HFM	-	25.4	density 131kg/m^3
	35	0.0330					
	31	0.0310	board	Probe	-	25.4	density 131kg/m^3
McFadden (1988)	24	0.0361	board	Probe and GHP	>3.2	>3.2	-
McCaa and Smith (1991)	24	0.0384	board	GHP, HFM, THA	2.8 ~ 3	152.4	density 12kg/m^3
	24	0.0378					density 15kg/m^3
Al-Hammad *et al.* (1994)	24	0.0330	board	GHP	±2 ~ ±4	-	density 48kg/m^3
	25	0.0350	board			-	density 32-37kg/m^3
Chyu *et al.* (1997b)	10	0.0310	pipe	Radial HFM	-	-	density 46.4kg/m^3
	20	0.0330					
	30	0.0340					
	40	0.0355					
	50	0.0360					
Salmon (2001)	10	0.0319	board	GHP and HFM	1.83	25	density 150-165kg/m^3 [1]$k=-7.7663\times10^{-3}+5.6153\times10^{-5}\rho+1.0859\times10^{-4}T$
	20	0.0330					
	30	0.0341					
	40	0.0352					
Wikes *et al.* (2002)	20	0.0311	pipe	Guarded Heated Pipe	±0.8	54	density 33kg/m^3 [1]$k=0.000183T+0.02742$
	30	0.0329					
	40	0.0347					
	50	0.0366					

[1] SI units: k (W/m-K), T (˚C) and ρ (kg/m^3)

Appendix A-1 (*continued*): Comparison among experimental methods and test results for fiberglass insulation (SI units)

Fiberglass							
Literature	Mean temperature	Thermal conductivity	Type	Method	Uncertainty /Deviation	Thickness	Description
	˚C	W/m-K			%	mm	
Whitaker and Yarbrough (2002)	20	0.0333	pipe	Guarded Heated Pipe	-27.5 ~ 9.6 deviation	50.8	density 86.5kg/m^3 ^{2}k=7.787×10^{-7}T^2+1.921×10^{-4}T+0.2141
	30	0.0341					
	40	0.0350					
	50	0.0359					
Abdou and Budaiwi (2005)	8	0.0441	board	GHP	-	5-100	density 13.1kg/m^3 k=0.0003368T+0.041433
	12	0.0455					
	24	0.0495					
	36	0.0536					
	40	0.0549					
	8	0.0338	board	GHP	-	5-100	density 27kg/m^3 k=0.000188T+0.030677
	12	0.0345					
	24	0.0367					
	36	0.0388					
	40	0.0395					
	8	0.0301	board	GHP	-	5-100	density 56kg/m^3 k=0.0001189T+0.02913
	12	0.0306					
	24	0.0320					
	36	0.0334					
	40	0.0339					
Bezjak and Zvizdic (2011)	23	0.0457	board	GHP	3.1	80	density 13kg/m^3
	23	0.0444		THW	8.1		
Cremaschi *et al.* (2012a; 2012b)	10	0.0330	pipe	HFM (cold pipe)	<±6	50.8	density 70kg/m^3 k=0.00010T+0.0320
	20	0.0340					
	30	0.0350					
	40	0.0360					

[1]: SI units: k (W/m-K) and T (˚C);
[2]: IP units: k (Btu-in/hr-ft^2-˚F) and T (˚F)

Table A-2: Comparison among experimental methods and test results for polyurethane insulation (SI units)

Polyurethane							
Literature	Mean temperature	Thermal conductivity	Type	Method	Uncertainty /Deviation	Thickness	Description
	˚C	W/m-K			%	mm	
Zehendner (1983)	10	0.0230	pipe	Guarded Heated Pipe	< ±3	20-26	density 39kg/m^3 Blowing agent: $CFCl_3$; Aging: 4~6 months with 0.3mm PVC jacketing
	20	0.0240					
	30	0.0250					
	40	0.0260					
	50	0.0270					
McFadden (1988)	24	0.0216	board	Probe and GHP	-	>3.2	-
Al-Hammad *et al.* (1994)	35	0.0240	board	GHP	±2 ~ ±4	-	density 32-35kg/m^3
Chyu *et al.*(1997a)	10	0.0182	pipe	HFM (hot pipe)	-	38.1	density 46kg/m^3
	20	0.0202					
	30	0.0222					
	40	0.0242					
	50	0.0262					
Abdou and Budaiwi (2005)	10	0.0212	board	HFM	-	5-100	density 44kg/m^3 [1]k=0.0001089T+0.020132
	20	0.0223					
	30	0.0234					
	40	0.0245					
	50	0.0256					
Adl- Zarrabi (2005)	20	0.0318	pipe	TPS			
	50	0.0358					
Ohmura (2007)	10	0.0450	board	Cyclic heat, THW, Hot disk	±10 (deviation)	20	density 119kg/m^3
	20	0.0475					
	25	0.0500					
Bezjak and Zvizdic (2011)	23	0.0235	board	GHP	3	100	density 42kg/m^3
	23	0.0294		THW	6.1		density 42kg/m^3

[1] SI units: k (W/m-K) and T (˚C)

Table A-3: Comparison among experimental methods and test results for extruded and expanded polystyrene insulation (SI units)

Extruded Polystyrene							
Literature	Mean temperature	Thermal conductivity	Type	Method	Uncertainty /Deviation	Thickness	Description
	˚C	W/m-K			%	mm	
McFadden (1988)	24	0.0274	board	Probe and GHP	-	>3.2	-
Abdou and Budaiwi (2005)	10	0.0277	board	HFM	-	5-100	density 35.8kg/m^3, [1]k=0.0000961T+0.026741
	20	0.0287					
	30	0.0296					
	40	0.0306					
	50	0.0315					
	10	0.0286	board	HFM	-	5-100	density 49.3kg/m^3, [1]k=0.0000706T+0.027846
	20	0.0293					
	30	0.0300					
	40	0.0307					
	50	0.0314					
Bezjak and Zvizdic (2011)	23	0.0357	board	GHP	3.1	50	density 40kg/m^3
	23	0.0352		THW	6.3		

[1] SI units: k (W/m-K) and T (˚C)

Table A-3 (*Continued*): Comparison among experimental methods and test results for extruded and expanded polystyrene insulation (SI units)

Expanded Polystyrene							
Litearture	Mean temperature	Thermal conductivity	Type	Method	Uncertainty /Deviation	Thickness	Description
	˚C	W/m-K			%	mm	
Pratt [1]	10	0.0346	board	-	-	-	density 16kg/m^3
	10	0.0331	board	-	-	-	density 24kg/m^3
McFadden (1988)	24	0.0418	board	Probe and GHP	-	>3.2	
Al-Hammad *et al.* (1994)	35	0.0380	board	GHP	±2 ~ ±4	-	density 16kg/m^3
	35	0.0360					density 20kg/m^3
	35	0.0350					density 24kg/m^3
	35	0.0320					density 26kg/m^3
Slamon (2001)	10	0.0319	board	GHP and HFM	1.83	25	density 40kg/m^3 [2]k=6.3054×10^{-4}-4.1993×10^{-5}ρ +1.1650×10^{-4}T
	20	0.0331					
	30	0.0343					
	40	0.0354					
Abdou and Budaiwi (2005)	7.5	0.0284	board	HFM	-	5-100	density 32.5kg/m^3, [2]k=0.0001045T+0.027658
	12	0.0289					
	23.5	0.0301					
	36	0.0314					
	40	0.0318					
Mar *et al.*(2008)	10	0.0310	board	GHP	-	-	density 40kg/m^3
	20	0.0330					
	30	0.0350					
	40	0.0360					
Bezjak and Zvizdic (2011)	10	0.0360	board	GHP	-	-	density 20kg/m^3
	23	0.0373	board	GHP	3.1	60	density 20kg/m^3
	23	0.0352		THW	6.8		
Lakatos and Kalmar (2012)	17	0.0489	board	HFM	-	50	density 10.2 kg/m^3
	17	0.0363					density 21.4 kg/m^3
	17	0.0340					density 26.0 kg/m^3
Jerman and Cerny (2012)	22	0.0370	board	IM (impulse method, transient method)	±5%		density 16.5 kg/m^3

[1]: referred by Tye(1969) [2]: SI units: k (W/m-K), T (˚C) and ρ (kg/m^3)

Table A-4: Comparison among experimental methods and test results for cellular glass, phenolic and PIR insulations (SI units)

Cellular Glass							
Literature	Mean temperature	Thermal conductivity	Type	Method	Uncertainty /Deviation	Thickness	Description
	˚C	W/m-K			%	mm	
Kaplar (1974)	10	0.055	board	GHP	-	50.8	density 148kg/m^3
Zehendner (1983)	10	0.0545	pipe	Guarded Heated Pipe	< ±3	50	density 137kg/m^3 Staggered joints with recommended joint sealant; Vapor barrier and sheet metal jacket were applied on the outside
	20	0.056					
	30	0.0575					
	40	0.06					
	10	0.06				73	density 140kg/m^3 Staggered joints with recommended joint sealant; Vapor barrier and sheet metal jacket were applied on the outside
	20	0.0625					
	30	0.065					
	40	0.066					
Whitaker and Yarbrough (2002)	20	0.0596	pipe	Guarded Heated Pipe	-2.5 ~ 4.4 deviation	50.8	density 136.2kg/m^3 $^2k=1.316\times10^{-6}T^2+3.574\times10^{-4}\times T+0.3825$
	30	0.0610					
	40	0.0626					
	50	0.0643					
Pittsburgh Corning Co.	10	0.0396	board	GHP	-	25.4	density 120kg/m^3 $^2k=0.25+0.00054T+4.6\times10^{-7}T^2+2\times10^{-11}T^2$
	20	0.0407					
	30	0.0418					
	40	0.0429					
Cremaschi *et al.* (2012a; 2012b)	10	0.0419	pipe	HFM (cold pipe)	±6	25.4	density 120kg/m^3[1] $k=0.00025T+0.0394$
	20	0.0444					
	30	0.0469					
	40	0.0494					
	10	0.0390	pipe		<±6	50.8	density 120kg/m^3[1] $k=0.00055T+0.0335$
	20	0.0445					
	30	0.0500					
	40	0.0555					

[1] SI units: k (W/m-K) and T (˚C);
[2] IP units: k (Btu-in/hr-ft^2-˚F) and T (˚F)

Appendix A-4 (*continued*): Comparison among experimental methods and test results for other common insulations (SI units)

Polyisocyanurate (PIR)							
Literature	Mean temperature	Thermal conductivity	Type	Method	Uncertainty /Deviation	Thickness	Description
	˚C	W/m-K			%	mm	
McFadden (1988)	24	0.0216	board	Probe and GHP	-	>3.2	-
Al-Hammad *et al.* (1994)	35	0.0230	board	GHP	±2 ~ ±4	50.8	density 32-37kg/m^3
Cremaschi *et al.* (2012a; 2012b)	10	0.0279	pipe	HFM (cold pipe)	<±6	50.8	density 50kg/m^3[1]k=0.00009T+0.0270
	20	0.0288					
	30	0.0297					
	40	0.0306					

[1] SI units: k (W/m-K) and T (˚C);
[2] IP units: k (Btu-in/hr-ft^2-˚F) and T (˚F)

Table A-5: Comparison among experimental methods and test results for elastomeric rubber and mineral wool insulation (SI units)

Mineral Wool							
Literature	Mean temperature	Thermal conductivity	Type	Method	Uncertainty /Deviation	Thickness	Description
	˚C	W/m-K			%	mm	
Zehendner (1983)	10	0.0315	pipe	Guarded Heated Pipe	< ±3	20-40	density 43-53kg/m^3 Mineral fibers bound with synthetic resin
	20	0.0325					
	30	0.033					
	40	0.035					
	50	0.0365					
	10	0.037	board (wrap around pipe)	Guarded Heated Pipe	< ±3	20	density 85kg/m^3 Laminates glued to aluminum film
	20	0.038					
	30	0.0395					
	40	0.041					
	50	0.0425					
McCaa and Smith (1991)	24	0.0494	board	GHP, HFM, THA	10.5 ~ 11 deviation	14-21	density 30kg/m^3
	24	0.0499					density 40kg/m^3
Whitaker and Yarbrough (2002)	20	0.0440	pipe	Guarded Heated Pipe	-29.7 ~ 31.5 deviation	50.8	density 145.8kg/m^3 $^2k=1.059\times10^{-6}T^2-8.21\times10^{-5}T+0.3060$
	30	0.0442					
	40	0.0446					
	50	0.0450					
Abdou and Budaiwi (2005)	10	0.0347	board	HFM	-	5-100	density 145.4kg/m^3 $^1k=0.0001263T+0.033425$
	20	0.0360					
	30	0.0372					
	40	0.0385					
	50	0.0397					
Bezjak and Zvizdic (2011)	23	0.0434	board	GHP	3	160	density 142kg/m^3
	23	0.0456		THW	8.3		
Jerman and Cerny (2012)	22	0.0370	board	IM (impulse method, transient method)	±5	25	density 70kg/m^3
	22	0.0360				25	density 100kg/m^3
	22	0.0410				25	density 170kg/m^3

¹ SI units: k (W/m-K) and T (˚C); ² IP units: k (Btu-in/hr-ft^2-˚F) and T (˚F)

Appendix A-5 (*Continued*): Comparison among experimental methods and test results for elastomeric rubber and mineral wool insulation (SI units)

Elastomeric Rubber							
Literature	Mean temperature	Thermal conductivity	Type	Method	Uncertainty /Deviation	Thickness	Description
	˚C	W/m-K			%	mm	
Wikes *et al.* (2002)	10	0.0382	board	GHP	±0.8	30.4	density 61kg/m^{3}[1]k=0.000133T+0.03684
	20	0.0395					
	30	0.0408					
	40	0.0422					
	50	0.0435					
	10	0.0372	pipe	Guarded Heated Pipe	±0.8	25.4	density 66kg/m^{3}[1]k=0.000156T+0.03567
	20	0.0388					
	30	0.0404					
	38	0.0416					
	50	0.0435					
Cremaschi *et al.* (2012a; 2012b)	10	0.0348	pipe	HFM (cold pipe)	< ±6	50.8	density 86kg/m^{3}[1]k=0.00014T+0.0334
	20	0.0362					
	30	0.0376					
	40	0.0390					

[1] SI units: k (W/m-K) and T (˚C); [2] IP units: k (Btu-in/hr-ft^{2}-˚F) and T (˚F)

Appendix B: CAD drawings of the experimental apparatus

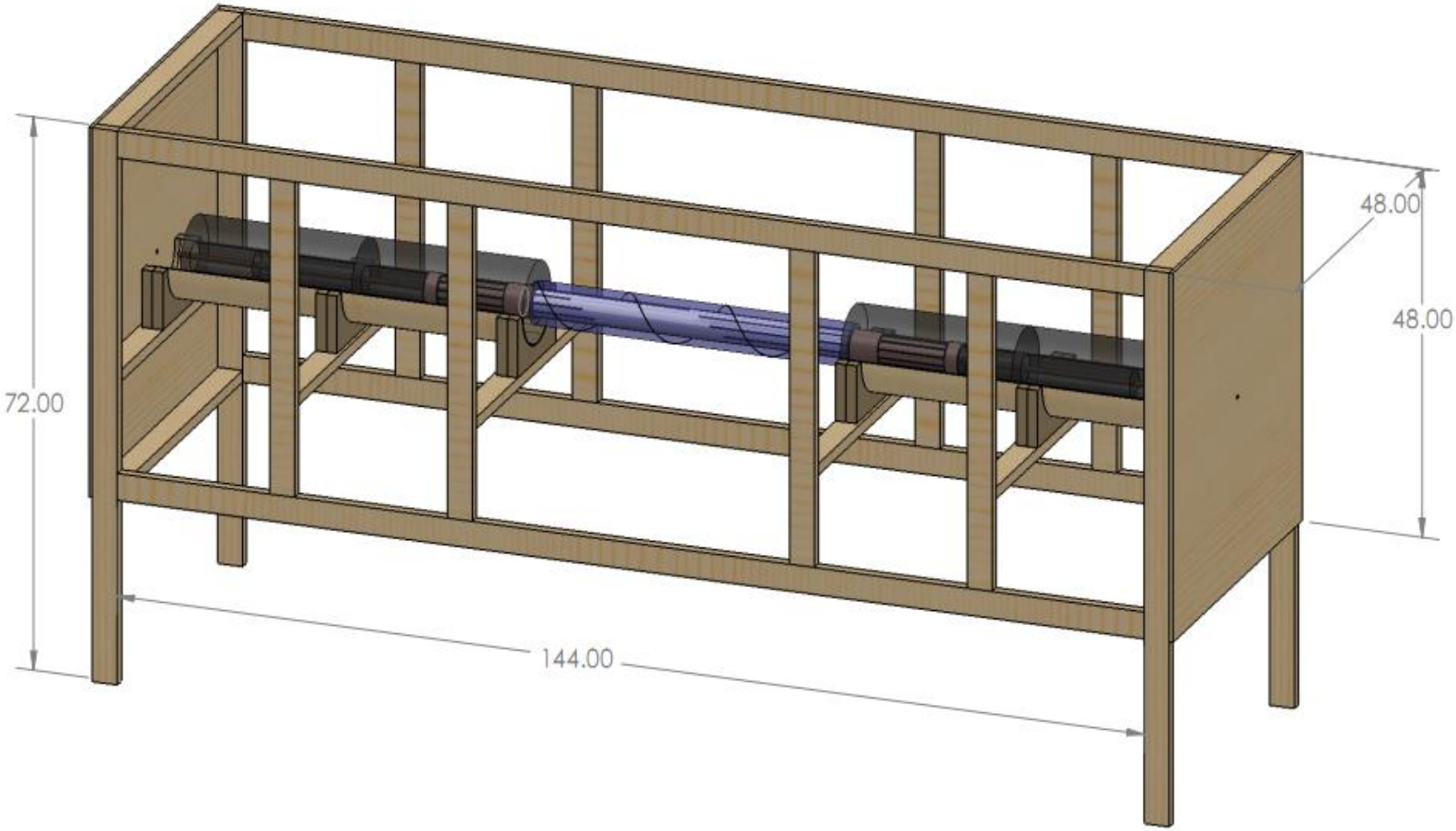

Figure B-1 3D drawing of the entire test apparatus (unit: inch)

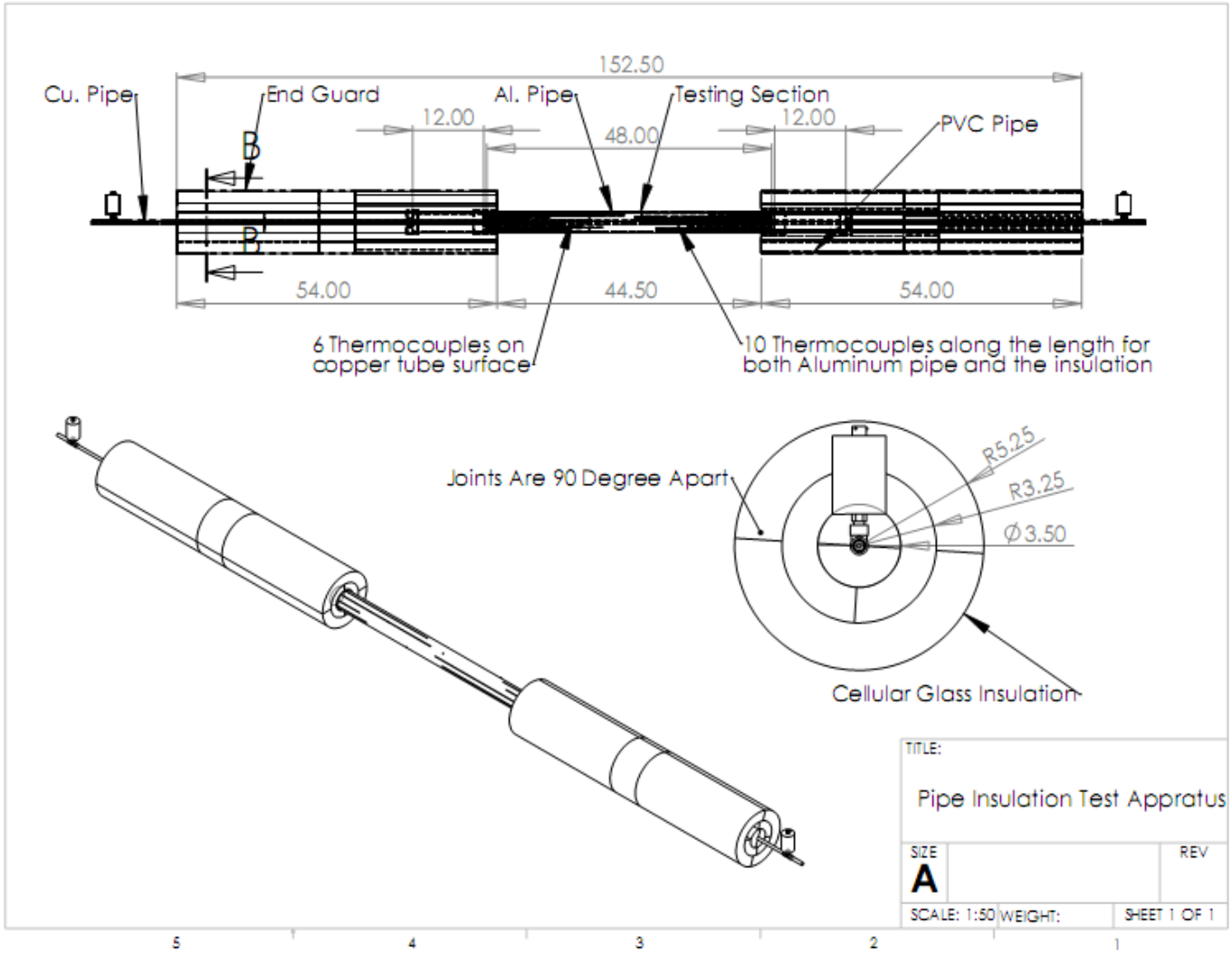

Figure B-2: Technical drawings of the Aluminum pipe with two end thermal guard sections (unit: inch)

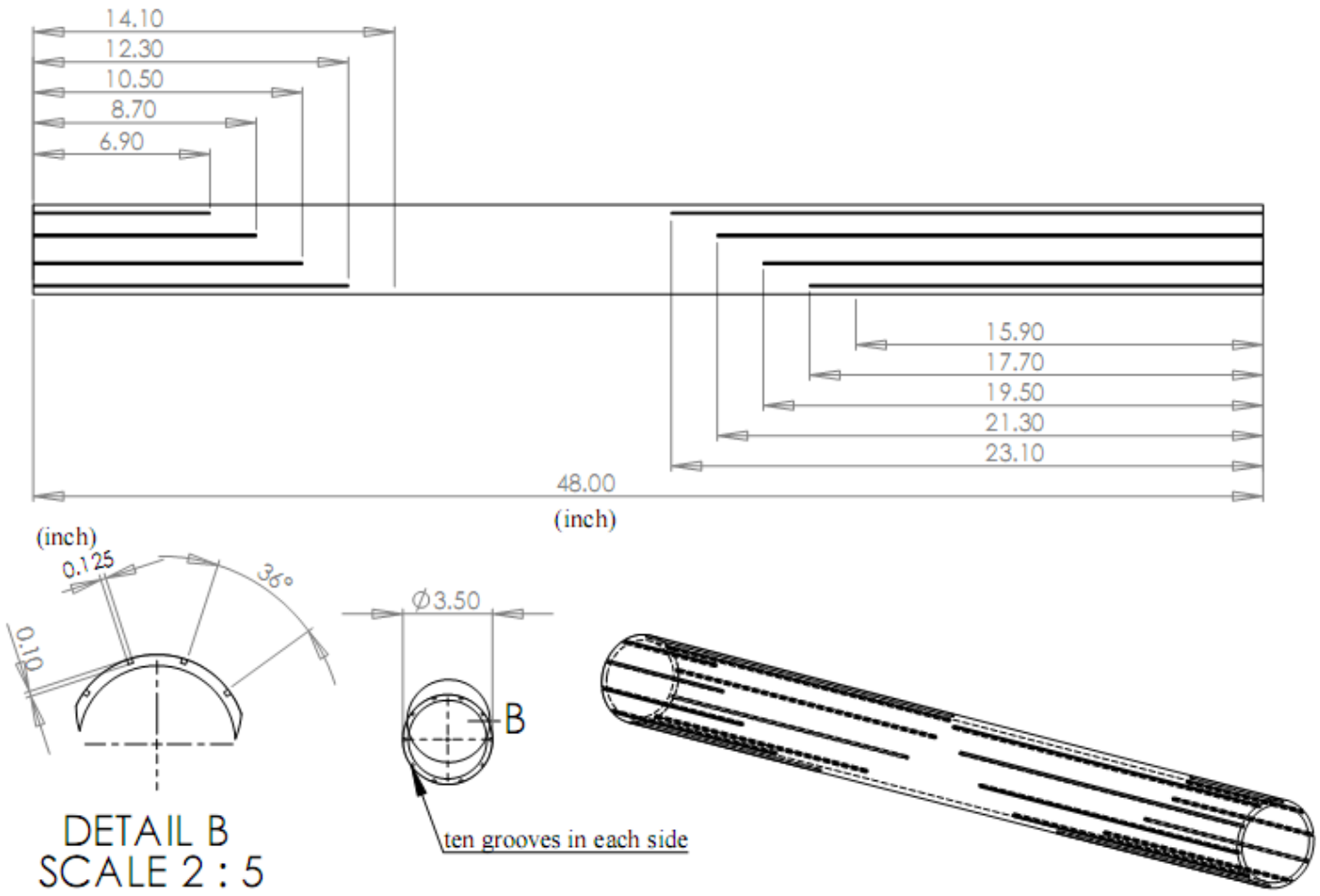

Figure B-3: Details of the grooves machined on the Aluminum pipe exterior surface (unit: inch)

Appendix C: Examples of experimental data sets

Table C-1: Experimental results for system P1-FG under dry condition (IP units)

RH	%	89.08	98.010	110.77	77.16
T_{Room}	F	17.30	16.635	14.19	20.62
T_{Outins}	F	86.77	95.739	109.59	74.94
T_{Al}	F	84.80	93.396	106.46	74.07
T_{Cu}	F	40.45	41.286	41.32	40.42
ΔT_{out}	F	31.33	30.582	28.09	33.60
ΔT_{in}	F	44.35	52.111	65.14	33.65
T_{sand}	F	9.12	10.704	13.23	6.82
T_{test}	F	35.89	35.934	34.70	37.01
k_{eff}	Btu-in/hr-ft^2-F	62.63	67.341	73.89	57.25
Q_{sand}	Btu/hr	2.71	2.709	2.75	2.67
k_{test}	Btu-in/hr-ft^2-F	21.66	25.422	31.88	15.97
k_{func} (1in)	Btu-in/hr-ft^2-F	0.2370	0.2367	0.2375	0.2302
ΔT_{Al}	F	0.23	0.230	0.23	0.23
ΔT_{Outins}	F	7.22	8.474	10.63	5.32

Table C-2: Experimental results for system P1-P1 under dry condition (IP units)

RH	%	38.75	34.930	29.51	24.18
T_{Room}	F	13.90	12.942	14.41	19.08
T_{Outins}	F	38.50	34.747	29.11	23.89
T_{Al}	F	36.38	32.582	27.41	22.45
T_{Cu}	F	4.90	4.819	4.38	4.13
ΔT_{out}	F	-5.39	-4.100	-2.98	-1.72
ΔT_{in}	F	31.48	27.763	23.03	18.31
T_{sand}	F	10.29	8.919	7.36	5.86
T_{test}	F	-0.25	0.359	0.70	1.20
k_{eff}	Btu-in/hr-ft^2-F	20.64	18.70	15.89	13.29
Q_{sand}	Btu/hr	0.41	0.405	0.40	0.40
k_{test}	Btu-in/hr-ft^2-F	13.46	11.569	9.49	7.49
k_{func} (1in)	Btu-in/hr-ft^2-F	0.0336	0.0328	0.0324	0.0322
ΔT_{Al}	F	0.02	0.021	0.02	0.02
ΔT_{Outins}	F	1.28	1.155	0.93	0.70

Table C-3: Experimental results for system P1-P2 under dry condition (IP units)

RH	%	110.02	99.872	90.20	79.56
T_{Room}	F	14.94	15.920	16.31	17.71
T_{Outins}	F	109.33	98.393	88.91	78.52
T_{Al}	F	106.92	95.542	86.77	77.02
T_{Cu}	F	39.92	39.907	40.73	40.84
ΔT_{out}	F	27.96	30.210	32.71	34.62
ΔT_{in}	F	66.99	55.635	46.04	36.18
T_{sand}	F	11.96	9.697	8.02	6.21
T_{test}	F	33.94	35.058	36.72	37.73
k_{eff}	Btu-in/hr-ft^2-F	73.42	67.724	63.75	58.93
Q_{sand}	Btu/hr	2.7713	2.7381	2.6809	2.6399
k_{test}	Btu-in/hr-ft^2-F	29.05	23.278	18.86	14.39
k_{func} (1in)	Btu-in/hr-ft^2-F	0.2127	0.2052	0.2009	0.1949
ΔT_{Al}	F	0.15	0.146	0.15	0.15
ΔT_{Outins}	F	9.69	7.759	6.29	4.80

Table C-4: Experimental results for system P1-ER under dry condition (IP units)

RH	%	77.25	87.35	96.97	110.12
T_{Room}	F	18.27	15.75	15.95	13.98
T_{Outins}	F	75.05	85.37	95.22	109.29
T_{Al}	F	73.97	83.60	93.62	106.43
T_{Cu}	F	41.43	41.56	40.11	39.82
ΔT_{out}	F	34.30	32.42	28.56	25.69
ΔT_{in}	F	32.54	42.04	53.52	66.61
T_{sand}	F	7.12	9.15	11.54	14.14
T_{test}	F	37.86	36.99	34.33	32.75
k_{eff}	Btu-in/hr-ft^2-F	57.70	62.58	66.87	73.12
Q_{sand}	Btu/hr	2.64	2.67	2.76	2.80
k_{test}	Btu-in/hr-ft^2-F	16.46	21.41	27.93	34.72
k_{func} (1in)	Btu-in/hr-ft^2-F	0.2455	0.2472	0.2533	0.2529
ΔT_{Al}	F	0.2388	0.2403	0.2416	0.2435
ΔT_{Outins}	F	5.49	7.14	9.31	11.57

Table C-5: Experimental results for system P1-FG under dry condition (IP units)

RH	%	8.97	8.32	7.50	7.00	8.82	7.18
T_{Room}	F	85.48	90.55	95.56	99.10	87.53	92.57
T_{Outins}	F	83.37	88.23	93.06	96.34	85.30	90.14
T_{Al}	F	36.88	36.98	36.57	36.37	36.68	36.67
T_{Cu}	F	26.85	25.79	24.04	23.04	26.10	24.97
ΔT_{out}	F	46.49	51.25	56.50	59.97	48.62	53.47
ΔT_{in}	F	10.03	11.19	12.53	13.33	10.58	11.69
T_{sand}	F	31.86	31.38	30.30	29.71	31.39	30.82
T_{test}	F	60.13	62.61	64.82	66.36	60.99	63.40
k_{eff}	Btu-in/hr-ft^2-F	2.60	2.61	2.62	2.63	2.60	2.61
Q_{sand}	Btu/hr	22.85	25.58	28.76	30.67	24.13	26.77
k_{test}	Btu-in/hr-ft^2-F	0.2426	0.2464	0.2513	0.2525	0.2450	0.2471
k_{func} (1in)	Btu-in/hr-ft^2-F	0.2334	0.2343	0.2352	0.2358	0.2337	0.2346
ΔT_{Al}	F	0.98	1.12	1.24	1.36	1.08	1.17
ΔT_{Outins}	F	1.49	1.74	1.85	1.96	1.79	2.02

Table C-6: Experimental results for system P2-FG2 under dry condition (IP units)

RH	%	21.13	18.23	13.72	9.96	10.71	5.75
T_{Room}	F	77.14	80.10	85.07	90.10	87.07	107.17
T_{Outins}	F	75.32	78.12	82.78	87.59	84.74	103.94
T_{Al}	F	37.81	37.57	37.83	37.85	37.75	37.63
T_{Cu}	F	27.67	26.64	25.70	24.31	24.94	19.37
ΔT_{out}	F	37.51	40.54	44.95	49.74	46.99	66.31
ΔT_{in}	F	10.14	10.94	12.13	13.54	12.81	18.26
T_{sand}	F	32.74	32.11	31.76	31.08	31.34	28.50
T_{test}	F	56.56	57.85	60.31	62.72	61.24	70.78
k_{eff}	Btu-in/hr-ft^2-F	2.5523	2.5605	2.5767	2.5928	2.5827	2.6456
Q_{sand}	Btu/hr	22.68	24.55	27.40	30.78	29.00	42.34
k_{test}	Btu-in/hr-ft^2-F	0.2499	0.2503	0.2520	0.2558	0.2552	0.2640
k_{func} (1in)	Btu-in/hr-ft^2-F	0.2361	0.2381	0.2419	0.2456	0.2433	0.2580
ΔT_{Al}	F	1.33	1.43	1.56	1.80	1.72	2.33
ΔT_{Outins}	F	1.31	1.46	1.88	2.35	2.05	3.23

Table C-7: Experimental results for system P2-FG3 under dry condition (IP units)

RH	%	21.13	18.23	13.72	9.96	10.71	5.75
T_{Room}	F	76.99	80.00	84.68	89.70	86.66	106.18
T_{Outins}	F	75.55	78.37	82.83	87.51	84.67	102.99
T_{Al}	F	37.97	37.74	37.95	37.92	37.84	37.50
T_{Cu}	F	28.01	27.00	26.15	24.85	25.43	20.19
ΔT_{out}	F	37.57	40.63	44.89	49.59	46.83	65.49
ΔT_{in}	F	9.96	10.74	11.80	13.07	12.41	17.31
T_{sand}	F	32.99	32.37	32.05	31.38	31.63	28.85
T_{test}	F	56.76	58.06	60.39	62.71	61.26	70.24
k_{eff}	Btu-in/hr-ft^2-F	2.4868	2.4991	2.5060	2.5173	2.5121	2.5581
Q_{sand}	Btu/hr	21.72	23.53	25.93	28.84	27.34	38.81
k_{test}	Btu-in/hr-ft^2-F	0.2444	0.2448	0.2443	0.2459	0.2468	0.2506
k_{func} (1in)	Btu-in/hr-ft^2-F	0.2364	0.2384	0.2420	0.2456	0.2434	0.2572
ΔT_{Al}	F	1.03	1.07	1.12	1.14	1.12	1.40
ΔT_{Outins}	F	0.76	0.88	1.09	1.32	1.18	1.85

Table C-8: Experimental results for system P2-FG4 under dry condition (IP units)

RH	%	15.59	13.52	11.45	9.88	8.76	7.31
T_{Room}	F	76.97	81.74	86.71	91.78	96.74	101.54
T_{Outins}	F	75.53	80.09	84.82	89.67	94.42	98.98
T_{Al}	F	40.49	40.50	40.68	40.82	40.73	40.74
T_{Cu}	F	31.28	29.95	28.79	27.63	25.94	24.68
ΔT_{out}	F	35.04	39.60	44.14	48.85	53.69	58.23
ΔT_{in}	F	9.21	10.55	11.89	13.20	14.79	16.06
T_{sand}	F	35.89	35.23	34.74	34.22	33.34	32.71
T_{test}	F	58.01	60.30	62.75	65.25	67.58	69.86
k_{eff}	Btu-in/hr-ft^2-F	2.6075	2.5875	2.5669	2.5458	2.5259	2.5060
Q_{sand}	Btu/hr	21.05	23.92	26.75	29.45	32.76	35.29
k_{test}	Btu-in/hr-ft^2-F	0.2427	0.2440	0.2448	0.2435	0.2464	0.2447
k_{func} (1in)	Btu-in/hr-ft^2-F	0.2431	0.2436	0.2442	0.2448	0.2453	0.2459
ΔT_{Al}	F	1.70	1.73	1.77	1.85	1.97	2.02
ΔT_{Outins}	F	2.15	2.41	2.52	2.65	2.80	3.03

Table C-9: Experimental results for system P2-FG5A under dry condition (IP units)

RH	%	15.59	13.52	11.45	9.88	8.76	7.31
T_{Room}	F	76.85	81.71	86.71	91.84	96.87	101.79
T_{Outins}	F	75.61	80.28	85.11	90.06	94.95	99.71
T_{Al}	F	39.74	39.53	39.50	39.44	39.27	39.41
T_{Cu}	F	32.58	31.22	30.07	28.92	27.67	26.73
ΔT_{out}	F	35.86	40.76	45.61	50.62	55.68	60.30
ΔT_{in}	F	7.17	8.30	9.43	10.51	11.60	12.68
T_{sand}	F	36.16	35.37	34.79	34.18	33.47	33.07
T_{test}	F	57.68	59.91	62.31	64.75	67.11	69.56
k_{eff}	Btu-in/hr-ft^2-F	3.0302	3.0082	2.9872	2.9655	2.9433	2.9238
Q_{sand}	Btu/hr	19.04	21.90	24.68	27.34	29.92	32.49
k_{test}	Btu-in/hr-ft^2-F	0.2621	0.2652	0.2671	0.2666	0.2652	0.2660
k_{func} (1in)	Btu-in/hr-ft^2-F	0.2328	0.2354	0.2382	0.2410	0.2437	0.2465
ΔT_{Al}	F	1.51	1.48	1.50	1.54	1.64	1.67
ΔT_{Outins}	F	1.27	1.24	1.29	1.29	1.37	1.42

Table C-10: Experimental results for system P2-FG5B under dry condition (IP units)

RH	%	14.74	13.88	11.58	9.31	9.14	7.98
T_{Room}	F	76.87	81.68	86.58	91.38	91.38	96.33
T_{Outins}	F	75.77	80.45	85.09	89.70	89.72	94.51
T_{Al}	F	36.62	36.82	34.91	34.19	34.17	33.99
T_{Cu}	F	28.48	27.74	24.13	22.38	22.38	20.95
ΔT_{out}	F	39.15	43.62	50.18	55.51	55.55	60.52
ΔT_{in}	F	8.15	9.09	10.78	11.81	11.79	13.03
T_{sand}	F	32.55	32.28	29.52	28.29	28.27	27.47
T_{test}	F	56.20	58.64	60.00	61.95	61.94	64.25
k_{eff}	Btu-in/hr-ft^2-F	2.6705	2.6535	2.6486	2.6347	2.6347	2.6188
Q_{sand}	Btu/hr	19.07	21.14	25.03	27.29	27.23	29.92
k_{test}	Btu-in/hr-ft^2-F	0.2445	0.2433	0.2504	0.2468	0.2461	0.2482
k_{func} (1in)	Btu-in/hr-ft^2-F	0.2390	0.2428	0.2449	0.2479	0.2479	0.2514
ΔT_{Al}	F	1.83	1.88	1.73	1.71	1.71	1.72
ΔT_{Outins}	F	1.58	1.78	1.97	2.16	2.16	2.25

Table C-11: Experimental results for system P2-CGA under dry condition (IP units)

RH	%	8.97	8.32	7.50	7.00	8.82	7.18
T_{Room}	F	84.00	88.92	93.79	97.14	85.90	90.82
T_{Outins}	F	81.46	86.25	90.88	93.98	83.43	88.10
T_{Al}	F	39.99	40.31	40.14	40.11	39.87	40.12
T_{Cu}	F	27.20	25.99	24.19	23.11	26.34	25.13
ΔT_{out}	F	41.47	45.95	50.74	53.87	43.56	47.99
ΔT_{in}	F	12.79	14.32	15.95	17.00	13.53	14.99
T_{sand}	F	33.59	33.15	32.16	31.61	33.10	32.63
T_{test}	F	60.72	63.28	65.51	67.04	61.65	64.11
k_{eff}	Btu-in/hr-ft^2-F	3.15	3.13	3.09	3.07	3.13	3.11
Q_{sand}	Btu/hr	35.30	39.26	43.21	45.75	37.12	40.84
k_{test}	Btu-in/hr-ft^2-F	0.3600	0.3613	0.3601	0.3591	0.3603	0.3599
k_{func} (1in)	Btu-in/hr-ft^2-F	0.3008	0.3033	0.3054	0.3069	0.3017	0.3041
ΔT_{Al}	F	0.79	0.80	0.85	0.93	0.79	0.81
ΔT_{Outins}	F	0.90	0.89	0.96	1.34	0.89	0.95

Table C-12: Experimental results for system P2-CGB under dry condition (IP units)

RH	%	14.74	13.88	11.58	9.31	9.14	7.98
T_{Room}	F	77.01	81.95	86.88	91.83	91.84	96.87
T_{Outins}	F	74.79	79.51	84.11	88.82	88.82	93.62
T_{Al}	F	40.02	40.55	38.93	38.67	38.68	38.83
T_{Cu}	F	29.00	28.13	24.36	22.50	22.50	20.98
ΔT_{out}	F	34.77	38.96	45.18	50.15	50.14	54.79
ΔT_{in}	F	11.02	12.42	14.57	16.17	16.18	17.85
T_{sand}	F	34.51	34.34	31.64	30.59	30.59	29.90
T_{test}	F	57.41	60.03	61.52	63.74	63.75	66.22
k_{eff}	Btu-in/hr-ft^2-F	3.0801	3.0516	2.9883	2.9487	2.9488	2.9145
Q_{sand}	Btu/hr	29.76	33.22	38.17	41.79	41.83	45.60
k_{test}	Btu-in/hr-ft^2-F	0.3457	0.3443	0.3412	0.3366	0.3369	0.3361
k_{func} (1in)	Btu-in/hr-ft^2-F	0.3493	0.3483	0.3478	0.3469	0.3469	0.3459
ΔT_{Al}	F	1.32	1.31	1.30	1.26	1.26	1.30
ΔT_{Outins}	F	1.56	1.72	1.76	1.88	1.87	1.95

Table C-13: Experimental results for system P2-ER1 under dry condition (IP units)

RH	%	11.18	8.97	8.32	7.50	7.00
T_{Room}	F	75.48	84.16	89.00	93.79	96.87
T_{Outins}	F	73.96	83.13	87.90	92.55	95.66
T_{Al}	F	38.23	38.32	38.50	38.16	38.04
T_{Cu}	F	28.33	25.90	24.68	22.82	21.71
ΔT_{out}	F	35.73	44.80	49.39	54.39	57.62
ΔT_{in}	F	9.90	12.43	13.82	15.34	16.34
T_{sand}	F	33.28	32.11	31.59	30.49	29.88
T_{test}	F	56.10	60.73	63.20	65.36	66.85
k_{eff}	Btu-in/hr-ft^2-F	2.60	2.62	2.62	2.63	2.64
Q_{sand}	Btu/hr	22.57	28.49	31.80	35.40	37.79
k_{test}	Btu-in/hr-ft^2-F	0.2670	0.2689	0.2723	0.2752	0.2773
k_{func} (1in)	Btu-in/hr-ft^2-F	0.0000	0.0000	0.0000	0.0000	0.0000
ΔT_{Al}	F	0.76	0.78	0.84	0.94	1.00
ΔT_{Outins}	F	2.53	3.39	3.82	4.11	4.04

Table C-14: Experimental results for system P2-ER2 under dry condition (IP units)

RH	%	11.18	8.97	8.32	7.50	7.00
T_{Room}	F	74.88	84.32	89.14	94.02	97.17
T_{Outins}	F	73.74	82.62	87.25	91.80	94.86
T_{Al}	F	37.19	36.74	36.74	36.22	35.97
T_{Cu}	F	28.81	26.26	25.16	23.33	22.36
ΔT_{out}	F	36.55	45.88	50.51	55.59	58.89
ΔT_{in}	F	8.37	10.48	11.59	12.88	13.61
T_{sand}	F	33.00	31.50	30.95	29.77	29.16
T_{test}	F	55.46	59.68	62.00	64.01	65.41
k_{eff}	Btu-in/hr-ft^2-F	2.47	2.50	2.51	2.53	2.54
Q_{sand}	Btu/hr	18.12	22.95	25.49	28.53	30.27
k_{test}	Btu-in/hr-ft^2-F	0.2488	0.2511	0.2533	0.2577	0.2581
k_{func} (1in)	Btu-in/hr-ft^2-F	0.2442	0.2465	0.2477	0.2488	0.2496
ΔT_{Al}	F	0.70	0.75	0.80	0.81	0.93
ΔT_{Outins}	F	1.57	1.64	1.67	1.82	1.77

Table C-15: Experimental results for system P2-PIR1 under dry condition (IP units)

RH	%	21.13	18.23	13.72	9.96	10.71
T_{Room}	F	77.13	80.20	85.27	90.32	87.17
T_{Outins}	F	73.97	76.71	81.29	86.02	83.15
T_{Al}	F	38.87	38.69	39.00	39.03	38.93
T_{Cu}	F	28.78	27.73	26.80	25.39	26.04
ΔT_{out}	F	35.09	38.02	42.29	46.99	44.22
ΔT_{in}	F	10.10	10.96	12.20	13.64	12.89
T_{sand}	F	33.82	33.21	32.90	32.21	32.49
T_{test}	F	56.42	57.70	60.15	62.53	61.04
k_{eff}	Btu-in/hr-ft^2-F	3.1691	3.1397	3.1258	3.0975	3.1089
Q_{sand}	Btu/hr	28.06	30.18	33.43	37.04	35.14
k_{test}	Btu-in/hr-ft^2-F	0.2482	0.2464	0.2454	0.2447	0.2467
k_{func} (1in)	Btu-in/hr-ft^2-F	0.1957	0.1961	0.1969	0.1978	0.1973
ΔT_{Al}	F	1.29	1.25	1.11	1.38	1.36
ΔT_{Outins}	F	1.18	1.23	2.13	2.26	1.92

Table C-16: Experimental results for system P2-PIR2 under dry condition (IP units)

RH	%	21.13	18.23	13.72	9.96	10.71
T_{Room}	F	77.13	80.11	84.94	89.93	86.91
T_{Outins}	F	76.02	78.89	83.47	88.32	85.47
T_{Al}	F	38.21	37.99	38.23	38.26	38.16
T_{Cu}	F	28.52	27.52	26.71	25.44	26.00
ΔT_{out}	F	37.81	40.90	45.24	50.06	47.31
ΔT_{in}	F	9.69	10.47	11.52	12.82	12.17
T_{sand}	F	33.36	32.75	32.47	31.85	32.08
T_{test}	F	57.11	58.44	60.85	63.29	61.82
k_{eff}	Btu-in/hr-ft^2-F	2.6645	2.6557	2.6553	2.6497	2.6505
Q_{sand}	Btu/hr	22.64	24.36	26.82	29.78	28.27
k_{test}	Btu-in/hr-ft^2-F	0.2532	0.2519	0.2506	0.2515	0.2526
k_{func} (1in)	Btu-in/hr-ft^2-F	0.1959	0.1964	0.1972	0.1980	0.1975
ΔT_{Al}	F	1.44	1.44	1.58	1.67	1.61
ΔT_{Outins}	F	1.92	1.92	2.52	2.38	2.37

Appendix D: System input file and output coefficients (wet condition)

Table D-1: System input file and output coefficients for fibrous pipe insulation systems (IP units)

INPUTS		Fibrous Pipe Insulation System				
Tempearture Profiles		IP Units	P1-FG	P2-FG4	P2-FG5A	P2-FG5B
Amb temp	T_amb	F	107.60	78.10	78.10	90.10
R.H.	RH_amb	%	81.00	54.80	54.80	84.00
Outins temp	T_outins	F	103.98	76.69	76.86	86.68
Cold pipe temp	T_al	F	41.60	38.40	40.60	41.90
Dew point	T_dp	F	100.44	60.58	60.58	84.56
Test Sample Geometries						
Test length	L	in	36	36	36	36
Insulation exterior diameter	D_o	in	7.5	7.5	7.5	7.5
Insulation interior diameter	D_i	in	3.5	3.5	3.5	3.5
Properties						
Dry thermal conductivity	k_dry	Btu-in/hr-ft^2-F	0.24	0.23	0.23	0.23
Permeability	P	US perms	1.39E-11	4.98E-14	1.39E-11	1.39E-11
Water density	rho	lbm/ft^3	62.4	62.4	62.4	62.4
Convection heat transfer coefficient	h	Btu/hr-ft^2-F	1.63	1.63	1.63	1.63
OUTPUTS						
Partial vapor pressure (cold pipe=dp)	P_v1	in. Hg	0.25	0.23	0.25	0.27
Partial vapor pressure	P_v2	in. Hg	1.96	0.53	0.53	1.18
Atmosphere pressure	P_amb	in. Hg	29.9	29.9	29.9	29.9
Diameter at dew point	D_dp	in	7.1478	5.4729	5.3610	7.1080
Insulation volume	V	ft^3	7.20E-01	7.20E-01	7.20E-01	7.20E-01
Condensate volume	V_cond	ft^3	6.36E-01	2.90E-01	2.70E-01	6.26E-01
Coefficient f1	f1	-	0.8828	0.4023	0.3748	0.8698
Coefficient f2	f2	-	1	1	1	1
Coefficient f3	f3	-	0.0742	1	0.0742	0.0742
Condensate mass flow rate	m_w_dot	lbm/hr	0.0180	0.0001	0.0012	0.0097
		lbm/day	1551.9907	5.9998	107.8038	838.9561
Coefficient C1	C1	-	4.50E-05	0	4.50E-05	4.50E-05
Coefficient C2	C2	-	0.0178	0.0178	0.0178	0.0178

Table D-1: System input file and output coefficients for fibrous pipe insulation systems (SI units)

INPUTS	Fibrous Pipe Insulation System					
Tempearture Profiles		SI Units	P1-FG	P2-FG4	P2-FG5A	P2-FG5B
Amb temp	T_amb	C	42.00	25.61	25.61	32.28
R.H.	RH_amb	%	81.00	54.80	54.8	84.00
Outins temp	T_outins	C	39.99	24.83	24.92	30.38
Cold pipe temp	T_al	C	5.33	3.56	4.78	5.50
Dew point	T_dp	C	38.02	15.88	15.88	29.20
Test Sample Geometries						
Test length	L	m	0.9144	0.9144	0.9144	0.9144
Insulation exterior diameter	D_o	m	0.1905	0.1905	0.1905	0.1905
Insulation interior diameter	D_i	m	0.0889	0.0889	0.0889	0.0889
Properties						
Dry thermal conductivity	k_dry	W/m-K	0.0343	0.0334	0.0335	0.0338
Permeability	P	ng/s-m-Pa	7.97E-10	2.85E-12	7.97E-10	7.97E-10
Water density	rho	kg/m^3	1000	1000	1000	1000
Convection heat transfer coefficient	h	W/m^2-C	9.26	9.26	9.26	9.26
OUTPUTS						
Partial vapor pressure (cold pipe=dp)	P_v1	Pa	892.8	788.7	859.2	903.4
Partial vapor pressure	P_v2	Pa	6648.4	1800.9	1800.9	4060.9
Atmosphere pressure	P_amb	Pa	101325	101325	101325	101325
Diameter at dew point	D_dp	m	0.1816	0.1390	0.1362	0.1805
Insulation volume	V	m^3	2.04E-02	2.04E-02	2.04E-02	2.04E-02
Condensate volume	V_cond	m^3	1.80E-02	8.20E-03	7.64E-03	1.77E-02
Coefficient f1	f1		0.8828	0.4023	0.3748	0.8698
Coefficient f2	f2		1	1	1	1
Coefficient f3	f3		0.0742	1	0.0742	0.0742
Condensate mass flow rate	m_w_dot	kg/s	2.26E-06	8.75E-09	1.57E-07	1.22E-06
		kg/day	0.1955	0.0008	0.0136	0.1057
Coefficient C1	C1	-	4.50E-05	0	4.50E-05	4.50E-05
Coefficient C2	C2	-	0.0178	0.0178	0.0178	0.0178

Table D-2: System input file and output coefficients for closed-cell pipe insulation systems (IP units)

INPUTS	Closed-cell Pipe Insulation System							
Tempearture Profiles			P2-CGA	P2-CGB	P2-ER	P1-P2	P2-P	P2-PIR
Amb temp	T_amb	C	32.61	32.11	32.55	35.78	42.04	41.90
R.H.	RH_amb	%	83	83.20	83.00	87.10	81.70	81.70
Outins temp	T_outins	C	30.39	30.38	31.13	34.68	40.75	40.69
Cold pipe temp	T_al	C	3.36	3.15	2.65	4.60	4.70	4.83
Dew point	T_dp	C	29.30	28.89	29.20	33.27	38.22	38.09
Test Sample Geometries								
Test length	L	m	0.9144	0.9144	0.9144	0.9144	0.9144	0.9144
Insulation exterior diameter	D_o	m	0.1651	0.1651	0.1651	0.1905	0.1905	0.1651
Insulation interior diameter	D_i	m	0.0889	0.0889	0.0889	0.0889	0.0889	0.0889
Properties								
Dry thermal conductivity	k_dry	W/m-K	0.0530	0.0496	0.0401	0.0335	0.0341	0.0364
Permeability	P	m^2/s	7.00E-15	7.00E-15	1.44E-13	1.30E-12	1.30E-12	5.80E-12
Water density	rho	kg/m^3	1000	1000	1000	1000	1000	1000
Convection heat transfer coefficient	h	W/m^2-C	9.26	9.26	9.26	9.26	9.26	9.26
OUTPUTS								
Partial vapor pressure (cold pipe=dp)	P_v1	Pa	777.6	766.1	739.4	848.4	854.4	862.2
Partial vapor pressure	P_v2	Pa	4089.4	3983.8	4047	5517.3	6720	6670.7
Atmosphere pressure	P_amb	Pa	101325	101325	101325	101325	101325	101325
Diameter at dew point	D_dp	m	0.1637	0.1633	0.1614	0.1855	0.1824	0.1549
Insulation volume	V	m^3	1.39E-02	1.39E-02	1.39E-02	2.04E-02	2.04E-02	1.39E-02
Condensate volume	V_cond	m^3	1.36E-02	1.35E-02	1.30E-02	1.90E-02	1.82E-02	1.16E-02
Coefficient f1	f1		0.9761	0.9691	0.9372	0.9343	0.8941	0.8317
Coefficient f2	f2		84.0770	84.0770	2.4372	11.6281	11.6281	1.9763
Condensate mass flow rate	m_w_dot	kg/s	1.77E-08	1.703E-08	1.01E-08	4.97E-07	5.98E-07	5.14E-07
		kg/day	0.0015	0.0015	0.0009	0.0429	0.0516	0.0444

Table D-2: System input file and output coefficients for closed-cell pipe insulation systems (SI units)

INPUTS	Closed-cell Pipe Insulation System							
Tempearture Profiles			P2-CGA	P2-CGB	P2-ER	P1-P2	P2-P	P2-PIR
Amb temp	T_amb	F	90.70	89.80	90.59	96.40	107.67	107.42
R.H.	RH_amb	%	83.00	83.20	83.00	87.10	81.70	81.70
Outins temp	T_outins	F	86.70	86.68	88.03	94.42	105.35	105.24
Cold pipe temp	T_al	F	38.05	37.67	36.77	40.28	40.46	40.69
Dew point	T_dp	F	84.74	84.00	84.56	91.89	100.80	100.56
Test Sample Geometries								
Test length	L	in	36	36	36	36	36	36
Insulation exterior diameter	D_o	in	6.5	6.5	6.5	7.5	7.5	6.5
Insulation interior diameter	D_i	in	3.5	3.5	3.5	3.5	3.5	3.5
Properties								
Dry thermal conductivity	k_dry	Btu-in/hr-ft^2-F	0.37	0.34	0.28	0.23	0.24	0.25
Permeability	P	US perms	1.22E-16	1.22E-16	2.52E-15	2.27E-14	2.27E-14	1.01E-13
Water density	rho	lbm/ft^3	62.4	62.4	62.4	62.4	62.4	62.4
Convection heat transfer coefficient	h	Btu/hr-ft^2-F	1.63	1.63	1.63	1.63	1.63	1.63
OUTPUTS								
Partial vapor pressure (cold pipe=dp)	P_v1	in. Hg	0.25	0.23	0.25	0.27	0.27	0.27
Partial vapor pressure	P_v2	in. Hg	0.53	0.53	1.96	1.18	1.18	1.18
Atmosphere pressure	P_amb	in. Hg	29.9	29.9	29.9	29.9	29.9	29.9
Diameter at dew point	D_dp	in	6.4446	6.4282	6.3534	7.3046	7.1828	6.0993
Insulation volume	V	ft^3	4.91E-01	4.91E-01	4.91E-01	7.20E-01	7.20E-01	4.91E-01
Condensate volume	V_cond	ft^3	4.79E-01	4.76E-01	4.60E-01	6.73E-01	6.44E-01	4.08E-01
Coefficient f1	f1		0.9761	0.9691	0.9372	0.9343	0.8941	0.8317
Coefficient f2	f2		84.0770	84.0770	2.4372	11.6281	11.6281	1.9763
Condensate mass flow rate	m_w_dot	lbm/hr	0.0001	0.0001	0.0001	0.0039	0.0047	0.0041
		lbm/day	12.1081	11.6795	6.9238	340.8483	409.8279	352.4262

Appendix E: Comparison results between simulation results and experimental data

Table E-1: Simulation results on closed-cell system P2-CGA

Days	T_{ins}		k_{exp}		k_{sim}		k_{dry}		$kratio_{exp}$	$kratio_{sim}$	Vw_{exp}	Vw_{sim}	Diff
	C	F	W/m-K	Btu-in/hr-ft^2-F	W/m-K	Btu-in/hr-ft^2-F	W/m-K	Btu-in/hr-ft^2-F			%	%	%
0	16.56	64.78	0.0511	0.3544	0.0525	0.3642	0.0497	0.3445	1.03	1.06	0.00001	0.00	2.78
8	16.90	65.46	0.0536	0.3714	0.0529	0.3666	0.0496	0.3440	1.08	1.07	0.15	0.09	-1.29
18	16.90	65.46	0.0548	0.3798	0.0532	0.3692	0.0496	0.3440	1.10	1.07	0.45	0.20	-2.81
28	16.90	65.46	0.0547	0.3793	0.0536	0.3717	0.0496	0.3440	1.10	1.08	0.23	0.31	-2.00
38	16.90	65.46	0.0543	0.3765	0.0540	0.3743	0.0496	0.3440	1.09	1.09	0.53	0.42	-0.59
49	16.90	65.46	0.0545	0.3782	0.0544	0.3771	0.0496	0.3440	1.10	1.10	0.91	0.54	-0.27
57	16.90	65.46	0.0549	0.3806	0.0547	0.3792	0.0496	0.3440	1.11	1.10	0.35	0.63	-0.38
65	16.90	65.46			0.0550	0.3811	0.0496	0.3440		1.11		0.72	
75	16.90	65.46			0.0553	0.3837	0.0496	0.3440		1.12		0.83	
85	16.90	65.46			0.0557	0.3862	0.0496	0.3440		1.12		0.94	
95	16.90	65.46			0.0561	0.3888	0.0496	0.3440		1.13		1.05	
100	16.90	65.46			0.0563	0.3901	0.0496	0.3440		1.13		1.10	

Table E-2: Simulation results on closed-cell system P2-CGA

Days	T_{ins}		k_{exp}		k_{sim}		k_{dry}		$kratio_{exp}$	$kratio_{sim}$	Vw_{exp}	Vw_{sim}	Diff
	C	F	W/m-K	Btu-in/hr-ft^2-F	W/m-K	Btu-in/hr-ft^2-F	W/m-K	Btu-in/hr-ft^2-F			%	%	%
0	17.01	65.67	0.0489	0.3389	0.0526	0.3650	0.0496	0.3439	0.99	1.06	0.00001	0.00	7.68
11	17.19	66.04	0.0502	0.3481	0.0531	0.3679	0.0496	0.3436	1.01	1.07	0.21	0.12	5.69
21	17.19	66.04	0.0506	0.3508	0.0534	0.3703	0.0496	0.3436	1.02	1.08	0.18	0.23	5.55
32	17.19	66.04	0.0511	0.3541	0.0538	0.3728	0.0496	0.3436	1.03	1.08	0.14	0.34	5.29
42	17.19	66.04	0.0508	0.3520	0.0542	0.3754	0.0496	0.3436	1.02	1.09	0.29	0.45	6.66
53	17.19	66.04	0.0512	0.3548	0.0545	0.3781	0.0496	0.3436	1.03	1.10	0.16	0.57	6.58
63	17.19	66.04	0.0517	0.3583	0.0549	0.3806	0.0496	0.3436	1.04	1.11	0.27	0.67	6.22
65	17.19	66.04			0.0549	0.3810	0.0496	0.3436		1.11		0.69	
75	17.19	66.04			0.0553	0.3834	0.0496	0.3436		1.12		0.80	
85	17.19	66.04			0.0557	0.3858	0.0496	0.3436		1.12		0.90	
95	17.19	66.04			0.0560	0.3883	0.0496	0.3436		1.13		1.01	
100	17.19	66.04			0.0562	0.3895	0.0496	0.3436		1.13		1.06	

Table E-3: Simulation results on closed-cell system P2-ER

Days	T_{ins}		k_{exp}		k_{sim}		k_{dry}		$kratio_{exp}$	$kratio_{sim}$	Vw_{exp}	Vw_{sim}	Diff
	C	F	W/m-K	Btu-in/hr-ft^2-F	W/m-K	Btu-in/hr-ft^2-F	W/m-K	Btu-in/hr-ft^2-F			%	%	%
0	16.56	64.78	0.0401	0.2777	0.0393	0.2724	0.0400	0.2771	1.00	0.98	0.00001	0.00	-1.91
8	17.26	66.18	0.0402	0.2786	0.0394	0.2729	0.0402	0.2786	1.00	0.98	0.10	0.05	-2.03
18	17.26	66.18	0.0400	0.2774	0.0394	0.2733	0.0402	0.2786	1.00	0.98	0.10	0.12	-1.50
28	17.26	66.18	0.0406	0.2814	0.0395	0.2736	0.0402	0.2786	1.01	0.98	0.21	0.18	-2.77
38	17.26	66.18	0.0404	0.2802	0.0395	0.2740	0.0402	0.2786	1.01	0.98	0.25	0.24	-2.22
49	17.26	66.18	0.0410	0.2841	0.0396	0.2744	0.0402	0.2786	1.02	0.99	0.29	0.31	-3.41
57	17.26	66.18	0.0405	0.2808	0.0396	0.2747	0.0402	0.2786	1.01	0.99	0.34	0.36	-2.19
65	17.26	66.18			0.0397	0.2749	0.0402	0.2786		0.99		0.41	
75	17.26	66.18			0.0397	0.2753	0.0402	0.2786		0.99		0.47	
85	17.26	66.18			0.0398	0.2756	0.0402	0.2786		0.99		0.54	
95	17.26	66.18			0.0398	0.2760	0.0402	0.2786		0.99		0.60	
100	17.26	66.18			0.0398	0.2762	0.0402	0.2786		0.99		0.63	

Table E-4: Simulation results on closed-cell system P1-P2

Days	T_{ins}		k_{exp}		k_{sim}		k_{dry}		$kratio_{exp}$	$kratio_{sim}$	Vw_{exp}	Vw_{sim}	Diff
	C	F	W/m-K	Btu-in/hr-ft^2-F	W/m-K	Btu-in/hr-ft^2-F	W/m-K	Btu-in/hr-ft^2-F			%	%	%
0	16.56	64.78	0.0297	0.2056	0.0326	0.2257	0.0329	0.2282	0.90	0.99	0.00	0.00	9.79
3	19.68	70.96	0.0369	0.2561	0.0340	0.2358	0.0335	0.2325	1.10	1.01	0.81	0.70	-7.93
7	19.68	70.96	0.0407	0.2823	0.0358	0.2481	0.0335	0.2325	1.21	1.07	1.63	1.53	-12.09
14	19.68	70.96	0.0438	0.3037	0.0393	0.2724	0.0335	0.2325	1.31	1.17	2.54	3.01	-10.30
21	19.68	70.96	0.0473	0.3278	0.0426	0.2951	0.0335	0.2325	1.41	1.27	4.72	4.50	-9.98
24	19.68	70.96	0.0484	0.3356	0.0439	0.3043	0.0335	0.2325	1.44	1.31	4.96	5.11	-9.33
30	19.68	70.96			0.0465	0.3227	0.0335	0.2325		1.39		6.32	
40	19.68	70.96			0.0512	0.3549	0.0335	0.2325		1.53		8.43	
50	19.68	70.96			0.0559	0.3874	0.0335	0.2325		1.67		10.54	
60	19.68	70.96			0.0606	0.4200	0.0335	0.2325		1.81		12.64	
80	19.68	70.96			0.0701	0.4861	0.0335	0.2325		2.09		16.86	
100	19.68	70.96			0.0798	0.5535	0.0335	0.2325		2.38		21.07	

Table E-5: Simulation results on closed-cell system P2-P

Days	T_{ins}		k_{exp}		k_{sim}		k_{dry}		$kratio_{exp}$	$kratio_{sim}$	Vw_{exp}	Vw_{sim}	Diff
	C	F	W/m-K	Btu-in/hr-ft^2-F	W/m-K	Btu-in/hr-ft^2-F	W/m-K	Btu-in/hr-ft^2-F			%	%	%
0	22.19	75.94	0.0340	0.2360	0.0330	0.2360	0.0340	0.2360	1.00	0.97	0.00	0.00	-3.20
9	22.79	77.13	0.0439	0.3042	0.0385	0.3042	0.0342	0.2368	1.28	1.13	2.38	2.36	-12.19
17	22.79	77.13	0.0469	0.3252	0.0426	0.3252	0.0342	0.2368	1.37	1.25	4.45	4.19	-9.24
23	22.79	77.13	0.0525	0.3642	0.0464	0.3642	0.0342	0.2368	1.54	1.36	6.70	5.92	-11.64
31	22.79	77.13	0.0595	0.4126	0.0505	0.4126	0.0342	0.2368	1.74	1.48	10.01	7.73	-15.21
37	22.79	77.13	0.0691	0.4793	0.0544	0.4793	0.0342	0.2368	2.02	1.59	13.08	9.46	-21.37
45	22.79	77.13	0.0846	0.5869	0.0597	0.5869	0.0342	0.2368	2.48	1.75	22.10	11.48	-29.48
50	22.79	77.13			0.0616	0.0000	0.0342	0.2368		1.80		12.67	
60	22.79	77.13			0.0674	0.0000	0.0342	0.2368		1.97		15.20	
70	22.79	77.13			0.0731	0.0000	0.0342	0.2368		2.14		17.73	
85	22.79	77.13			0.0817	0.0000	0.0342	0.2368		2.39		21.53	
100	22.79	77.13			0.0904	0.0000	0.0342	0.2368		2.65		25.33	

Table E-6: Simulation results on closed-cell system P2-PIR

Days	T_{ins}		k_{exp}		k_{sim}		k_{dry}		$kratio_{exp}$	$kratio_{sim}$	Vw_{exp}	Vw_{sim}	Diff
	C	F	W/m-K	Btu-in/hr-ft^2-F	W/m-K	Btu-in/hr-ft^2-F	W/m-K	Btu-in/hr-ft^2-F			%	%	%
0	22.41	76.37	0.0368	0.2553	0.0371	0.2574	0.0364	0.2522	1.01	1.02	0.00	0.00	0.81
9	22.77	77.08	0.0416	0.2885	0.0430	0.2981	0.0364	0.2522	1.14	1.18	2.16	2.98	3.33
17	22.77	77.08	0.0427	0.2963	0.0473	0.3277	0.0364	0.2522	1.17	1.30	4.19	5.28	10.61
23	22.77	77.08	0.0443	0.3073	0.0513	0.3560	0.0364	0.2522	1.22	1.41	5.98	7.46	15.82
31	22.77	77.08	0.0466	0.3229	0.0557	0.3858	0.0364	0.2522	1.28	1.53	9.64	9.75	19.50
37	22.77	77.08	0.0502	0.3481	0.0598	0.4147	0.0364	0.2522	1.38	1.64	11.61	11.93	19.13
45	22.77	77.08	0.0559	0.3876	0.0597	0.4138	0.0364	0.2522	1.54	1.64	16.04	14.48	6.77
50	22.77	77.08			0.0676	0.4689	0.0364	0.2522		1.86		15.98	
60	22.77	77.08			0.0739	0.5126	0.0364	0.2522		2.03		19.17	
70	22.77	77.08			0.0804	0.5571	0.0364	0.2522		2.21		22.37	
85	22.77	77.08			0.0903	0.6257	0.0364	0.2522		2.48		27.16	
100	22.77	77.08			0.1005	0.6970	0.0364	0.2522		2.76		31.95	

Table E-7: Simulation results on fibrous system P1-FG

Days	T_{ins}		k_{exp}		k_{sim}		k_{dry}		$kratio_{exp}$	$kratio_{sim}$	Vw_{exp}	Vw_{sim}	Diff	a
	C	F	W/m-K	Btu-in/hr-ft^2-F	W/m-K	Btu-in/hr-ft^2-F	W/m-K	Btu-in/hr-ft^2-F			%	%	%	
0	23.67	74.60	0.0397	0.2755	0.0335	0.2324	0.0383	0.2656	1.04	0.88	0.12	0.0005	-15.64	0.9800
3	23.67	74.60	0.0989	0.6858	0.1007	0.6979	0.0383	0.2656	2.58	2.63	1.66	2.87	1.77	0.7146
5	23.67	74.60	0.1004	0.6959	0.1064	0.7379	0.0383	0.2656	2.62	2.78	4.26	4.76	6.03	0.7077
8	23.67	74.60	0.1212	0.8403	0.1152	0.7984	0.0383	0.2656	3.16	3.01	7.03	7.54	-4.98	0.6977
11	23.67	74.60	0.1242	0.8609	0.1239	0.8589	0.0383	0.2656	3.24	3.23	11.33	10.21	-0.23	0.6880
12	23.67	74.60	0.1250	0.8665	0.1268	0.8788	0.0383	0.2656	3.26	3.31	10.93	11.07	1.41	0.6849
20	23.67	74.60			0.1482	1.0275	0.0383	0.2656		3.87		17.28		0.6624
30	23.67	74.60			0.1696	1.1760	0.0383	0.2656		4.43		23.17		0.6411
40	23.67	74.60			0.1848	1.2810	0.0383	0.2656		4.82		27.11		0.6268
50	23.67	74.60			0.1945	1.3487	0.0383	0.2656		5.08		29.56		0.6179
60	23.67	74.60			0.2005	1.3899	0.0383	0.2656		5.23		31.01		0.6127
80	23.67	74.60			0.2060	1.4280	0.0383	0.2656		5.38		32.34		0.6079
100	23.67	74.60			0.2071	1.4361	0.0383	0.2656		5.41		32.76		0.6063
150	23.67	74.60			0.2085	1.4456	0.0383	0.2656		5.44		32.95		0.6057
200	23.67	74.60			0.2086	1.4459	0.0383	0.2656		5.45		32.96		0.6056
250	23.67	74.60			0.2086	1.4460	0.0383	0.2656		5.45		32.96		0.6056
350	23.67	74.60			0.2086	1.4460	0.0383	0.2656		5.45		32.96		0.6056

Table E-8: Simulation results on fibrous system P2-FG5A

Days	T_{ins}		k_{exp}		k_{sim}		k_{dry}		$kratio_{exp}$	$kratio_{sim}$	Vw_{exp}	Vw_{sim}	Diff	a
	C	F	W/m-K	Btu-in/hr-ft^2-F	W/m-K	Btu-in/hr-ft^2-F	W/m-K	Btu-in/hr-ft^2-F			%	%	%	
0	14.12	57.42	0.0392	0.2718	0.0395	0.2736	0.0381	0.2645	1.03	1.03	0.00	0.00	0.68	0.9800
9	15.20	59.35	0.0563	0.3900	0.0504	0.3491	0.0382	0.2649	1.47	1.32	0.27	0.60	-10.49	0.9061
16	15.20	59.35	0.0562	0.3899	0.0513	0.3555	0.0382	0.2649	1.47	1.34	0.33	1.06	-8.83	0.9044
30	15.20	59.35	0.0563	0.3901	0.0531	0.3681	0.0382	0.2649	1.47	1.39	1.15	1.96	-5.64	0.9012
37	15.20	59.35	0.0567	0.3931	0.0540	0.3743	0.0382	0.2649	1.48	1.41	1.25	2.40	-4.79	0.8996
44	15.20	59.35	0.0537	0.3726	0.0549	0.3803	0.0382	0.2649	1.41	1.44	1.51	2.83	2.07	0.8980
55	15.20	59.35	0.0559	0.3879	0.0562	0.3895	0.0382	0.2649	1.46	1.47	1.66	3.46	0.43	0.8957
60	15.20	59.35			0.0568	0.3935	0.0382	0.2649		1.49		3.74		0.8947
70	15.20	59.35			0.0579	0.4013	0.0382	0.2649		1.51		4.26		0.8928
90	15.20	59.35			0.0599	0.4152	0.0382	0.2649		1.57		5.20		0.8895
110	15.20	59.35			0.0616	0.4270	0.0382	0.2649		1.61		5.97		0.8866
130	15.20	59.35			0.0630	0.4367	0.0382	0.2649		1.65		6.60		0.8844
150	15.20	59.35			0.0641	0.4445	0.0382	0.2649		1.68		7.10		0.8825
170	15.20	59.35			0.0650	0.4502	0.0382	0.2649		1.70		7.49		0.8786
190	15.20	59.35			0.0657	0.4550	0.0382	0.2649		1.72		7.79		0.8774
210	15.20	59.35			0.0662	0.4587	0.0382	0.2649		1.73		8.02		0.8766
260	15.20	59.35			0.0670	0.4644	0.0382	0.2649		1.75		8.37		0.8752
360	15.20	59.35			0.0676	0.4685	0.0382	0.2649		1.77		8.62		0.8742
460	15.20	59.35			0.0677	0.4694	0.0382	0.2649		1.77		8.67		0.8740
560	15.20	59.35			0.0677	0.4696	0.0382	0.2649		1.77		8.68		0.8740

Table E-9: Simulation results on fibrous system P2-FG5B

Days	T_{ins}		k_{exp}		k_{sim}		k_{dry}		$kratio_{exp}$	$kratio_{sim}$	Vw_{exp}	Vw_{sim}	Diff	a
	C	F	W/m-K	Btu-in/hr-ft^2-F	W/m-K	Btu-in/hr-ft^2-F	W/m-K	Btu-in/hr-ft^2-F			%	%	%	
0	16.16	61.08	0.0354	0.2452	0.0327	0.2270	0.0355	0.2464	0.99	0.92	0.00	5.1850 9E-10	-7.39	0.9800
4	18.89	66.00	0.0825	0.5718	0.0701	0.4860	0.0359	0.2487	2.30	1.95	3.03	2.07	-15.00	0.8326
11	18.89	66.00	0.0918	0.6362	0.0788	0.5465	0.0359	0.2487	2.56	2.20	8.55	5.60	-14.10	0.8198
21	18.89	66.00	0.0979	0.6788	0.0911	0.6313	0.0359	0.2487	2.73	2.54	14.55	10.21	-6.99	0.8031
32	18.89	66.00	0.1026	0.7113	0.1022	0.7083	0.0359	0.2487	2.86	2.85	13.09	14.41	-0.42	0.7879
42	18.89	66.00	0.1032	0.7156	0.1097	0.7608	0.0359	0.2487	2.88	3.06	16.28	17.34	6.31	0.7792
53	18.89	66.00	0.1070	0.7416	0.1175	0.8147	0.0359	0.2487	2.98	3.28	15.12	19.69	9.86	0.7676
60	18.89	66.00			0.1197	0.8302	0.0359	0.2487		3.34		20.78		0.7648
70	18.89	66.00			0.1238	0.8582	0.0359	0.2487		3.45		21.92		0.7607
80	18.89	66.00			0.1262	0.8746	0.0359	0.2487		3.52		22.70		0.7579
90	18.89	66.00			0.1278	0.8858	0.0359	0.2487		3.56		23.22		0.7560
100	18.89	66.00			0.1288	0.8932	0.0359	0.2487		3.59		23.57		0.7547
120	18.89	66.00			0.1300	0.9014	0.0359	0.2487		3.62		23.95		0.7534
140	18.89	66.00			0.1305	0.9049	0.0359	0.2487		3.64		24.11		0.7528
160	18.89	66.00			0.1301	0.9018	0.0359	0.2487		3.63		24.18		0.7525
180	18.89	66.00			0.1308	0.9071	0.0359	0.2487		3.65		24.21		0.7524
200	18.89	66.00			0.1309	0.9073	0.0359	0.2487		3.65		24.22		0.7524
250	18.89	66.00			0.1309	0.9075	0.0359	0.2487		3.65		24.23		0.7523
350	18.89	66.00			0.1309	0.9075	0.0359	0.2487		3.65		24.23		0.7523

Table E-10: Simulation results on fibrous system P2-FG4

Days	T_{ins}		k_{exp}		k_{sim}		k_{dry}		$kratio_{exp}$	$kratio_{sim}$	Vw_{exp}	Vw_{sim}	Diff	a
	C	F	W/m-K	Btu-in/hr-ft^2-F	W/m-K	Btu-in/hr-ft^2-F	W/m-K	Btu-in/hr-ft^2-F			%	%	%	
0	14.09	57.36	0.0363	0.2513	0.0322	0.2230	0.0351	0.2434	1.03	0.92	0.00	0.00001	-11.26	1.03
55	14.11	57.40	0.0351	0.2430	0.0325	0.2252	0.0351	0.2434	1.00	0.93	0.25	0.19	-7.31	0.9793
100	14.11	57.40			0.0327	0.2270	0.0351	0.2434		0.93		0.34		0.9787
150	14.11	57.40			0.0330	0.2289	0.0351	0.2434		0.94		0.51		0.9780
200	14.11	57.40			0.0333	0.2307	0.0351	0.2434		0.95		0.66		0.9774
300	14.11	57.40			0.0338	0.2340	0.0351	0.2434		0.96		0.95		0.9763
400	14.11	57.40			0.0342	0.2369	0.0351	0.2434		0.97		1.19		0.9754
500	14.11	57.40			0.0345	0.2392	0.0351	0.2434		0.98		1.39		0.9746
600	14.11	57.40			0.0348	0.2410	0.0351	0.2434		0.99		1.54		0.9740
800	14.11	57.40			0.0351	0.2434	0.0351	0.2434		1.00		1.75		0.9732
984	14.11	57.40			0.0353	0.2447	0.0351	0.2434		1.01		1.85		0.9728

Appendix F: VBA codes sample

F-1 Sample VBA code of the thermal conductivity model under dry condition (for fibrous)

```
Attribute VB_Name = "PIT"

Sub lamdacal(ByRef c_rad As Double, ByRef a As Double, ByRef lamda_tot() As Double, ByRef
lamda_exp() As Double, _
ByRef Niter As Integer)

Dim L As Double
Dim D_o As Double
Dim D_i As Double
Dim D_x1_t As Double
Dim D_x1_b As Double
Dim D_x2_t As Double
Dim D_x2_b As Double
Dim D_exp As Double
Dim delta_js_ip As Double
Dim delta_js As Double
Dim delta_air As Double
Dim lamda_g As Double
Dim lamda_pg As Double
Dim lamda_rad As Double
Dim lamda_s As Double
Dim lamda_ins_t(20) As Double
Dim lamda_ins_b(20) As Double
Dim lamda_series_t(20) As Double
Dim lamda_series_b(20) As Double
Dim lamda_parallel_t(20) As Double
Dim lamda_parallel_b(20) As Double
Dim lamda_js As Double
Dim lamda_air As Double
Dim n As Double
Dim T(20) As Double
Dim R_s_o_t As Double
Dim R_s_o_b As Double
Dim R_g_i_t As Double
Dim R_g_i_b As Double
Dim R_1_t As Double
Dim R_1_b As Double
Dim R_g_o_t As Double
Dim R_g_o_b As Double
Dim R_s_i_t As Double
Dim R_s_i_b As Double
Dim R_2_t As Double
Dim R_2_b As Double
Dim R_series_t As Double
Dim R_series_b As Double
Dim R_g As Double
Dim R_s As Double
Dim R_g_parallel_t As Double
```

```
Dim R_g_parellel_b As Double
Dim R_s_parallel_t As Double
Dim R_s_parallel_b As Double
Dim R_parallel_t As Double
Dim R_parallel_b As Double
Dim R_ins_t As Double
Dim R_ins_b As Double
Dim R_air As Double
Dim R_js As Double
Dim R_tot(20) As Double
Dim i As Integer
Dim BlowingAgent As String

Const pi = 3.14

Call ReadPIT(D_i, D_exp, delta_js, L, lamda_s, lamda_js, n, Niter, T(), lamda_exp())

'delta_air = delta_js / 4
delta_air = (((D_i + delta_js) ^ 2 + D_i ^ 2) / 2) ^ 0.5 - D_i
D_o = (pi * D_exp - 2 * delta_js) / pi
D_x1_t = (n * (D_o ^ 2 - D_i ^ 2) + D_i ^ 2) ^ 0.5
D_x2_t = (D_o ^ 2 - n * (D_o ^ 2 - D_i ^ 2)) ^ 0.5
D_x1_b = D_x1_t
D_x2_b = D_x2_t

' air thermal conductivity
lamda_air = 0.024

Call ReadBlowingAgent(BlowingAgent)

For i = 1 To Niter
   If (BlowingAgent = "CO2") Then
      'cellular glass (func curve fitted in the range 10 to 30 C)
      lamda_pg = 0.0145570153 + 0.0000807263962 * T(i) - 5.83658784E-09 * T(i) ^ 2
   End If
   If (BlowingAgent = "C5H12") Then
      'PIR(func curve fitted in the range 10 to 30 C)
      lamda_pg = 0.0126236067 + 0.000084379968 * T(i) + 0.00000012136 * T(i) ^ 2
   End If
   If (BlowingAgent = "Air") Then
      '(func curve fitted in the range 10 to 30 C)
      lamda_pg =0.0236351784 + 0.0000756184913 * T(i) - 2.49407342E-08 * T(i) ^ 2
   End If

   If (n > 0.999) Then
      lamda_rad = 0
   Else
      lamda_rad = c_rad * 10 ^ (-10) * (T(i) + 273.15) ^ 3
   End If

   'thermal conductivity in the pores
   lamda_g = lamda_pg + lamda_rad

   'pure insulation thermal conductivity
   'series thermal conductivity
   'case 1: solid phase in the exterior layer
```

```
    R_s_o_t = 2 * WorksheetFunction.Ln(D_o / D_x1_t) / (2 * pi * lamda_s * L)
    R_g_i_t = 2 * (WorksheetFunction.Ln(D_x1_t / D_i)) / (2 * pi * lamda_g * L)
    R_1_t = R_s_o_t + R_g_i_t
    R_1_b = R_1_t
       'case 2: gas phase in the exterior layer
    R_g_o_t = 2 * WorksheetFunction.Ln(D_o / D_x2_t) / (2 * pi * lamda_g * L)
    R_s_i_t = 2 * WorksheetFunction.Ln(D_x2_t / D_i) / (2 * pi * lamda_s * L)
    R_2_t = R_s_i_t + R_g_o_t

    If (R_1_t > R_2_t) Then
       R_series_t = R_1_t
    Else
       R_series_t = R_2_t
    End If

    R_series_b = R_series_t

    lamda_series_t(i) = WorksheetFunction.Ln(D_o / D_i) / (pi * R_series_t * L)
    lamda_series_b(i) = WorksheetFunction.Ln(D_o / D_i) / (pi * R_series_b * L)

    'parallel thermal codnuctivity
    R_g = WorksheetFunction.Ln(D_o / D_i) / (2 * pi * lamda_g * L)
    R_s = WorksheetFunction.Ln(D_o / D_i) / (2 * pi * lamda_s * L)
    R_g_parallel_t = 2 * R_g / n
    R_s_parallel_t = 2 * R_s / (1 - n)

    R_parallel_t = 1 / (1 / R_s_parallel_t + 1 / R_g_parallel_t)
    R_parallel_b = R_parallel_t
    lamda_parallel_t(i) = WorksheetFunction.Ln(D_o / D_i) / (pi * R_parallel_t * L)
    lamda_parallel_b(i) = WorksheetFunction.Ln(D_o / D_i) / (pi * R_parallel_b * L)

    R_ins_t = 1 / (a / R_series_t + (1 - a) / R_parallel_t)
    R_ins_b = 1 / (a / R_series_b + (1 - a) / R_parallel_b)
    lamda_ins_t(i) = WorksheetFunction.Ln(D_o / D_i) / (pi * R_ins_t * L)
    lamda_ins_b(i) = WorksheetFunction.Ln(D_o / D_i) / (pi * R_ins_b * L)

    ' combined insulation thermal conductivity with airgaps and joint sealant
    R_air = 2 * WorksheetFunction.Ln((D_i + 2 * delta_air) / D_i) / (2 * pi * lamda_air * L)
    R_js = (D_o - D_i) / (4 * lamda_js * delta_js * L)
    R_tot(i) = 1 / (1 / R_js + 1 / (R_ins_t) + 1 / (R_air + R_ins_b))

    lamda_tot(i) = WorksheetFunction.Ln(D_exp / D_i) / (2 * pi * R_tot(i) * L)
Next i

Call WritePIT(D_o, a, c_rad, lamda_tot(), lamda_ins_t(), lamda_ins_b(), lamda_series_t(),
lamda_series_b(), lamda_parallel_t(), lamda_parallel_b(), Niter)
End Sub
```

F-2 Sample VBA code of the thermal conductivity model under dry condition (for fibrous)

```
Sub WetPIT(ByRef a As Double, ByRef u_fs As Double, ByRef V_w_t As Double, V_w_b As Double,
ByRef lamda_tot() As Double, ByRef lamda_exp() As Double, ByRef Niter As Integer, _
ByRef Nufs As Integer, ByRef CaseNum As Integer)

Dim L As Double
Dim D_o As Double
Dim D_i As Double
Dim D_xw1_t As Double
Dim D_xw1_b As Double
Dim D_xw2_t As Double
Dim D_xw2_b As Double
Dim D_pd1_t As Double
Dim D_pd1_b As Double
Dim D_pd2_t As Double
Dim D_pd2_b As Double
Dim D_x1_t As Double
Dim D_x1_b As Double
Dim D_x2_t As Double
Dim D_x2_b As Double
Dim D_exp As Double
Dim delta_js_ip As Double
Dim delta_js As Double
Dim delta_jac_ip As Double
Dim delta_jac As Double
Dim delta_air As Double
Dim delta_water As Double
Dim h_amb(20) As Double
Dim h_sat(20) As Double
Dim lamda_g As Double
Dim lamda_pg As Double
Dim lamda_rad As Double
Dim lamda_s As Double
Dim lamda_ins_t(20) As Double
Dim lamda_ins_b(20) As Double
Dim lamda_series_t(20) As Double
Dim lamda_series_b(20) As Double
Dim lamda_parallel_t(20) As Double
Dim lamda_parallel_b(20) As Double
Dim lamda_js As Double
Dim lamda_air As Double
Dim lamda_water As Double
Dim lamda_aw As Double
Dim M_water As Double
Dim n As Double
Dim T(20) As Double
Dim Tk(20) As Double
Dim R_aw_b As Double
Dim R_s1_t As Double
Dim R_s1_b As Double
Dim R_g1_t As Double
Dim R_g1_b As Double
```

```
Dim R_w1_t As Double
Dim R_w1_b As Double
Dim R_pd1_t As Double
Dim R_pd1_b As Double
Dim R_1_t As Double
Dim R_1_b As Double
Dim R_s2_t As Double
Dim R_s2_b As Double
Dim R_g2_t As Double
Dim R_g2_b As Double
Dim R_w2_t As Double
Dim R_w2_b As Double
Dim R_pd2_t As Double
Dim R_pd2_b As Double
Dim R_2_t As Double
Dim R_2_b As Double
Dim R_series_t As Double
Dim R_series_b As Double
Dim R_g As Double
Dim R_s As Double
Dim R_w As Double
Dim R_pd As Double
Dim R_g_parallel_t As Double
Dim R_g_parellel_b As Double
Dim R_s_parallel_t As Double
Dim R_s_parallel_b As Double
Dim R_w_parallel_t As Double
Dim R_w_parallel_b As Double
Dim R_pd_parallel_t As Double
Dim R_pd_parallel_b As Double
Dim R_parallel_t As Double
Dim R_parallel_b As Double
Dim R_ins_t As Double
Dim R_ins_b As Double
Dim R_air As Double
Dim R_js As Double
Dim R_tot(20) As Double
Dim rho_water As Double
Dim V_a As Double
Dim V_pd_t As Double
Dim V_pd_b As Double
Dim Vol_air As Double
Dim Vol_ins As Double
Dim Vol_water_t As Double
Dim Vol_water_b As Double
Dim Dv As Double
Dim P_amb As Double
Dim P_sat As Double
Dim dh_v As Double
Dim i As Integer
Dim b_t As Double
Dim b_b As Double
Dim c_rad As Double
Dim BlowingAgent As String
Dim Jacketing As String
```

```
Const pi = 3.1415926
Const Rv = 286.9

If (CaseNum = 2) Then
   Call ReadPITAppUfs(D_i, D_exp, delta_js, L, lamda_s, lamda_js, n, Niter, a, c_rad, V_w_t, V_w_b,
Nufs, T(), lamda_exp(), h_amb(), h_sat())
End If

If (CaseNum = 3) Then
   Call ReadPITAppWet(D_i, D_exp, delta_js, L, lamda_s, lamda_js, n, Niter, a, c_rad, V_w_t, V_w_b,
u_fs, T(), lamda_exp(), h_amb(), h_sat())
End If

If (CaseNum = 4) Then
   Call ReadPITAppa(D_i, D_exp, delta_js, L, lamda_s, lamda_js, n, Niter, c_rad, V_w_t, V_w_b, u_fs,
T(), lamda_exp(), h_amb(), h_sat())
End If

D_o = (pi * D_exp - 2 * delta_js) / pi

Vol_ins = pi * (D_o ^ 2 - D_i ^ 2) / 4 * L
Vol_water_t = V_w_t * Vol_ins
Vol_water_b = V_w_b * Vol_ins

rho_water = 1000
M_water = Vol_air * rho_water

Call ReadBlowingAgent(BlowingAgent)
Call ReadJacketingCase2(Jacketing, delta_jac)

For i = 1 To Niter
Tk(i) = T(i) + 273.15

   ' air and water thermal conductivity
   '(func curve fitted in the range 5 to 80 C)
   lamda_water = 0.5466 + 0.002189 * T(i) - 0.00001025 * T(i) ^ 2

   If (BlowingAgent = "CO2") Then
      'cellular glass (func curve fitted in the range 10 to 30 C)
      lamda_pg = 0.0145570153 + 0.0000807263962 * T(i) - 5.83658784E-09 * T(i) ^ 2
   End If
   If (BlowingAgent = "C5H12") Then
      'PIR(func curve fitted in the range 10 to 30 C)
      lamda_pg = 0.0126236067 + 0.000084379968 * T(i) + 0.00000012136 * T(i) ^ 2
   End If
   If (BlowingAgent = "Air") Then
      '(func curve fitted in the range 10 to 30 C)
      lamda_pg = 0.0236351784 + 0.0000756184913 * T(i) - 2.49407342E-08 * T(i) ^ 2
   End If

   If (n > 0.999) Then
      lamda_rad = 0
   Else
      lamda_rad = c_rad * 10 ^ (-10) * Tk(i) ^ 3
   End If
```

```
'Thermal conductivity of jacketing
lamda_jac = 0

If (Jacketing = "ASJ") Then
   '1 mil (0.001") Al foil +10 mil (0.01") paper
   lamda_jac = 0.09 * (236.291064 - 0.0254620174 * T(i) + 0.000744945368 * T(i) ^ 2) + 0.91 * 0.18
End If

If (Jacketing = "ASJ&PVC") Then
   '1 mil (0.001") Al foil +9 mil (0.009") paper+20 mil (0.02") PVC
   lamda_jac = 0.0322 * (236.291064 - 0.0254620174 * T(i) + 0.000744945368 * T(i) ^ 2) + 0.3226 *
0.18 + 0.65 * 0.19
End If

If (Jacketing = "Saran") Then
   '4 mil (0.004") paper
   lamda_jac = 0.18
End If

'case 1: solid phase in the exterior layer, gas phase between the water film and solid phase
D_xw1_t = (2 * V_w_t * (D_o ^ 2 - D_i ^ 2) + D_i ^ 2) ^ 0.5
D_xw1_b = (2 * V_w_b * (D_o ^ 2 - D_i ^ 2) + D_i ^ 2) ^ 0.5
D_x1_t = (n * (D_o ^ 2 - D_i ^ 2) + D_i ^ 2) ^ 0.5
D_x1_b = D_x1_t

'case 2: gas phase in the exterior layer, solid phase between the water film and gas phase
D_x2_t = ((1 - n) * (D_o ^ 2 - D_i ^ 2) + D_i ^ 2) ^ 0.5
D_x2_b = D_x2_t
D_xw2_t = (2 * V_w_t * (D_o ^ 2 - D_i ^ 2) + D_x2_t ^ 2) ^ 0.5
D_xw2_b = (2 * V_w_t * (D_o ^ 2 - D_i ^ 2) + D_x2_b ^ 2) ^ 0.5

'series thermal conductivity
'case 1: solid phase in the exterior layer, gas phase between the water film and solid phase
R_w1_t = 2 * WorksheetFunction.Ln(D_xw1_t / D_i) / (2 * pi * lamda_water * L)
'R_pd1_t = 2 * WorksheetFunction.Ln(D_pd1_t / D_xw1_t) / (2 * pi * lamda_pd * L)
R_g1_t = 2 * (WorksheetFunction.Ln(D_x1_t / D_xw1_t)) / (2 * pi * lamda_g * L)
R_s1_t = 2 * WorksheetFunction.Ln(D_o / D_x1_t) / (2 * pi * lamda_s * L)

R_1_t = R_s1_t + R_g1_t + R_w1_t

R_w1_b = 2 * WorksheetFunction.Ln(D_xw1_b / D_i) / (2 * pi * lamda_water * L)
'R_pd1_b = 2 * WorksheetFunction.Ln(D_pd1_b / D_xw1_b) / (2 * pi * lamda_pd * L)
R_g1_b = 2 * (WorksheetFunction.Ln(D_x1_b / D_xw1_b)) / (2 * pi * lamda_g * L)
R_s1_b = 2 * WorksheetFunction.Ln(D_o / D_x1_b) / (2 * pi * lamda_s * L)

R_1_b = R_s1_b + R_g1_b + R_w1_b

'case 2: gas phase in the exterior layer, solid phase between the water film and gas phase
R_s2_t = 2 * WorksheetFunction.Ln(D_x2_t / D_i) / (2 * pi * lamda_s * L)
R_w2_t = 2 * WorksheetFunction.Ln(D_xw2_t / D_x2_t) / (2 * pi * lamda_water * L)
'R_pd2_t = 2 * WorksheetFunction.Ln(D_pd2_t / D_xw2_t) / (2 * pi * lamda_pd * L)
R_g2_t = 2 * (WorksheetFunction.Ln(D_o / D_xw2_t)) / (2 * pi * lamda_g * L)

R_2_t = R_s2_t + R_w2_t + R_g2_t

R_s2_b = 2 * WorksheetFunction.Ln(D_x2_b / D_i) / (2 * pi * lamda_s * L)
```

```
R_w2_b = 2 * WorksheetFunction.Ln(D_xw2_b / D_x2_b) / (2 * pi * lamda_water * L)
R_g2_b = 2 * (WorksheetFunction.Ln(D_o / D_xw2_b)) / (2 * pi * lamda_g * L)

R_2_b = R_s2_b + R_w2_b + R_g2_b

If (R_1_t > R_2_t) Then
   R_series_t = R_1_t
Else
   R_series_t = R_2_t
End If

If (R_1_b > R_2_b) Then
   R_series_b = R_1_b
Else
   R_series_b = R_2_b
End If

lamda_series_t(i) = WorksheetFunction.Ln(D_o / D_i) / (pi * R_series_t * L)
lamda_series_b(i) = WorksheetFunction.Ln(D_o / D_i) / (pi * R_series_b * L)

'parallel thermal conductivity
R_g = WorksheetFunction.Ln(D_o / D_i) / (2 * pi * lamda_g * L)
R_s = WorksheetFunction.Ln(D_o / D_i) / (2 * pi * lamda_s * L)
R_w = WorksheetFunction.Ln(D_o / D_i) / (2 * pi * lamda_water * L)
'R_pd = WorksheetFunction.Ln(D_o / D_i) / (2 * pi * lamda_pd * L)

R_g_parallel_t = R_g / (n / 2 - V_w_t)
R_s_parallel_t = 2 * R_s / (1 - n)
R_w_parallel_t = R_w / V_w_t
'R_pd_parallel_t = R_pd / V_pd_t

R_g_parallel_b = R_g / (n / 2 - V_w_b)
R_s_parallel_b = 2 * R_s / (1 - n)
R_w_parallel_b = R_w / V_w_b

R_parallel_t = 1 / (1 / R_s_parallel_t + 1 / R_g_parallel_t + 1 / R_w_parallel_t)
R_parallel_b = 1 / (1 / R_s_parallel_b + 1 / R_g_parallel_b + 1 / R_w_parallel_b)
lamda_parallel_t(i) = WorksheetFunction.Ln(D_o / D_i) / (pi * R_parallel_t * L)
lamda_parallel_b(i) = WorksheetFunction.Ln(D_o / D_i) / (pi * R_parallel_b * L)

'lamda_ins_b(i) = lamda_series_b(i) * a + lamda_parallel_b(i) * (1 - a)
R_ins_t = 1 / (a / R_series_t + (1 - a) / R_parallel_t)
R_ins_b = 1 / (a / R_series_b + (1 - a) / R_parallel_b)
lamda_ins_t(i) = WorksheetFunction.Ln(D_o / D_i) / (pi * R_ins_t * L)
lamda_ins_b(i) = WorksheetFunction.Ln(D_o / D_i) / (pi * R_ins_b * L)

' combined insulation thermal conductivity with airgaps and joint sealant
If (lamda_jac = 0) Then
   R_jac = 0
Else
   R_jac = 2 * WorksheetFunction.Ln(D_o / D_i) / (2 * pi * lamda_jac * L)
End If

R_tot(i) = 1 / (1 / R_ins_t + 1 / R_ins_b) + R_jac
lamda_tot(i) = WorksheetFunction.Ln(D_exp / D_i) / (2 * pi * R_tot(i) * L)
```

```
Next i

If (CaseNum = 2) Then
   Call WritePITUfs(u_fs, lamda_tot(), Niter)
End If

If (CaseNum = 3) Then
   Call WritePITAppWet(D_o, M_water, lamda_tot(), lamda_ins_t(), lamda_ins_b(), lamda_series_t(),
lamda_series_b(), lamda_parallel_t(), lamda_parallel_b(), Niter)
End If

If (CaseNum = 4) Then
   Call WritePITAppa(a, D_o, M_water, lamda_tot(), lamda_ins_t(), lamda_ins_b(), lamda_series_t(),
lamda_series_b(), lamda_parallel_t(), lamda_parallel_b(), Niter)
End If

End Sub
```

F-3 VBA code of Nelder-Mead optimization (Modification on an existing optimization code)

```
Attribute VB_Name = "NelderMead"
''''''
```

```
ndim = 2   'number of independent variables
m = ndim + 1

ReDim Xtemp(ndim) As Double  'redim the working variables
ReDim Xall(m, ndim) As Double
ReDim Y(m) As Double
ReDim deltaX(ndim) As Double


' Call InitArrayOfDoubles(Xtemp, 1.534965, 0.122097, 1.975156, 1.412954) 'initial guesses
Call InitArrayOfDoubles(Xtemp, 0.5, 0.5) 'initial guesses
Call InitArrayOfDoubles(deltaX, 0.05, 0.05) 'deltas


Call Nelder_Mead(ndim, Xtemp, Xall, Y, deltaX, iserror, CaseNum)

End Sub

Sub NM_wet(ByRef CaseNum As Integer)
Dim ndim As Integer, m As Integer
Dim Xtemp() As Double, Xall() As Double, Y() As Double, deltaX() As Double
Dim iserror As Boolean

ndim = 1   'number of independent variables
m = ndim + 1

ReDim Xtemp(ndim) As Double  'redim the working variables
ReDim Xall(m, ndim) As Double
ReDim Y(m) As Double
ReDim deltaX(ndim) As Double


' Call InitArrayOfDoubles(Xtemp, 1.534965, 0.122097, 1.975156, 1.412954) 'initial guesses
Call InitArrayOfDoubles(Xtemp, 0.5) 'initial guesses
Call InitArrayOfDoubles(deltaX, 0.01) 'deltas


Call Nelder_Mead(ndim, Xtemp, Xall, Y, deltaX, iserror, CaseNum)

End Sub



' Nelder Mead Simplex Routine
'''''''
```

```
Dim i As Integer, j As Integer, limit As Integer, num As Integer
Dim m As Integer
Dim movename As String 'Added by JDS
Dim row_number As Integer 'Added by JDS
Dim column_number As Integer 'Added by JDS

'redimension the arrays
ReDim Xsum(ndim)
ReDim Xtry(ndim)
m = ndim + 1

'initialize the constant variables

' Nelder Mead constants for reflection, expansion and contraction
alpha = 1#   'JDS: These don't seem to be used again
beta = 0.5   'JDS: These don't seem to be used again
gamma = 2#   'JDS: These don't seem to be used again

' convergence criterion
converge = 10 ^ (-5)
MaxIt = 500 '1000
iserror = False
      'copy all the input coordinates for initial point into Xall
      For i = 1 To ndim
         Xall(1, i) = Xtemp(i)
      Next i

      'generate coordinates of other points..
      For i = 2 To m
         For j = 1 To ndim
            If (i = j + 1) Then
               Xall(i, j) = Xall(1, j) + deltaX(j)
            Else
               Xall(i, j) = Xall(1, j)
            End If
         Next j
      Next i

      'generate the function values for m points
      For i = 1 To m
         For j = 1 To ndim
            Xtry(j) = Xall(i, j)
         Next j


         Call calculate_func(Xtry, Y(i), iserror, CaseNum)
         If iserror = True Then
         Exit Sub
         End If

      Next i
' Write initial simplex to output worksheet; added by JDS 9-4-00

For i = 1 To ndim + 1
   For j = 1 To ndim
```

```
      row_number = 2
      column_number = 1 + (i - 1) * (ndim + 1) + j
      Worksheets("Output").Cells(row_number, column_number) = Xall(i, j)
      Next j
   column_number = 1 + i * (ndim + 1)
   Worksheets("Output").Cells(row_number, column_number) = Y(i)
   Next i


      ' start iterations for convergence...
      'For limit = 1 To MaxIt 'start iterations

      'calculate Xsum()
      For j = 1 To ndim
         sum = 0#
         For i = 1 To m
            sum = sum + Xall(i, j)
         Next i
         Xsum(j) = sum
      Next j


' Begin iterations
For num = 1 To MaxIt

iserror = False
      'find the function values for the highest and the lowest points
      'and the actual high and low points
      Call HighLow_point(m, Yhi, Ylo, Y2hi, Xhi, Xlo, X2hi, Y)

      rtol = 2# * Abs(Yhi - Ylo) / (Abs(Yhi) + Abs(Ylo) + (0.0000000001))
      If rtol < converge Then
         temp = Y(1)
         Y(1) = Y(Xlo)
         Y(Xlo) = temp
         For j = 1 To ndim
            temp = Xall(1, j)
            Xall(1, j) = Xall(Xlo, j)
            Xall(Xlo, j) = temp
         Next j
         ' exit the for loop
         Exit For
      End If

      'Begin New Iteration
      'First extrapolate by a factor of -1
      Call Amotry(ndim, Xhi, -1#, Xsum, Xall, Y, Ytry, iserror, CaseNum)
      movename = "Reflection" 'JDS 9-4-00
      If iserror = True Then
         iserror = False
      'Exit Sub
      End If

      'if the trial point is better than the best point try EXPANSION
      If Ytry <= Y(Xlo) Then
         Call Amotry(ndim, Xhi, 2#, Xsum, Xall, Y, Ytry, iserror, CaseNum)
```

```
        movename = "Expansion"  'JDS 9-4-00
        If iserror = True Then
           iserror = False
        ' Exit Sub
        End If


      ElseIf Ytry >= Y(X2hi) Then
        'the reflected point is worse than the second highest point
        'find CONTRACTION point
        Ysave = Y(Xhi)
        Call Amotry(ndim, Xhi, 0.5, Xsum, Xall, Y, Ytry, iserror, CaseNum)
        movename = "Contraction"  'JDS 9-4-00

        If iserror = True Then
           iserror = False
        'Exit Sub
        End If

        'if cant seem to get rid of that high point
        'better contract around the lowest (best) point
        If Ytry >= Ysave Then
           For i = 1 To m
              If i <> Xlo Then
                 For j = 1 To ndim
                    Xall(i, j) = Xsum(j) = 0.5 * (Xall(i, j) + Xall(Xlo, j))
                    Xtry(j) = Xsum(j)
                 Next j
                 Call calculate_func(Xtry, Y(i), iserror, CaseNum)
                 movename = "Multiple Contraction"  'JDS 9-4-00

                    iserror = False ' JDS: This is strange. 9-4-00
                 If iserror = True Then
                    iserror = False
                 'Exit Sub
                 End If

              End If
           Next i

           'calculate Xsum()

           For j = 1 To ndim
              sum = 0#
              For i = 1 To m
                 sum = sum + Xall(i, j)
              Next i
              Xsum(j) = sum
           Next j

        End If
      End If

' Write simplex to output worksheet; added by JDS 9-4-00

For i = 1 To ndim + 1
```

```
    For j = 1 To ndim

      row_number = num + 2
      column_number = 1 + (i - 1) * (ndim + 1) + j
      Worksheets("Output").Cells(row_number, column_number) = Xall(i, j)
      Next j
    column_number = 1 + i * (ndim + 1)
    Worksheets("Output").Cells(row_number, column_number) = Y(i)
    Next i
    column_number = column_number + 1
    Worksheets("Output").Cells(row_number, column_number) = movename



Next num

End Sub

'Calculate the Function Value
Sub calculate_func(x() As Double, ByRef value As Double, ByRef iserror As Boolean, ByRef CaseNum
As Integer)

iserror = False
Dim lamda_exp(20) As Double ' Holds 20 measured values of the thermal resistance
Dim lamda_tot(20) As Double
Dim a As Double
Dim c_rad As Double
Dim V_w_t As Double
Dim V_w_b As Double
Dim u_fs As Double
Dim i As Integer
Dim Niter As Integer
Dim Nufs As Integer
Dim SSQE As Double

'Sum of the Squares of the Error

'Call InitArrayOfDoubles(R_exp, 3.933, 4.502, 4.955, 5.337, 3.492, 4.179, 4.694, 5.115)
'Call InitArrayOfDoubles(DT, 5, 7.5, 10#, 12.5, 3.5, 6, 8.5, 11)

SSQE = 0

If (CaseNum = 1) Then

    a = x(1)
    c_rad = x(2)
    Call lamdacal(c_rad, a, lamda_tot(), lamda_exp(), Niter)

    If a > 1 Or a < 0 Then

       SSQE = 10000

    End If

    If c_rad < 0 Then
```

```
        SSQE = 10000
    Else
    For i = 1 To Niter
        SSQE = SSQE + (lamda_tot(i) - lamda_exp(i)) ^ 2
    Next i
    End If
End If
If (CaseNum = 2) Then
    u_fs = x(1)
    If u_fs > 1 Or u_fs < (V_w_t + V_w_b) Then
        SSQE = 10000
    Else
        Call WetPIT(a, u_fs, V_w_t, V_w_b, lamda_tot(), lamda_exp(), Niter, Nufs, CaseNum)
        If u_fs < (V_w_t + V_w_b) Then
            SSQE = 10000
        Else
            SSQE = SSQE + (lamda_tot(Nufs) - lamda_exp(Nufs)) ^ 2
        End If
    End If
End If
If (CaseNum = 4) Then
    a = x(1)
    'If a > 1 Or a < 0 Then
    '    SSQE = 0
    'Else
        Call WetPIT(a, u_fs, V_w_t, V_w_b, lamda_tot(), lamda_exp(), Niter, Nufs, CaseNum)
        If a > 1 Or a < 0 Then
            SSQE = 10000
        Else
```

```
            SSQE = SSQE + (lamda_tot(Niter) - lamda_exp(Niter)) ^ 2

        End If



End If

value = SSQE

End Sub


' find the maximum of two
Sub Maxx(a As Double, b As Double, ByRef C As Double)
   If (a >= b) Then
      C = a
   Else
      C = b
   End If
End Sub

' find the highest and the lowest points
Sub HighLow_point(num As Integer, Yhi As Double, Ylo As Double, Y2hi As Double, Xhi As Integer,
Xlo As Integer, X2hi As Integer, Y() As Double)
Dim count As Integer

Yhi = Y(1)
Ylo = Y(1)
Xhi = 1
Xlo = 1

'Find out the Highest Point
For count = 2 To num
   If Y(count) > Yhi Then
      Yhi = Y(count)
      Xhi = count
   End If
Next count

'Find out the Lowest Point
For count = 2 To num
   If Y(count) < Ylo Then
      Ylo = Y(count)
      Xlo = count
   End If
Next count

Y2hi = Ylo
X2hi = Xlo

'Find out the Second highest Point
For count = 1 To num
   If Y(count) <> Yhi Then
```

```
      If Y(count) > Y2hi Then
         Y2hi = Y(count)
         X2hi = count
      End If
   End If
Next count

End Sub

' the actual function evaluation routine
Sub Amotry(ByRef ndim As Integer, hi As Integer, fac As Double, _
                  Xsum() As Double, Xall() As Double, Y() As Double, _
                  ByRef Ytrial As Double, ByRef iserror As Boolean, ByRef CaseNum As Integer)
Dim L As Integer
Dim fac1, fac2 As Double
Dim Xtry() As Double


'redimension
ReDim Xtry(ndim)

fac1 = (1# - fac) / ndim
fac2 = fac1 - fac

For L = 1 To ndim
   Xtry(L) = Xsum(L) * fac1 - Xall(hi, L) * fac2
Next L

' evaluate function at the trial point
Call calculate_func(Xtry, Ytrial, iserror, CaseNum)
If iserror = True Then
'Exit Sub
End If

'if its better than the highest point replace the highest point
If (Ytrial < Y(hi)) Then
   Y(hi) = Ytrial
   For L = 1 To ndim
      Xsum(L) = Xsum(L) + Xtry(L) - Xall(hi, L)
      Xall(hi, L) = Xtry(L)
   Next L
End If

End Sub
```

.

VITA

Shanshan Cai

Candidate for the Degree of

Doctor of Philosophy

Thesis: THERMAL PERFORMANCE OF MECHANICAL PIPE INSULATION SYSTEMS AT BELOW-AMBIENT TEMPERATURE

Major Field: Mechanical Engineering

Biographical:

Education:

Completed the requirements for the Doctor of Philosophy in Mechanical Engineering at Oklahoma State University, Stillwater, Oklahoma in December, 2013.

Completed the requirements for the Master of Science in Mechanical Engineering at Oklahoma State University, Stillwater, Oklahoma in 2009.

Completed the requirements for the Bachelor of Science in Building Environment and Equipment Engineering at Huazhong Univeristy of Science and Technology, Wuhan, China in 2007.

Experience: Research/Teaching Assistant in Oklahoma State University

Professional Memberships: ASHRAE Student Member